

Regulation of mechanical feedback amplification in the *Drosophila* ear

Dissertation

for the award of the degree

"Doctor rerum naturalium" (Dr.rer.nat.)

of the Georg-August-Universität Göttingen

within the doctoral program Biology

of the Georg-August University School of Science (GAUSS)

submitted by

Narges Bodaghabadi (Lux)

from Tehran, Iran

Göttingen, 2021

Thesis Committee

Prof. Dr. Martin Göpfert

Department of Cellular Neurobiology, University of Göttingen

Prof. Dr. Tobias Moser

Institute for Auditory Neuroscience & InnerEarLab, University Medical Center Göttingen

Prof. Dr. Jörg Großhans

Institute of Biochemistry and Molecular Cell Biology, University Medical Center Göttingen

Members of the Examination Board

Prof. Dr. Ralf Heinrich

Dept. Cellular Neurobiology, University of Göttingen

Dr. Jan Clemens

Neural Computation and Behavior group, European Neuroscience Institute

Dr. Gerd Vorbrüggen

Dept. of Molecular Development, Max Planck Institute for Biophysical Chemistry

Date of oral examination: 17th November 2021

Layout of the dissertation

This thesis starts with a general introduction followed by a materials and methods section. The first half of the thesis deals with the enzymatic control of mechanical amplification in fly hearing, while the second half is allocated to the role of the gene *invertebrate GAP43 like (igl)* in the audition. The thesis ends with a summary of an initial project on *inactivation no afterpotential D (inaD)* that was ceased after the first two years of my Ph.D. due to technical issues.

Table of contents

Abstract	6
I Preface	9
I.I The model organism <i>Drosophila melanogaster</i>	9
I.II Chordotonal neurons	10
I.III Anatomy of the <i>Drosophila</i> hearing organ	11
I.IV Mechanism of hearing	13
I.V Ion Channels	13
I.VI Mechanical amplification	15
II Materials and Methods	17
II.I Fly husbandry; feeding regimes; and treatment	17
II.II GAL4/UAS System	22
II.III Cloning	23
II.IV Quantitative reverse transcription PCR (RT-qPCR)	27
II.V Double Header tool	28
II.VI Immunohistochemistry and confocal microscopy	29
II.VI.I Adult JO staining	29
II.VI.II Larva lch5 staining	30
II.VI.III Used antibodies	31
II.VII Hearing assessment using Laser Doppler vibrometry	32
II.VII.I Preparation	32
II.VII.II Free fluctuation measurement	33
II.VII.III Intensity-characteristics of sound receiver vibrations	34
II.VIII NAAM assay	35
II.IX Western blot	36
II.X TdT-mediated dUTP-X nick end labeling (TUNEL) assay	37
II.XI Electron microscopy	38
II.XII Prolonged depolarizing afterpotential (PDA) recordings	39

II.XIII	Statistical analyses	39
1.	Chapter I: Enzymatic control of mechanical amplification in fly hearing.....	40
1.1.	Introduction	40
1.1.1.	NAD ⁺ pathways	40
1.1.2.	Precedence for NAAM function in JO	42
1.1.3.	TRPV channel agonists.....	43
1.1.4.	EF-hand domains function in NAAM.....	44
1.1.5.	Chapter overview	45
1.2.	Results.....	47
1.2.1.	<i>Naam</i> expression in chordotonal neurons, cap, and scolopale cells.....	47
1.2.2.	NAAM localization in scolopale cells and JO neurons	49
1.2.3.	Auditory defects in <i>Naam</i> mutant flies	51
1.2.4.	NAAM substrate and product effects on hearing	55
1.2.5.	Overexpressed <i>Nmnat</i> in <i>Naam</i> mutant flies	58
1.2.6.	Cell type-specific rescue of hearing in the <i>Naam</i> mutant flies.....	60
1.2.7.	EF-hand domains role in NAAM enzymatic activity	63
1.2.8.	Auditory effects caused by <i>Naam</i> overexpression	69
1.2.9.	Auditory phenotype in double <i>iav</i> and <i>Naam</i> mutants.....	74
1.2.10.	NOMPC and <i>lav</i> channel disturbance in <i>Naam</i> mutant flies.....	76
1.2.11.	Apoptosis assay	77
1.2.12.	Altered mitochondrial features in <i>Naam</i> mutant flies	79
1.2.13.	Disrupted microtubule acetylation pattern in <i>Naam</i> mutant flies.....	80
1.3.	Discussion.....	82
1.3.1.	NAAM performance in hearing (modes of action)	82
1.3.2.	Enzymatically controlled TRPV channel agonist.....	83
1.3.3.	<i>Naam</i> expression pattern	84
1.3.4.	EF-hand domains function in NAAM enzyme	85
1.3.5.	<i>Naam</i> orthologs.....	87
1.3.6.	NAD ⁺ salvage pathway enzymes.....	88
1.3.7.	Additional <i>Naam</i> mutant characteristics	89
1.4.	Conclusion	92
2.	Chapter II. <i>Drosophila</i> GAP43 like (<i>igl</i>) in auditory neuron cilia.....	93
2.1.	Introduction	93
2.2.	Results.....	98
2.2.1.	<i>igl</i> expression pattern	98
2.2.2.	IGL cellular localization	101
2.2.3.	<i>igl</i> , a cilium compartment gene.....	102

2.2.4. Hearing impairment in <i>igl</i> mutant flies.....	108
2.3. Discussion.....	112
2.3.1. <i>igl</i> expression pattern and its protein localization	112
2.3.2. RFX regulation of IGL	113
2.3.3. IGL role in hearing.....	114
References.....	116
Appendix.....	131
Unveiling the role of the visual scaffolding protein INAD in hearing.....	131
Transgenic flies	132
The contribution of INAD to JO function, including auditory transduction and mechanical amplification	135
Cellular expression of the <i>inaD</i> gene.....	137
INAD protein localization	139
Uncovering <i>inaD</i> mutations with a deficiency line	139
Rescuing the mutant phenotype	142
Supplement pictures	148
List of figures	163
List of tables	166
List of abbreviations	167
Acknowledgments.....	169
Declaration.....	170
Curriculum vitae	171

Abstract

Ears achieve their exquisite sensitivity using positive mechanical feedback (Ashmore et al., 2010). Like pushing a swing augments its swing, sound-induced vibrations are enhanced by motile responses of auditory receptor cells on a cycle-by-cycle basis (Manley, 2001; Göpfert et al., 2005; Ashmore et al., 2010). This positive mechanical feedback boosts auditory sensitivity and is prone to feedback oscillations. The gain of this amplification needs to be controlled critically to adjust the sensitivity of hearing. Low amplification will hamper sensitive hearing, whereas excessive amplification can lead to large, self-sustained feedback oscillations that can be measured acoustically as spontaneous otoacoustic emissions, i.e. sounds emitted by the ear (Ashmore et al., 2010). The outer hair cells in the mammalian inner ear mediate the amplification through a voltage-dependent motor molecule, prestin (Fettiplace, 2006; Geurten et al., 2013). Four features of the active amplification are frequency-specific amplification, self-sustained oscillations (spontaneous otoacoustic emission), power gain, and compressive nonlinearity (Hudspeth, 2008). Amplification has been reported also in the hearing organ of non-mammalian vertebrates and insects (Manley, 2001; Nadrowski et al., 2011). The amplification in the *Drosophila* hearing organ is the focus of this thesis.

Stabilizing the gain of mechanical amplification is crucial for hearing, yet how this stabilization is achieved is little understood. In *Drosophila*, Nanchung (Nan)-Inactive (lav) transient receptor potential vanilloid (TRPV) channels have been identified to negatively regulate amplification, whereby the loss of Nan-lav leads to hyper-amplification, with the antenna displaying large, self-sustained oscillations in the absence of sound stimuli (Göpfert et al., 2006). Excess amplification also ensues from mutations in the flies' single calmodulin gene (Senthilan et al., 2012), implicating TRPV channels and calcium in the endogenous regulation of the amplification gain. How TRPV channel activity and calcium levels are controlled, however, has remained mysterious. In the course of my work, I had a deeper look into this control, unraveling a metabolic feedback that regulates amplification (part 1) and identifying a novel molecular player in the regulation of the amplification gain (part 2).

Part I: Enzymatic control of mechanical amplification in fly hearing

The *Drosophila* auditory neurons are ciliated with Nan and lav both localizing to the proximal cilium region in an interdependent manner, assembling into Nan-lav

heteromers (Gong et al., 2004). Hints that the open probability of the TRPV channel might be important comes from the action of pymetrozine, a synthetic insecticide whose molecular targets are Nan-lav TRPVs (Nesterov et al., 2015). Pymetrozine activates Nan-lav channels, leading to ciliary calcium influx and reducing the mechanical amplification gain (Nesterov et al., 2015). Apparently, activating Nan-lav reduces the gain of mechanical amplification, but what controls internally the activity of Nan-lav?

Nicotinamidase is a component of the nicotinamide adenine dinucleotide (NAD⁺) salvage pathway that generates NAD⁺ from niacin equivalents, such as nicotinamide. Nicotinamidase converts nicotinamide into nicotinic acid, whereby nicotinamide is an agonist of Nan-lav TRPV channels that, at least *in vitro*, activates Nan-lav (Upadhyay et al., 2016). The application of nicotinamide on the *Drosophila* larvae elicits calcium signals in the chordotonal neurons (Upadhyay et al., 2016), much like pymetrozine (Nesterov et al., 2015).

My work documented that, unlike pymetrozine, nicotinamide is an endogenous activator of Nan-lav channels, linking Nan-lav activity to metabolism. I identified the fly's nicotinamidase (NAAM), as a central player in the regulation of mechanical amplification in fly hearing. By analyzing a null mutation that disrupts *Naam* expression, I found that loss of NAAM not only abolishes sound-evoked electrical Johnston's organ responses and mechanical amplification but also affects TRPV channels expression and localization.

Judged from my results, loss of *Naam* leads to the accumulation of nicotinamide and, thus, excessive Nan-lav opening, thereby reducing the gain of mechanical amplification in fly hearing. Consistent with such a scenario, supplementing the fly food of wild-type flies with nicotinamide also reduced the amplification gain, whereas feeding *Naam* mutant flies with NAD⁺ or nicotinic acid did not rescue mechanical amplification. Hence, rather than the lack of the NAAM product, it seems to be the accumulation of the NAAM substrate, nicotinamide, that reduces the amplification gain. Apparently, NAAM links mechanical amplification in hearing to metabolism, regulating the amplification gain by modulating nicotinamide levels and, thus, Nan-lav activity.

Drosophila NAAM is particular in that it bears aminoterminal EF-hand domains, besides the isochorismatase-like domain. The evolutionary conserved EF-hand domains might regulate the enzyme activity by binding to Ca²⁺. In the course of this thesis, I found that the EF-hand domains have a direct effect on the NAAM enzymatic activity. NAAM with missense point mutation or deletion in the EF-hand domains did not rescue the hearing defect in the *Naam* mutant flies, and the same was observed in *in vitro* assays

of the enzymatic reaction. Manipulating the EF-hand domains of *Naam* affected NAAM localization, leaving the question open, how exactly the EF-hand domains contribute to the NAAM function.

Part II: *Drosophila* GAP43 like (*igl*) in auditory neuron cilia

(IGL, Invertebrate GAP43 like), the fly ortholog of the vertebrate key “growth” and “plasticity” protein GAP43, is reportedly abundant in neurons (Neel and Young, 1994). I found that *igl* is expressed in auditory receptor neurons, with IGL protein localizing to their cilia. In effect, sequence analysis identified the binding motif of the ciliary transcription factor RFX in the *igl* promoter/enhancer region, putting IGL forward as a novel cilium compartment protein. Consistent with this notion, I could show that the expression of IGL protein is RFX-dependent, with the loss of RFX abolishing ciliary localization of the IGL. Moreover, I discovered an RFX DNA binding motif in human GAP43, adding a new twist to GAP43 regulation and suggesting that *igl* might be a conserved cilium gene. Precedence for a GAP43 cilium connection comes from newborn rat olfactory receptor neurons, whose cilia are strongly stained by antibodies against GAP43 (Verhaagen et al., 1989).

Notwithstanding these intriguing results, there was not a proper available mutant for this gene. The non-in-frame GFP cassette insertion in *igl*^{M102290} flies leads to the reduction in the mechanical amplification as well as the power of the antenna’s mechanical free fluctuations. Hence, in contrast to TRPVs and calmodulin, *Drosophila* IGL seems to positively control the amplification gain in the fly’s auditory system. This seems intriguing given that the *igl* sequence comprises IQ motifs and reportedly binds calmodulin (Neel and Young, 1994).

I Preface

Human beings perceive the surrounding environment through at least five senses, touch, smell, audition, taste, and vision. Enabling communication, hearing is one of the most important senses, the defect of which can be an immense challenge for affected individuals and society. Like touch, hearing happens through the conversion of mechanical stimuli to electrical signals, a process known as mechano-electrical transduction (Kung, 2005). The sound stimulus (pressure or particle velocity) gets converted to the electrical signals, in the sound detector organ, such as an ear. The processing of the converted signals in the brain leads to auditory perception. Whereas the importance of hearing is undeniable, the genetic underpinning of deafness is not fully understood (Senthilan et al., 2012).

I.I The model organism *Drosophila melanogaster*

Apart from vertebrates, hearing is widespread in insects (Göpfert and Hennig, 2016). The fruit fly, *Drosophila melanogaster* (*D. melanogaster*), for example, communicates acoustically and hears with antennal ears (Ewing, 1978). The antenna's distal part acts as a sound receiver whose vibrations are picked up by Johnston's organ (JO), a large stretch receptor organ in the proximal part of the antenna (Albert and Göpfert, 2015). The JO shows a partial molecular parallel with the vertebrate inner ear (Lu et al., 2009). Of 274 genes identified in a screen for *Drosophila* auditory organ genes (Senthilan et al., 2012), every fifth has a cognate gene that is implicated in human hearing disorders, besides many genes that had been associated with hearing before. This illustrates the evolutionary conservation of the systems as exemplified by *atonal* (*ato*). *Ato* encodes the transcription factor that specifies JO neurons and can functionally be substituted with *Math1/Atoh1* in mice (or *ATOH1* in humans), which is implicated in hair cell specification in the vertebrate ear (Bermingham et al., 1999). Furthermore, ciliogenesis in all ciliated sensory neurons and chordotonal neurons, are controlled by transcription factors RFX and Fd3F respectively, which are evolutionary conserved, and functioning downstream of *Ato* (Cachero et al., 2011). Unlike *Drosophila*, mammalian's RFX does not affect the development of primary cilia (kinocilia) in the ear; however, it is needed for the maintenance of normally-developed hair cells (Elkon et al., 2015).

Not only common genetics and molecular similarities, but also parallel function between vertebrate cochlea (snail-like structure in the inner ear) and *Drosophila* ears, make *Drosophila* a useful model for hearing studies. Like the cochlea, JO displays key characteristics that are ascribed to the cochlear amplifier in the vertebrate hearing organ (Göpfert and Robert, 2003 a; Göpfert et al., 2006; Nadrowski et al., 2008; Ashmore et al., 2010).

The growing gene modification tools in *Drosophila* to create targeted mutation, and transgenic flies (Venken and Bellen, 2005; Diao et al., 2015), besides its complete sequenced genome, makes *Drosophila* a favorite model organism.

I.II Chordotonal neurons

The peripheral nervous system in *Drosophila* is composed of two sensory neuron types (Brewster and Bodmer, 1995). Type I sensory neurons are monodendritic, which are in association with numerous support cells. Type I sensory neurons originate from individual ectodermal precursor cells and are split into two groups (Brewster and Bodmer, 1995). The chordotonal neurons in the first group have internally located stretch receptors, while the second group has externally located sensory organs like chemo- and mechanosensory neurons (Brewster and Bodmer, 1995).

The second type of sensory neurons (type II) in *Drosophila* are non-ciliated multidendritic neurons that, with one exception, lack any connection to the support cells (Brewster and Bodmer, 1995).

Chordotonal organs detect the relative movement of two joints directly or indirectly with extero- and proprioceptive function in insects and other arthropods (Krishnan and Sane, 2015). The chordotonal organs with extero-function in *Drosophila* are involved in sound (Göpfert and Hennig, 2016), gravity (Kamikouchi et al., 2009), and wind sensation (Yorozu et al., 2009). The biggest chordotonal organ in adult *Drosophila* is known as JO (Azusa Kamukouchi, Tkashi Shimada, 2006).

Chordotonal neurons in *Drosophila* larvae are categorized into four groups: lateral pentascolopidial chordotonal (lch5), single lateral chordotonal (lch1), ventral chordotonal A (vchA), and ventral chordotonal B (vchB) (Halachmi et al., 2016). The larval chordotonal organs are involved in proprioception, touch (Caldwell et al., 2003), and vibration sensation (Zhang et al., 2013).

I.III Anatomy of the *Drosophila* hearing organ

Drosophila detects sound via one pair of antennae that are located in front of the head between the eyes. Each antenna is composed of three main parts that are the 1) scape, the 2) pedicel, and the 3) funiculus (Figure 1).

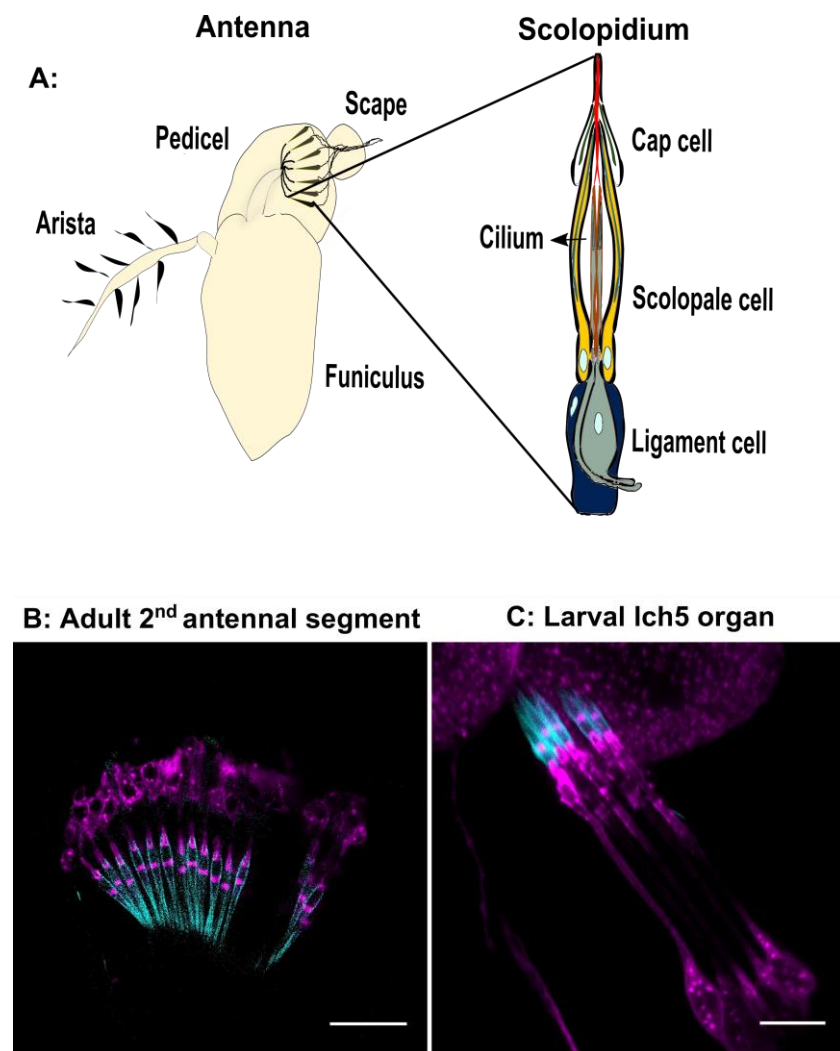


Figure 1. *Drosophila* hearing organ.

A: schematic picture of an antenna, and a scolopidium, B: adult 2nd antennal segment, and C: larval lateral chordotonal organ (lch5), depicted in cyan for scolopale rods and magenta for neurons. Scale bars: 20 μm in panel B and 10 μm in panel C.

- 1) The scape is the first and basal part of the insects' antenna that allows the fly to actively move the antenna, containing muscles connecting to the head.

- 2) The pedicel contains the JO, which is composed of approximately 250 multicellular stretch receptor units, the scolopidia. These receptor units harbor several accessory cells and two to three bipolar ciliated monodendritic neurons, each (Caldwell and Eberl, 2002; Todi et al., 2004). These JO neurons can serve as potential progenitor cells for JO neurogenesis (Hernandez et al., 2021).

All cells in a scolopidium originate from one precursor cell that differentiates into various cell types. Based on the projection of JO neurons in the antennal mechanosensory and motor center in the brain (AMMC), they can be categorized into five groups named A-E. A and B are mainly responding to vibrational stimuli, while C and E react to sustained deflection by wind (Yorozu et al., 2009) and gravity (Kamikouchi et al., 2009). Subgroup-D reacts to both antennal vibrations and static deflection (Matsuo et al., 2014).

Accessory cells, such as cap and ligament cells are anchored to the cuticle via cap- and ligament-attachment cells respectively, with the cap cells conveying antennal vibrations to the mechanosensory cilia of the neurons (Kernan, 2007). Another accessory cell, the scolopale cell, encompasses the cilium of each scolopidium and builds a scolopale space that is rich in K^+ (Eberl, 1999). This composition resembles the endolymph space in the inner ear, which surrounds the inner and outer hair cells in the vertebrate hearing system. The scolopale cells also harbor intracellular actin-based scolopale rods that presumably provide mechanical support (Roy et al., 2013).

- 3) The funiculus together with the arista, a featherlike appendix to the funiculus (the antenna distal segment), serves as a sound receiver (Göpfert and Robert, 2002). In response to sound, the funiculus rotates about its longitudinal axis and transduces the signal to the pedicel via a hook. The funiculus is also an olfactory detector, housing mostly the olfactory sensory neurons (Carlson, 1996).

The Ich5 (Figure 1) is the most studied chordotonal organ in *Drosophila* larvae. The Ich5 organs are serially located in the lateral position of the seven abdominal segments and are required for proprioception (Caldwell et al., 2003) and sound-induced vibration perception (Zhang et al., 2013). The Ich5 in the *Drosophila* larvae shares great functional and morphological features with the *Drosophila* adult JO (Zhang et al., 2013). They have

the *ato* proneural gene in their developmental program (Jarman et al., 1993) and use equivalent mechanotransduction channels for detecting sound (Zhang et al., 2013).

I.IV Mechanism of hearing

A major function of hearing in *Drosophila* is the detection of conspecific courtship songs (Bennet-Clark, 1971). By fanning one of their wings, male flies produce sounds in the range of 100-300 Hz and in two forms, a sine and a pulse song (Greenspan and Ferveur, 2000; Dickson, 2008). In response to sound particle velocity, the sound receiver in the antenna (funiculus and arista) will be rotated, whereby the neurons in JO will be contracted or stretched. Due to the fast response of JO neurons to sound stimuli, it is assumed that the transduction of the signal is mediated through a directly force-gated ion channel (Albert et al., 2007). Within the cilia, in the JO of *Drosophila*, the vibrations are transduced into electrical signals (mechano-electrical transduction), either by No mechanoreceptor potential C (NOPMC), TRPN channels in the cilium tips, or by heteromeric TRPV channels formed by Nan and lav that reside in the proximal cilium region (Albert and Göpfert, 2015). The signal then will be propagated to the AMMC in the brain.

I.V Ion Channels

Ion channels are transmembrane proteins with a narrow hydrophilic pore that are transporters of ions through the membrane. They also contain intracellular and extracellular domains, which contribute to the closing, opening, or gating of the channel. In all cells, ion channels contribute to the cell membrane potential, the cell volume, and cellular signaling.

Transient receptor potential (TRP) channels are a family of nonselective cationic channels that have more diversity in activation modes and selectivity compared to other ion channels (Montell, 2005). TRP channels are tetrameric ion channels with extended cytosolic C and N terminal regions (Pedersen et al., 2005). Each subunit of the TRP channel contains six transmembrane regions, with a pore loop between the fifth and the sixth one (K. Venkatachalam, 2007). TRP channels are categorized into seven groups based on sequence similarity: TRPN (NOPMC), TRPV (vanilloid), TRPC (canonical), TRPA (ankyrin), TRPM (melastatin), TRPML (mucolipin), and TRPP (polycystic) (Pedersen et al., 2005). TRP channels are also categorized based on their common

features. The first group (TRPA, TRPC, TRPV, TRPN, TRPM) has either N-terminal variable intracellular ankyrin repeats for membrane anchoring and protein interaction or C-terminal TRP domain involving in channel multimerization and gating modulation. The second group (TRPML, TRPP) has a long extracellular region between S1 and S2 while lacking the features of the first group (Kadowaki, 2015).

All seven TRP categories are present in *Drosophila*; however, in mice and humans, the TRPN channel is missing (Fowler and Montell, 2013). *Drosophila* TRPN (=NOMPC) channels are required for mechanosensation (Effertz et al., 2011; Yan et al., 2013) and noxious cold temperatures perception (Turner et al., 2016). TRPC with its three members mediate proprioception (Akitake et al., 2015), cold sensation, and photosensation (Rosenzweig et al., 2008). TRPA has four members with fundamental functions in sensations, namely nociception (Tracey et al., 2003), and gravity sensing (Sun et al., 2009). TRPM mediates Zn^{2+} (Georgiev et al., 2010) and Mg^{2+} (Hofmann et al., 2010) homeostasis. Besides, it involves in cold sensations (Turner et al., 2016). In contrary to all TRP channels, TRPML and TRPP have not been reported to be involved in any sensory perception.

Among TRP channels, TRPV (Vanilloid) has been studied extensively. The TRPV channels are homo- or hetero-tetrameric, non-specific cation channels. They are divided into six and two subfamilies in mammals and *Drosophila*, respectively. Each Monomer has 3 - 5 N-terminal ankyrin repeats. In mammals, the TRPV channels have various thermosensitivity, perceiving heat in different thresholds (Patapoutian et al., 2003).

The two TRPV channels in *Drosophila*, *Nan*, and *lav* are required for mechano- (Kim et al., 2003; Lehnert et al., 2013) and cold sensation (Kwon et al., 2010). The *lav* expression is restricted to chordotonal neurons, whereas *nan* is expressed broadly in chordotonal and multidendritic neurons (Nesterov et al., 2015).

In *Drosophila* JO, there is compelling evidence in favor of the hypothesis that NOMPC is the mechano-electrical transduction channel (Göpfert et al., 2006; Effertz et al., 2011, 2012). The NOMPC channels are located in the cilium tips (Lee et al., 2010) and harbor 29 N-terminal ankyrin domains as a gating spring in each subunit (Howard and Bechstedt, 2004). In *nompC* mutant flies, there is a residual NOMPC-independent, wind- and gravity-neuronal response (Effertz et al., 2011) with a complete loss of the mechanical amplification by auditory JO neurons, unlike the facilitated amplification in *nan* and *lav* mutants (Göpfert et al., 2006). In *nompC* and *nan* double mutants, the mechanical amplification is completely abolished, resembling the *nompC* mutant phenotype (Göpfert et al., 2006). The studies indicate that NOMPC is required for the

nonlinear amplification, whereas *Nan-lav* is needed for adjusting the amplification, and *nompC* is epistatic to *nan* (Göpfert et al., 2006; Effertz et al., 2011, 2012).

I.VI Mechanical amplification

The hearing in *Drosophila* is actively amplified (Nadrowski et al., 2011). This process is comparable to the cochlear amplification in the mammalian auditory system (Dallos, 1992; Ashmore et al., 2010). The amplification enhances the mechanical sensitivity in mammals and *Drosophila* by a factor of 100 (Liberman et al., 2002) and 10 (Göpfert et al., 2006), respectively.

In mammals, the sound travels along the basilar membrane within the cochlea and vibrates the basilar membrane tonotopically (tonotopy from Greek *tono* = frequency and *topos* = place) (Talavage et al., 2004). The tonotopical displacement of the basilar membrane depends on the various width and stiffness of the membrane, which by itself is a linear, passive process (Olson et al., 2012). Cochlear amplification is an active process with four characteristics that increase the acute sensitivity of sound perception in mammals. The four characteristics of the cochlear amplifier are 1) an otoacoustic emission (self-sustained oscillations), 2) compressive nonlinearity, 3) frequency-specific amplification, and 4) active amplification (Hudspeth, 2008). The principal players of the cochlear amplification are the outer hair cells, having prestin in their membrane, mediating electromechanical feedback amplification (Ashmore, 1987; Dallos, 1992; Liberman et al., 2002). The mammalian ear produces signals in the absence of the sound stimulus, by a process known as otoacoustic emission. The ear also amplifies faint sounds (compressive nonlinearity) (Hudspeth, 2008) and increases the auditory sensitivity, broadening the dynamic range (Ashmore et al., 2010). Active amplification ascribes to the situation that the output energy of a system exceeds the input (Hudspeth, 2008). Depriving the mammalian ear of energy reduces the hearing sensitivity to less than 1 % of the normal situation (Ruggero and Rich, 1991). The hearing organ in *Drosophila* also demonstrates features equivalent to the cochlear amplifier (Lu et al., 2009).

In mammals, mechano-electrical transduction happens through actin-based stereocilia (McGrath et al., 2017), whereas in *Drosophila*, it happens via axoneme-based cilia (Kernan, 2007). Concerning the microtubule axonemes, the cilia of *Drosophila* JO neurons resemble immotile primary cilia (9+0), yet the proximal cilium region bears axonemal dynein arms, allowing for force generation (Albert and Göpfert, 2015). The

axonemal dynein motor together with the mechano-electrical transduction channel provides a mechanical amplification mechanism, analogous to the cochlear amplifier in mammalian ears (Ashmore et al., 2010; Karak et al., 2015). By assisting sound-induced antennal vibrations on a cycle-by-cycle basis, the ciliary motility exerts positive mechanical feedback on the antenna's vibrations, enhancing minute vibrations induced by faint sounds, nonlinearly boosting auditory sensitivity (Nadrowski et al., 2008).

The first chapter of my thesis deals with the involvement of the *Naam* gene in *Drosophila* hearing. Nicotinamide (the substrate of the NAAM enzyme) is known as an agonist of *Caenorhabditis elegans* (*C. elegans*) OSM-9 and OCR-4, the orthologs of *Drosophila* Nan and Iav channels (Upadhyay et al., 2016). The external application of nicotinamide on *Drosophila* larvae elicited cytosolic Ca²⁺ influx in the chordotonal neurons through both Nan and Iav channels (Upadhyay et al., 2016). What is the function of endogenous nicotinamide in the hearing of adult *Drosophila*, and how does *Drosophila* metabolic state relate to the mechanical amplification in hearing? These are the questions that have been thoroughly addressed in this thesis.

II Materials and Methods

II.I Fly husbandry; feeding regimes; and treatment

Drosophila melanogaster fly strains were obtained from Bloomington Drosophila Stock Center (BDSC) or Vienna Drosophila Resource Center (VDRC) unless otherwise stated (Table 1). They were kept at 18°C for maintenance or 25°C chambers for speeding up crosses, with 60 % humidity and 12 hours light, dark cycles. 7000 ml fly food contains 500 g yeast, 500 g sugar, 20 g salt, 60 g agar, 250 g wheat, 6-liter water with 1-liter apple juice (Tegut, Göttingen, Germany), and 30 ml propionic acid (Sigma-Aldrich, Munich, Germany, #687081).

Table 1. Fly lines

Genotype	Description	Type	Source
w^{1118}	w^{1118}	Wild type control	BDSC# 3605
<i>Canton-S</i>	<i>Canton-S</i>	Wild type control	BDSC# 64349
$cn^1 bw^1$	$cn^1 bw^1$	Wild type control	BDSC# 264
w^* ; <i>Dnai2-Gal4</i>	<i>Dnai2-Gal4</i>	chordotonal neurons driver III chromosome	Somdatt a Karak
$y^1 w^*$; <i>Mi{MIC}igl</i> ^{MI02290}	<i>igl</i> ^{MI02290}	Mutant II chromosome	BDSC# 34310
$y^1 w^*$; <i>Mi{MIC}igl</i> ^{MI12785}	<i>igl</i> ^{MI12785}	Mutant II chromosome	BDSC# 59097
$y^1 w^{67c23}$; <i>Mi{PT-GFSTF.1}igl</i> ^{MI02290-GFSTF.1}	<i>igl::EGFP::igl</i>	GFP tagged II chromosome	BDSC# 60527

Materials and Methods

$y^1 w^*$; $Mi\{Trojan-GAL4.1\}igl^{MI12785-TG4.1/SM6a}$	$igl^{MI12785-Gal4}$	Gal4 II chromosome	BDSC# 76744
$P\{KK105109\}VIE-260B$	$igl-RNAi$	RNAi II chromosome	VDR# v100159
$y^1 w^*$; $Mi\{Trojan-GAL4.1\}igl^{MI102290-TG4.1/SM6a}$	$igl^{MI102290-Gal4}$	Gal4 II chromosome	This work
$y^1 w^*$; $Mi\{PT-GFSTF.1\}igl^{MI12785-GFSTF.1}$	$igl::EGFP::igl$	GFP tagged II chromosome	This work
w^{1118} ; $Df(2R)Exel7135/CyO$	$igl-Df$	Deficiency II chromosome	BDSC# 7879
w^{1118} ; $PBac\{w[+mC]=PB\}Rfx^{c02503}$	Rfx^{c02503}	Mutant III chromosome	BDSC# 10923
$y^1 w^*$; $Mi\{y[+mDint2]=MIC\}Rfx^{MI00053/TM6B, Tb^1}$	$Rfx^{MI00053}$	Mutant III chromosome	BDSC# 30604
$y^1 v^1$; $P\{y[+t7.7]v[+t1.8]=TRiP.JF03277\}attP2$	$RNAi-igl$	RNAi III chromosome	BDSC# 29598
$P\{KK105109\}VIE-260B$	$RNAi-igl$	RNAi II chromosome	VDR# v100159
$UAS-igl/TM3$	$UAS-igl$	III chromosome	This work
$y^1 w^*$; $Mi\{MIC\}Naam^{MI12364/TM3, Sb^1 Ser^1}$	$Naam^{MI12364}$	Mutant III chromosome	BDSC# 58512
$y^1 w^*$; $Mi\{Trojan-GAL4.1\}Naam^{MI12364-TG4.1/TM3, Sb^1 Ser^1}$	$Naam^{MI12364-Gal4}$	Gal4 III chromosome	This work

y^1 w^* ; $Mi\{PT-GFSTF.1\}$ $Naam^{MI12364-GFSTF.1}/TM3, Sb^1 Ser^1$	$Naam::EGFP::Naam$	GFP tagged III chromosome	This work
$w^{1118}; Df(3R)BSC809/TM6C, Sb^1$ cu^1	$Naam-Df$	Deficiency III chromosome	BDSC# 27380
$Naam-Gal4/CyO$	$Naam-Gal4$	Gal4 II chromosome	Pingkalai R Senthila n
$UAS-Naam/CyO$	$UAS-Naam$	II chromosome	This work
$UAS-Naam::GFP/CyO$	$UAS-Naam::GFP$	II chromosome	This work
$UAS-Naam-3EF/CyO$	$UAS-Naam-3EF$	II chromosome	This work
$UAS-Naam-EF-point$ $mutation/CyO$	$UAS-Naam-EF-point$ $mutation$	II chromosome	This work
$UAS-Naam-delta EF/CyO$	$UAS-Naam-delta EF$	II chromosome	This work
$UAS-PNC1/CyO$	$UAS-PNC1$	II chromosome	This work
y^1 w^* ; $P\{w[+mC]=UAS-$ $Nmnat.Z\}2/CyO$	$UAS-Nmnat$	II chromosome	BDSC# 39699
y^1 w^* ; $Tl\{Tl\}Nmnat^{C344S.C345S.EGFP}/TM3,$ $P\{w[+mC]=GAL4-Kr.C\}DC2,$ $P\{w[+mC]=UAS-$ $GFP.S65T\}DC10, Sb^1$	$Nmnat::GFP::Nmnat$ $C344S.C345S$	Mutant III chromosome	BDSC# 80089
y^1 w^* ; $Tl\{Tl\}Nmnat^{wt.EGFP}$	$Nmnat::GFP::Nmnat$	GFP tagged III chromosome	BDSC# 80087
y^1 w^* ; $Mi\{Trojan-$ $GAL4.1\}Naprt^{MI10235-TG4.1}/SM6a$	$Naprt^{MI10235}-Gal4$	Gal4 II chromosome	BDSC# 77803
y^1 w^* ; $Mi\{MIC\}nompC^{MI12787}/SM6a$	$nompC^{MI12787}$	Mutant	BDSC#

Materials and Methods

		II chromosome	58601
<i>nompC</i> ^{MI12787} -Gal4	<i>nompC-Gal4</i>	Gal4 II chromosome	This work/Ra doslaw Katana
<i>y</i> ¹ <i>w</i> [*] ; <i>TI{CRIMIC.TG4.1}inaD</i> ^{CR00769-TG4.1}	<i>inaD-Gal4</i>	Gal4 II chromosome	BDSC# 80653
<i>inaD</i> ^{2, TGEM} -Gal4	<i>inaD-Gal4</i>	Gal4 II chromosome	This work
<i>cn</i> ¹ <i>bw</i> ¹ , <i>inaD</i> ¹	<i>inaD</i> ¹	Mutant II chromosome	(Tsunod a et al., 1997)
<i>w</i> ¹¹¹⁸ ; <i>Df(2R)BSC864/Dp(2;2)Cam16</i> , <i>b</i> ¹ <i>bw</i> ¹	<i>inaD-Df</i>	Deficiency II chromosome	BDSC# 29987
<i>UAS-inaD/TM3</i>	<i>UAS-inaD</i>	III chromosome	This work
<i>UAS-inaD-GFP/TM3</i>	<i>UAS-inaD-GFP</i>	III chromosome	This work
<i>inaD</i> ^{hs.PT}	<i>inaD</i> ^{hs}	III chromosome	(Tsunod a et al., 2001)
<i>P(GMR-inaD-GFP); inaD</i> ¹	<i>inaD</i> ^{GMR.GFP}	I chromosome	(Sanxari dis and Tsunoda , 2010)
<i>w</i> [*] ; <i>p {+mW inaD. inaD}</i>	<i>p {+mW inaD}</i>	III chromosome	This work
<i>UAS-YFP; CyO/Sp</i> ¹ ; <i>α-Tub85E-Trojan-Gal4/TM3-Sb</i> ¹	<i>α-Tub85E Trojan-Gal4</i>	Gal4 III chromosome	Radosla w Katana
<i>w</i> ¹¹¹⁸ ; <i>P{GMR-GAL4.w}2/CyO</i>	<i>GMR-GAL4</i>	GAL4	BDSC# 9146

		II chromosome	
$w^{1118};$ $P\{w[+mC]=UASRedStinger\}4/Cy$ O	$UAS-nuclear\ RFP$	Reporter II chromosome	BDSC# 8546
$w^*;$ $P\{y[+t7.7]\ w[+mC]=1XUAS-$ $IVS-mCD8::GFP\}attP2$	$UAS-mCD8::GFP$	Reporter III chromosome	BDSC# 32190
$y^1\ w^*;$ $PBac\{y[+mDint2]$ $w[+mC]=20XUAS-$ $6XGFP\}VK00018/CyO,$ $P\{Wee-$ $P.ph0\}Bacc[Wee-P20]$	$UAS-6XGFP$	Reporter II chromosome	BDSC# 52261

To test whether the substrate or the product of NAAM that is nicotinamide (Sigma-Aldrich, Munich, Germany, #72340) and nicotinic acid (Sigma-Aldrich, Munich, Germany, #N4126) respectively, affect JO function, I fed w^{1118} flies with 10 mM of either compound plus 1 % sucrose (Merck KGaA, Darmstadt, Germany, #57-50-1), for three hours after overnight starvation (Figure 2). Control flies were fed with only 1 % sucrose. The same procedure was followed using 50 μ M NAAM inhibitor (Sigma-Aldrich, Munich, Germany, #349496). To assess the recovery probability of JO function in treated flies, I put the respective flies on a 1 % sucrose regimen for another 3 hours.



Figure 2. Experimental plan.

Schematic picture of the experiment for detecting nicotinamide and nicotinic acid effect on *Drosophila* hearing. Flies were fed with nicotinic acid or nicotinamide plus 1 % sucrose for three hours after overnight starvation. Control flies were fed with only 1 % sucrose.

To test the possibility of restored auditory perception in *Naam* mutant flies through the effect of nicotinic acid or β -Nicotinamide adenine dinucleotide hydrate (NAD^+) (Sigma-Aldrich, Munich, Germany, #N7004), I fed the flies with 10 mM nicotinic acid or NAD^+ plus 1 % sucrose for three hours after overnight starvation (Figure 2).

In all treatments, I tried different concentrations of substances and continued the experiments with the lowest concentration of each substance affecting hearing.

II.II GAL4/UAS System

I used Gal4/UAS system for recovering the hearing perception in *Naam*, *igl*, and *inaD* mutant flies, as well as, analyzing the expression pattern of the respective genes. Upstream activating sequence (UAS) and Gal4, which are adopted from yeast, are extensively used in *Drosophila* to study gene expression and function (Fischer et al., 1988). Gal4 is a transcription factor that can recognize the UAS motif and drive the expression of the gene downstream of UAS, such as, for example, the gene encoding enhanced green fluorescent protein (eGFP). In this particular case, the expression of eGFP demonstrates the time and tissue expression pattern of the Gal4 transcription factor (Figure 3).

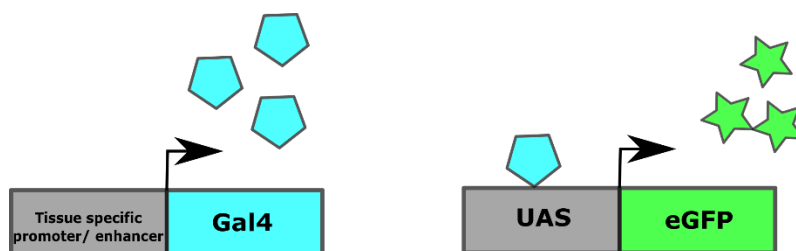


Figure 3. Schematic of Gal4/UAS system.

Gal4 transcription factor is expressed under the promoter of a specific gene and drives the expression of the eGFP reporter by recognizing the UAS motif.

II.III Cloning

Cloning of UAS constructs for rescuing mutant phenotypes, overexpressing a gene, or (in this project) determining the function of EF-hand domains in NAAM (Table 2) was done as described below.

Table 2. List of clonings

Construct name	Gene	Used restriction enzymes	Plasmid	Insert-size (bp)
<i>Naam</i>	<i>Naam</i>	EcoRI-Xbal	pUAST attp	1074
<i>Naam::GFP</i>	<i>Naam</i>	EcoRI-NotI-Xbal	pUAST attp	1074
<i>Naam_3 EF</i>	<i>Naam</i>	EcoRI-Xbal	pUAST attp	1188
<i>Naam_EF_point mutation</i>	<i>Naam</i>	EcoRI-Xbal	pUAST attp	1074
<i>Naam_delta_EF</i>	<i>Naam</i>	EcoRI-Xbal	pUAST attp	801
<i>Ce_PNC1</i>	<i>PNC1</i>	EcoRI-Xbal	pUAST attp	1009
<i>Naam_EF_point mutation::GFP</i>	<i>Naam</i>	EcoRI-NotI-Xbal	pUAST attp	1074
<i>Naam_delta_EF::GFP</i>	<i>Naam</i>	EcoRI-NotI-Xbal	pUAST attp	801
<i>igl RA</i>	<i>igl</i>	XhoI-Xbal	pUAST attp	2514
<i>inaD RA::GFP</i>	<i>inaD</i>	EcoRI-Xbal	pUAST attp	2295
<i>inaD RA</i>	<i>inaD</i>	EcoRI-Xbal	pUAST attp	2295
<i>inaD RB</i>	<i>inaD</i>	EcoRI-Xbal	pUAST attp	2331

RNA extraction, complementary DNA (cDNA) synthesis, and polymerase chain reaction (PCR):

To extract total RNA from the antennae or the heads of desired flies, a Zymo research (Zymo Research Europe GmbH, Freiburg, Germany, #R2030) RNA isolation kit was used according to the manufacturer's protocol. RNA concentration was measured using a NanoDrop 1,000 (Thermo Scientific, Schwerte, Germany).

The RNA was converted to complementary DNA (cDNA), using LunaScript® RT SuperMix Kit (New England Biolabs, Ipswich, MA, NEB #E3010). The cDNA was used as a template for amplification by PCR using appropriate primers (mentioned in Table 3).

Precise amplification of the cDNA template for cloning or sequencing was done by Phusion® High-Fidelity DNA Polymerase (Thermo Fisher Scientific, Osterode am Harz, Germany, # F-530XL). A Bio-Rad MyIQ thermal cycler (Thermo Fisher Scientific, Osterode am Harz, Germany) was used for DNA amplification.

Table 3. Used Primers

Gene	Short name	Application	Sequence
<i>Ce_PNC1</i>	Ce_PNC1_EcoRI_Rv	Cloning	CTGTGAATTCTTACTTCTTCACGAT CCTTTGAACC
<i>Ce_PNC1</i>	Ce_PNC1_Xbal_Fw	Cloning	ACGATCTAGAATGTTTCCCTGCCC AAAGCT
<i>Naam</i>	Naam_delta_EF_EcoRI_Fw	Cloning	ACGAGAATTCATGGTGCACCGG
<i>Naam</i>	Naam_delta-EF_Xbal_Rv	Cloning	CTGTTCTAGATTAGTATGAGGGCC TG
<i>Naam</i>	Naam_GFP_NotI_Rv	Cloning	CTGTGCGGCCGCGTATGAGGGC CTGAAGCCATT
<i>Naam</i>	Naam_Xbal_Rv	Cloning	CTGTTCTAGATTAGTATGAGGGCC TGAAGCCATT
<i>Naam</i>	Naam_EcoRI_Fw	Cloning	ACGAGAATTCATGGATTCACCTAC ACCGCCAATT
<i>Naam</i>	Naam_EF point mutation_EcoRI_Fw	Cloning	CACGGCATTTCGGCAAGGGCAGTG ATGACCGCC
<i>Naam</i>	Naam_EF point mutation_Xbal_Rv	Cloning	GATATTCGCCGTCTTCGGTACGAA TGGCGATGG
<i>Naam</i>	Naam_Rv	RT-qPCR	GAGGTCCTTGTGCAGCTC
<i>Naam</i>	Naam_Fw	RT-qPCR	CGATAATCTGTGCGAGCTCTG
<i>Naam</i>	Naam_Fw	RT-qPCR	CGTTGGACTIONCGGATTCCG
<i>Naam</i>	Naam_Rw	RT-qPCR	CCTTGACCTGATTAGTGTGG
<i>igl</i>	igl_RA	RT-qPCR	GACGAGGACGAAGCAAAAGCCG
<i>igl</i>	igl_RC	RT-qPCR	GCAACACATTCACAACACAAACAG
<i>igl</i>	igl_RB	RT-qPCR	GCCTTTCTGCAGAAGAGCCAAG
<i>igl</i>	igl_Fw	RT-qPCR	GCTAGAGGCTGAATTCGATC

<i>igl</i>	<i>igl</i> _Rv	RT-qPCR	CTCCTGAATGTCCTCGTC
<i>igl</i>	<i>igl</i> _RA_XhoI_Fw	Cloning	ACGActcgagATGGGCTGCAACACCA GCC
<i>igl</i>	<i>igl</i> _RC_XbaI_Rv	Cloning	CTGTTCTAGACTACTCGGGATTGG CATCCTTGCG
<i>InaD</i>	<i>InaD</i> _EcoRI_Fw	Cloning	ACGAGAATTCATGGTTCAGTTCCT GGGCAAACAG
<i>InaD</i>	<i>InaD</i> _XbaI_Rv	Cloning	CTGTTCTAGACTAGGCCTTGGGTG CCTCCGTACGTA
<i>Rpl32</i>	Reference gene	RT-qPCR	ATG CTA AGC TGT CGC ACA AA
<i>Rpl32</i>	Reference gene	RT-qPCR	GCG CTT GTT CGA TCC GTA
pUAST attB	pUAST attB_Fw	sequencing	TAAACAAGCGCAGCTGAACA
pUAST attB	pUAST attB_Rv	sequencing	TGCTCCCATTCATCAGTTCC

Gel electrophoresis:

After PCR, the samples were loaded on 1 % agarose (Chemsolute, Renningen, Germany, #99200500) gel containing 0.005 % Roti®-Gel Stain (Roth, Karlsruhe, Germany, #3865.2) for nucleic acids visualization. The gel was run in 1X TBE (89.15 mM Tris base, 88.95 mM boric acid, and 2 mM Na₂EDTA) (AppliChem, Darmstadt, Germany, #A2264, #A2940, #A2937) buffer at 110 V for 40 minutes, in a Bio-Rad Wide Mini Sub Cell GT electrophoresis machine (Bio-Rad™, Feldkirchen, Germany). A Thermo Scientific Generuler (Thermo Fisher Scientific, Osterode am Harz, Germany, #SM0331) was used as a DNA ladder. After visualization of the gel by an iBrightCL1000 gel documentation system (Thermo Fisher Scientific, Osterode am Harz, Germany), the sample on the gel was excised and cleaned up by Macherey-Nagel NucleoSpin® Gel and the PCR Clean-up kit (Thermo Fisher Scientific, Osterode am Harz, Germany, #740609.50S) for further usage.

Restriction digestion and Ligation:

PCR products and appropriate cloning vectors (pUAST-attB for UAS construct <https://www.addgene.org/vector-database/5556/>) (Figure 4), were digested using appropriate restriction enzymes (1U) and 2X Tango buffer (Thermo Fisher Scientific,

Osterode am Harz, Germany, #BY5) at 37 °C for 2 hours. Subsequently, they were separated by size with gel electrophoresis, and the desired digested products were purified from the gel.

Purified digested insert and vector were used with a 3:1 molar ratio for ligation by 10X ligation buffer and 1U, T4 DNA ligase (Thermo Fisher Scientific, Osterode am Harz, Germany, #EL0011) in a total volume of 20 µl reaction mixture. Ligation was carried out overnight at 4 °C.

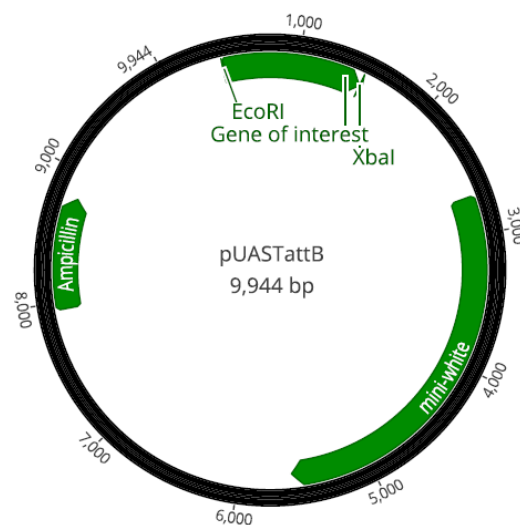


Figure 4: Generated plasmid map.

The pUAS-attB plasmid with inserted gene of interest is depicted. Here EcoRI and XbaI restriction enzymes were used for digestion (picture was made in Geneious Prime 2020.1.1).

Transformation, Mini-preparation, and Sequencing:

Heat shock was used as a method for transformation. 50 µl XL1-Blue competent cells (Agilent, Frankfurt, Germany, #200249) with 5 µl ligation mixture were incubated for 30 minutes on ice, followed by 50 seconds at 42 °C and 3 minutes on ice. Subsequently, 950 µl of room temperature (RT), SOB medium (281.3 mM Tryptone (Roth, Karlsruhe, Germany, #8952.2), 15.6 mM Yeast extract (Roth, Karlsruhe, Germany, #2363.2), 8.5 mM NaCl (Merck KGaA, Darmstadt, Germany, #1.06404), 2.5 mM KCl (Merck KGaA, Darmstadt, Germany, # 7447-40-7)) was added and incubated for 45 minutes in the Innova 40 shaker incubator (Thermo Fisher Scientific, Osterode am Harz, Germany) with 250 rpm. LB agar (Sigma-Aldrich, Munich, Germany, # 22700025) plates containing appropriate antibiotics (ampicillin for pUAS-attB) (AppliChem, Darmstadt, Germany, #A0839), were used for culturing bacteria in a chamber (37 °C) overnight. On the next day, single colonies were picked and applied for colony PCR with vector primers, to make

sure that the colonies have the desired inserts and are not the reassembled empty vectors.

Each colony containing the insert was incubated overnight at 37 °C in a 7 ml liquid LB medium (Sigma-Aldrich, Munich, Germany, # 12780052) with appropriate antibiotics. The plasmids were purified using a NucleoSpin® Plasmid kit from Machery-Nagel (Thermo Fisher Scientific, Osterode am Harz, Germany).

Sequencing of the plasmids by microsynth SEQLAB (Göttingen, Germany) verified the desired sequences in the plasmids. The plasmids were finally sent to BestGene® (CA, U.S.A.) for embryo injections.

Vector, pMC4 containing the cDNA of *C.elegans PNC1* with exon 1a was provided by Wendy Hanna-Rose (Crook et al., 2014).

II.IV Quantitative reverse transcription PCR (RT-qPCR)

For quantifying the expression of desired genes (*Naam*, *igl*, and *inaD*) in different genotypes, I used Luna® Universal qPCR Master Mix (New England Biolabs, Ipswich, MA, NEB #M3003). The cDNA and appropriate primers (Table 3) in a Bio-Rad MyiQ Single-Color Real-Time PCR Detection System were used for the reaction (Table 4). For calculating primer efficiency, I used Thermo Scientific Web Tools ›qPCR Efficiency Calculator. The difference of the gene expression levels ($2^{-(\Delta\Delta Ct)}$) (Livak and Schmittgen, 2001) between the threshold cycle (CT) values of the desired gene and *Rpl32* as a reference gene was calculated in the mutant flies or specific tissue of the flies and depicted relative to the respective tissues in the control *w¹¹¹⁸* flies. At least three biological replicates with three PCRs for each replicate were conducted.

Table 4. Quantitative RT-PCR protocol

*The temperature was subsequently increased by 0,5 °C in each cycle.

Temperature (°C)	95,0	95,0	63,0	72,0	95,0	55,0	55,0 - 95,0 *
Time (mm:ss)	03:00	00:10	00:30	00:30	01:00	01:00	00:10
Cycle	1X	40X			1X		81X

II.V Double Header tool

One approach for tagging genes in *Drosophila* is the random integration of a Minos-mediated integration cassette (MiMIC) (Venken et al., 2011) into the genome and the subsequent replacement with *T2A-GAL4* (Lee et al., 2018; Li-Kroeger et al., 2018). This cassette can also be replaced with an artificial exon that encodes a Green fluorescent protein (GFP) tag (Nagarkar-Jaiswal et al., 2015) *in vivo* by Cre recombination without embryo injection (Li-Kroeger et al., 2018) (Figure 5).

With this method, I created internally GFP-tagged proteins (protein trap) and T2A-GAL4 lines for the desired genes (gene trap) from available MiMIC lines. Double Header (DH) is a cassette that has EGFP in one direction and T2A-GAL4 in another direction. Using the *attB* sequence in DH for replacing it with MiMIC cassette in the gene of interest leads to the respective T2A-GAL4 or GFP-tagged protein.

Making a T2A-GAL4 or GFP tagged protein by DH method is a four crosses procedure. For the first cross, the MiMIC line was crossed to an appropriate DH line regarding the reading frame and the chromosome number. In the next cross, by introducing the recombinase in the genomic background, recombination mediates cassette exchange. By selecting the yellow flies, whose color reflects the absence of the MiMIC cassette and its genetic marker, one can establish a line by crossing it to a proper double balancer (Figure 5) (The details of the method can be found in (Li-Kroeger et al., 2018)).

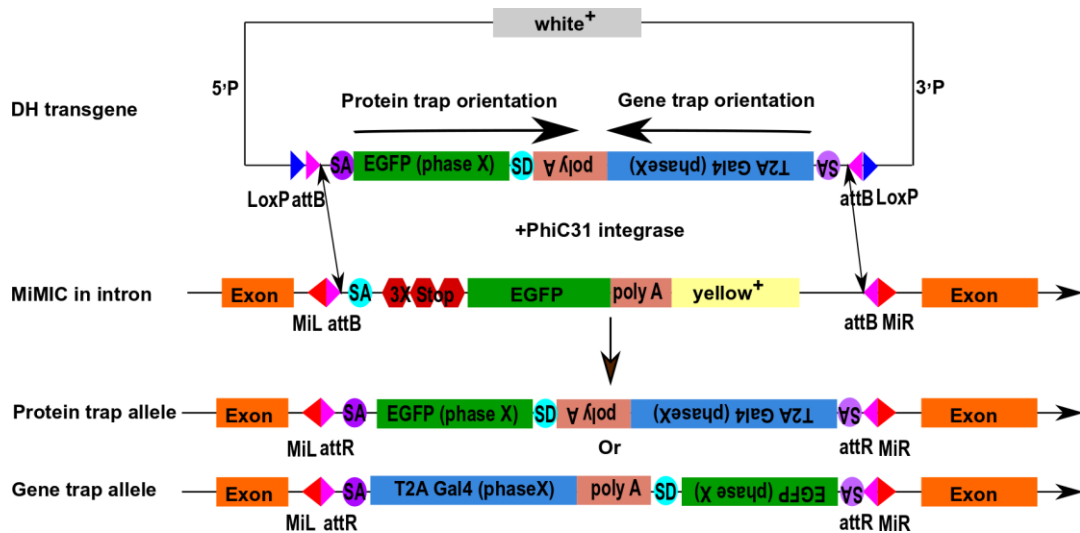


Figure 5. Double Header tool.

The Double Header cassette can be replaced with Minos-mediated integration cassette (MiMIC), and based on the landing orientation, gives rise to gene trapped, Gal4 line or protein-tagged, GFP line. Modified from Li-Kroeger et al., 2018.

II.VI Immunohistochemistry and confocal microscopy

II.VI.I Adult JO staining

Flies of defined ages were anesthetized with CO₂. The heads were dissected and fixed in 4 % paraformaldehyde (PFA) (Roth, Karlsruhe, Germany, #0335.3) diluted in phosphate buffer saline (PBS) (Chemsolute, Renningen, Germany, #8461) with 0.3 % Triton-X-100 (0.3 % PBST) (Sigma-Aldrich, Munich, Germany, #93443) at pH 7.4 for 1 hour at RT. The dissected heads were oriented upwards in albumin-gelatin and were sequentially fixed in PFA 6 %, overnight, and methanol (AppliChem, Darmstadt, Germany, #161091) for 15 minutes (washing steps with water in between is mandatory).

The fixed samples were cut into 40-micron thick slices with a blade on a Leica Ultracut S microtome and collected in PBS. The slices were immersed in blocking solution (5 % Normal Goat Serum (GE Healthcare, Munich, Germany), 2 % Bovine Serum Albumin (MP Biochemicals, Heidelberg, Germany), and 1 % PBST) for at least an hour. Subsequently, the samples were probed with the first antibody (Table 5) diluted in blocking solution overnight. The slices were washed four times, each time 20 minutes with 0.3 % PBST. Afterward, the samples were incubated for 2 hours with secondary antibody (Table 5) diluted in 0.3 % PBST 1:300. The slices were washed four times with

0.3 % PBST, each time for 30 minutes, and were mounted by DABCO (Sigma-Aldrich, Munich, Germany, #D2522).

II.VI.II Larva Ich5 staining

The larvae were mechanically immobilized from the anterior and posterior ends using 0.1 mm diameter stainless steel insect pins (Minutiens, ENTOMORAVIA – Austerlitz Insect Pins, Slavkov u Brna, Czech Republic). The larvae were cut longitudinally through the middle between the tracheae. The brain and peripheral nervous system were exposed after removing internal floating organs/tissues. The fillet was fixed in 4 % PFA diluted in 0.3 % PBST for 40 minutes at RT. Subsequently, it was washed three times for 30 minutes with PBS and then twice for 20 minutes with 0.3 % PBST. The larval fillet was immersed in blocking solution for one hour at RT and then incubated with primary antibodies (Table 5) overnight at 4 °C. The following day after extensive washing (5 times) with 0.1 % PBST for 20 minutes, secondary antibodies (Table 5) were added and left for two hours at RT. After washing with 0.3 % PBST (4 times, 20 minutes each), the samples were mounted with DABCO.

The sections were imaged with a Leica TCS SP8 Laser Scanning Confocal Microscope 63 × oil numerical aperture 1.0 objective (Leica Biosystems, Nussloch, Germany). The lasers, 405 nm diode laser, 488 nm Argon gas laser, 561, and 633 were used. The images were further analyzed with ImageJ (Version 1.53d).

II.VI.III Used antibodies

Table 5. Used antibodies

List of antibodies	Concentration	Source
Anti-GFP chicken	1:1000	Catalog no. GTX13970 (GeneTex, Irvine, CA, USA)
FluoTag®-X4 anti-GFP	1:1000	Catalog no. N0304 (NanoTag Biotechnologies GmbH, Göttingen, Germany)
Anti-RFP rat	1:1000	Catalog no. 5F8 (ChromoTek, Germany)
Anti-acetylated tubulin mouse	1:1000	Catalog no. T7451 (Sigma-Aldrich, Munich, Germany)
Anti-NOMPC rabbit	1:300	Yuh-Nung Jan
Anti-lav rat	1:300	Changsoo Kim
Anti-InaD rabbit	1:500	Susan Tsunoda
Anti-InaD rabbit	1:500	Olaf Voolstra
Anti-nc82 mouse	1:50	Catalog no. AB_2314866 (Developmental Studies Hybridoma Bank, Iowa)
Alexa Fluor 488 anti-chicken	1:300	Catalog no. A21316 (Thermo Fisher Scientific, Osterode am Harz, Germany)
Alexa Fluor 488 anti-mouse	1:300	Catalog no. A32723 (Thermo Fisher Scientific, Osterode am Harz, Germany)
Alexa Fluor 546 anti-mouse	1:300	Catalog no. A-11030 (Thermo Fisher Scientific, Osterode am Harz, Germany)
Alexa Fluor 488 anti-rabbit	1:300	Catalog no. A11008 (Thermo Fisher Scientific, Osterode am Harz, Germany)
Alexa Fluor 546 anti-rat	1:300	Catalog no. A-11081 (Thermo Fisher Scientific, Osterode am Harz, Germany)

Cy3-conjugated goat anti-HRP	1:300	Catalog no. 123165021 (Jackson ImmunoResearch, Newmarket, UK)
488-conjugated goat anti-HRP	1:300	Catalog no. 123545021 (Jackson ImmunoResearch, Newmarket, UK)
Alexa Fluor 633 Phalloidin	1:100	Catalog no. A22284 (Thermo Fisher Scientific, Osterode am Harz, Germany)
Anti-22C10	1:50	Catalog no. AB_528403 (Developmental Studies Hybridoma Bank, Iowa)
DAPI	1:1000	Catalog no. D9542 (Sigma-Aldrich, Munich, Germany)
Anti- β -Tubulin mouse	1:500	Catalog no. AB_2315513 (Developmental Studies Hybridoma Bank, Iowa)
Anti-mouse HRP	1:2500	Catalog no. G-21040 (Thermo Fisher Scientific, Osterode am Harz, Germany)
Anti-chicken HRP	1:2500	Catalog no. A16054 (Thermo Fisher Scientific, Osterode am Harz, Germany)

II.VII Hearing assessment using Laser Doppler vibrometry

JO neurons transduce sound-induced antennal vibrations into electrical signals and, in addition, actively boost these vibrations, enhancing auditory sensitivity (Göpfert et al., 2003, 2005). The following is an established noninvasive method for probing JO function (Albert et al., 2006, 2007).

II.VII.I Preparation

For mechanical measurement, flies were mounted with wax to eliminate unwanted animal movements (Figure 6). Further, dental glue was used on the connection of the scape to the head for the right antenna, while the left one was

completely glued. An air table (Linus Photonics series 63 table, #436356401 (dimensions 900 × 1200 × 100 mm)) was used to cancel environmental vibrations.

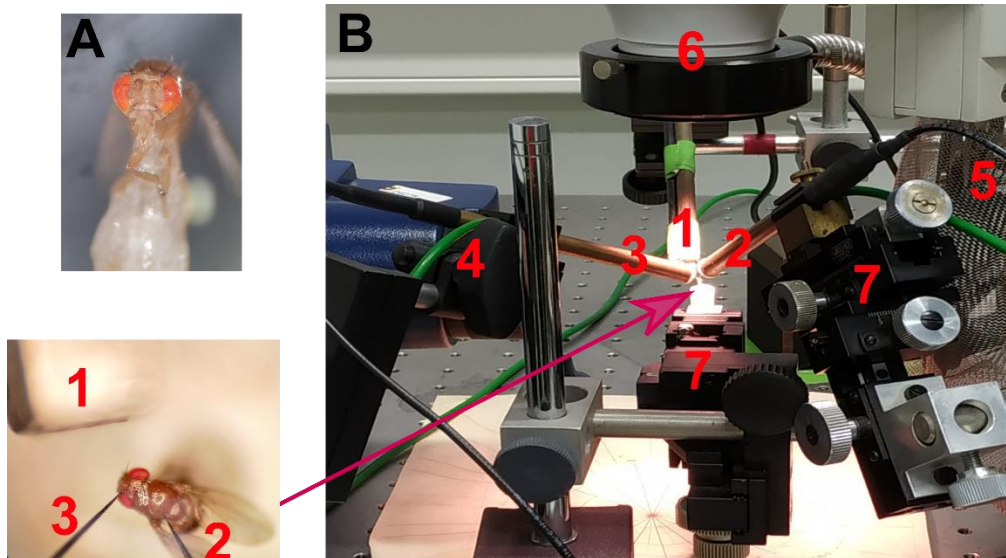


Figure 6: Laser Doppler vibrometry (LDV) set up.

A: a mounted fly on a plastic rod B: LDV set up 1) microphone 2) reference electrode 3) recording electrode 4) laser 5) loudspeaker 6) microscope 7) micromanipulators

II.VII.II Free fluctuation measurement

Free fluctuation measurement is the recording of the thermal motion and the active movements of the JO neurons in the absence of external stimuli. The velocities of the fluctuation as a time trace were measured by a Polytec PSV-400 Laser Doppler Vibrometer (LDV). For analyzing the fluctuations, the recorded velocity-time trace $X(t)$ was converted into a displacement-time trace $X(t) = \int X(t)dt$ (Albert et al., 2006). Individual best frequency (iBF) is determined as the frequency at which the antennal fluctuation reaches the peak in the velocity spectrum. The power spectral density (PSD) (nm^2/Hz) was determined from the power spectrum and is a fluctuation power across frequencies, the integration of which, between 100 and 1,500 Hz lead to systems power (nm^2) calculation (Göpfert and Robert, 2003 b).

II.VII.III Intensity-characteristics of sound receiver vibrations

To assess the intensity characteristics of the receiver vibrations, the mounted flies were stimulated with pure tones at the iBF of the sound receiver. Tones were generated by a loudspeaker (Visaton, Haan, Germany, #W130S). Stimulus particle velocities were measured by Emkay NR 3158 pressure gradient microphone (Knowles Electronics Inc., Itasca, Illinois, USA), positioned next to the flies' antenna. The intensity of the sound was dampened by an attenuator (Custom-build resistor-based attenuator) between 0 - 100 dB.

The extracellular neuronal activity from the antennal nerve in the form of compound action potential (CAP), was recorded by a tungsten recording electrode, which was inserted between the 1st antennal segment and the head capsule, whereas the reference electrode was placed into the thorax. To assess the intensity characteristics of the CAP response, CAP amplitudes were normalized and then plotted against sound particle velocity (SPV) or antennal displacement.

The mechanical sensitivity is the division of the antennal displacement by the microphone response. The amplification gain is calculated as a ratio between the mechanical sensitivity in the high- and low-intensity regimes. The amplification gain provides a simple measurement of auditory integrity and has been used to categorize auditory phenotypes (Table 6) (Senthilan et al., 2012).

Table 6. Auditory phenotypes based on amplification gain values (Senthilan et al., 2012)

auditory phenotypes	severely impaired	moderately impaired	normal	hypersensitive
amplification gain	< 1.5	1.5 - 5	5 - 15	> 15

SPV or antennal displacement amplitude correlated to the 10 % of the maximum CAP amplitude of the Hill fitted plots are ascribed to SPV or displacement threshold (working definition).

Additional LDV Setup:

The extracellular amplifier (4-channel amplifier, MA102) works in conjunction with a battery-powered isolated low noise preamplifier (model MA101, Electronics workshop,

Institute for Zoology, University of Cologne), which uses an optical separation method (diode and photo-diode) to eliminate electrical interference.

The humbug (Quest Scientific, BC, Canada) reduces the electrical noise associated with 50 Hz. The A/D converter (Cambridge Electronic Devises, micro 1401 MKII, Cambridge, England) digitizes the analog displacement signals from the LDV output, the amplified CAP signal, and the stimulus amplitude after the manual attenuation. The stimulus further goes into the HiFi amplifier (dB Technologies, MA1060, BO, Italy) and the loudspeaker.

II.VIII NAAM assay

The PNC1 assay (Chang, 2018) is a method to assess the activity of the NAD⁺ consuming enzymes. In this assay, the direct product of the NAD⁺ hydrolysis, nicotinamide, is converted into nicotinic acid and NH₄⁺ (ammonia) by pyrazinamidase/nicotinamidase 1 (PNC1) enzyme. The NH₄⁺ in reaction with ortho-phthalaldehyde (OPT) and dithiothreitol (DTT) produce the fluorescent 1-alkylthio-substituted isoindoles. This fluorescent signal is proportional to the amount of produced nicotinamide from the NAD⁺ consumption. NAAM assay was obtained from the PNC1 assay. To assess NAAM enzymatic activity, I used 40 μM nicotinamide (Sigma-Aldrich, Munich, Germany, #72340) and different extracted and enriched NAAM enzymes for producing NH₄⁺ and subsequently the fluorescent signal.

For enzyme expression, about 50,000 *Drosophila* Schneider 2 (S2) cells were transfected (Effectene Transfection Reagent, (Qiagen, Hilden, Germany, #301425)) with *UAS-Naam::GFP*, *Naam_EF_point mutation::GFP*, and *Naam_delta_EF::GFP* plasmids, according to the protocol from Qiagen Effectene® Transfection Reagent (provided by Dr. Philip Hehlert). Subsequently, the enzymes were enriched by a GFP selector (NanoTag, Göttingen, Germany, #N0310).

For conducting the fluorescent reaction, 100 μL of the reaction buffer (1 mM DTT (Thermo Fisher Scientific, Osterode am Harz, Germany, #R0861) in PBS (pH = 7.4)), as well as the extracted and enriched enzymes with or without 40 μM nicotinamide, were incubated at 37 °C on a plate shaker for three hours.

To develop the fluorescent reaction, 100 μL pre-warmed OPT developer (OPT (Sigma-Aldrich, Munich, Germany, #P0657) in pure ethanol (AppliChem, Darmstadt,

Germany, #141086) (33.3 mM) and DTT in PBS (14.28 mM), with three to seven ratio respectively) was added to each reaction reagent under dim light.

After incubation at RT for one hour on a plate shaker, the fluorescence was read at excitation 420 (± 10) nm and emission 460 (± 20) nm using BioTek™ Synergy™ Mx Multi Detection Top Monochromator-Based Microplate Reader w/Gen5 Software (Thermo Fisher Scientific, Osterode am Harz, Germany).

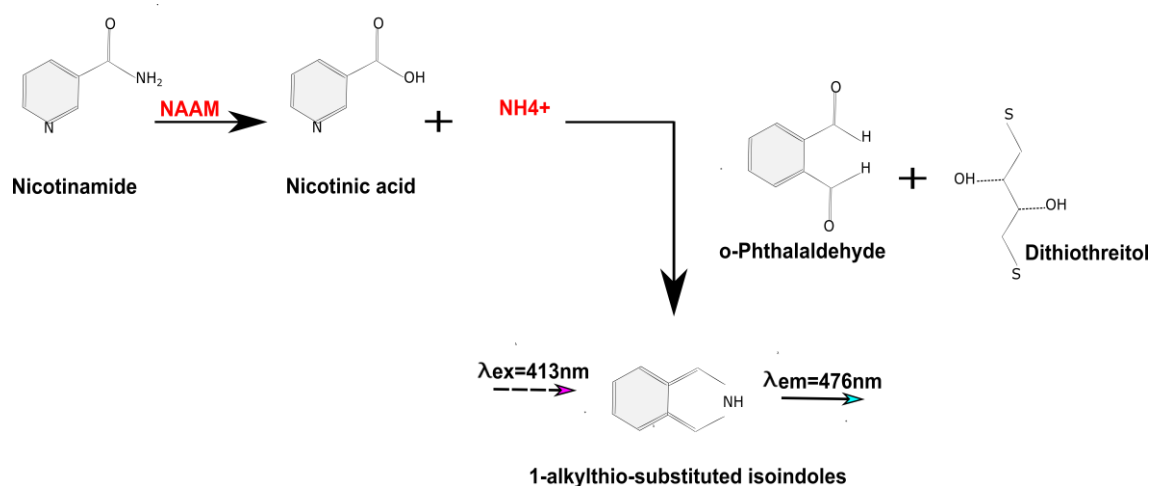


Figure 7. Schematic of NAAM assay.

In the NAAM assay, the fluorescence intensity and by that the nicotinamide concentration was measured to evaluate the NAAM enzymatic activity.

II.IX Western blot

For determining the size and purity of the NAAM enzymes after enrichment by a GFP selector, I used western blot according to the protocol from Abcam Company (Abcam, 2013). I diluted the extracted and enriched NAAM enzyme in 200 μl PBS, and boiled the samples for five minutes at 95 $^\circ\text{C}$ in 2X laemmli buffer (4 % SDS (Roth, Karlsruhe, Germany, #2326.2), 10 % 2-mercaptoethanol (AppliChem, Darmstadt, Germany, #A1108), 20 % glycerol (AppliChem, Darmstadt, Germany, #A2926), 0.004 % bromophenol blue, 0.125 M Tris-HCl (Roth, Karlsruhe, Germany, #9090.3), pH = 6.8). I prepared 10 % SDS gel with separating, and stacking gel (H_2O , acrylamide (Merck KGaA, Darmstadt, Germany, #100639), tris (pH = 8.8) (Roth, Karlsruhe, Germany, #AE15.2), 20 % SDS, 10 % Ammonium persulfate (Merck KGaA, Darmstadt, Germany, #A3678), TEMED (SERVA, Heidelberg, Germany, #35925)). I loaded 10 μl of each sample in separate wells plus a pre-stained protein ladder (Thermo Fisher Scientific, Osterode am Harz, Germany, #26619) for determining the proteins' molecular weight. I

ran the gel for 30 minutes at 70 V, and subsequently for 90 minutes at 100 V, in running buffer (24.76 mM Tris base, 250.13 mM glycine (Chemsolute, Renningen, Germany, # 9366), 3.47 mM SDS, pH = 8.3). After running the gel, I transferred the separated samples, from the gel to the nitrocellulose membrane (Roth, Karlsruhe, Germany, #9200.1), using transfer buffer (20 mM Tris base, 153.66 mM glycine, 20 % methanol, pH = 8.3) for 90 minutes at 180 mA (wet western blotting). To avoid unspecific antibody binding, the membrane was incubated for two hours at RT in 5 % bovine serum albumin (BSA) (Roth, Karlsruhe, Germany, #8076.4) prepared in Tris-buffered saline with 0.05 % Tween® 20 detergent (Sigma-Aldrich, Munich, Germany, #P1379) (TBS-T) (19.81 mM Tris, pH = 7.5, 150.58 mM NaCl). Afterward, the membrane was incubated overnight in GFP first antibody (Table 5) diluted in 5 % BSA. The following day, after three washes with TBS-T, each for 10 minutes, the membrane was incubated with anti-chicken HRP (Table 5) (secondary antibody) diluted in TBS-T for one hour at RT. After three more washes with TBS-T, each for 10 minutes Pierce™ ECL Western Blotting Substrate (Thermo Fisher Scientific, Osterode am Harz, Germany, #32209) was added to the membranes, and the bands were detected with an iBrightCL1000 gel documentation system.

II.XTdT-mediated dUTP-X nick end labeling (TUNEL) assay

I used TUNEL assay to test for presumable apoptosis in *Naam* mutant flies. For this assay, an *in situ* cell death detection kit, Fluorescein, (Sigma-Aldrich, Munich, Germany, # 11684795910) was used. The sample preparation was described in section II.VI.I. After incubation of the dissected tissue in blocking solution, the samples were treated with 5 µl TDT enzyme and 45 µl reaction solution and incubated for 1 h at 37°C. Subsequently, the samples were washed and mounted using DABCO. As a positive control, DNase I (Qiagen, Hilden, Germany, #79254) was used before the application of the TDT enzyme and its reaction solution. Unspecific endonuclease, DNase I, cleave DNA that can be recognized by the TDT enzyme.

II.XI Electron microscopy

For imaging the chordotonal organ in the *Drosophila* antenna, I used the electron microscopy method. The antennae were cut in cold haemolymph-like HL3 medium (70 mM NaCl, 20 mM MgCl₂·6H₂O (Merck KGaA, Darmstadt, Germany, #7791-18-6), 10 mM NaHCO₃ (Merck KGaA, Darmstadt, Germany, #144-55-8), 5 mM Trehalose dihydrate (Merck KGaA, Darmstadt, Germany, #6138-23-4), 115 mM sucrose, 5 mM HEPES (Merck KGaA, Darmstadt, Germany, #7365-45-9), 5 mM KCL, and 1 mM CaCl₂ (Merck KGaA, Darmstadt, Germany, #10043-52-4), pH = 7.2). The samples were incubated overnight at 4°C with 4 % paraformaldehyde and 2.5 % glutaraldehyde (Science Service, Germany, #E16216) in 0.1 M phosphate buffer (Natriumphosphat monobasisch Monohydrat (Merck KGaA, Darmstadt, Germany, #10049-21-5), Natriumphosphat Dihydrat (Merck KGaA, Darmstadt, Germany, #10028-24-7)) with 0.5 % NaCl. The following day after three washes with 0.1 M phosphate buffer for 15 minutes each, samples were incubated for 4 hours with 2 % osmium tetroxide (OsO₄) (Roth, Karlsruhe, Germany, #8088.1) in 0.1 M phosphate buffer (pH = 7.4) for further fixation.

After three more washes with 0.1 M phosphate buffer for 15 minutes, samples were dehydrated in a serial dilution with acetone (50 %, 70 %, and 90 %) (Merck KGaA, Darmstadt, Germany, #67-64-1), each for 20 minutes, and 100 % Acetone for 3 X 20 minutes. Following infiltration with acetone/EPON (2:1, 1:1, 1:3, and 100 % EPON) (EPON is composed of Glycid ether 100 (SERVA, Heidelberg, Germany, #21045), 2-Dodecenylsuccinic acid anhydride (SERVA, Heidelberg, Germany, #20755), Methyladac anhydride (SERVA, Heidelberg, Germany, #29452), and 2,4,6-Tris (dimethylaminomethyl) phenol (SERVA, Heidelberg, Germany, #36975).), each for 2 h, samples were embedded in EPON and polymerized for 24 h at 60°C.

Samples were cut with an ultra-microtome (Leica EM UC7, Leica Biosystems, Nussloch, Germany) into 70 nm slices and placed onto a copper grid coated with 1.3 % Formvar (Merck KGaA, Darmstadt, Germany, #12164).

For contrasting, samples were incubated with 4 % Uranylacetat-dihydrate (SERVA, Heidelberg, Germany, #77870.01) for 20 minutes, followed by three washes with distilled water. Imaging was done with a LEO 902 transmission electron microscope (Zeiss, Oberkochen, Germany) by Nicola Schwedhelm-Domeyer and Hanna Pies.

II.XII Prolonged depolarizing afterpotential (PDA) recordings

I used PDA recordings for assessing the phototransduction in *inaD*¹ mutant flies and the flies that were rescued for the *inaD*¹ mutation. PDA is a simple and efficient way for the functional assessment of phototransduction. PDA recording is based on the bi-stable nature of rhodopsin. With a blue stimulus, rhodopsin photoconverts to its active form, metarhodopsin (M^{*}). Metarhodopsin can be photoconverted back to the rhodopsin via an orange stimulus. First, the flies were mounted as previously described in section II.VII. The tungsten recording electrode was inserted in one eye and the reference electrode into the thorax. After the flies adapted to darkness for five minutes, the stimulus was applied. The stimulus protocol contains one orange stimulus, two blue stimuli, and two subsequent orange stimuli, each with 10 s duration and 10 s intervals. The orange stimulus (590nm) and the blue one (470nm) were produced using superluminescent LEDs (Mouser Electronics, Munich, Germany, #LB W5SN-GYHZ-25-Z, LY W5SN-JYKY-46).

II.XIII Statistical analyses

Data were analyzed and plotted by GraphPad Prism and Excel. Two-tailed Mann-Whitney-U tests with the Bonferroni correction were used for statistical analysis. Statistical significances are indicated with not significant = ns ($P > 0.05$), * ($P \leq 0.05$), ** ($P \leq 0.01$), *** ($P \leq 0.001$), **** ($P \leq 0.0001$). Some data are displayed in barplots with standard deviation, and some are displayed in scatter dot plots with a black line in the middle that represents the median. The individual CAP response was normalized calculated as $((V - V_{\min}) / (V_{\max} - V_{\min}))$. A Hill equation that was used for fitting the plots is $f(x) = y_{\min} + ((y_{\max} - y_{\min}) / (1 + Ix / mI^n))$.

1. Chapter I: Enzymatic control of mechanical amplification in fly hearing

1.1. Introduction

1.1.1. NAD⁺ pathways

Nicotinamide adenine dinucleotide (NAD⁺) is a redox carrier with a fundamental role as a coenzyme in energy metabolism. NAD⁺ is also an essential cofactor in non-redox reactions mediated by NAD⁺ consuming enzymes, orchestrating growth, signaling, and development (Covarrubias et al., 2021). The NAD⁺-dependent non-redox reactions, unlike the NAD⁺-dependent redox reactions, consume NAD⁺, irreversibly (Lin, 2007). For maintaining the cellular NAD⁺ levels, there are two NAD⁺ synthesis pathways. Eukaryotes can synthesize NAD⁺ through a salvage pathway from vitamin B3 derivatives such as nicotinamide, nicotinic acid, and dietary nicotinamide riboside (NR) (Bieganowski and Brenner, 2004) or, alternatively, through a *de novo* pathway from tryptophan (Rongvaux et al., 2003; Gossmann et al., 2012), termed the kynurenine pathway.

Many invertebrates and mammals, unlike some nematodes, insects, and yeasts (Gossmann et al., 2012), can use tryptophan in the kynurenine pathway to produce NAD⁺ (Imai and Guarente, 2014). Several enzymes participate in the kynurenine pathway, namely tryptophan 2,3 dioxygenase (*vermillion* in flies), kynurenine 3-monooxygenase (*cinnabar* in flies), and 3-hydroxyanthranilic acid oxygenase (absent in flies) (Campesan et al., 2011). The genes *cinnabar* and *vermillion* are expressed in the fly eye and play role in eye color pigmentation (Tearle, 1991). 3-hydroxyanthranilic acid oxygenase enzyme, the final enzyme of the kynurenine pathway, is not present in *Drosophila* (Linzen, 1974; Campesan et al., 2011). This missing enzyme in *Drosophila* might still be unraveled as was exemplified by the discovery of uridine monophosphate phosphoribosyl transferase in *C.elegans*, which is functioning instead of quinolinic acid phosphoribosyltransferase (McReynolds et al., 2017).

In the salvage pathway from invertebrates, including *D. melanogaster* and most bacterial species, the NAAM enzyme transforms nicotinamide to nicotinic acid and finally produces NAD⁺ through the Preiss-Handler Pathway (Marletta et al., 2015). In the vertebrates' salvage pathway, the first enzyme is known as nicotinamide phosphoribosyltransferase (NAMPT) that converts nicotinamide to nicotinamide mononucleotide (NMN). In other words, NAMPT and NAAM use the same substrate

(Vrablik et al., 2009) and coexist only in some organisms (Gossmann et al., 2012), but not in *Drosophila*.

NAD⁺-consuming enzymes such as poly ADP-ribose polymerase (PARP), CD38, and silent information regulators (sirtuins), produce nicotinamide, which has an inhibitory feedback effect on the NAD⁺-consuming enzymes (Bitterman et al., 2002; Audrito et al., 2011). From an evolutionary perspective, the development of diversified NAD⁺-dependent signaling pathways, which are mediated by, e.g., sirtuins and PARP, rely on a transition to the exclusive usage of NAMPT for NAD⁺ salvage synthesis with a higher recycling capacity (Bockwoldt et al., 2019). The coevolution of nicotinamide N-methyltransferase (NNMT) (nicotinamide consuming enzyme) with NAMPT contributes not only to the high turnover for NAD⁺-dependent signaling through the elimination of the nicotinamide but also to enhance the NAMPT affinity to the nicotinamide (Bockwoldt et al., 2019).

Nicotinate phosphoribosyltransferase (NAPRTase), NAD synthetase (NADS), and nicotinamide mononucleotide adenylyltransferase (NMNAT) are three conserved enzymes in the Preiss-Handler pathway in both eukaryotes and prokaryotes. Previous work in our lab indicated that at least the first enzyme of the NAD⁺-salvage pathway, NAAM, is enriched in the fly's hearing organ (Senthilan et al., 2012).

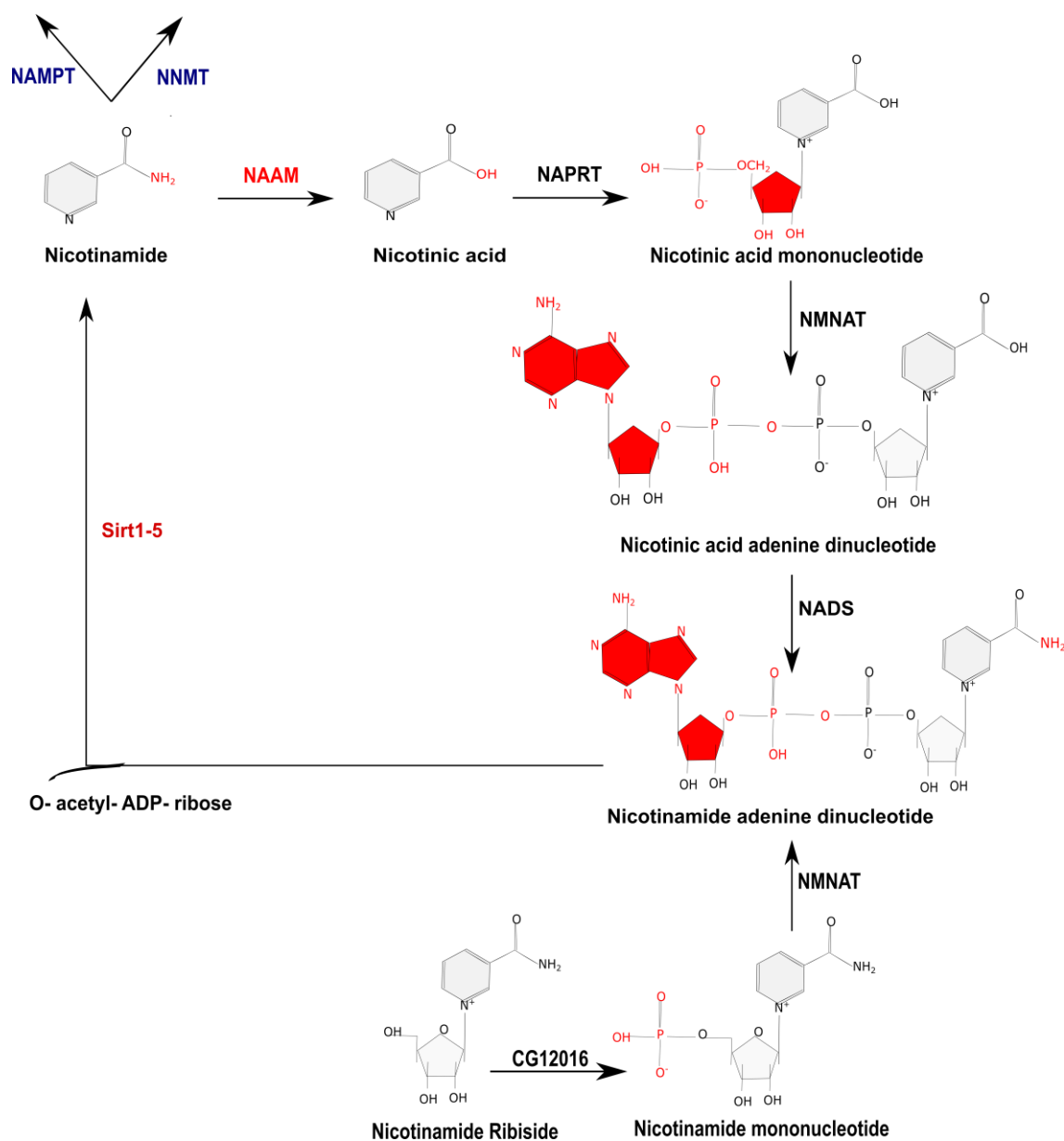


Figure 8. Salvage pathway of NAD⁺ synthesis.

Nicotinamidase (NAAM) is the first enzyme in the NAD⁺ salvage pathway. The NAAM substrate, nicotinamide, is also consumed by nicotinamide phosphoribosyltransferase (NAMPT) or nicotinamide N-methyltransferase (NNMT). The two enzymes, NAMPT and NNMT, are absent in *Drosophila*. Nicotinamide inhibits sirtuins and other NAD⁺-consuming enzymes. The list of the enzymes in the graph: nicotinate phosphoribosyltransferase (NAPRT), NAD synthetase (NADS), nicotinamide mononucleotide adenyltransferase (NMNAT).

1.1.2. Precedence for NAAM function in JO

One screening in 2012 by Senthilan et al. (Senthilan et al., 2012) demonstrated that *ato*-based JO knockout down-regulates the expression of 274 genes in the second antennal segment. According to the screening results, *Naam* expression was also down-

regulated upon JO disruption. The further experiment demonstrated that driving *UAS-2XEGFP* reporter with *Naam-Gal4* (*Naam-Gal4>2XEGFP*) labels JO scolopale cells (Senthilan et al., 2012) and assessing auditory JO function in *Naam*^{KG10548} mutant flies (made by insertion of the P transposable element in *Naam* gene (Bellen et al., 2004)) revealed a significant hearing impairment compared to wild-type (WT) flies (Senthilan et al., 2012).

Another screening by Natascha Zhang (unpublished data) is based on specific ablation of different neuronal groups (AB or CE) in JO and further analysis of gene expression profiles of the 2nd antennal segment cells. This screening also demonstrated that the expression level of *Naam* was decreased after JO neurons ablation, confirming its expression dependency on the presence of JO neurons (Table 7). In the table, the numbers are representing *Naam* gene expression in the 2nd antennal segment cells after AB, CE, or all JO neuronal ablation (red columns), compared to the WT flies (blue columns).

Table 7. Screening result for *Naam* gene

Gene _ID	AB Neurons ablated			CE Neurons ablated			ALL Neurons ablated			<i>w</i> ¹¹¹⁸		
	<i>Naam</i>	31236	29608	23022	35518	11535	25690	9625	9536	14279	48466	12523

1.1.3. TRPV channel agonists

Nicotinamide acts on Nan-lav TRPV channels in *Drosophila* (Upadhyay et al., 2016). In *C. elegans*, Nan and lav orthologs, are termed OSM-9 and OCR-4, which also assemble into heterotetrameric TRPV channels (Upadhyay et al., 2016). The OSM-9 and OCR-4 heterotetrameric channels are activated by nicotinamide, and, at least in *C. elegans*, nicotinamide seems to act as an internal OSM-9 and OCR-4 channels modulator (Upadhyay et al., 2016). In *Drosophila*, however, the external application of nicotinamide on the WT third instar larvae elicited calcium signals in the chordotonal neurons and reduced the response to a vibrational stimulus (Upadhyay et al., 2016).

Two commercial insecticides, pymetrozine, and pyrifluquinazon were shown to act as the agonist of insects Nan-lav complexes, as well (Nesterov et al., 2015). In

insects, these insecticides silence the stretch receptor cells by enhancing the ciliary Ca^{2+} influx (Nesterov et al., 2015).

How endogenous nicotinamide affects the *Drosophila* Nan-lav TRPV channels is not known. However, according to the similar structure of nicotinamide to pymetrozine and pyrifluquinazon, I assumed a similar effect to the insecticide might be observed. The *Arabidopsis nic-1-1* (*Naam* ortholog) mutation results in a higher nicotinamide concentration compared to controls (Sattar et al., 2019). I hypothesized that in *Naam* mutant flies, there might be an accumulation of the NAAM substrate (nicotinamide), as well. Considering the agonistic effect of nicotinamide on Nan and lav channels (Upadhyay et al., 2016), one can expect the exerted NAAM role via soluble internal nicotinamide on the TRPV channels, and by this effect, hearing.

There might be a link between the metabolic state (NAD^+ metabolism) and the sensory function of the Nan-lav TRPV channels (Upadhyay et al., 2016). It might also be possible that the NAAM role in hearing is independent of the NAD^+ metabolism.

1.1.4. EF-hand domains function in NAAM

A first automatic annotation of protein domains from the Interpro/Pfam database (Blum et al., 2021) assigned two generic EF-hand domains and one isochorismatase-like domain to the *Drosophila Naam*. The EF-hand domains are helix-loop-helix structures, with about two-thirds of them binding Ca^{2+} ion (Kretsinger and Schaffer, 2021). In chimeric proteins, having a non-EF hand catalytic region besides the EF-hand domains, the conformational changes in the EF-hand-domains upon Ca^{2+} binding will affect the functionality of the attached catalytic region (Kretsinger and Schaffer, 2021). Respectively, the NAAM enzyme as a chimeric protein could also be affected by Ca^{2+} binding to the EF-hand domains.

I inferred that there might be a possible modulatory role of the EF-hand domains to the enzymatic function of NAAM since BLAST searches excluding insects or Arthropoda against *Naam* resulted in many nicotinamidase sequences containing EF-hand domains. Bacteria, Fungi, and Viridiplantae do not have the EF-hand-domain in their NAAM ortholog proteins. The NAAM enzymes, having EF-hand domains, presumably appeared in the early bilaterian lineage; however, it has been lost in

Chordata (exception: *Branchiostoma belcheri*), and *C. elegans* acquired a nematode-specific domain (Figure 9).

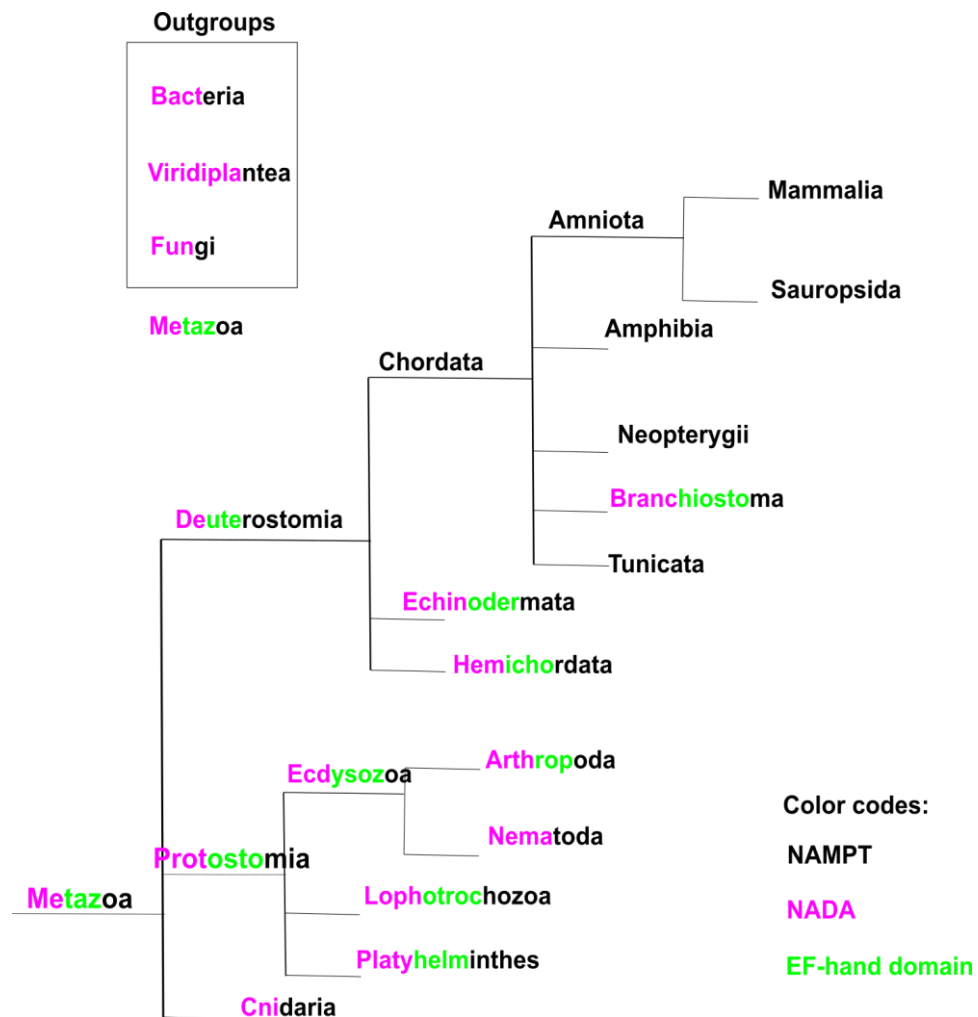


Figure 9. The evolutionary conservation of the EF-hand domains in the NAAM enzyme.

NADA in magenta stands for nicotinamide deamidase that includes NAAM enzyme, as well. The color codes are explained in the right-low corner of the figure. The EF-hand domain (green) is present in all species having NADA except bacteria, fungi, plants (Viridiplantae), and cnidarians. Nematodes, like *C. elegans*, acquired a nematode-specific domain. The branch length is not correct. The figure was modified from (Bockwoldt et al., 2019).

1.1.5. Chapter overview

Given that NAAM is necessary for hearing (Senthilan et al., 2012), and the NAAM substrate, nicotinamide, is the agonist of the TRPV channels (Upadhyay et al., 2016), I addressed the following questions: Is nicotinamide an internal agonist of the TRPV channels in *Drosophila*? Is the deafness in *Naam* mutants related to the agonistic

function of NAAM substrate, nicotinamide, on TRPV channels? Do the conserved EF-hand domains in the NAAM have effects on the NAAM performance? And is there a connection between the TRPV channels modulation and the energy status of the JO?

NAAM might play a role as a mediator of energy sensors, a modulator of hearing, or both in the *Drosophila* auditory organ. For uncovering the possibility of NAAM functions in hearing as an energy sensor, I treated the *Naam* mutant flies with the NAAM product (nicotinic acid) or NAD⁺, the end product of the NAD⁺ salvage pathway. Besides, I generated a fly, overexpressing the rate-limiting enzyme of the NAD⁺ salvage pathway, NMNAT, in *Naam* mutant background for recovering the auditory perception in the mutant flies. In either case (treating the *Naam* mutant flies with nicotinic acid, NAD⁺, or overexpressing NMNAT in the *Naam* mutant flies), rescuing the hearing defect would support the assumption that NAAM functions through energy modulation.

For studying the effect of the conserved EF-hand domains in NAAM, I made constructs with ablated EF-hand-domains attached to the intact core enzyme. Using these constructs for rescuing the hearing defect in the *Naam* mutant flies and further *in vitro* assay shed light on the importance of the EF-hand domains in NAAM enzymatic function.

I also tested for potential cell death due to the TRPV channel hyperactivation and ionic imbalance across the membrane. Necrosis had been shown to arise from the loss of the *Naam* orthologs in *C. elegans* OLQ and uv1 cells (Upadhyay et al., 2016). In this thesis, I studied cell death in the *Naam* mutant flies.

Besides the involvement of NAAM in the TRPV channel modulation, NAAM, as the first enzyme in the NAD⁺ salvage pathway, is involved in energy metabolism and NAD⁺-dependent enzyme modulation. The changes in the function of the NAD⁺-dependent deacetylase, as an NAD⁺-consuming enzyme, were investigated through monitoring the changes in the tubulin acetylation pattern of the chordotonal organs as a secondary read-out.

NAD⁺ is also a crucial electron donor in the oxidative phosphorylation pathway. Considering that oxidative phosphorylation happens in the inner membrane of the mitochondria and the problems that *Naam* mutation might cause in the NAD⁺ production pathway, I examined the overall changes in mitochondria features via electron microscopy.

1.2. Results

According to the FlyBase website, the *Naam* gene has two transcripts and one unique polypeptide (Larkin et al., 2021). To assess *Naam* gene expression and NAAM protein localization in JO, I generated *GAL4*, and *GFP* lines for the *Naam* gene by the Double Header tool (materials and methods, section II.V) from a MiMIC line, *Naam*^{MI12364} (Figure 10).

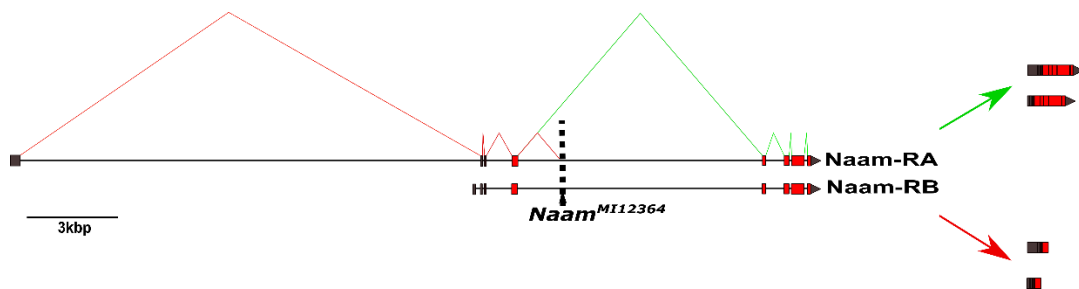


Figure 10. *Naam* transcripts.

Naam transcripts and the position of the MiMIC insertion in the intron of *Naam* are depicted. The MiMIC line, *Naam*^{MI12364}, was used for making *Gal4* and *GFP* lines. In the MiMIC line, both truncated transcripts (red arrow) due to the aberrant splicing of the *Naam* transcripts (red line) and normal transcripts (green arrow) due to alternative splicing (green line) can be present.

1.2.1. *Naam* expression in chordotonal neurons, cap, and scolopale cells

In this thesis, I used two *Gal4* lines for detecting the *Naam* gene expression pattern: *Naam-Gal4* that was made by fusion of *Gal4* to 1 kb of the *Naam* promoter (Senthilan et al., 2012) and the *Naam*^{MI12364}-*Gal4* that was made by the Double Header tool in this work. Driving a reporter, nuclear red fluorescent protein (=nuclear RFP) (*UAS-red-stinger*), with *Naam-Gal4* (*Naam-Gal4*>*red-stinger*) and *Naam*^{MI12364}-*Gal4* (*Naam*^{MI12364}-*Gal4*>*red-stinger*) induced fluorescence signals in scolopale and cap cells in the adult *Drosophila* JO and the mechanosensory lch5 chordotonal organs of larvae (Figure 11). To assess the identity of the labeled cells, JO neurons were counterstained with anti-HRP as a neuronal marker with a distinct staining pattern in the cilium. Anti-HRP labels sugar residues of glycoproteins that are secreted in two bands in the cilium (Sun and Salvaterra, 1995). The first band demarks the junction between the dendritic inner segment and the cilium, whereas the second band occurs halfway up the cilium, separating the proximal and distal cilium regions (Zanini et al., 2018).

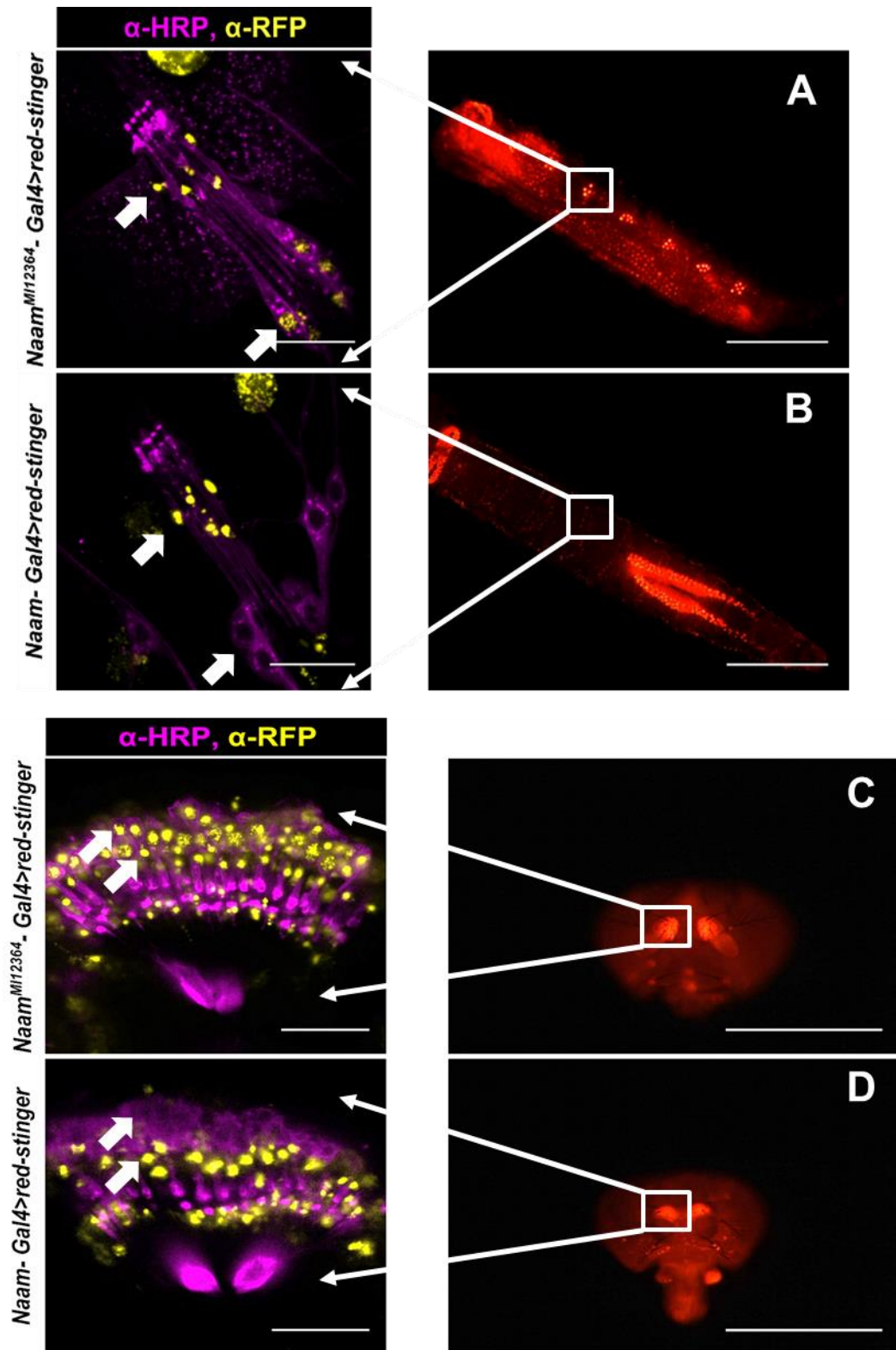


Figure 11. *Naam* expression in JO and Ich5 chordotonal organs.

Driving a reporter, nuclear RFP (*UAS-red-stinger*), with *Naam-Gal4* (*Naam-Gal4>red-stinger*) labels scolopale and cap cells of the larval chordotonal organ, Ich5 (B), and the adult *Drosophila* JO (D) (yellow). Driving the same reporter with *Naam^{MI12364}-Gal4* (*Naam^{MI12364}-Gal4>red-stinger*) additionally labels oenocytes and neurons (A, C) (yellow). The white arrows point to the expression patterns of the two drivers in the scolopale cells and the JO neurons. Anti-HRP labels the neurons (magenta). Scale bars: 20 μ m and 1 mm for fluorescent pictures.

As it is depicted in Figure 11, both *Naam^{MI12364}-Gal4* and *Naam-Gal4* lines label scolopale and cap cells in chordotonal organs, including JO and the larval Ich5 organ. In addition, *Naam^{MI12364}-Gal4*, which carries Gal4 in the native *Naam* sequence, labels oenocytes and chordotonal neurons. Apparently, *Naam-Gal4* reproduces endogenous gene expression only partially, and *Naam* is expressed in three cell types within chordotonal organs, that is scolopale cells, cap cells, and chordotonal neurons. Using the respective driver lines to express the membrane-tethered GFP (*UAS-mCD8::GFP*) and the cytoplasmic GFP (*20XUAS-6XGFP*) produced the same result as obtained with nuclear RFP (*UAS-red-stinger*) (Supplement Figure 69).

Driving the *UAS-mCD8::GFP* with the *Naam^{MI12364}-Gal4* (*Naam^{MI12364}-Gal4>mCD8::GFP*) demonstrated the *Naam* expression in the brain, in the antennal lobe (AL), and the antennal mechanosensory and motor center (AMMC) (Figure 12). Expression was also observed in the femoral chordotonal organ in the leg of adult flies and their haltere pedicel (Supplement Figure 70). Despite the importance of the NAD⁺ salvage pathway, the expression of *Naam* in *Drosophila* is remarkably restricted (Figure 12).

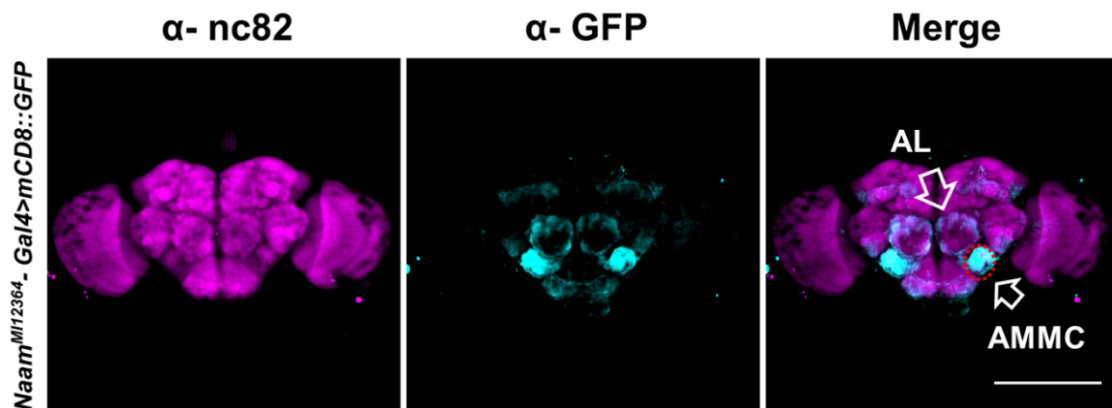


Figure 12. *Naam* expression pattern in the *Drosophila* brain.

Expression of *Naam* (cyan) in the antennal lobe (AL) and the antennal mechanosensory and motor center (AMMC), revealed by driving *UAS-mCD8::GFP* with *Naam^{MI12364}-Gal4* (*Naam^{MI12364}-Gal4>mCD8::GFP*). The neuropil is counterstained with α -nc82 that labels synapses (magenta). Scale bar: 200 μ m.

1.2.2. NAAM localization in scolopale cells and JO neurons

To show NAAM protein localization within chordotonal organs, I generated internally GFP-tagged native protein using the Double Header tool (Figure 5). The tagged

proteins were found to localize to the scolopale cells in both JO and Ich5, whereby also some staining was seen in the mechanosensory neurons of JO (Figure 13).

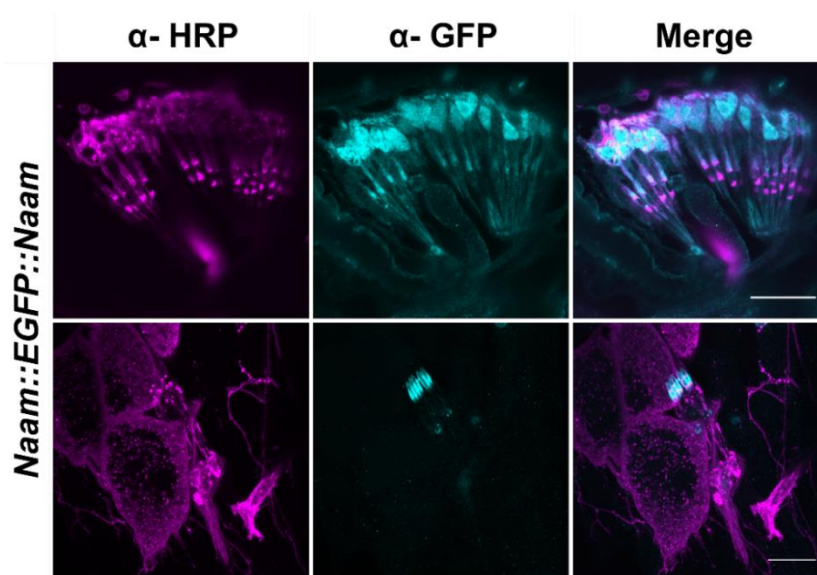


Figure 13. NAAM localization in scolopale cells and JO neurons.

NAAM::EGFP::NAAM (cyan) was found to localize to the scolopale cells in both JO (Upper panel) and Ich5 (lower panel), whereby also some staining was seen in the mechanosensory neurons of JO. Anti-HRP labels the neurons (magenta). Scale bars: 20 μ m.

Inserting a GFP cassette into the *Naam* gene might affect protein function. Hearing measurements in the respective flies demonstrated a hearing defect, including absences of frequency tuning, mechanical amplification, and nerve responses (Supplement Figure 71). This observation indicates that the GFP signal in *Naam::EGFP::Naam* flies might not represent the position of the WT protein (further discussion in 1.2.7.1 section). For detecting the relative location of NAAM to the scolopale rods, double staining with anti-GFP and phalloidin in *Naam::EGFP::Naam* flies was performed. It revealed that NAAM localizes to the luminal side of the scolopale rods (Figure 14).

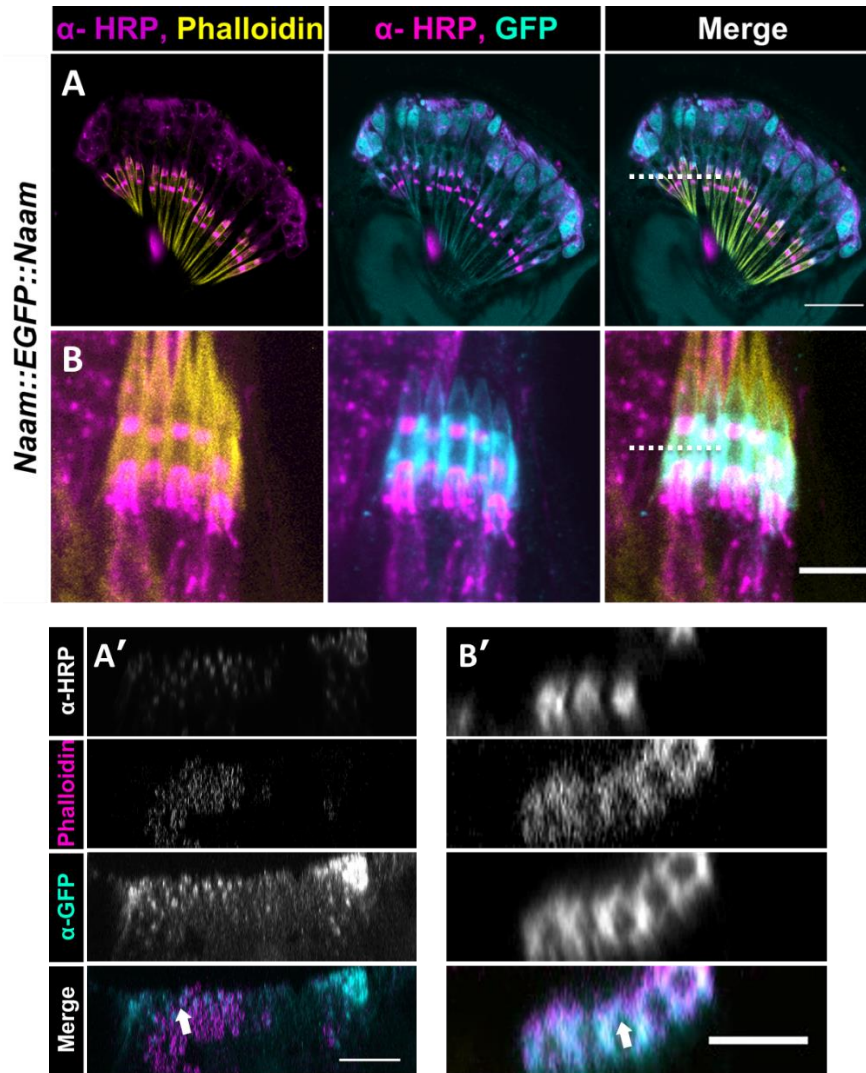


Figure 14. Localization of NAAM relative to the scolopale rods.

The cross-sections (white dotted lines) of the images from JO (A) and *lch5* (B) demonstrate that NAAM (cyan) localizes to the luminal side of the scolopale rods (A', B') (white arrows) (Scolopale rods are in yellow (A, B), and magenta (A', B')). Anti-HRP labels the neurons in magenta (A, B). Scale bars: 20 μm in panel A and 5 μm in panel B.

1.2.3. Auditory defects in *Naam* mutant flies

Analysis of RT-qPCR results with two different sets of primers showed that *Naam*^{*MI12364*} can be considered as a knockout (KO) mutant (Figure 15). I used the respective flies for analyzing the hearing functionality in *Naam* KO mutant.

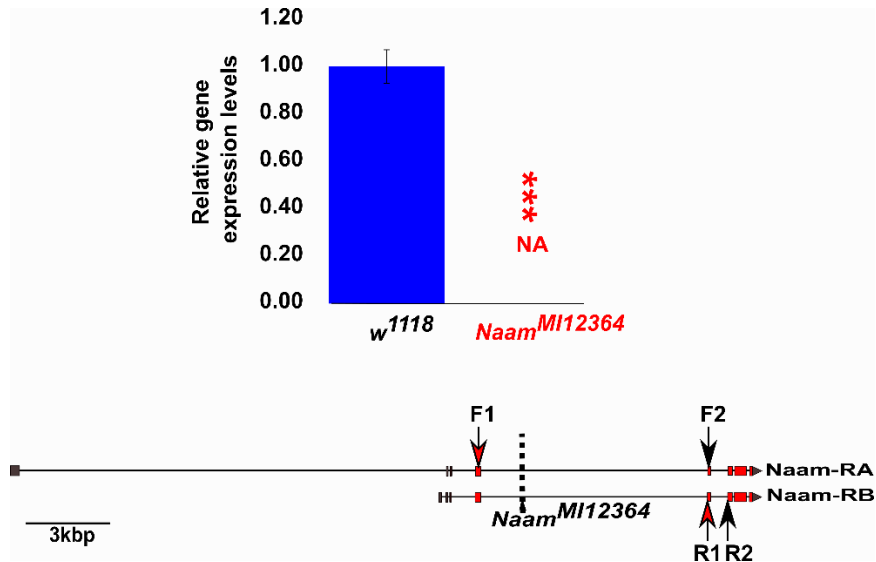


Figure 15. *Naam* expression analysis.

Analysis of RT-qPCR results revealed that *Naam^{MI12364}* can be considered as a KO mutant. Mann-Whitney U test was used for statistical analysis. The statistical significance level is $p < 0.001$ (***). $n = 7$ biological replicates, with five one-day-old flies per replicate (the whole flies), were used. Two sets of primers (F1R1 and F2R2) were used for the RT-qPCR. NA = Not Applicable. The error bars represent standard deviations.

Loss of NAAM in *Naam^{MI12364}* mutants impaired JO function. Measurements of the antennal mechanics revealed an altered mechanical frequency tuning, signaling a loss of mechanical amplification provided by JO neuron motility (Figure 16, panel B). Furthermore, antennal nerve recordings revealed a complete loss of sound-evoked antennal nerve potentials (Figure 16, panel C).

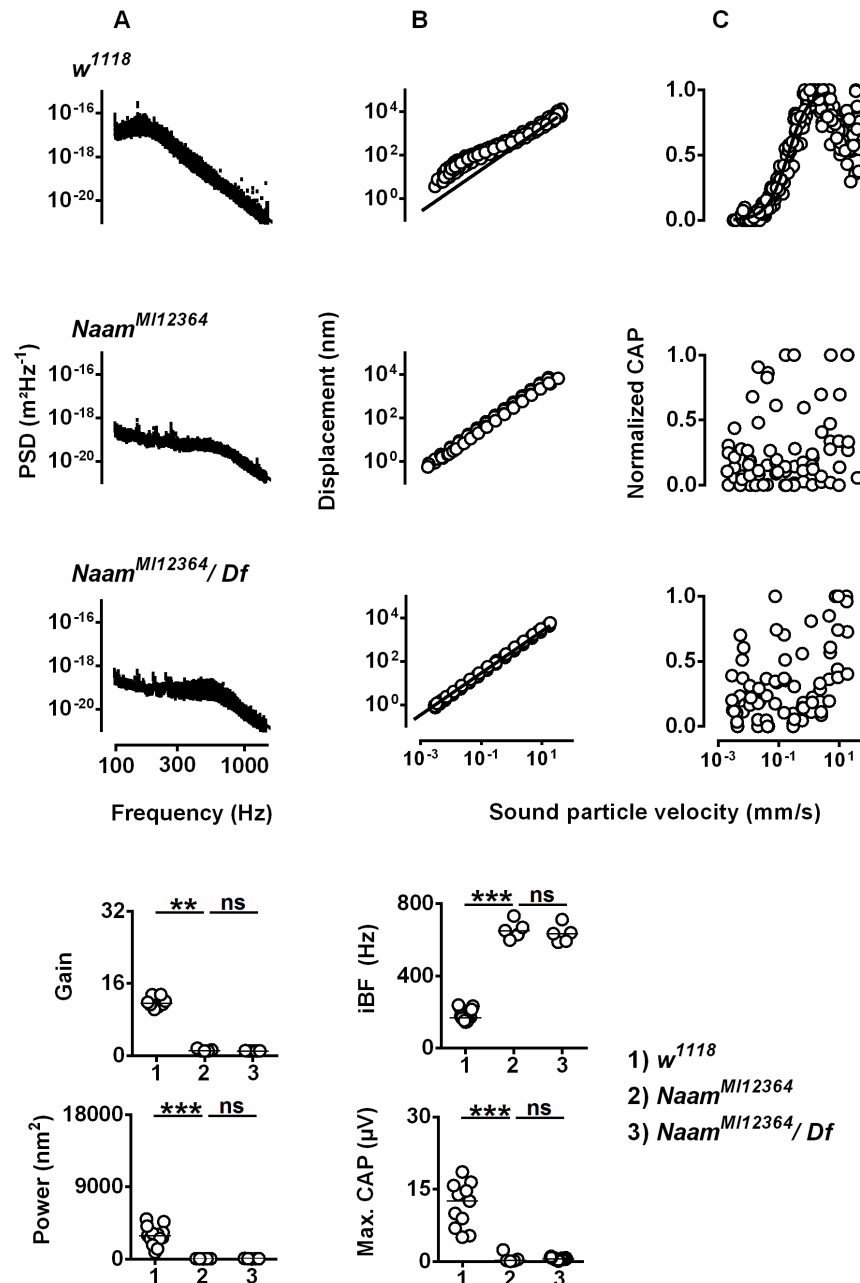


Figure 16. Auditory defects in *Naam* mutant flies.

Top: power spectra of the mechanical fluctuations of the antennal sound receiver (A) as well as antennal displacement (B), and normalized compound action potential (CAP) amplitudes (C) as a function of the sound particle velocity in wild type flies, homozygous *Naam*^{MI12364} mutant flies, and flies in which the *Naam*^{MI12364} allele was uncovered by the deficiency *Df(3R)BSC809*. Bottom: corresponding amplification gain, individual best frequencies, power of the receiver fluctuations, and maximum CAP amplitudes. In the mutant flies, mechanical amplification is lost, and so are sound-evoked CAPs in the antennal nerve. $n \geq 5$ flies/genotype. Two-tailed Mann-Whitney-U tests with the Bonferroni correction were used for statistical analysis. Statistical significances are indicated with ns ($P > 0.05$), ** ($P \leq 0.01$), *** ($P \leq 0.001$).

Additional evidence for the auditory relevance of the *Naam* gene was obtained when *w*¹¹¹⁸ wild-type flies, starved overnight, were kept for three hours on 1 % sucrose solution supplemented with an irreversible nicotinamidase inactivator, Pyrazincarbonitril (Seiner et al., 2010). Pyrazincarbonitril at a concentration of 50 μM caused the same

hearing defects as seen in the *Naam*^{MI12364} mutant flies (Figure 17) (Data provided by Sabrina Weber).

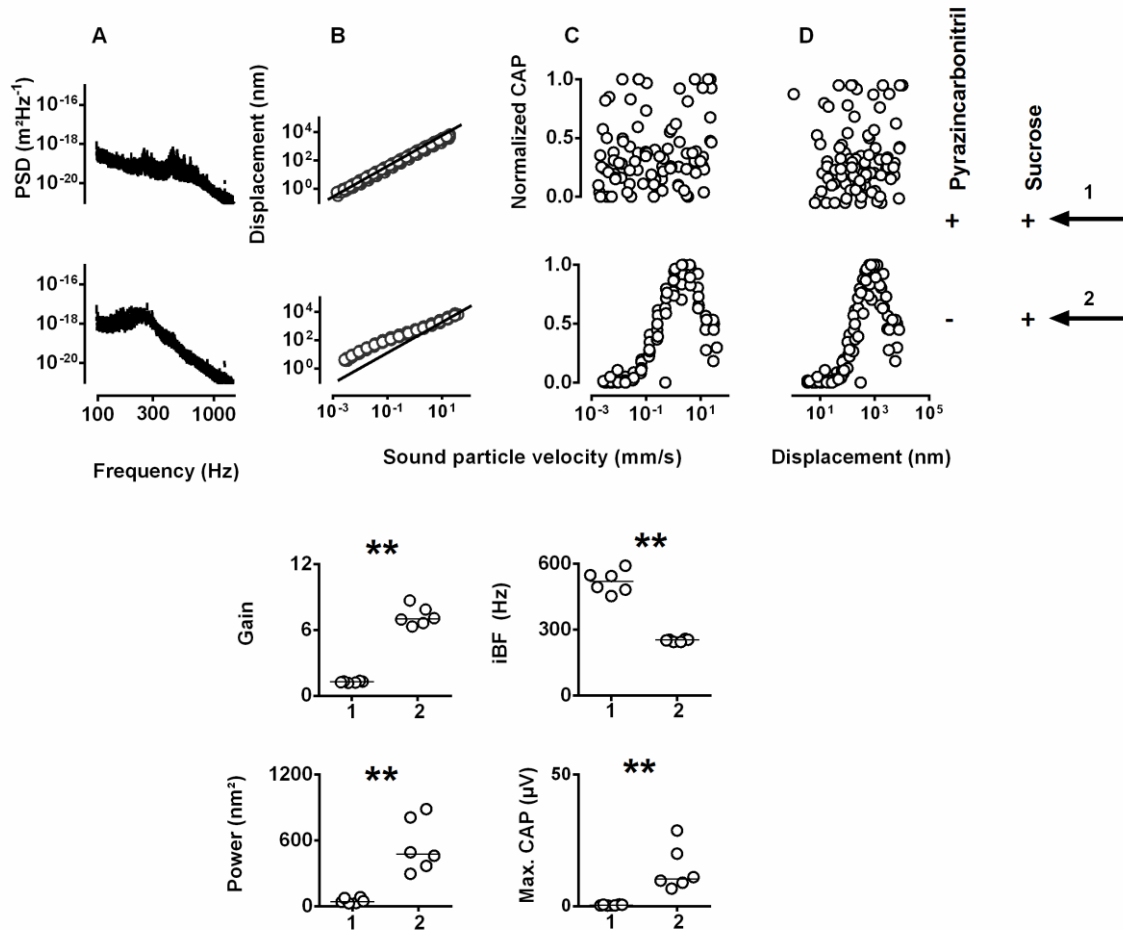


Figure 17. Effects of a NAAM inactivator on hearing.

Top: power spectra of the mechanical fluctuations of the antennal sound receiver (A) as well as antennal displacement (B), normalized compound action potential (CAP) amplitudes (C) as a function of the sound particle velocity, and CAP amplitude as a function of antennal displacement (D) in Pyrazincarbonitril-fed *w*¹¹¹⁸ wild-type flies and control sucrose-fed *w*¹¹¹⁸ flies. Bottom: corresponding amplification gain, individual best frequencies, power of the receiver fluctuations, and maximum CAP amplitudes. The *w*¹¹¹⁸ flies, starved overnight, and were kept for three hours on 1 % sucrose solution supplemented with a 50 μ M Pyrazincarbonitril (only 1 % sucrose solution was used as a food in control flies). The *w*¹¹¹⁸ flies treated with Pyrazincarbonitril demonstrated a loss of mechanical amplification and sound-evoked CAP in the antennal nerve. *Naam* mutant flies and *w*¹¹¹⁸ flies treated with Pyrazincarbonitril showed the same hearing defect that strengthens *Naam* involvement in *Drosophila* hearing. $n \geq 5$ flies/genotype. Two-tailed Mann-Whitney-U tests were used for statistical analysis. Statistical significance is indicated with ** ($P \leq 0.01$).

1.2.4. NAAM substrate and product effects on hearing

Loss of NAAM enzyme caused hearing loss in the *Naam* mutant flies (Figure 16). The hearing loss might be a consequence of the accumulated NAAM substrate, nicotinamide, or the deprivation of NAAM product, nicotinic acid. To test this, I treated wild-type flies with 10 mM nicotinamide or nicotinic acid.

Keeping wild-type flies, starved overnight, for three hours on 1 % sucrose solution and 10 mM nicotinic acid left hearing unaffected, whereas keeping them on medium supplemented with 10 mM nicotinamide for three hours, caused the hearing loss (hypo-amplification). The nicotinamide effect was reversible, with normal hearing being restored within 3 hours after the flies (not the measured flies) had been transferred to 1 % sucrose solution (Figure 18).

Given that nicotinamide activates Nan-lav channels (Upadhyay et al., 2016), I also tested whether supplementing the food with nicotinic acid or nicotinamide affects *iav*¹ null mutants whose JO neuron cilia lack both lav and Nan (Gong et al., 2004). Loss of Nan-lav electrically silences JO neurons and causes mechanical hyper-amplification (Göpfert et al., 2006). This hyper-amplification persisted in both treatments, either with nicotinamide, or nicotinic acid, documenting that the loss of Nan-lav renders the flies resistant to nicotinamide (Figure 18).

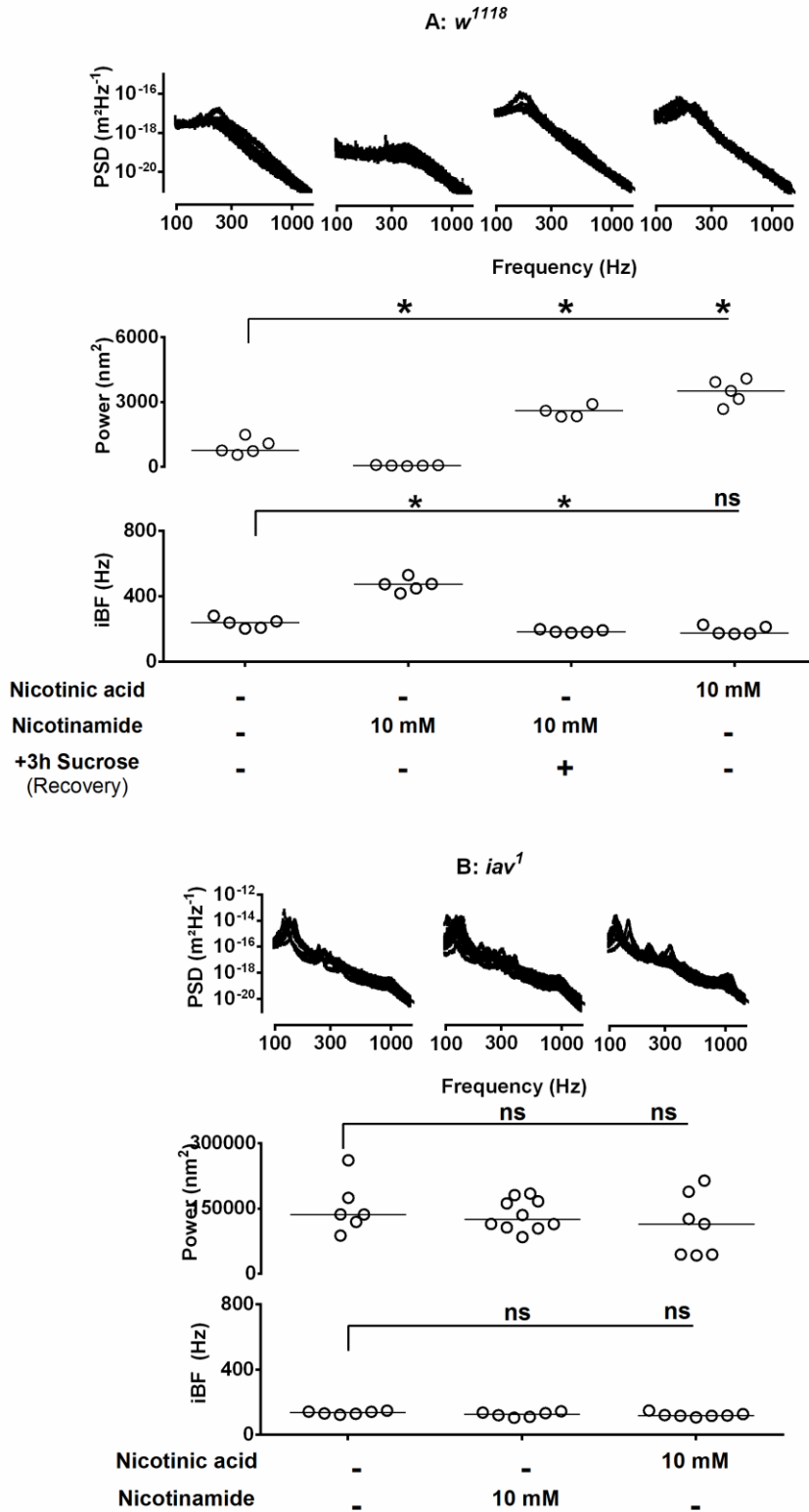


Figure 18. Nicotinamide and nicotinic acid feeding effects on hearing.

Flies, starved overnight, were kept for three hours on 1 % sucrose solution (controls) or 1 % sucrose solution supplemented with either 10 mM nicotinamide or nicotinic acid. Nicotinamide, but not nicotinic acid, disrupted hearing in *w¹¹¹⁸* flies (A) but not in *iav¹* mutants (B). Normal hearing in nicotinamide-treated *w¹¹¹⁸* flies was restored after the flies had been kept for three extra hours on 1 % sucrose solution. $n \geq 5$ flies/genotype. Two-tailed Mann-Whitney-U tests with the Bonferroni correction were used for statistical analysis. Statistical significances are indicated with ns ($P > 0.05$), * ($P \leq 0.05$).

Because NAAM is the first enzyme in the NAD⁺ salvage pathway, it seems possible that the hearing loss in the *Naam* mutant flies partially arises from defects in energy homeostasis or disruption of the NAD⁺ consuming enzymes functions. To test this possibility, and to distinguish between the roles of nicotinamide as the TRPV channel agonist and the modulator of the NAD⁺ bioavailability, I treated the *Naam* mutant flies with the NAAM product, nicotinic acid, or the end product of the NAD⁺ salvage pathway, NAD⁺. Keeping *Naam*^{MI12364}/*Df(3R)BSC809* mutant flies, starved overnight, on 1 % sucrose solution plus 10 mM nicotinic acid or NAD⁺ did not recover the auditory perception (Figure 19). Likewise, exposing homozygous *Naam*^{MI12364} mutant flies for longer durations (for monitoring long-term effects) to various nicotinic acid and NAD⁺ concentrations (for monitoring dose-dependent effects) did not recover the auditory perception (Supplement Figure 72-Figure 73).

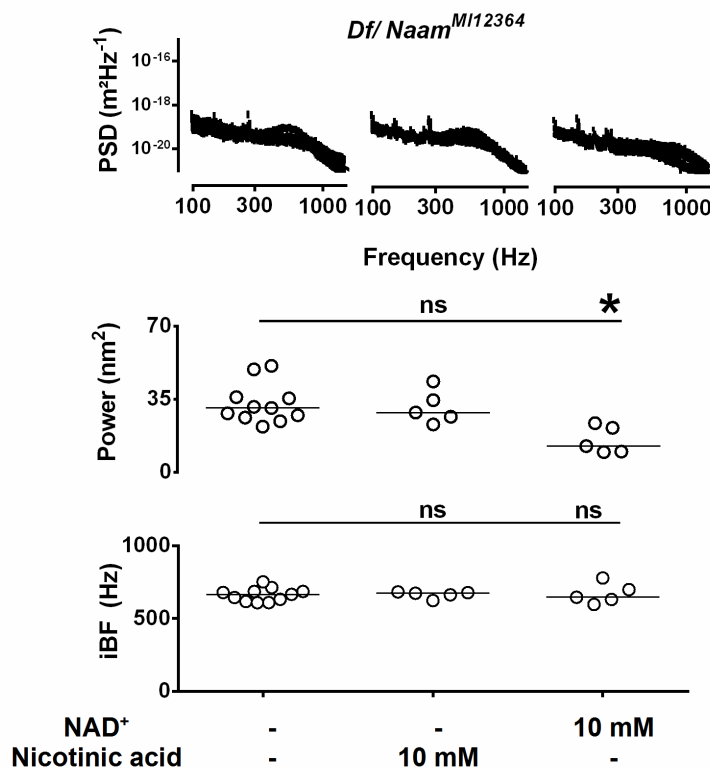


Figure 19. Absence of nicotinic acid or NAD⁺ rescue effect on hearing of the *Naam* mutant flies. Keeping *Df(3R)BSC809/Naam*^{MI12364} mutant flies, starved overnight, on 1 % sucrose solution plus 10 mM nicotinic acid or NAD⁺ did not recover the auditory perception. $n \geq 5$ flies/treatment. Two-tailed Mann-Whitney-U tests with the Bonferroni correction were used for statistical analysis. Statistical significance are indicated with ns ($P > 0.05$), * ($P \leq 0.05$).

1.2.5. Overexpressed *Nmnat* in *Naam* mutant flies

NMNAT is the rate-limiting enzyme in the NAD⁺ salvage pathway (Mori et al., 2014) (Figure 8). NMNAT converts the nicotinic acid mononucleotide into the nicotinic acid adenine dinucleotide, for that reason, the NMNAT overexpression should lead to elevated levels of the nicotinic acid adenine dinucleotide and the end product, NAD⁺. Treating *Naam*^{MI12364}/*Df(3R)BSC809* mutant flies with nicotinic acid or NAD⁺ did not recover the hearing perception in *Naam* mutant flies (Figure 19). It is not known whether the respective flies uptake the nicotinic acid or NAD⁺ in the food. For overcoming the mentioned problem with the feeding experiment, I enhanced *Nmnat* levels endogenously by driving *UAS-Nmnat* with the *Naam*^{MI12364}-*Gal4* driver (*Naam*^{MI12364}-*Gal4*>*Nmnat*). Overexpressing *Nmnat* in flies with homozygous *Naam*^{MI12364}-*Gal4* background could not rescue the hearing impairment in the respective flies (Figure 20) (*Naam*^{MI12364}-*Gal4* homozygous flies have a hearing impairment and can be used both as a *Naam* driver and a mutant). The overexpression of *Nmnat* with *Naam*^{MI12364}-*Gal4* in *Naam* deficiency background (*Df(3R)BSC809*) also did not recover the hearing perception in the *Naam* mutant flies (Supplement Figure 74).

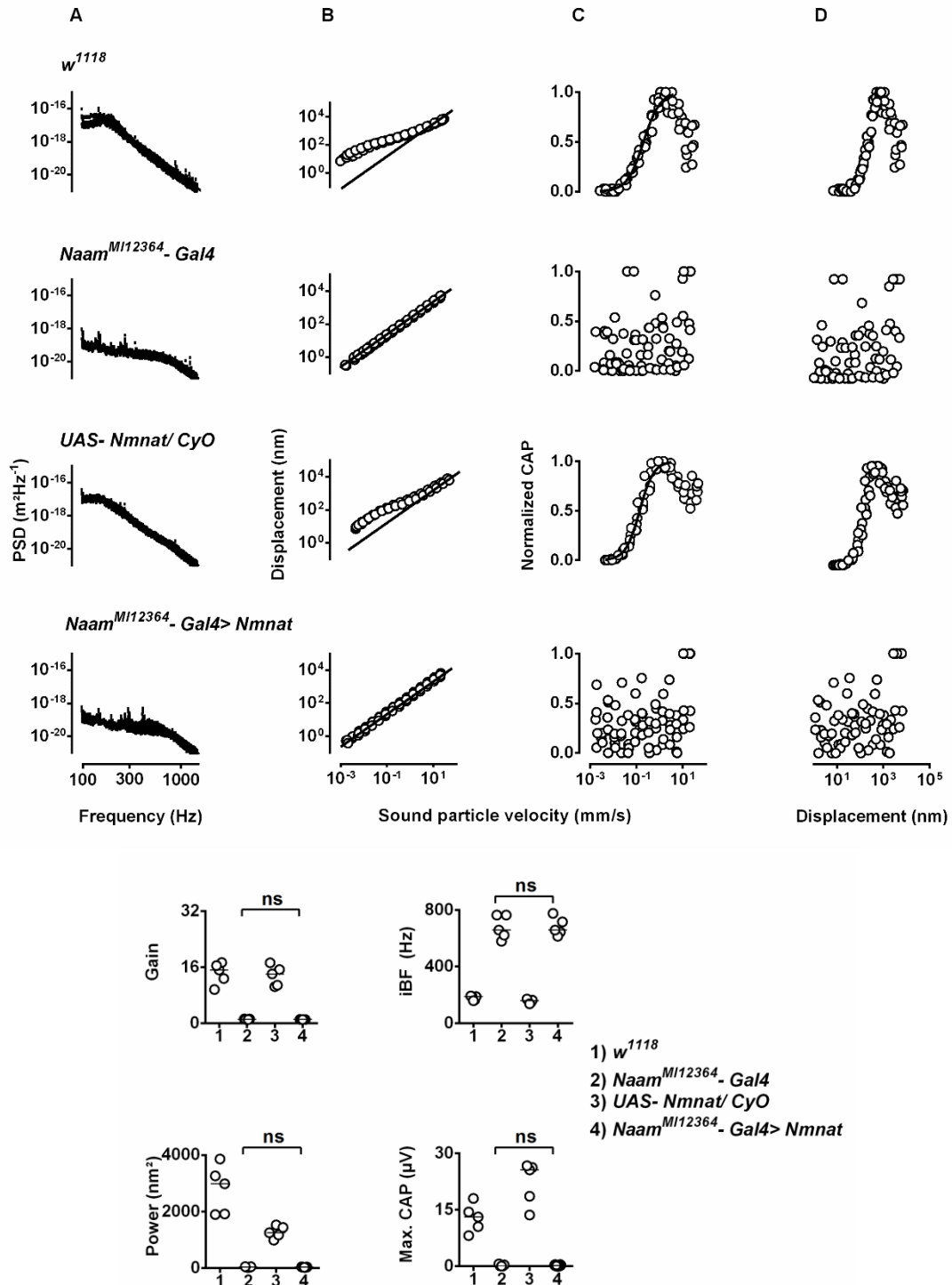


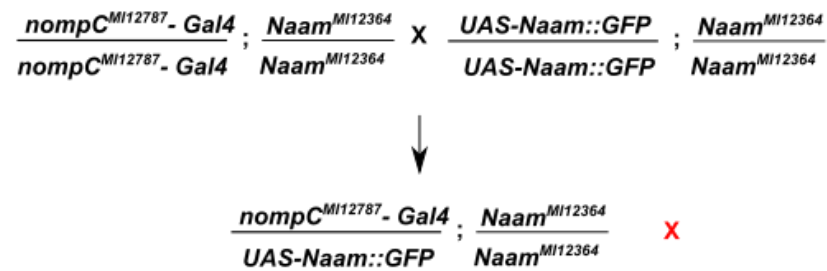
Figure 20. *Nmnat* overexpression effects on the hearing of the *Naam* mutant flies.

Top: power spectra of the mechanical fluctuations of the antennal sound receiver (A) as well as antennal displacement (B), normalized compound action potential (CAP) amplitudes (C) as a function of the sound particle velocity, and CAP amplitude as a function of antennal displacement (D) in wild type flies, homozygous *Naam^{MI12364}-Gal4* mutant flies, *UAS-Nmnat/CyO* control flies, and flies that overexpress *Nmnat* with *Naam^{MI12364}-Gal4* driver (*Naam^{MI12364}-Gal4>Nmnat*). Bottom: corresponding amplification gain, individual best frequencies, power of the receiver fluctuations, and maximum CAP amplitudes. Overexpressing *Nmnat* in the *Naam* mutant background (4) did not recover the mechanical amplification and sound-evoked CAPs in the antennal nerve of the *Naam* mutant flies (2). $n \geq 5$ flies/genotype. Two-tailed Mann-Whitney-U tests with the Bonferroni correction were used for statistical analysis. Statistical significance is indicated with ns ($P > 0.05$).

1.2.6. Cell type-specific rescue of hearing in the *Naam* mutant flies

NAAM is expressed by both JO neurons and supporting scolopale cells (Figure 11), suggesting that fly hearing might require NAAM function in both cell types. To test this hypothesis, I used cell type-specific *Gal4* drivers to drive the expression of a rescue-construct, *UAS-Naam::GFP*, in the *Naam* mutant background. Driving the rescue-construct with the JO neuronal driver, *nompC^{MI12787}-Gal4* (*nompC^{MI12787}-Gal4>Naam::GFP*), in the homozygous *Naam^{MI12364}* mutant background did not rescue the hearing defect (data not shown) (Figure 21, A), which was not expected. After several attempts to eliminate the probable problems, I found that changing the genetic background of the mutant flies to *Naam^{MI12364}/Df(3R)BSC809* led to the rescued hearing, restoring the antenna best frequencies, mechanical amplification, and sound-evoked electrical potentials in the flies with *nompC^{MI12787}-Gal4>Naam::GFP* (Figure 21, B). A potential negative effect of the excessive truncated NAAM protein on the hearing of *Drosophila* might be the underlying reason for the unsuccessful hearing recovery attempts in the homozygous *Naam^{MI12364}* flies (Figure 10). After realizing that the homozygous *Naam^{MI12364}* mutant flies are different from the *Naam^{MI12364}/Df(3R)BSC809* mutant flies, I repeated all the previous experiments with *Naam^{MI12364}/Df(3R)BSC809*, as well, and in some cases, presented the data of both results.

A:



B:

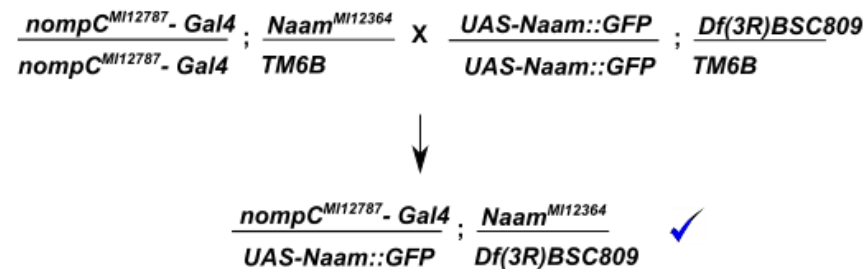


Figure 21. Crossing scheme of the cell type-specific rescue of hearing in the *Naam* mutant flies.

Driving the rescue-construct, *UAS-Naam::GFP*, with the JO neuronal driver, *nompC^{MI12787}-Gal4* (*nompC^{MI12787}-Gal4*>*Naam::GFP*), in the homozygous *Naam^{MI12364}* mutant background, did not rescue the hearing defect (A) whereas, *nompC^{MI12787}-Gal4*>*Naam::GFP* in the *Naam^{MI12364}/Df(3R)BSC809* mutant background rescued the hearing defect (B).

Driving the rescue-construct, in the scolopale cells (*Naam-Gal4*>*Naam::GFP*) of *Naam^{MI12364}/Df(3R)BSC809* mutant flies, rescued hearing partially, restoring frequency tuning and mechanical amplification, but not the sound-evoked potentials (Figure 22).

Apparently, NAAM presence in the chordotonal neurons is required for the generation of sound-evoked potentials and mechanical amplification.

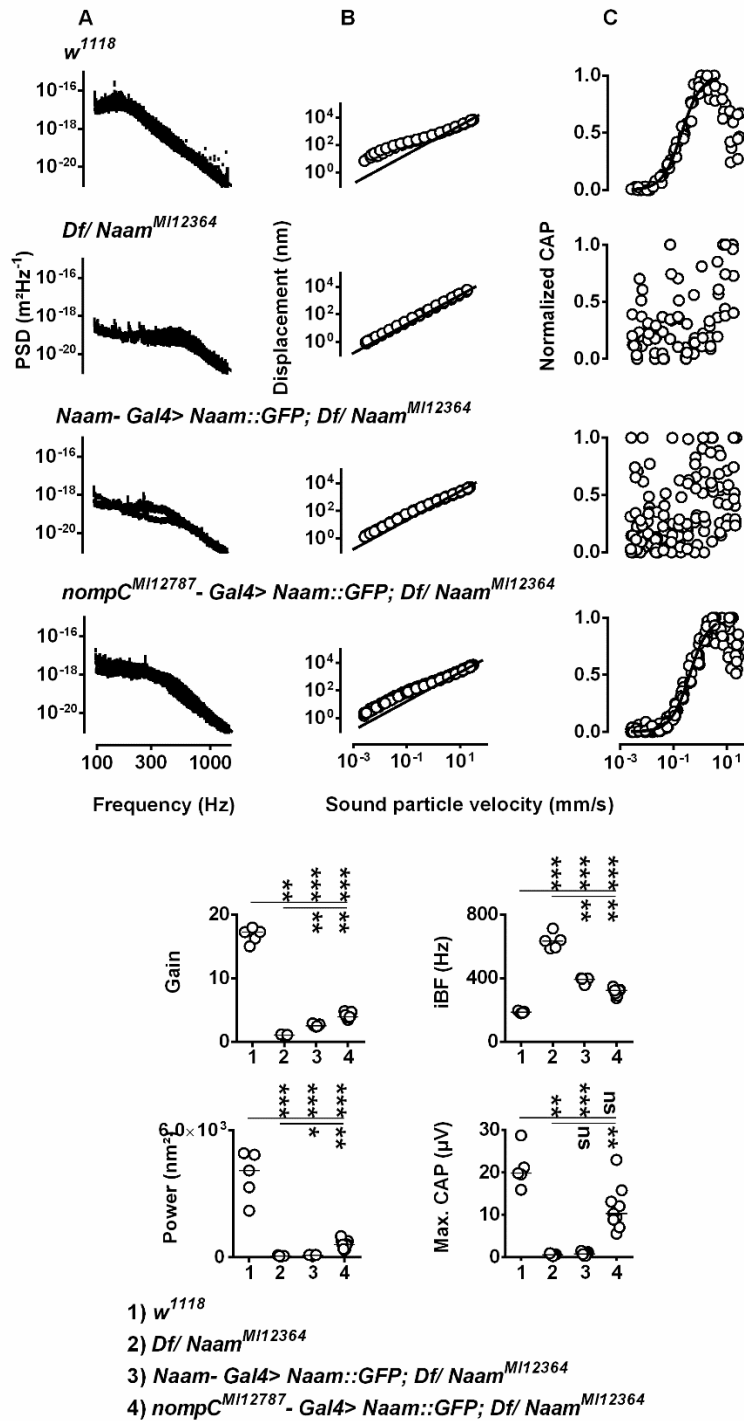


Figure 22. Cell type-specific rescue of the *Naam* mutant flies.

Top: power spectra of the mechanical fluctuations of the antennal sound receiver (A) as well as antennal displacement (B), and normalized compound action potential (CAP) amplitudes (C) as a function of the sound particle velocity in wild type flies, *Naam*^{MI12364}/*Df*(3R)*BSC809* mutant flies, and flies that expressing *UAS-Naam::GFP* with the *Naam-Gal4* (*Naam-Gal4*>*Naam::GFP*) or *nompC*^{MI12787}-*Gal4* (*nompC*^{MI12787}-*Gal4*>*Naam::GFP*) drivers in *Naam*^{MI12364}/*Df*(3R)*BSC809* background. Bottom: corresponding amplification gain, individual best frequencies, power of the receiver fluctuations, and maximum CAP amplitudes. Driving *UAS-Naam::GFP* with both neuronal (4) and scolopale (3) drivers restored mechanical amplification. In contrast to the neuronal driver, driving the *UAS-Naam::GFP* construct with the scolopale driver did not recover the neuronal response. $n \geq 5$ flies/genotype. Two-tailed Mann-Whitney-U tests with the Bonferroni correction were used for statistical analysis. Statistical significances are indicated with ns ($P > 0.05$), * ($P \leq 0.05$), ** ($P \leq 0.01$), and *** ($P \leq 0.001$).

1.2.7. EF-hand domains role in NAAM enzymatic activity

The presence of conserved aminoterminal EF-hand domains in NAAM suggests that NAAM activity might be calcium-dependent. To explore the functional relevance of the EF-hand domains in the NAAM enzyme, I generated one *UAS-Naam* construct without the EF-hand domains, one with missense point mutations in the EF-hand domains (incapable of binding to Ca^{2+} ions), and one with three EF-hand domains. Missense point mutations included D26, 28G, and D69G amino-acid changes, which are predicted to impair calcium-binding (Kawasaki et al., 1998). In addition, a UAS construct was generated for *PNC1*, the *Naam* ortholog of *C. elegans* that natively doesn't possess EF-hand domains (Figure 23).

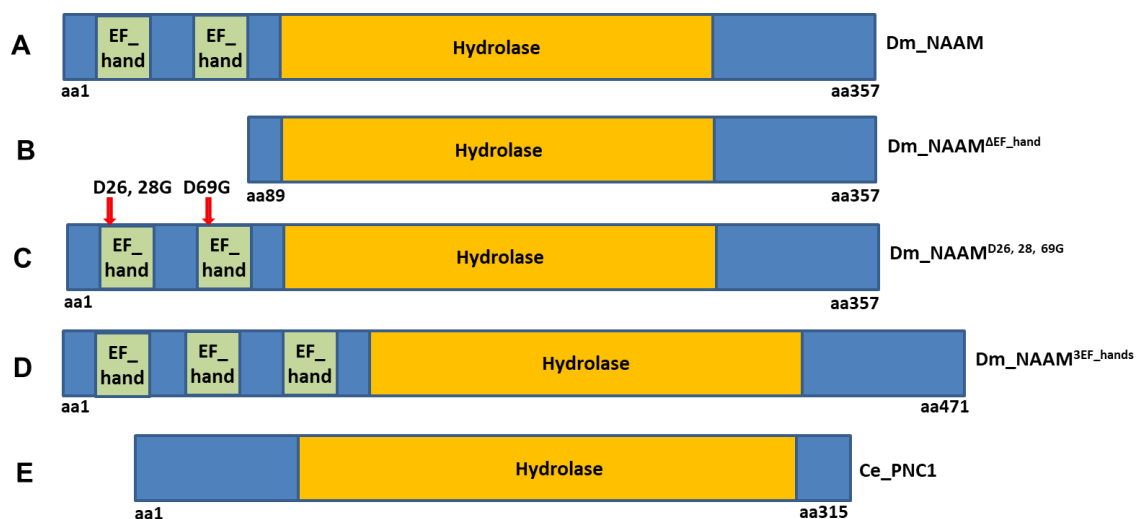


Figure 23. Schematic picture of the generated NAAM constructs.

The NAAM enzyme has two EF-hand domains for Ca^{2+} binding and an isochorismatase-like domain for hydrolase capability. For evaluating the function of EF-hand domains, *UAS-Naam* constructs without EF-hands (B), EF-hands with missense mutations (C), and three EF-hands (D) were generated. Besides, *PNC1* from *C. elegans* (E) was also used for the same purpose.

I also generated a *UAS-Naam::GFP* construct (Figure 24). The respective construct encodes a C-terminal GFP-tagged NAAM protein, which is different from the internally GFP-tagged NAAM protein made by the Double Header tool (Figure 13).

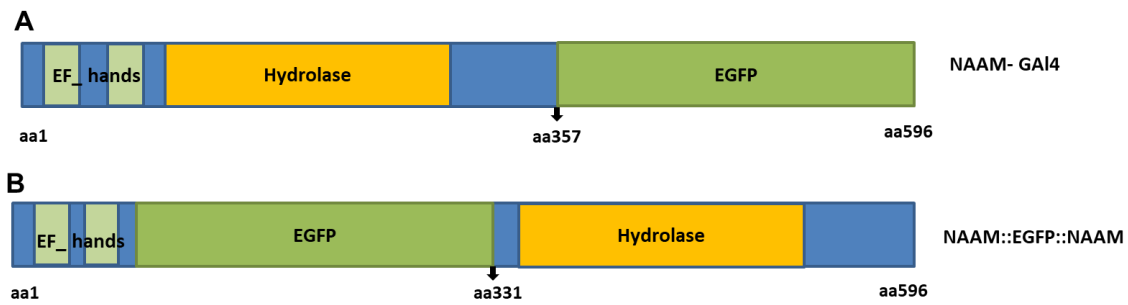


Figure 24. The differences between the two NAAM GFP-tagged proteins.

The first picture is a NAAM protein (NAAM::GFP) encoded by the *UAS-Naam::GFP* construct. The flies carrying *UAS-Naam::GFP* were made by embryo injections (section II.III). In the respective protein, the EGFP is attached to the C-terminus of the NAAM protein (A). The second picture is a NAAM protein (NAAM::EGFP::NAAM) encoded by the *Naam::EGFP::Naam* gene. The flies carrying the *Naam::EGFP::Naam* gene were made by the Double Header tool from the *Naam^{MI12364}* line (section II.V). In this protein, the EGFP is located between the EF-hand and the isochorismatase-like domains (B). In both conditions, the NAAM protein is tagged with EGFP.

The GFP signals in homozygous *Naam^{MI12364}-Gal4>Naam::GFP* flies were visible in the antenna (Supplement Figure 75). Having *Naam^{MI12364}-Gal4>Naam::GFP* flies in the *Naam Df(3R)BSC809* background labels JO neurons and supporting scolopale cells (Supplement Figure 76), corroborating the expression pattern of the *Naam* gene.

1.2.7.1. Rescue potential of *UAS-Naam* with or without modified EF-hand domains

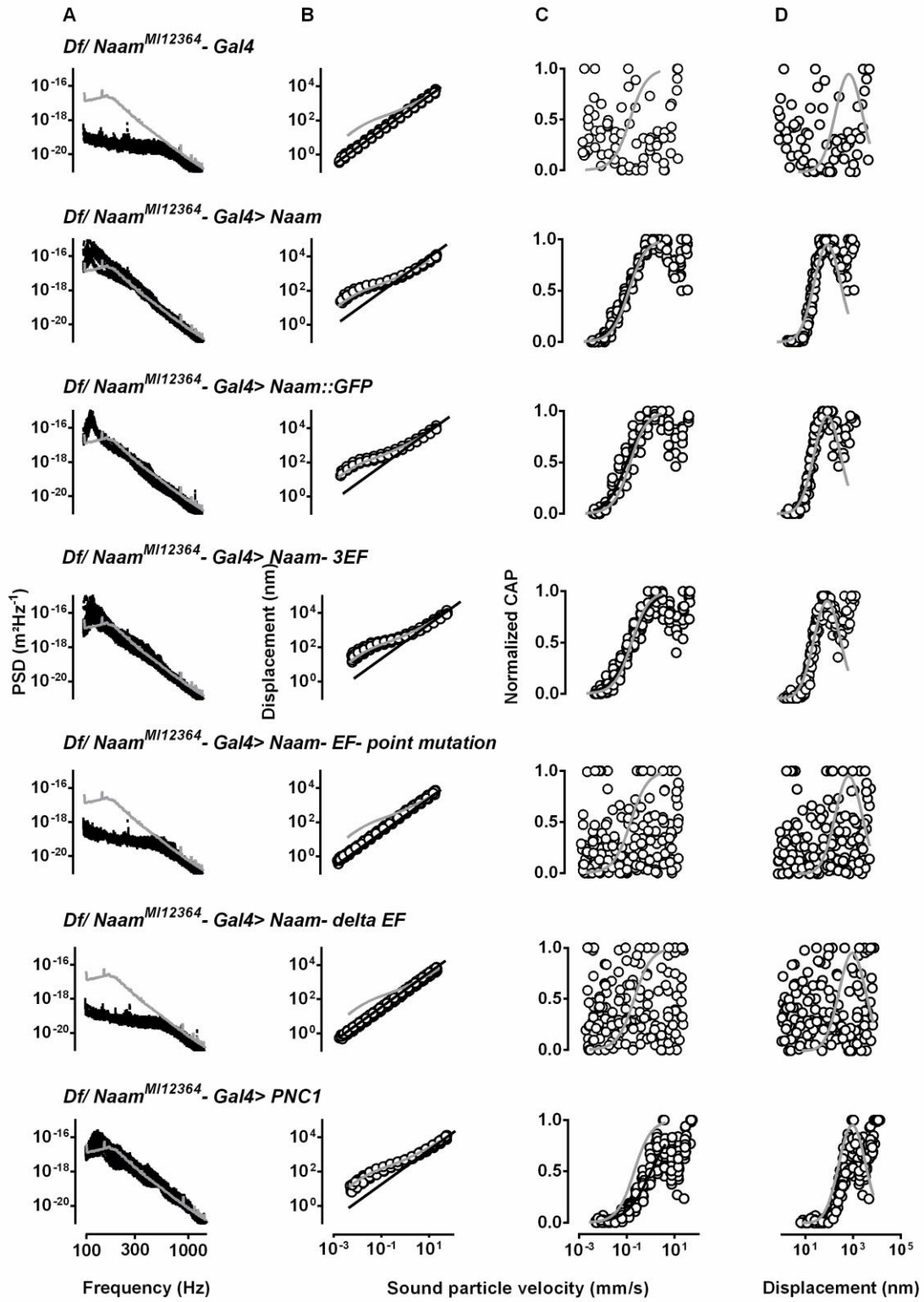
For functional assessment of the EF-hand domains in the NAAM enzyme, I used the generated *UAS-Naam* constructs (Figure 23) for rescuing the hearing impairment in the *Naam* mutant flies. I could use homozygous *Naam^{MI12364}-Gal4* flies as a *Naam* driver and a *Naam* mutant (Figure 20). For the reason that was described in section 1.2.6 and depicted in Figure 21, using homozygous *Naam^{MI12364}-Gal4* mutant flies might affect the fly's hearing negatively (due to probable excessive truncated NAAM proteins). Crossing homozygous *Naam^{MI12364}-Gal4* flies into the flies carrying *UAS-Naam* constructs (*UAS-Naam*, *UAS-Naam::GFP*, *UAS-Naam-3EF*, *UAS-Naam-EF-point mutation*, and *UAS-PNC1* but not *UAS-Naam-delta-EF*), in homozygous *Naam^{MI12364}-Gal4* background, recovered the nerve response but not mechanical amplification (Supplement Figure 77)

However, using *Naam^{MI12364}-Gal4/Df(3R)BSC809* mutant flies instead of homozygous *Naam^{MI12364}-Gal4* flies, carrying *UAS-Naam* constructs, rescued hearing completely, including frequency tuning, mechanical amplification, and nerve responses except in flies carrying the impaired NAAM EF-hand domains (*UAS-Naam-EF-point mutation* and *UAS-Naam-delta EF*). Among the rescued flies, the line with *UAS-PNC1*

and *UAS-Naam-3EF* showed significant differences in the SPV threshold (materials and methods, section II.VII.III) compared to WT flies. The hearing recovery phenotypes that were obtained with *UAS-Naam* and *UAS-Naam::GFP* were equivalent, and parameters describing their auditory performance showed no statistical difference (Figure 25).

The hearing was normal in control flies, which are homozygous *UAS-Naam*, *UAS-Naam::GFP*, *UAS-Naam-3EF*, *UAS-Naam-EF-point mutation*, *UAS-Naam-delta-EF*, and *UAS-PNC1* (Supplement Figure 78).

Chapter I - Results



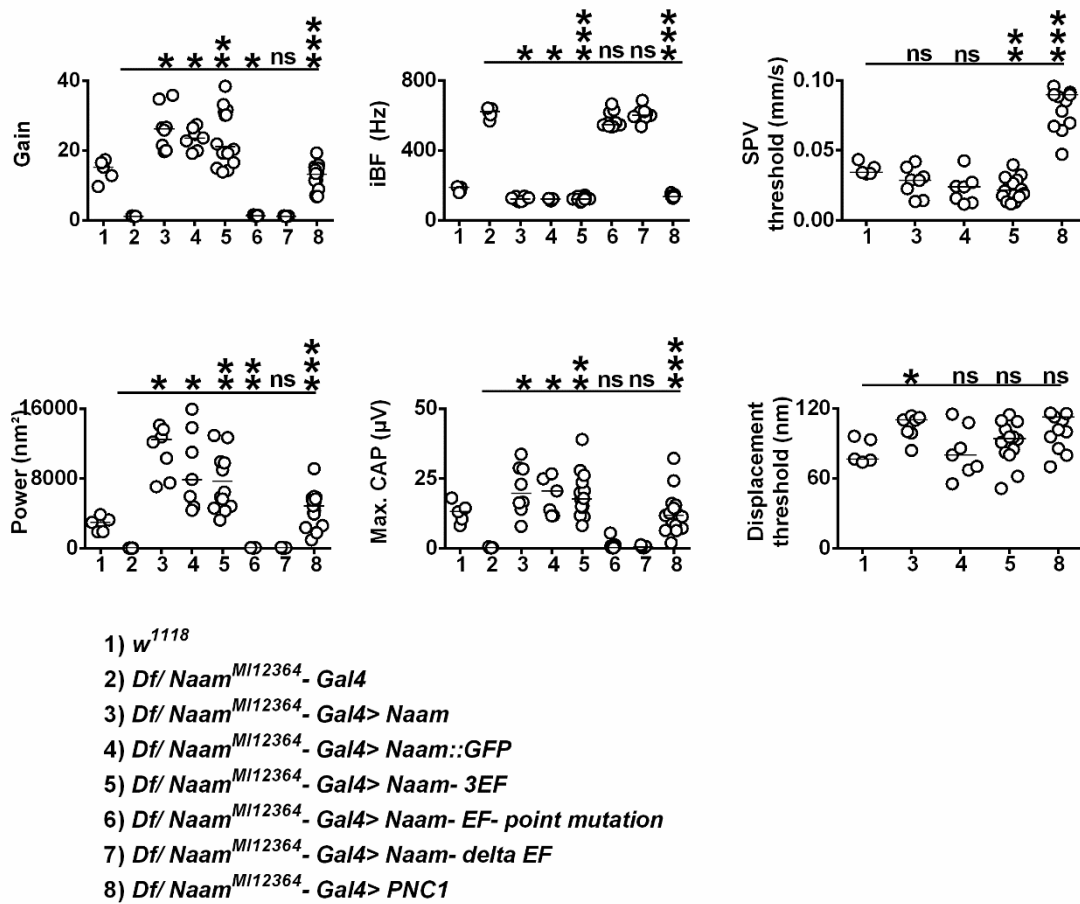


Figure 25. Rescue potential of *UAS-Naam* with and without EF-hand domains mutation.

Top: power spectra of the mechanical fluctuations of the antennal sound receiver (A) as well as antennal displacement (B), normalized compound action potential (CAP) amplitudes (C) as a function of the sound particle velocity, and CAP amplitude as a function of antennal displacement (D) in wild type flies, $Naam^{MI12364} - Gal4/Df(3R)BSC809$ mutant flies, and flies carrying various *UAS-Naam* constructs in the $Naam^{MI12364} - Gal4/Df(3R)BSC809$ background. Bottom: corresponding amplification gain, individual best frequencies, power of the receiver fluctuations, maximum CAP amplitudes, sound particle velocity (SPV) threshold, and displacement threshold. Expressing any *UAS-Naam* constructs rescued hearing in *Naam* mutant flies, including frequency tuning, mechanical amplification, and nerve responses except for those with impaired EF-hand domains (*UAS-Naam-EF-point mutation* and *UAS-Naam-delta EF*). Among the flies with recovered hearing, the line carrying *UAS-PNC1* and *UAS-Naam-3EF* showed significant differences in the SPV threshold compared to WT flies. The ghost graphs represent w^{1118} as a control. $n \geq 5$ flies/genotype. Two-tailed Mann-Whitney-U tests with the Bonferroni correction were used for statistical analysis. Statistical significances are indicated with ns ($P > 0.05$), * ($P \leq 0.05$), ** ($P \leq 0.01$), and *** ($P \leq 0.001$).

The internally GFP-tagged NAAM protein that was made by the Double Header tool (1.2.2 section) has the GFP cassette between the EF-hand domains and the core of the enzyme. These flies displayed hearing defects (supplement Figure 71), indicating that the EF-hand domains might need to be near to the core of the NAAM enzyme for its proper function. This observation is consistent with the recovered hearing in the *Naam* mutant flies expressing *UAS-Naam* constructs with functional EF-hand domains (Figure 25).

1.2.7.2. Disrupted *in vitro* NAAM enzymatic activity with ablated EF-hand domains

Additional evidence for the necessity of the EF-hand domains in the NAAM enzymatic function comes from the *in vitro* NAAM assay (section II.VIII). This assay relies on ammonium detection, the byproduct of the nicotinamide hydrolysis, through a colorimetric reaction (Figure 7).

Using the yeast PNC1 enzyme for converting nicotinamide in the fly extracts from the whole wild type or *Naam* mutant flies did not lead to significant changes in the fluorescence signal within the reaction. The same results were observed when I used the expressed NAAM enzyme by S2 cells, without purification, for converting 40 μ M nicotinamide (from Sigma-Aldrich) into nicotinic acid and ammonium (probably the presence of other enzymes in the extracts from the flies and the cells have inhibitory effects on the function of PNC1 or NAAM enzymes). For the extracts from the flies, one problem might be the free NH₃ or NH₄ in the malpighian tubules and hemolymph (Browne and O'Donnell, 2013), which can saturate the detection capacity of the assay.

Extracted and enriched GFP-tagged NAAM from S2 cells; however, could convert nicotinamide (from Sigma-Aldrich) into nicotinic acid and ammonium. The produced ammonium led to significant changes in the fluorescence signals compared to controls, in which the nicotinamide was not added. By contrast, GFP-tagged NAAM without (EF-hand domains) or with missense point mutations in the EF-hand domains could not produce significant amounts of ammonium from nicotinamide, and the changes in the fluorescent signals were lower than the reaction mediated by the GFP-tagged NAAM (Figure 26, panel A). This observation is consistent with the recovery of the hearing perception in the *Naam* mutant flies by the expression of *Naam::GFP* but not *Naam* with impaired EF-hand domains (*Naam-EF-point mutation* and *Naam-delta EF*) (Figure 25).

Imaging the S2 cells expressing GFP-tagged NAAM revealed cytosolic localization; however, GFP-tagged NAAM without (EF-hand domains) or with missense point mutations in the EF-hand domains caused NAAM mislocalization (Figure 26, panel C). In western blots, each extracted and enriched enzyme showed one band between 55 and 70 kDa (plus two additional weak bands for NAAM::GFP without EF-hand domains). Indeed, the expected sizes of the NAAM enzymes are in the range of 55 - 70 kDa (67.2 kDa for NAAM::GFP, 67.0 kDa for NAAM::GFP with missense point mutations

in the EF-hand domains, and 56.4 kDa for NAAM::GFP without EF-hand domains (<https://www.aatbio.com/tools/calculate-peptide-and-protein-molecular-weight-mw>). This observation indicates an absence of protein degradation. (Figure 26, panel B).

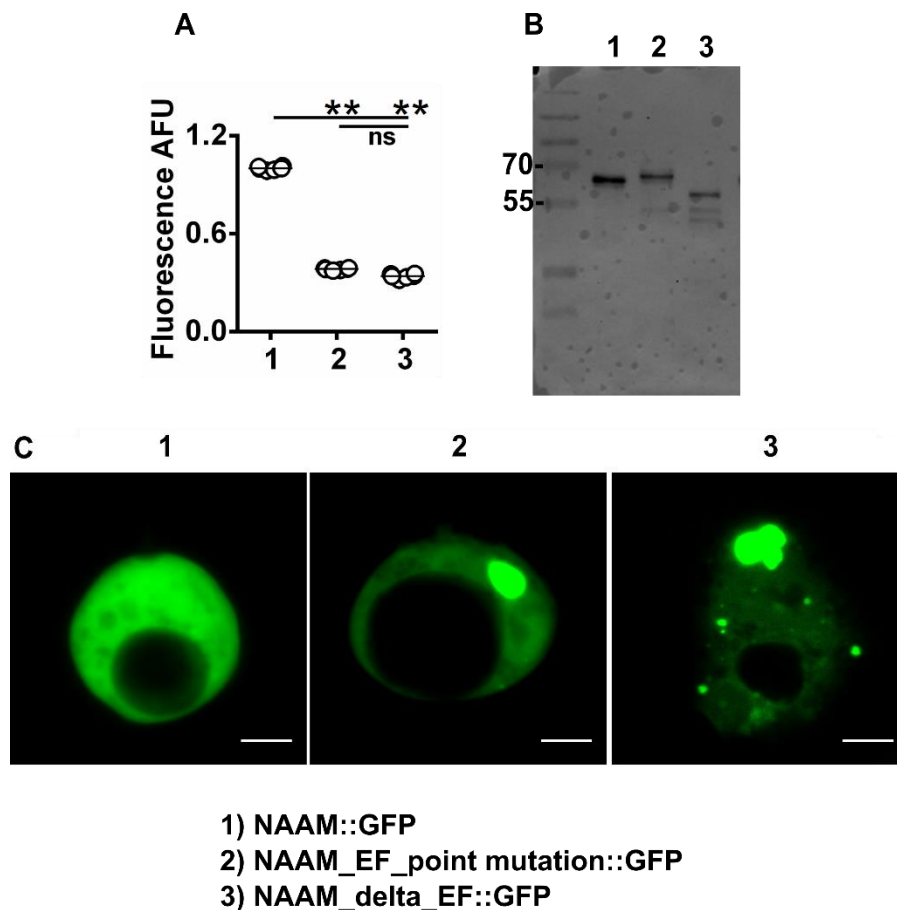


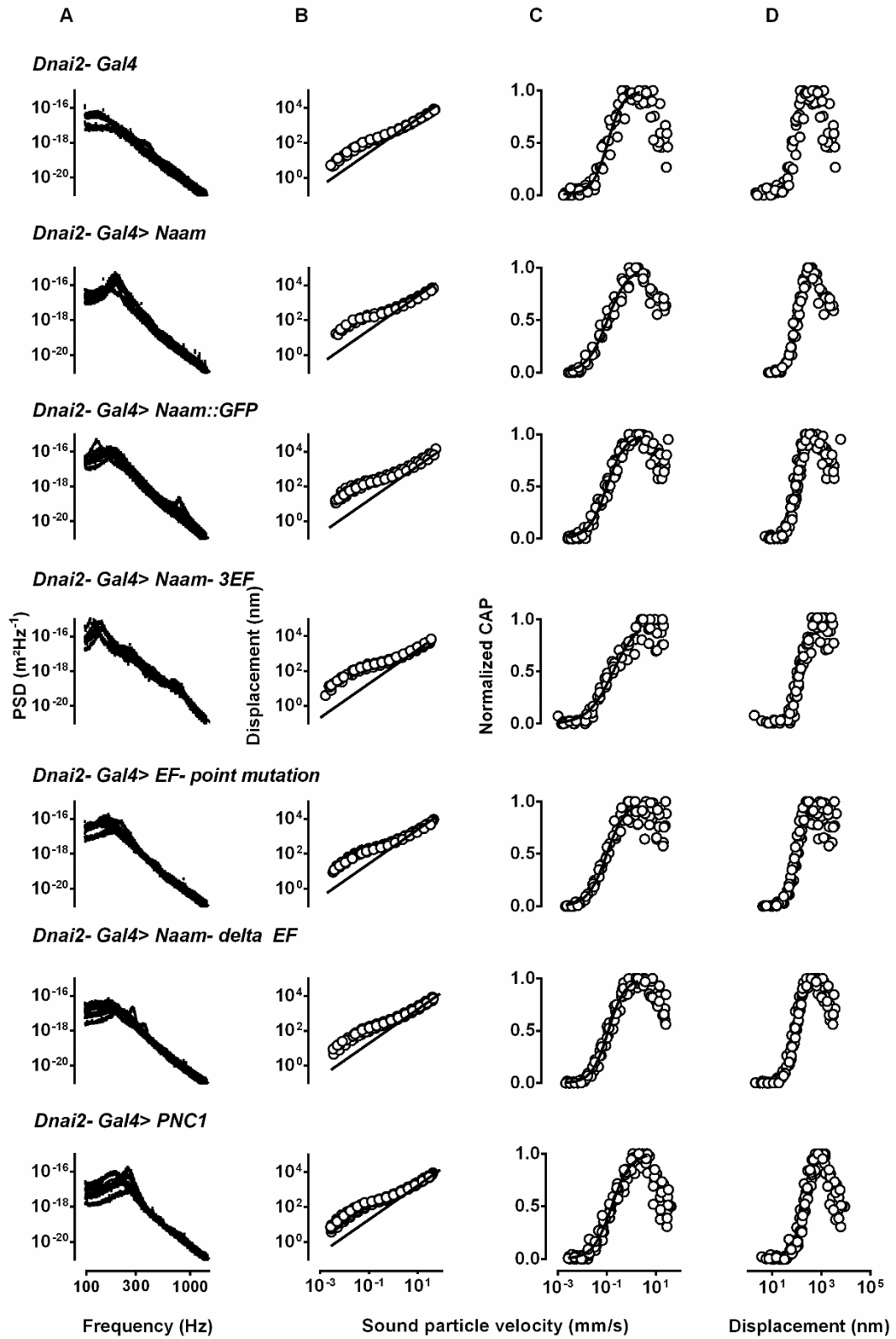
Figure 26. *In vitro* NAAM enzymatic activity with or without EF-hand domains ablation.

A: Fluorescence signals in an arbitrary fluorescent unit (AFU) demonstrated that extracted and enriched NAAM::GFP enzyme (1) from S2 cells has more enzymatic activity compared to NAAM-EF-point mutation::GFP (2) or NAAM-delta EF::GFP enzymes (3) ($n = 6$). Mann-Whitney-U test with the Bonferroni correction was used for statistical analysis. Statistical significances are indicated with ns ($P > 0.05$), and ** ($P \leq 0.01$). B: Western blot probing for GFP showed bands corresponding to the expected sizes for each enzyme. C: The image from the S2 cells expressing GFP-tagged NAAM revealed cytosolic localization; however, NAAM without (EF-hand domains) or with missense point mutations in the EF-hand domains showed NAAM mislocalization. Scale bars: 5 μ m.

1.2.8. Auditory effects caused by *Naam* overexpression

Loss of NAAM impaired hearing (Figure 16), and keeping wild-type flies on 1 % sucrose solution supplemented with NAAM substrate (nicotinamide) but not NAAM product (nicotinic acid) recapitulated the hearing defect seen in the *Naam* mutant flies

(Figure 18). It seems that the auditory performance depends on the nicotinamide levels, which might be affected by NAAM overexpression. To test this possibility, I crossed flies carrying different *UAS-Naam* constructs (Figure 23) into *Dnai2-Gal4* (the chordotonal receptor driver) flies to overexpress various NAAM proteins. The increased NAAM enzyme levels might lead to nicotinamide reduction and nicotinic acid elevation (I quantified neither of the two substances in the respective flies). I suspected facilitated mechanical amplification in the hearing of the flies overexpressing NAAM due to the presumable reduction of the TRPV channel agonist, nicotinamide (Upadhyay et al., 2016).



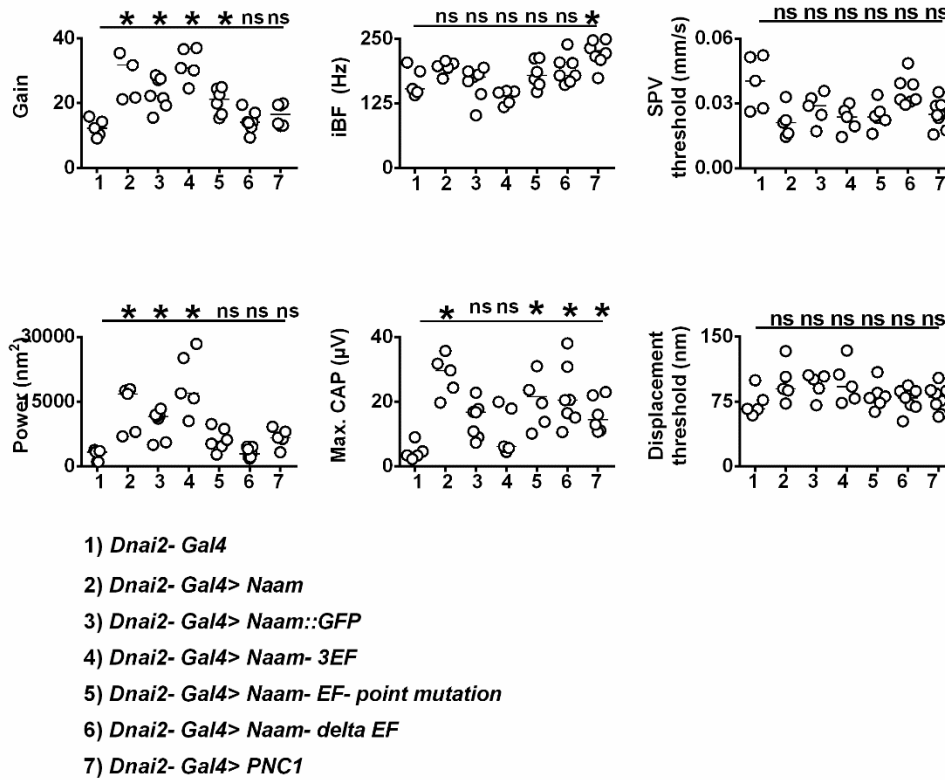


Figure 27. *Naam* overexpression effects on hearing.

Top: power spectra of the mechanical fluctuations of the antennal sound receiver (A) as well as antennal displacement (B), normalized compound action potential (CAP) amplitudes (C) as a function of the sound particle velocity, and CAP amplitude as a function of antennal displacement (D) in the chordotonal receptor driver, *Dnai2-Gal4* flies, and flies expressing various *UAS-Naam* constructs with *Dnai2-Gal4* driver. Bottom: corresponding amplification gain, individual best frequencies, power of the receiver fluctuations, maximum CAP amplitudes, sound particle velocity (SPV) threshold, and displacement threshold. There is a mechanical hyper-amplification in flies overexpressing each of the (generated) *UAS-Naam* constructs, in the chordotonal neurons, except *UAS-Naam-delta EF* and *UAS-PNC1* (6 - 7). The power of the antenna's mechanical free fluctuations was also increased upon overexpression of each *UAS-Naam* construct except the one with manipulated or absent EF-hand domains (5 - 7). $n \geq 5$ flies/genotype. Two-tailed Mann-Whitney-U tests with the Bonferroni correction were used for statistical analysis. Statistical significances are indicated with ns ($P > 0.05$), * ($P \leq 0.05$).

As shown in Figure 27, overexpressing each of the (generated) *UAS-Naam* (except *UAS-Naam-delta EF* and *UAS-PNC1*) constructs in the chordotonal neurons facilitate mechanical amplification in the flies hearing. The power of the antenna's mechanical free fluctuations was also increased upon overexpression of each *UAS-Naam* construct except the one with manipulated or absent EF-hand domains (Figure 27).

Consistent with this data, keeping the flies overexpressing NAAM, starved overnight, for three hours on 1 % sucrose solution supplemented with 10 mM nicotinamide left hearing unaffected (Figure 28). This observation is in contrast to the impaired hearing phenotype in WT flies that were treated with the same concentration of nicotinamide (Figure 18). Treating the flies overexpressing NAAM with higher nicotinamide concentration (80 mM), however, elicited hearing defects (Figure 28). In other words, NAAM overexpression in the chordotonal neurons resulted in significantly more resistance to (fed) nicotinamide-induced deafness.

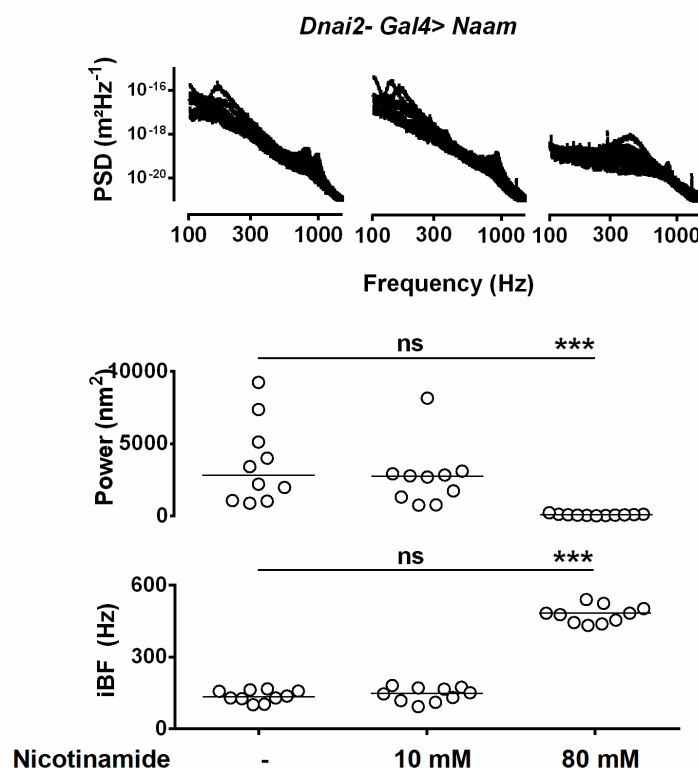


Figure 28. Nicotinamide effects on flies with overexpressed *Naam*.

Keeping the flies overexpressing NAAM, starved overnight, for three hours on 1 % sucrose solution supplemented with 80 mM (but not 10 mM) nicotinamide elicited hearing defects. $n \geq 5$ flies/genotype. Two-tailed Mann-Whitney-U tests with the Bonferroni correction were used for statistical analysis. Statistical significance is indicated with ns ($P > 0.05$).

Compatible with the higher rescue potential of the neuronal driver (*nompC^{MI12787}-Gal4*) compared to the scolopale cell driver (*Naam-Gal4*) (Figure 22), the power of the antenna's mechanical free fluctuations of the flies overexpressing *Naam* with a neuronal driver (*Dnai2-Gal4>Naam*) was significantly higher compared to the scolopale driver (*Naam-gal4>Naam*) (Supplement Figure 79)

1.2.9. Auditory phenotype in double *iav* and *Naam* mutants

Oral administration of nicotinamide impaired hearing in wild-type flies but left hearing, in *iav*¹ mutants, unaffected (Figure 18), suggesting that nicotinamide affects hearing by acting on Nan-lav channels, with Nan-lav and NAAM operating in the same pathway. To test this hypothesis, I generated a double *iav* and *Naam* mutant line and studied the genes for epistasis.

Consistent with data in section 1.2.4, the hearing phenotype, including antenna best frequencies, and mechanical amplification, in flies with *iav* and *Naam* double mutations resembled the hearing defect in the *iav* but not *Naam* mutant flies (Figure 29).

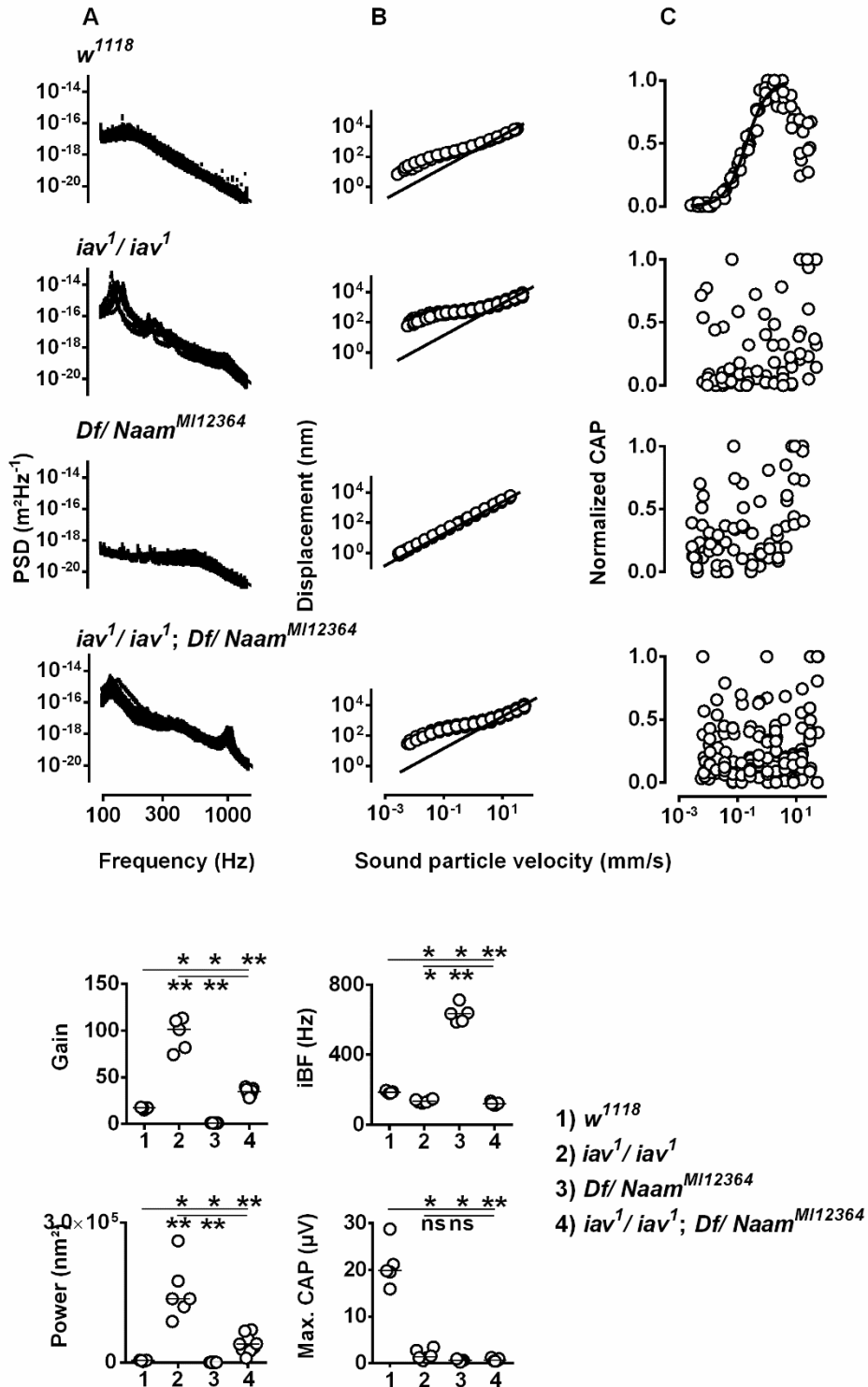


Figure 29. The auditory phenotype in double *Naam* and *iav* mutant flies.

Top: power spectra of the mechanical fluctuations of the antennal sound receiver (A) as well as antennal displacement (B), and normalized compound action potential (CAP) amplitudes (C) as a function of the sound particle velocity in wild type flies, *iav*¹ mutant flies, *Naam*^{MI12364}/*Df*(3*R*)*BSC809* mutant flies, and *iav*¹ mutant flies with *Naam*^{MI12364}/*Df*(3*R*)*BSC809* background. Bottom: corresponding amplification gain, individual best frequencies, power of the receiver fluctuations, and maximum CAP amplitudes. Observing the *iav*¹ hearing defect for the double *Naam* and *iav*¹ mutant flies endorse the hypothesis that NAAM functions through the agonistic effect of nicotinamide on the TRPV channel. $n \geq 5$ flies/genotype. Two-tailed Mann-Whitney-U tests with the Bonferroni correction were used for statistical analysis. Statistical significances are indicated with ns ($P > 0.05$), * ($P \leq 0.05$), ** ($P \leq 0.01$).

1.2.10. NOMPC and *iav* channel disturbance in *Naam* mutant flies

Since NAAM and TRPV channels in *Drosophila* are operating in the same pathway (Figure 29), NAAM might affect TRPV channel expression and localization. Besides the TRPV channels in the proximal cilium region of the JO neurons (Gong et al., 2004), hearing in *Drosophila* also relies on TRPN (=NOMPC) channels that reside in the cilium tips (Lee et al., 2010; Effertz et al., 2011). I tested for the presumable effects of NAAM on both *iav* and NOMPC channels.

Using RT-qPCR, I found increased expression of both *iav* and *nompC* in homozygous *Naam*^{MI12364} mutant flies compared to *w*¹¹¹⁸ control flies (Figure 30).

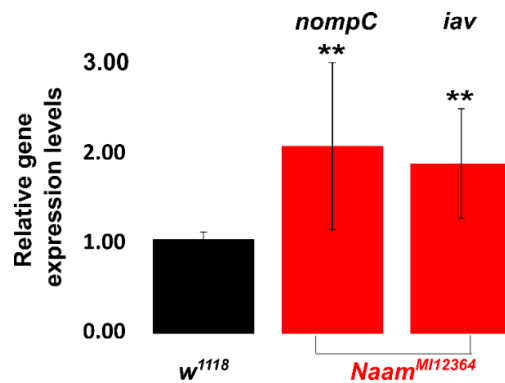


Figure 30. *nompC* and *iav* expression levels in the *Naam* mutant flies compared to *w*¹¹¹⁸.

The data from RT-qPCR revealed that *nompC* and *iav* in homozygous *Naam*^{MI12364} mutant flies (red columns) have higher expression levels compared to *w*¹¹¹⁸ as a control (black column). Mann-Whitney-U test with the Bonferroni correction was used for statistical analysis. The statistical significance level is $p < 0.01$ (**). $n = 3$ biological replicates, with five one-day-old flies per biological replicate (the whole fly was used). The error bars represent standard deviations.

The staining on the samples from homozygous *Naam*^{MI12364} mutant larvae with NOMPC and *iav* antibodies demonstrated disrupted channel localization (Figure 31). The HRP band signals were also abnormal in the respective larvae compared to the *w*¹¹¹⁸ control larvae (Figure 31), which indicates that *Naam* might be required for the integrity of the lateral chordotonal organ, lch5.

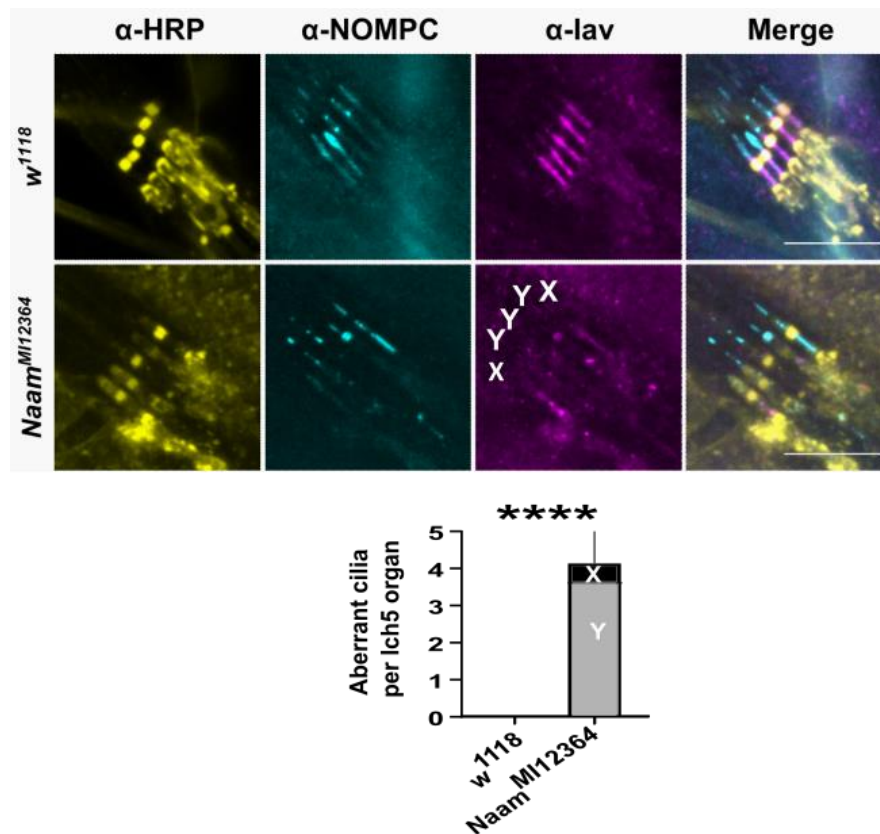


Figure 31. Disrupted channel localization in *Naam* mutant larvae.

In lch5 of *Naam^{M12364}* homozygous larvae, the localization of NOMPC (cyan) and lav (magenta) were disrupted. Anti-HRP labels the neurons (yellow). The presence of the lav signal in the proximal cilium region is marked as “X” and the absence of it as “Y”. Scale bar: 10 μ m. The number of aberrant cilia per lch5 organ is also depicted (numbers of lch5 = 10). Mann-Whitney-U test was used for statistical analysis **** ($P \leq 0.0001$).

Plotting (the existing) signal amplitudes of NOMPC, lav, and HRP along the longitudinal neuronal axis showed the same pattern as in *w¹¹¹⁸*, control flies, however, with a higher deviation from the mean (Supplement Figure 80).

1.2.11. Apoptosis assay

External nicotinamide application on *Drosophila* larvae has an agonistic effect on the TRPV channel activity (Upadhyay et al., 2016), and prolonged TRPV channel activation causes cell death in TRPV1-expressing HEK cells (Han et al., 2007) and *C. elegans* OLQ and uv1 cells (Upadhyay et al., 2016). Indicating from the previous data in this thesis (Figure 16, Figure 18), nicotinamide levels might be raised in the homozygous *Naam* mutant flies. Elevated nicotinamide levels could induce prolonged activation of the

TRPV channels. I tested for the potential cell death in the JO neurons, expressing the respective channels.

To test for apoptosis, I performed TUNEL stainings, which detect double DNA strand breaks during apoptosis. In one day old *Naam*^{MI12364} and *Naam*^{MI12364}-*Gal4* flies, no signal of (already occurred) apoptosis was observed in JO cells (Figure 32). This finding is consistent with the absence of apoptosis in nicotinamide or nicotinic acid-treated *w*¹¹⁸ (Figure 33). Thus apoptosis cannot be the cause of hearing loss in the *Naam* mutant flies.

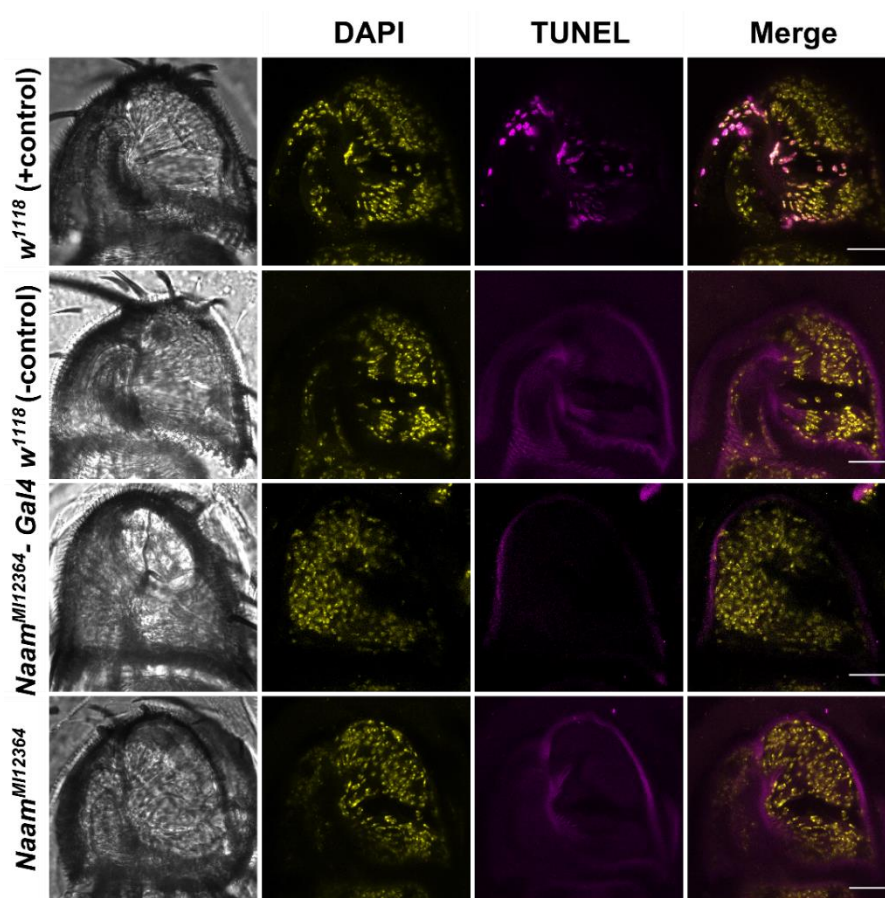


Figure 32. Absence of apoptosis in *Naam* mutant flies.

TUNEL assay for apoptosis detection was used. This assay demonstrated no apoptosis signal (magenta) in *Naam* mutants and *w*¹¹⁸-negative control samples. The *w*¹¹⁸-positive control sample was treated with endonuclease, DNase I, before TUNEL staining. DAPI labels nuclear DNA (yellow). Scale bars: 20 μ m.

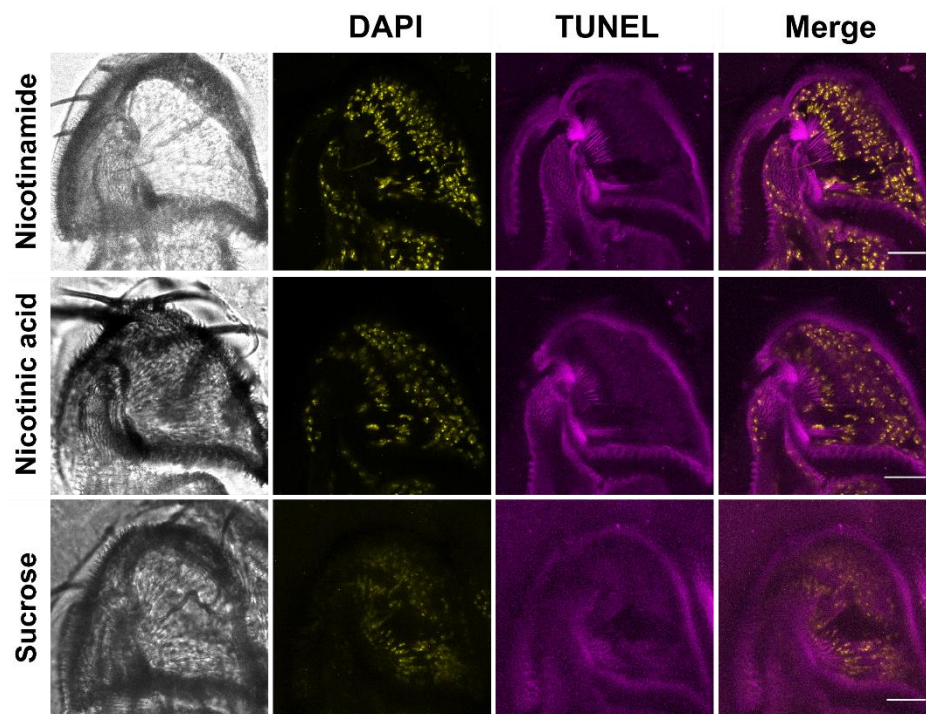


Figure 33. Absence of apoptosis in nicotinamide or nicotinic acid-treated w^{1118} . TUNEL assay for apoptosis detection was used. This assay demonstrated no apoptosis signal (magenta) in w^{1118} flies treated with 1 % sucrose, 10 mM nicotinamide, or 10 mM nicotinic acid. DAPI labels nuclear DNA (yellow). Scale bars: 20 μm .

1.2.12. Altered mitochondrial features in *Naam* mutant flies

The attempts to recover the hearing perception in the *Naam* mutant flies by increasing NAD^+ levels were not successful (Figure 19 and Figure 20). This observation indicates that the hearing defect in the respective flies is not solely due to the reduction in the NAD^+ levels. Given that disrupted glycolysis but not mitochondrial dysfunction is the underlying cause of gonad developmental delay in *C. elegans pnc-1* mutant (Wang et al., 2015), looking into mitochondrial features could lead to a better understanding of the NAAM function in hearing. Electron microscopy images were taken by Nicola Schwedhelm-Domeyer and Hanna Pies. Analyzing these data from *Naam*^{MI12364} compared to w^{1118} , both at one day old, demonstrated a minor but significant reduction in JO mitochondria diameter and area with increment in mitochondrial number (Figure 34).

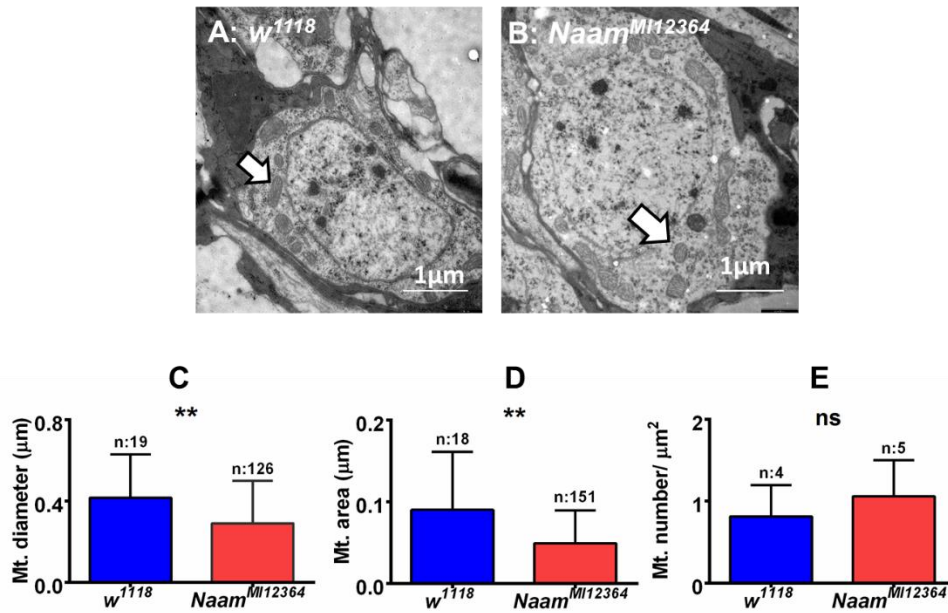


Figure 34. Altered mitochondrial features in *Naam* mutant flies.

Electron microscopy data demonstrated reduction in JO mitochondrial diameter (C) and area (D) with increment in mitochondrial number per μm² (E) in *Naam^{M12364}* mutant (B) compared to *w¹¹¹⁸* control (A) flies. Mann-Whitney U test was used for statistical analysis. Statistical significances are indicated with ns ($P > 0.05$), ** ($P \leq 0.01$).

1.2.13. Disrupted microtubule acetylation pattern in *Naam* mutant flies

Microtubule acetylation is mediated mostly by *Drosophila* α-tubulin acetylase (dTAT) (Yan et al., 2018), while microtubule deacetylation can be mediated by sirtuins, which is an NAD⁺-dependent enzyme. Using an antibody against acetylated tubulin, I tested the microtubule acetylation pattern in JO neurons. I discovered that in wild-type JO neurons, the acetylation is confined to the distal region and the dendritic inner segment but absent from the proximal cilium region between the two HRP bands (Figure 35). Accordingly, NOMPC in the cilium tips associates with acetylated microtubules, consistent with the situation in larval touch receptors (Yan et al., 2018). Nan-lav channels, by contrast, associate with non-acetylated microtubules in the proximal cilium region, which also harbors axonemal dynein arms.

I also found that the compartmentalized pattern of acetylation is disrupted in *Naam* mutant flies. Unlike in controls, microtubules in the proximal ciliary region were also partly acetylated (Figure 35). The same acetylation phenotype ensued when control flies were treated with nicotinamide, whereby the compartmentalized acetylation pattern was restored when the flies were subsequently kept on sucrose for three hours (Figure

36). The reversibility effect of nicotinamide might indicate the half-life of the nicotinamide that, i. e., maximum after three hours, needs to be replaced.

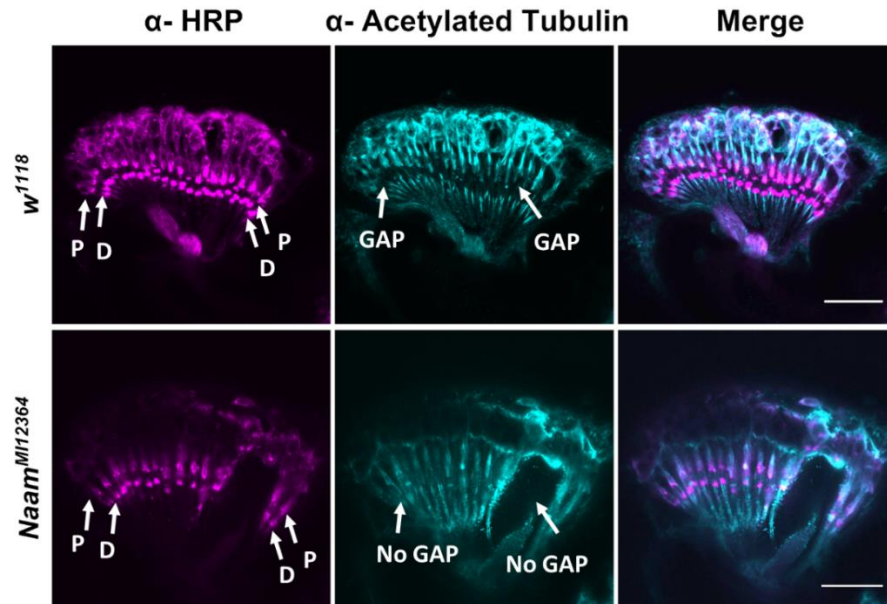


Figure 35. Disrupted tubulin acetylation pattern in *Naam* mutant flies.

Tubulin acetylation pattern (cyan) in the JO of the *Naam*^{M12364} mutant flies (lower panel) is disrupted compare to *w*¹¹¹⁸ control flies (upper panel). Anti-HRP labels the neurons (magenta). Scale bars: 20 μ m.

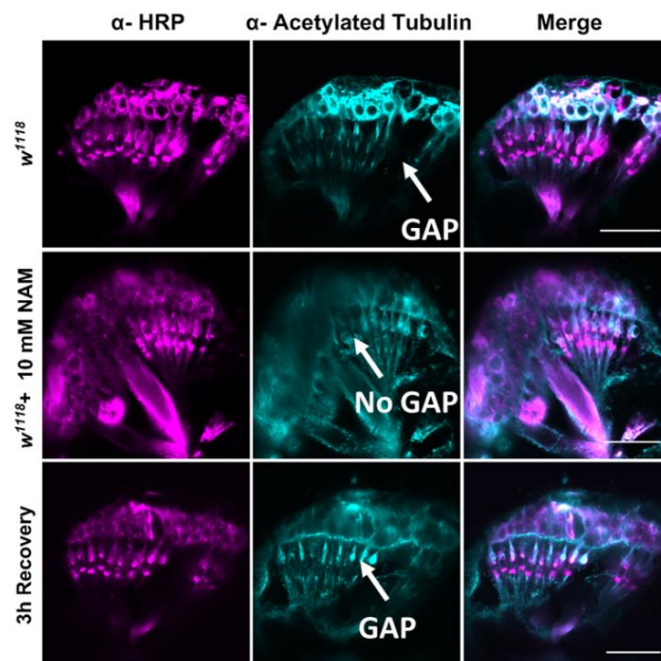


Figure 36. Disrupted tubulin acetylation pattern upon nicotinamide treatment.

Tubulin acetylation (cyan) pattern in *w*¹¹¹⁸ flies was disrupted upon nicotinamide (NAM) treatment. The flies that were fed with 10 mM nicotinamide and further with 1 % sucrose, each for three hours, showed a recovered tubulin acetylation pattern. Like hearing, the acetylation pattern is reversibly disrupted. Anti-HRP labels the neurons (magenta). Scale bars: 20 μ m.

1.3. Discussion

1.3.1. NAAM performance in hearing (modes of action)

NAAM is the first enzyme in the NAD⁺ salvage pathway. In *Drosophila*, the NAAM enzyme affects adult hearing, as the disruption of *JO* reduced the *Naam* expression levels, and the *Naam*^{KG10548} mutant flies displayed a hearing impairment (Senthilan et al., 2012). In this thesis, I used the line *Naam*^{MI12364} for generating intragenic Gal4 (*Naam*^{MI12364}-*Gal4*) and GFP-tagged (*Naam::EGFP::Naam*) lines. I showed that *Naam* is extensively expressed in the antenna with the protein localizing in the JO neurons and scolopale cells. Judging from RT-qPCR results, *Naam*^{MI12364} mutants show significantly reduced *Naam* transcript levels compared to control flies. I used the respective flies as a proper *Naam* KO mutant for hearing assessment, and I showed that the loss of NAAM causes deafness. Since the NAAM enzyme is involved in energy metabolism, observing the hearing impairment in the *Naam* mutant flies was not unexpected. Some studies suggest that the NAAM function might be related to factors other than energy contribution (Vrablik et al., 2009, 2011).

Mutations in *C. elegans pnc-1* (the *Naam* ortholog) result in various phenotypes that can be categorized into three subgroups: 1) one that can be mimicked by adding *pnc-1* substrate (nicotinamide) to WT organisms, 2) one that can be rescued by adding *pnc-1* product (nicotinic acid), and 3) one that is the consequence of both nicotinamide accumulation and lack of nicotinic acid (Vrablik et al., 2009, 2011). For example, the lack of NAD⁺ causes a perturbation in *C. elegans* gonad development, which can be rescued by adding nicotinic acid. *sir-2.1* in *C. elegans*, the ortholog for *D. melanogaster sirt-1* showed reduced activity in *pnc-1* mutants; however, the *sir-2.1* mutation did not lead to perturbation in *C. elegans* gonad development. On the other hand, reduced PME-1/PARP1 activity (NAD⁺ consumers) ameliorates the gonad developmental delay, which leads to the conclusion that NAD⁺ but not the NAD⁺ consumer enzymes are the underlying reason for the gonad developmental delay (Wang et al., 2015).

By feeding experiment in *Drosophila*, I revealed that the application of nicotinamide by itself recapitulates the *Naam* mutant phenotype. Besides, I showed that feeding the *Naam* mutant flies with nicotinic acid or NAD⁺ did not recover the hearing perception, which indicates that the observed phenotype in the respective flies might not be solely due to the deprivation of the nicotinic acid or NAD⁺.

NAD⁺ has different bioavailability in distinct subcellular compartments. Regulation and response to NAD⁺ perturbation are subsequently affected by NAD⁺ compartmentalization (Nikiforov et al., 2011). Despite that, NAD⁺ biosynthetic intermediates can freely move between tissues (Lan and Henderson, 1968), as restoration of NAD⁺ salvage biosynthesis outside the gonad partially rescued the gonad developmental delay (Crook et al., 2014). According to these studies, I assumed that the free movement of the consumed nicotinamide and nicotinic acid in *Drosophila* can reach any tissue including, the chordotonal organs.

I also tried to recover the hearing perception in the *Naam* mutant flies by overexpressing the rate-limiting enzyme in the NAD⁺ salvage pathway, NMNAT. NMNAT also mediates the last step of the NAD⁺ production from nicotinamide riboside. In the *Naam* mutant flies overexpressing NMNAT, the attempts to increase the NAD⁺ levels yet contributed to no recovery in the hearing perception. This observation is consistent with the previous result, in which the treatment of the *Naam* mutant flies with nicotinic acid or NAD⁺ did not recover the hearing perception. In conclusion, the hearing impairment in the *Naam* mutant flies most probably depends on nicotinamide accumulation rather than NAD⁺ reduction.

Drosophila NAAM overexpression, through increasing Sirt2 function, increases life span and protects neurons from oxidative stress (Balan et al., 2008). Mammals have seven sirtuins, NAD⁺-dependent Histone/protein deacetylase with different cellular localizations and functions. Sirtuins play fundamental roles in animals, especially in aging and metabolism, through the deacetylation of various targets (Michishita et al., 2005). One can, here, also consider the effect of *Naam* mutation through sirtuins on hearing (discussion, section 1.3.7.2). Further investigation on *Drosophila* sirtuins can lighten the pathway.

1.3.2. Enzymatically controlled TRPV channel agonist

Besides the involvement of nicotinamide in the NAD⁺ salvage pathway, it is particularly interesting for its agonistic action on the Nan-lav channels (Upadhyay et al., 2016). In 2016, Upadhyay et al. demonstrated that nicotinamide, is an internal agonist of the *C. elegans* OSM-9 and OCR-4, the orthologs of *Drosophila* Nan and lav TRPV channels, and the external application of it on WT *Drosophila* larvae induces a Ca²⁺ influx in the chordotonal neurons (Upadhyay et al., 2016). This study suggests that, in the

absence of NAAM, nicotinamide accumulation leads to a persistent TRPV channel activation, leading to excitotoxic calcium entry into JO mechanoreceptors, similar as caused by the synthetic TRPV channel agonist, pymetrozine (Nesterov et al., 2015). This hypothesis perfectly matches the outcome of feeding flies with nicotinamide substrate. In flies that overexpress *Naam*, more NAAM enzyme activity made them more resistant to the hearing impairment induced by the nicotinamide treatment compared to WT flies. In the respective flies, presumably, the higher rate of nicotinamide conversion leads to less TRPV channel activation.

Feeding *iav*¹ mutant flies with nicotinamide left hearing unaffected. This observation is strong evidence that the auditory effects seen in the *Naam* mutant flies are TRPV-channel dependent. The hearing phenotype in the *Naam* and *iav* double mutant flies, which resembles *iav*¹ hearing defects, reinforces the functionality of nicotinamide through the TRPV channel, and it places *Naam* downstream of NAAM in a signaling pathway.

Nicotinamide is used extensively in stem cell applications for modulating different cellular functions and promoting cell survival via kinase cascades (Meng et al., 2018). Beyond the distinct role of nicotinamide as a TRPV channel agonist, its role as a selective kinase inhibitor, independent of the NAD⁺ pathway must also be taken into consideration.

1.3.3. *Naam* expression pattern

I used two Gal4 drivers, *Naam-Gal4* (Senthilan et al., 2012) and *Naam*^{MI12364}-*Gal4* (this work), for showing the *Naam* expression pattern. The *Naam-Gal4* labeled scolopale and cap cells; however, the *Naam*^{MI12364}-*Gal4* driver showed expression not only in scolopale and cap cells but also in neurons and oenocytes, which involves in fatty acid and hydrocarbon metabolism (Makki et al., 2014). *Naam-Gal4* has a partial *Naam* promoter with extragenic location (Senthilan et al., 2012), whereas the intragenic *Naam*^{MI12364}-*Gal4* driver (this work) has the native *Naam* promoter, mimicking the *Naam* expression pattern. The different expression patterns of the two Gal4 lines might signal the presence of various *Naam* promoters. Using an online promoter prediction tool (Reese, 2001; Madeira et al., 2019), I found many presumable promoters, which need further careful promoter analysis. Studying the promoter(s) of *Naam* might unravel the function of NAAM in the scolopale cells. Knowing the NAAM function in scolopale cells is particularly interesting since the attempts to recover the complete hearing perception

in the *Naam* mutant flies by driving the *Naam* expression with the scolopale driver (*Naam-Gal4*), unlike the neuronal driver (*nompC^{MI12787}-Gal4*), were not successful. This observation indicates that *Naam* expression in neurons is necessary for the proper mechanosensation, whereas the function of NAAM in the scolopale cells is remained to be discovered.

1.3.4. EF-hand domains function in NAAM enzyme

NAAM has two conserved EF-hand domains besides a core isochorismatase-like domain. This implicates that the EF-hand-domains might be an ancestral feature of nicotinamidase (NAAM/PNC1) enzymes. To clarify the function of the EF-hand-domains in the NAAM enzyme, I designed recombinant *Naam* flies with different EF-hand-domains. Driving wild-type *UAS-Naam*, but not *Naam* with mutated or deleted EF-hand domains, with *Naam^{MI12364}-Gal4* (*Naam^{MI12364}-Gal4*>*Naam*), recovered the hearing perception in the *Naam* mutant flies. Moreover, an *in vitro* NAAM assay revealed that NAAM protein with ablated EF-hand domains does not form a complete functional enzyme. The images of the S2 cells expressing *UAS-Naam::GFP* showed cytoplasmic localization of GFP-tagged NAAM, which was disrupted upon EF-hand domains modifications.

C. elegans PNC1, which lacks EF-hand-domains, but not NAAM without (EF-hand domains) or with mutated EF-hand-domains, rescued the hearing defect in the *Naam* mutant flies. This observation suggests that the EF-hand-domains are not needed for the PNC1 function. Aligning NAAM sequences from different species indicates that the N-terminal EF-hand domains might co-occur with a conserved C-terminal sequence (amino acid 322 - 357, especially R328). The C-terminal in a predicted 3D structure from AlphaFold (Jumper et al., 2021) intercedes between the EF-hand domains and the core of the enzyme (Figure 37). This conserved C-terminal is missing in the *C. elegans* PNC1 and other species having nicotinamidase enzyme without EF-hand domains. Possibly the C-terminal sequence silences the enzyme activity when the EF-hand domains are compromised, which could explain why NAAM without (EF-hand domains) or with mutated EF-hand domains cannot rescue the hearing defect in the *Naam* mutant flies. To test this hypothesis, one needs to make *UAS-Naam* constructs with mutated or deleted C-terminal together with mutated or deleted EF-hand domains and assess the functionality of the respective enzyme with *in vitro* NAAM assay or its potential for

recovering the hearing perception in the *Naam* mutant flies. Since the C-terminal in *C. elegans* is absent, PNC1 is active and recovers the auditory perception in the *Naam* mutant flies.

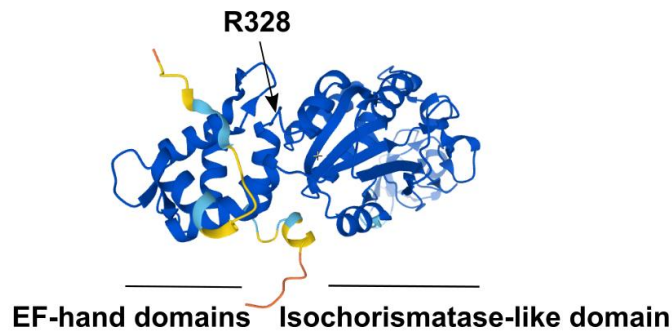


Figure 37. Predicted 3D structure of NAAM.

The image is made by AlphaFold (Jumper et al., 2021). In the image the position of the conserved R328 between the EF-hand and the isochorismatase-like domains is shown.

Following this, I proposed a mechanism for tight TRPV channel modulation that can be supported by the results from this thesis, however, it has not been proved.

In this mechanism, I assumed that: 1) The functional NAAM enzyme is localized in the JO neurons, since the GFP-tagged NAAM enzyme showed localization in the JO neurons, and driving the *UAS-Naam::GFP* expression in the JO neurons (*nompC^{MI12787}-Gal4>Naam::GFP*) rescued the hearing loss in the *Naam* mutant flies. 2) The NAAM enzyme becomes active upon binding to the Ca^{2+} ions. This assumption is solely made to describe the mechanism.

Hypothetically, in conditions with low Ca^{2+} concentration in the JO neurons, Ca^{2+} detaches from the NAAM EF-hand domains and silences the enzyme. The substrate of the enzyme, nicotinamide, in return, will be increased, activating Nan-lav TRPV channels. Following increased TRPV channel activation, the concentration of Ca^{2+} ions would be increased in the JO neurons. The subsequent Ca^{2+} binding to the NAAM EF-hand domains activates the enzyme to consume the agonist of the TRPV channels and reduce the channels hyperactivity (Figure 38).

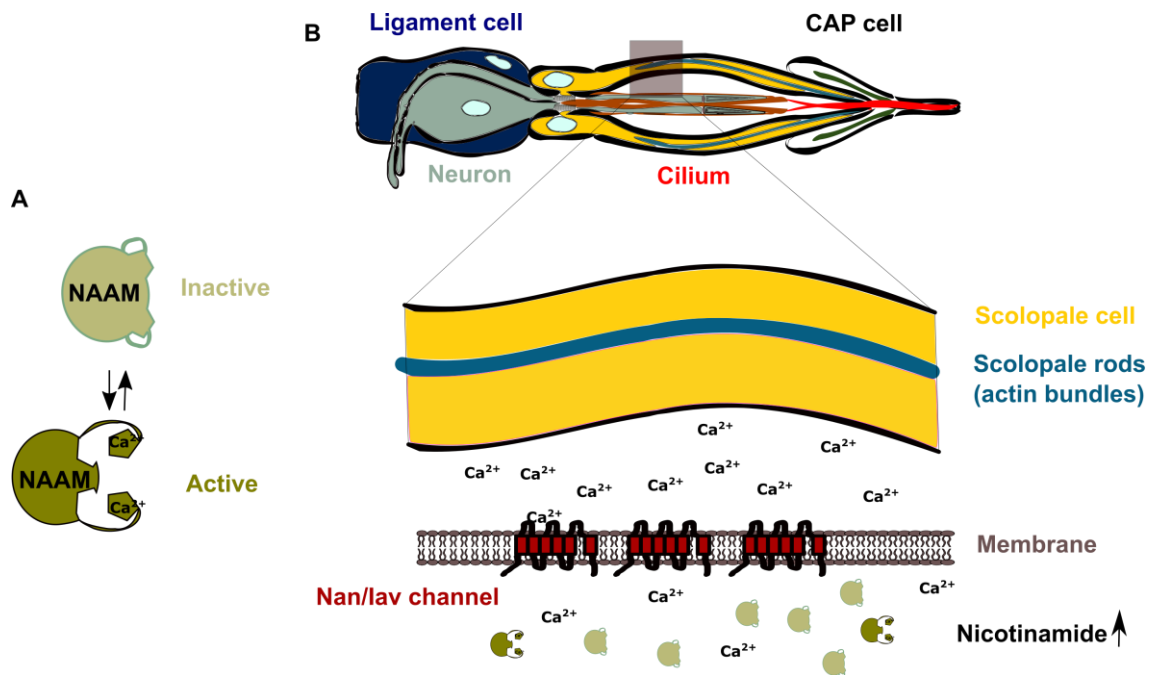


Figure 38. Schematic picture of the proposed NAAM function in the JO.

On the left (A), it is assumed that Ca^{2+} binding to the NAAM EF-hand domains activates the enzyme. (B), in conditions with low Ca^{2+} concentration in the JO neurons, Ca^{2+} detaches from the NAAM EF-hand domains and silences the enzyme. The substrate of the enzyme, nicotinamide (NAM), in return, will be increased, activating Nan-lav TRPV channels. Following increased Nan-lav TRPV channel activation, the concentration of Ca^{2+} ions would be increased in the JO neurons. The subsequent Ca^{2+} binding to the NAAM EF-hand domains activates the enzyme to consume the agonist of TRPV channels and reduce the TRPV channels hyperactivity.

It is also known that TRPV1 (vanilloid receptor 1 in mammals) agonists induce the TRPV1 channel internalization (Liu et al., 2019). In the same way, the nicotinamide might also exert its function by modulating TRPV channels abundance on the membrane.

1.3.5. *Naam* orthologs

The vertebrates' first enzyme in the NAD^+ salvage pathway, NAMPT, has intra- and extracellular functions (NAMPT and NAAM in *Drosophila* have the same substrate). While intracellular NAMPT (iNAMPT) is required for NAD^+ production, the secreted extracellular counterpart (eNAMPT) acts as a cytokine (Galli et al., 2020). Intra- and extracellular functions have also been described for the *C. elegans* PNC-1, which has two secreted and intracellular isoforms. The two PNC-1 isoforms are the outcome of transcription from two different promoters (Crook et al., 2014). According to these studies and the preliminary observation in this work, NAAM might also possess two intra- and

extracellular forms. Furthermore, one can support this hypothesis by observing the extracellular form of NAAM in S2 cells expressing *Naam*.

Despite the importance of the NAD⁺ salvage pathway, the expression of NAMPT in mice (Revollo et al., 2007), NAAM in *Drosophila* (Chintapalli et al., 2007), and PNC1 in *C. elegans* (Vrablik et al., 2009) are not widespread in tissues. These studies indicate that NAMPT, PNC-1 (Crook et al., 2014), and presumably NAAM might function, cell non-autonomously. Investigating the probable function of NAAM in other tissues that do not express NAAM might contribute to a better understanding of the NAAM function in the JO.

1.3.6. NAD⁺ salvage pathway enzymes

Unlike the *Drosophila* NAD⁺ salvage pathway from nicotinamide, that of vertebrates' bypasses nicotinic acid production. Vertebrates can still produce NAD⁺ from nicotinic acid by the Preiss-Handler pathway. The conversion of the NAD⁺ consuming enzymes byproduct, nicotinamide, to nicotinic acid (or NMN in vertebrates) is the actual recycling part of the NAD⁺ salvage pathway.

Unlike *C.elegans pnc-1* or *Drosophila Naam* mutants, the mammalian *Nampt* mutants are lethal (Revollo et al., 2007). This observation indicates that the NAD⁺ production from nicotinamide is playing a vital role in vertebrates, whereas flies without NAAM might still be able to produce an adequate amount of NAD⁺ for survival.

NAPRT, the next enzyme after NAAM in the *Drosophila* NAD⁺ salvage pathway (also the first enzyme in the Preiss-Handler pathway), produces NAMN from nicotinic acid. I used *Naprt*^{MI10235}-*Gal4* flies to show the *Naprt* expression in JO and malpighian tubules (Supplement Figure 81). The respective flies are homozygous lethal. The human ortholog of the *Naprt* gene expresses intra- and extracellular proteins with various functions (Audrito et al., 2020).

NMNAT, the next enzyme after NAPRT (or NAMPT in vertebrates) in the NAD⁺ salvage pathway, has different cellular localizations that are modulated in a condition-dependent manner (Ruan et al., 2015; Todorovic, 2016). In *Drosophila*, through alternative splicing, the expression of the cytoplasmic neuroprotective *Nmnat* variant increases compared to its nuclear counterpart in response to stress (Ruan et al., 2015). The neuroprotection activity of NMNAT is independent of its NAD⁺ synthesis activity (Zhai et al., 2006). Hearing in *Nmnat* mutant flies was impaired, and GFP-tagged NMNAT demonstrated localization in the nuclei of JO mechanoreceptors (Supplement Figure 82 and Figure 83). Many available *Nmnat* mutant flies are homozygous lethal.

Unlike the homozygous lethal *Naprt* and *Nmnat* mutant flies, the homozygous *Naam* mutant flies are viable. This observation indicates that the energy metabolism in the homozygous *Naprt* and *Nmnat* mutant flies is heavily disturbed, which causes death. However, homozygous *Naam* mutant flies without having the first step of the NAD⁺ salvage pathway can still produce NAD⁺ from nicotinic acid or NR.

Besides NAD⁺ synthesis, NAMPT, NAPRT, and NMNAT demonstrate a second function, which might suggest a probable secondary function for NAAM, as well (Table 8).

Table 8. NAD salvage pathway enzymes.

† This step is in the Preiss-Handler pathway and absent from the mammalian NAD⁺ salvage pathway.

* The presence of other functions besides NAD⁺ synthesis.

	NAM to NMN (H) NAM to NA (<i>D</i>)	† NA to NAMN	NMN to NAD NAMN to NAAD	NAAD to NAD
	NAMPT/NAAM	NAPRT	NMNAT	NADSYN
Human (H)	Intra- and extracellular (adipokine*) (Galli et al., 2020)	Intra- and extracellular (adipokine*) (Audrito et al., 2020)	Cytoplasm, nucleus, mitochondria (Todorovic, 2016)	predicted in the cytoplasm (Gaudet et al., 2011)
<i>Drosophila</i> (<i>D</i>)	Antenna, oenocytes Intra- (cytoplasm), and extracellular (preliminary data)	Malpighian tubules and JO, predicted in the cytosol (Gaudet et al., 2010)	Cytoplasm and nucleus (Neuroprotection*) (Ruan et al., 2015)	predicted in the cytoplasm (Gaudet et al., 2010)

1.3.7. Additional *Naam* mutant characteristics

1.3.7.1. Absence of apoptosis in *Naam* mutant flies

Prolonged activation of human TRPV channels causes cell death (Reilly et al., 2003; Ryskamp et al., 2011), as exemplified by excess TRPV1 function, which disrupts microtubule integrity and causes cell death (Han et al., 2007). Likewise, cell death arises

from nicotinamide accumulation, in *C. elegans* mechanosensory neurons, through TRPV channel activation (Upadhyay et al., 2016). In *C. elegans*, the excitotoxic death can be suppressed by LET-23 EGFR through LET-60 Ras/MAPK and phosphatidylcholine biosynthesis pathways (Crook et al., 2016). In this study, the TUNEL assay did not show any signal of (already occurred) apoptosis in the *Naam* mutants and the nicotinamide-fed flies. One can look into the functionality of the probable similar pathway to the one in *C. elegans* and test whether the respective pathway suppresses cell death in *Naam* mutant flies.

1.3.7.2. Disrupted microtubule acetylation pattern in *Naam* mutant flies

In addition to the hearing loss, *Naam* mutation is also affecting the microtubule acetylation pattern. A compartmentalized microtubule acetylation pattern in fly auditory neurons was observed for the first time. However, the existence of different domains within (axonal) individual microtubules was already demonstrated by immunoelectron microscopic studies (Ahmad et al., 1993). Acetylation of stable microtubules protects them from mechanical stress, rendering them softer and more resistant to damage induced by mechanical bending (Janke and Montagnac, 2017). Microtubule acetylation has been documented for various mechanosensory cells (Chalfie and Au, 1989; Akella et al., 2010) and, in *Drosophila*, it has been documented for touch-sensitive larval mechanosensory neurons (Yan et al., 2018). In the respective neurons, acetylation facilitates the gating of the transient receptor potential NOMPC (=TRPN1), a mechanotransduction channel. This channel tethers to microtubules with its amino-terminal ankyrin repeat domains to convey mechanical stimuli towards the channel pore, mechano-gates the channel (Cheng et al., 2010).

In cilium tips, where NOMPC occurs (Lee et al., 2010), microtubules are acetylated, whereas, in the proximal cilium region, where Nan-lav channels sit (Gong et al., 2004), they are not. I also identified NAAM as a protein, is required for this compartmentalized acetylation. If NAAM is absent, the microtubules are acetylated throughout.

Altered acetylation patterns also result if the flies are transiently treated with nicotinamide, yet here the effects are reversible. Nicotinamide, in addition to activating TRPVs, might independently affect microtubule acetylation through sirtuin signaling since sirtuin is an NAD⁺ dependent deacetylase. Testing whether Nan-lav interacts with microtubules using pull-downs would reveal more. This would be particularly interesting

as there is a rumor that Nan-lav channels can be mechanoactivated, which, analogous to NOMPC, might require microtubules (Zhang et al., 2015). It might be calcium entry through Nan-lav that modulates microtubule acetylation, similar as was presumed for mammalian TRPV1 (Goswami and Hucho, 2008).

Acetylation is one among many post-translational microtubule modifications (Hammond et al., 2008). One can assess other modifications (namely glutamylation, glycylation, phosphorylation, and palmitoylation) and their probable function in JO.

1.3.7.3. Mitochondrial dynamics in the *Naam* mutant flies

Mitochondria can adapt to the cellular environment not only via changes in their function but also through modifications in their structures and morphology, which is known as mitochondrial dynamics (Tilokani et al., 2018). Several studies revealed that the NAD⁺ levels decline with age and diseases (Liu et al., 2008; Imai and Guarente, 2014). There is a link between the NAD⁺ level and mitochondrial dynamics. Reduction in NAD⁺ level deteriorates mitochondrial function while recovering the NAD⁺ level via administration of NAD⁺ precursors like NMN. (Klimova et al., 2019) or NR (Schöndorf et al., 2018) can restore mitochondrial function. Deregulated glycolysis but not impaired mitochondrial function is an underlying cause for gonad developmental delay in *C. elegans pnc-1* mutant (Wang et al., 2015). Unlike the gonad developmental delay in *C. elegans*, the hearing defect in the *Naam* mutant flies is not solely due to the presumed reduction in the NAD⁺ level, since the attempts to restore hearing defect in the *Naam* mutant flies by increasing NAD⁺ levels were not successful. The *Naam* mutations, however, can cause changes in the mitochondrial features through the disrupted NAD⁺ salvage pathway. In this study, electron microscopy data revealed increased mitochondrial numbers with reduced diameter and area in the JO of the *Naam* mutant flies compared to wild-type flies. Further evaluation of the JO mitochondrial function is mandatory to interpret the link between metabolism, the *Naam* mutation, and the TRPV channels modulation.

1.4. Conclusion

In this study, I showed that Nan-lav TRPV channels do not function properly without NAAM. NAAM is the first enzyme in the NAD⁺ salvage pathway, and, in this thesis, I have demonstrated an additional function of NAAM in hearing. Remarkably, I provide a possible model to explain the observed phenotypes. I proposed that, in high Ca²⁺ concentration, Ca²⁺ binding to the NAAM EF-hand domains activates the enzyme. The active enzyme consumes nicotinamide (the endogenous agonist of the TRPV channels), makes TRPV channels inactive, and in this way modulates the activity of the TRPV channels.

Probably there is a link between JO energy level and the mechanical amplification in hearing. When energy levels are low, high NAD⁺ levels enable the NAD⁺ consuming enzymes to produce more nicotinamide (TRPV channel agonist) and regulate the hearing sensitivity according to the energy availability in the JO.

While a very interesting and fundamental modulator of the JO mechanical amplification has been revealed in this study, a lot has to be done to shed light on the exact mechanism of NAAM in the JO, particularly the neuronal signals.

2. Chapter II. *Drosophila* GAP43 like (*igl*) in auditory neuron cilia

2.1. Introduction

Growth-associated protein 43 (GAP43), also known as F1, neuromodulin, B-50, G50, and pp46, is a protein in humans that is abundant in neuronal growth cones (Holahan, 2017). GAP43 contributes to neurite outgrowth, plasticity, and nerve regeneration after injury. With Ca^{2+} increment, calmodulin detaches from the GAP43 IQ motif (calmodulin-binding motif (Cheney and Mooseker, 1992; Porter et al., 1993; Xie et al., 1994)) and binds to Ca^{2+} . The Ca^{2+} /calmodulin complex, via LIM kinase (LIMk) and Ca^{2+} /calmodulin-dependent protein kinase II (CamKII), indirectly enhance neurite outgrowth. However, phosphorylated GAP43, which is mediated by protein kinase C (PKC), directly contributes to neurite outgrowth via interaction with phosphatidylinositol 4, 5-bisphosphate (PIP2). The interactions of presynaptic proteins with phosphorylated GAP43 lead to enhanced plasticity and facilitated vesicle exo- and endocytosis (Figure 39) (Holahan, 2017).

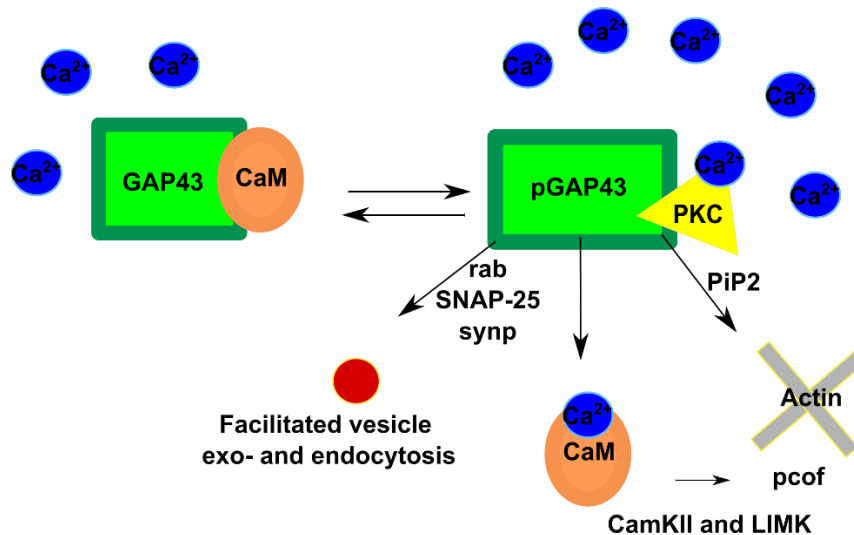


Figure 39. GAP43 mode of action.

Upon Ca^{2+} increment, calmodulin (CaM) leaves the IQ motif in GAP43 and binds to Ca^{2+} . The Ca^{2+} /calmodulin complex through LIM kinase (LIMk) and Ca^{2+} /calmodulin-dependent protein kinase II (CamKII) phosphorylates cofilin (pcof), which indirectly leads to neurite outgrowth. On the other hand, phosphorylated GAP43 (pGAP43) by protein kinase C (PKC) directly leads to neurite outgrowth via interaction with phosphatidylinositol 4, 5-bisphosphate (PIP2). The interaction of pGAP43 with synaptophysin (synp), rabatin (rab), and synaptosomal-associated protein 25 (SNAP-25) facilitates vesicle exo- and endocytosis and subsequently high plasticity.

GAP43 has two transcripts (splice variants). ‘The IQ motif in all vertebrates’ *GAP43* is located in a conserved region. *GAP43* is a membrane-associated protein (Meiri and Gordon-Weeks, 1990) through palmitoylation of two cysteine residues at its amino terminus (Zuber et al., 1989). In murine *GAP43*, serine⁴¹ is phosphorylated by PKC (Apel et al., 1990). This modification has important functional consequences (Benowitz and Routtenberg, 1987) that need to be conserved. Phosphorylation of *GAP43* at serine⁴¹ introduces negative charges at a position close to the calmodulin-binding site in *GAP43* that disrupt calmodulin/*GAP43* binding interaction. In this way, *GAP43* can release calmodulin locally in the neurons (Chapman et al., 1991).

The overall similarity in amino acid composition and similar biochemical activity suggest vertebrate *GAP43* as a functional homolog to invertebrate *GAP43* like (IGL) in *Drosophila* (Neel and Young, 1994). Calmodulin-binding domain, protein kinase C (PKC) phosphorylation site, and membrane association of *GAP43* (Alexander et al., 1988; Zuber et al., 1989; Apel et al., 1990) that mapped to its first 57 residues in a highly conserved region endorse *GAP43* as a functional homolog of IGL (Neel and Young, 1994) (Figure 42). Vertebrate *GAP43* also share neuronal expression pattern with *igl* (Neel and Young, 1994).

The data from the FlyBase website showed that the *igl* gene in *Drosophila* encodes three transcripts (Figure 40) and two polypeptides (Figure 41) (Larkin et al., 2021). The two proteins of IGL are 25 and 13 kDa.

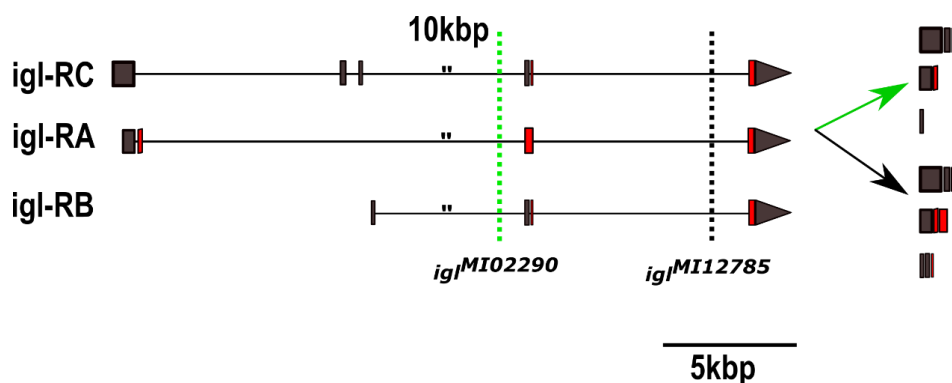


Figure 40. *igl* transcripts and the position of two MiMIC insertions.

The three *igl* transcripts and the position of two MiMIC insertions (dotted lines) in the introns of *igl* are depicted. The MiMIC lines were used for making Gal4 lines and GFP-tagged proteins. The MiMIC cassettes have stop codons that should stop the spliceosome. The truncated transcripts have been depicted for *igl*^{MI02290} in green and *igl*^{MI12785} in black.

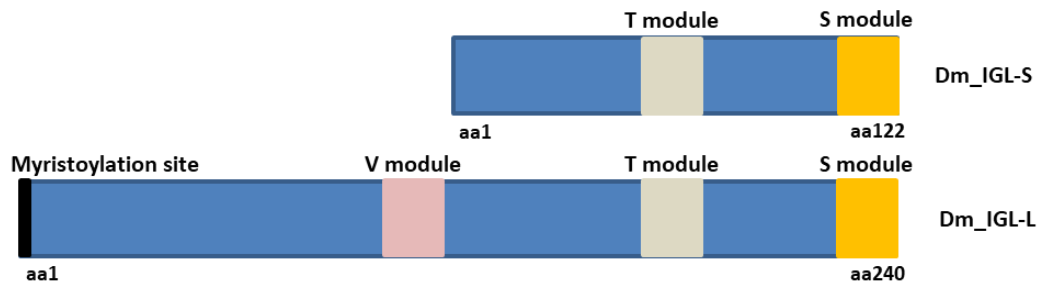


Figure 41. Two IGL translated proteins.

Small (S) and large (L) IGL proteins contain two and three IQ motifs (V, T, and S modules), respectively. These modules are calmodulin-binding motifs containing amino acids, isoleucine (commonly), and glutamine (invariably).

IGL has been identified as a *Drosophila* calmodulin (D-CaM) binding protein by an interaction assay in yeast using IGL sequences as bait (Yamanaka et al., 1987). IGL has three IQ modules, the three of which have independent calmodulin binding capacity (Neel and Young, 1994) with sensitivity to serine phosphorylation of the modules (Alexander et al., 1987). In *Drosophila*, serine in the S module (serine²²⁷) is the target of phosphorylation. The phosphorylated serine²²⁷ regulates the calmodulin/IGL interaction similar to the function of the phosphorylated serine⁴¹ in GAP43 (Neel and Young, 1994). In IGL-L, the myristoylation of the second glycine anchors it to the membrane (Neel and Young, 1994), similar to the function of the cysteine palmitoylation in GAP43 (Figure 42). The alignment of IGL-L protein with human Neurogranin (NRGN) and GAP43 revealed 53 % and 37 % similarity, respectively, due to the conserved IQ motifs (Figure 42).

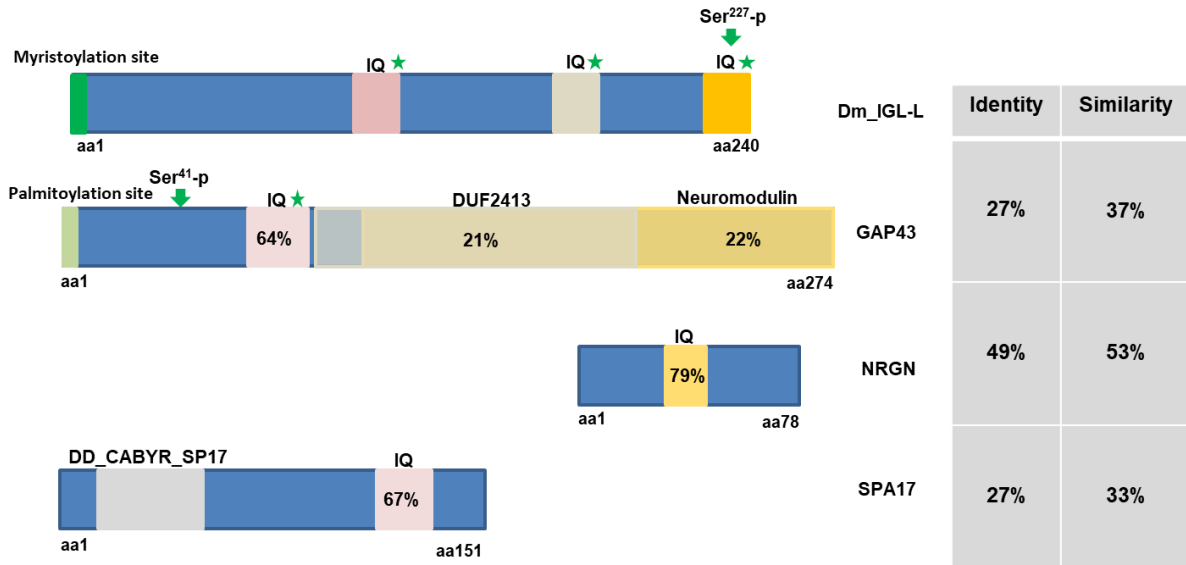


Figure 42. IGL and its human orthologs.

The motifs of IGL protein and the human orthologs of IGL (GAP43, NRGN, and SPA17) have been depicted. The identity value of each motif to the IGL is written in the respective motif boxes. The identity and similarity value of each protein compared to IGL is listed in the table (protein alignment made by DIOPT Version:8 (Hu et al., 2011)). Unlike the absence of significant sequence homology between IGL and GAP43, the conserved IQ motifs, membrane attachment sites (myristoylation and palmitoylation), and phosphorylated serines (Ser²²⁷-P and Ser⁴¹-P) endorse IGL as GAP43 functional homolog.

The expression of *igl* starts in embryos older than 12 hours and is restricted to the nervous system (Neel and Young, 1994). This expression pattern indicates that *igl* has no function in neurite outgrowth, while they are already completed before the *igl* peak mRNA expression time (Campos-Ortega and Hartenstein, 2013). It may offer that it involves in establishment or maintenance of synaptic contacts (Neel and Young, 1994).

The screening by Natascha Zhang (unpublished data) that is based on specific JO neuronal ablation (AB or CE) and further analysis of gene expression profiles in the 2nd antennal segment cells is shown for the *igl* gene in Table 9. In the table, numbers representing *igl* gene expression after AB, CE, or all JO neuronal ablation (red columns), compared to the WT flies (blue columns). The expression level of *igl* is decreased after all JO neuronal ablation, indicating its expression dependency on the presence of the JO neurons (Table 9).

While this gene has shown abundant expression in the nervous system, its role in *Drosophila* hearing as a novel bona fide function is the focus of this chapter.

Table 9. Screening result for *igl* gene

Gene_ID	AB Neurons ablated			CE Neurons ablated			ALL Neurons ablated			<i>w¹¹¹⁸</i>		
<i>igl</i>	6348	5610	4621	9542	2623	6405	2638	1851	2224	12301	2975	6328

2.2. Results

2.2.1. *igl* expression pattern

The data from the FlyBase website demonstrated that the *igl* gene has three transcripts (*igl-RA* (2.5 kb), *igl-RB* (1.9 kb), and *igl-RC* (2.7 kb)) and two unique polypeptides (25, 13 kDa) (Larkin et al., 2021). The transcript, *igl-RA*, encodes the larger IGL protein (IGL-L, 25 kDa), whereas the other two *igl* transcripts, *igl-RB*, and *igl-RC*, encode the smaller IGL protein (IGL-S, 13 kDa) (Neel and Young, 1994; Larkin et al., 2021). The two IGL proteins have distinct features. Despite the differences in the length of the proteins, they have different numbers of calmodulin-binding sites (three in IGL-L versus two in IGL-S). Besides, IGL-L but not IGL-S has a membrane attachment site. It seems that the two IGL proteins have different functions. For understanding the contribution of the respective proteins in *Drosophila* hearing, I analyzed the expression levels of *igl* transcripts. It was shown that the *igl-RA* transcript is virtually absent from the fly's head (Neel and Young, 1994). By RT-qPCR on samples from whole flies, whole flies without antennae, and antennae, I confirmed that the shortest transcript of *igl*, *igl-RB*, is the most abundant transcript in the whole flies and antennae, whereas the *igl-RA* is confined to the antenna (Figure 43).

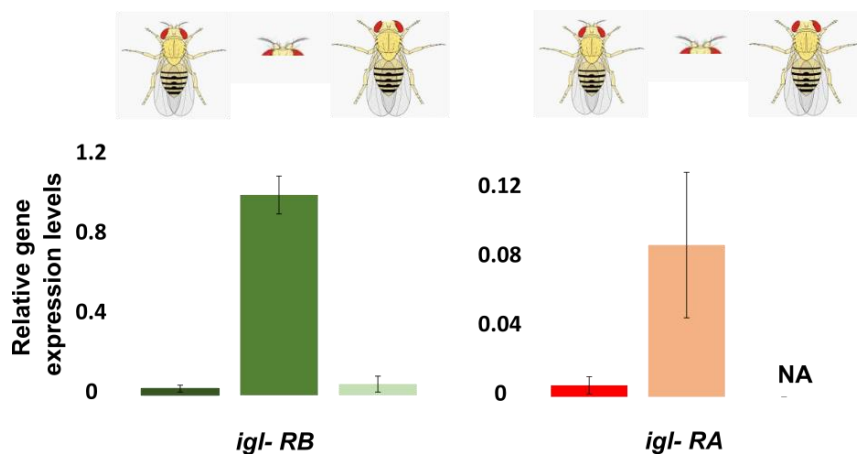


Figure 43. *igl* transcripts levels.

Levels of *igl* transcripts (*igl-RA* and *igl-RB*) in whole flies, whole flies without antennae, and antennae demonstrate *igl-RB* as the most abundant transcript in samples from the whole flies and antennae (~10 times more than *igl-RA*). The absence of *igl-RA* in samples from the whole flies without antennae demonstrates that *igl-RB* is the transcript with a more widespread expression pattern, and *RA* is restricted to the antenna. *igl-RC* expression presented a very low level only in the antenna (not shown). One-day-old *w¹¹⁸* flies were used for this assessment with $n = 3$ biological replicates and two sets of primers for each transcript. Five complete flies, five complete flies without antennae, and hundred antennae were used in each biological replicates. NA = Not Applicable. The error bars represent standard deviations.

For analyzing the expression pattern of the *igl* gene and the localization of the IGL proteins, I made intragenic Gal4 and GFP-tagged lines from flies carrying MiMIC cassettes, MI02290 and MI12785, using the Double Header tool (materials and methods, section II.V). The two MiMIC cassettes are inserted in two different introns of *igl*.

I made *igl Gal4* drivers from both *igl*^{MI12785} and *igl*^{MI02290} flies (Figure 40). The *Gal4* lines might demonstrate the expression pattern of the three *igl* transcripts without distinction (Table 10).

I used *igl*^{MI02290} flies for tagging IGL-L. Based on the position of the MiMIC cassette (Figure 40), exchanging MI02290 with a GFP cassette, it would be hard to predict having an N-terminal GFP-tagged IGL-S protein. First, the GFP cassette has no immediate start codon and Kozak sequence. There is an in-frame methionine in the GFP that comes on the 78th codon, meaning that even if it codes for a protein, it will lack the N-terminal 78 amino acids of GFP and is ineffective. Second, the remainder of the UTR will be in the coding region that can cause either frameshift or early stop codons. Unlike IGL-S, GFP-tagged IGL-L would be the outcome of exchanging MI02290 cassette with GFP since the cassette is located after the first exon of *igl-RA* (Figure 40). The GFP line generated from *igl*^{MI12785} was used for tagging the two IGL proteins without distinction (IGL-S and IGL-L) (Table 10).

Table 10. Possible *igl GAL4* and *GFP* lines

GAL4 lines		GFP lines	
<i>igl</i> ^{MI12785} - <i>Gal4</i>	<i>igl-RA, RB, RC</i>	<i>igl</i> ^{MI12785} - <i>GFP</i>	IGL-L and IGL-S
<i>igl</i> ^{MI02290} - <i>Gal4</i>	<i>igl-RA, RB, RC</i>	<i>igl</i> ^{MI02290} - <i>GFP</i>	IGL-L

Using the generated *igl GAL4* lines from *igl*^{MI12785} and *igl*^{MI02290} (not shown) for driving the expression of the cytoplasmic GFP, *20XUAS-6XGFP*, (*igl*^{MI12785} or *igl*^{MI02290}-*Gal4*>*6XGFP*), I demonstrated *igl* expression in the neurons of the chordotonal organ in larval lch5 and adult JO (Figure 44). The same results were obtained from both *igl Gal4* drivers.

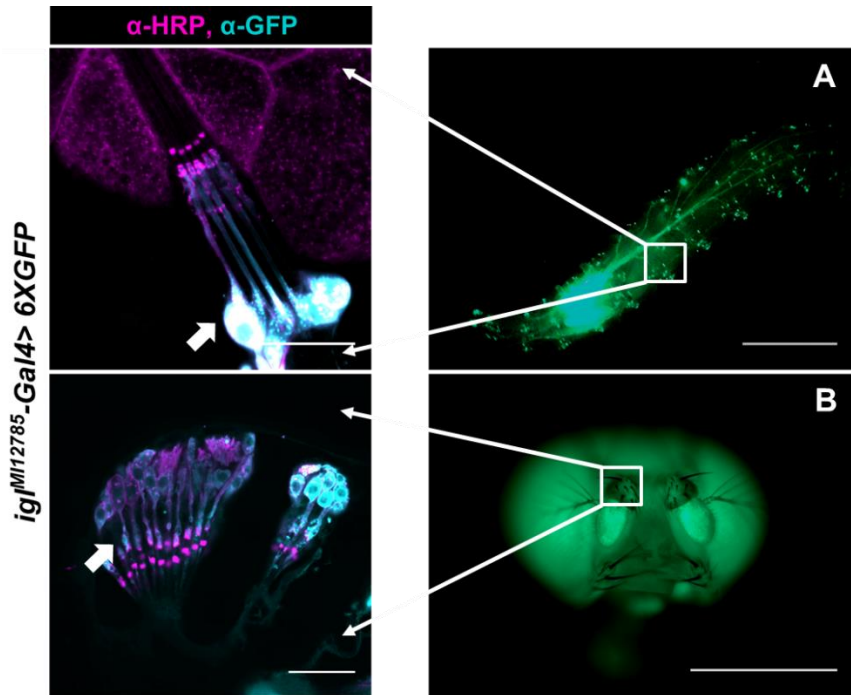


Figure 44. *igl* expression pattern.

Driving 20XUAS-6XGFP with *igl*^{MI12785}-Gal4 (*igl*^{MI12785}-Gal4>6XGFP) or *igl*^{MI02290}-Gal4 (*igl*^{MI02290}-Gal4>6XGFP) (not shown) (cyan) labels chordotonal neurons both in the larval Ich5 (A) and the adult JO (B). Anti-HRP labels the neurons (magenta). Scale bars: 20 μ m in the left panels and 1 mm in the right panels.

Driving the membrane-tethered GFP, *UAS-mCD8::GFP*, with the *igl* Gal4 drivers, (*igl*^{MI12785} or *igl*^{MI02290}-Gal4>*mCD8::GFP*), labeled the optic lobes and mushroom bodies in the *Drosophila* brain (Figure 45). The same results were obtained from both *igl* Gal4 drivers. Observing *igl* expression in the brain is consistent with the study that showed limited *igl* expression in the cells of the central and peripheral nervous system, including the brain (Neel and Young, 1994).

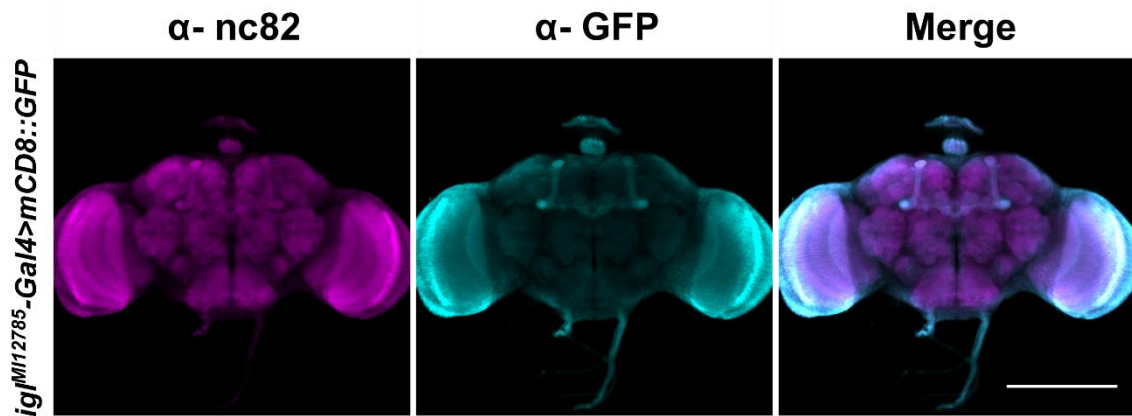


Figure 45. *igl* expression pattern in *Drosophila* brain.

Driving *UAS-mCD8::GFP* with *igl^{M12785}-Gal4* driver (*igl^{M12785}-Gal4>mCD8::GFP*) demonstrated intensive expression in the optic lobes and mushroom bodies (cyan). The neuropil is counterstained with α -nc82 that labels synapses (magenta). Scale bar: 200 μ m.

2.2.2. IGL cellular localization

I demonstrated *igl* expression in the neurons of the chordotonal organ (Figure 44). Moreover, for showing the localization of the IGL proteins, I used the GFP lines that were made from the *igl* MiMIC flies (Table 10). By tagging the native IGL proteins with GFP, I found that, within JO and larval chordotonal neurons, IGL-L protein is confined to the cilia (Figure 46), whereas IGL-S has a more widespread pattern. The IGL-L localization in the cilia suggests that *igl* constitutes a novel cilium compartment gene.

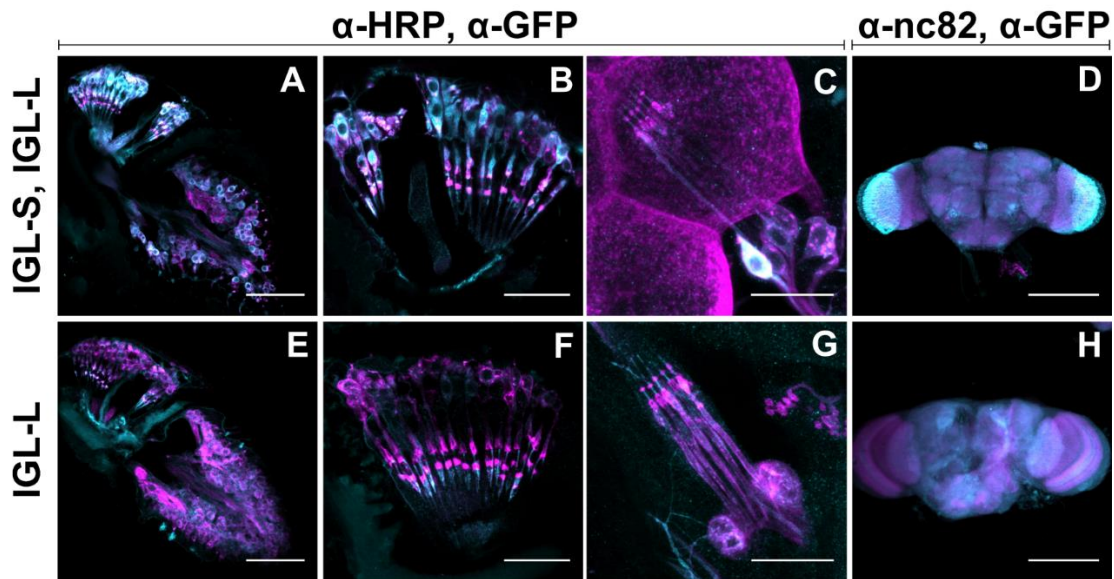


Figure 46. Cellular localization of IGL in JO and Ich5.

IGL localization (cyan) in the antenna (A, E), the JO (B, F), the Ich5 (C, G), and the brain (D, H) demonstrated that IGL-L (E, F, G, and H) has a more restricted localization compared to IGL-S. Anti-HRP labels the neurons (A-C and E-G in magenta). The neuropil is counterstained with α -nc82 that labels synapses (D and H in magenta). Scale bars: 40 μ m in panels A and E, 20 μ m in panels B, F, C, and G, 200 μ m in panels D and H.

2.2.3. *igl*, a cilium compartment gene

2.2.3.1. Conserved RFX DNA binding motif in *igl* promoter

RFX is a transcription factor under the *ato* control (Cachero et al., 2011) that regulates ciliogenesis core genes. To test the possibility that *igl* is a cilium compartment gene, I screened for an RFX DNA binding motif in the *igl* promoter. Indeed, such motif is present and conserved across *Drosophila* species (Figure 47). Besides the RFX DNA binding motif in the *igl* promoter, I also found a conserved RFX DNA binding motif in GAP43, the human ortholog of *igl* (Figure 48). The comparison of the RFX DNA binding motif between mammalian GAP43 and *Drosophila igl* is shown in Figure 49, made by (<http://weblogo.berkeley.edu/logo.cgi>).

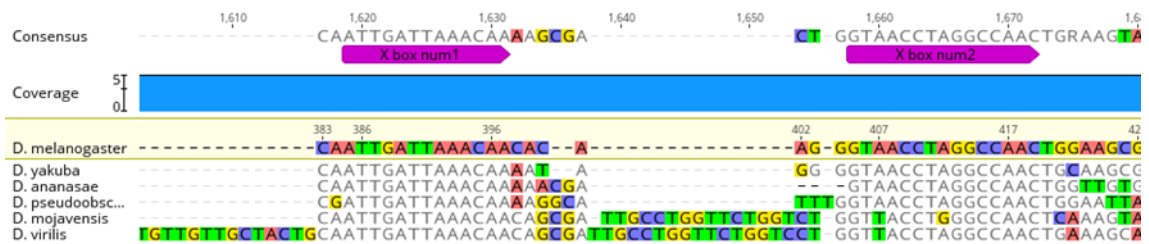


Figure 47. RFX DNA binding motif (X-box promoter motif) conservation in *Drosophila* species. *D. melanogaster* (NM_057712.5), *D. yakuba* (XM_002091366.2), *D. ananasae* (XM_001958894.3), *D. pseudoobscura* (XM_001360607.4), *D. mojavensis* (XM_002006116.3), and *D. virilis* (XM_002049654.3) in their *igl* promoter regions were aligned for a conservation assessment of the X-box motif. For clarity, only six *Drosophila* species are depicted. The sequence closely resembles those found in the promoters of *nan* and *iav*, the two known ciliary genes (Kim et al., 2003; Gong et al., 2004). The picture was made in Geneious Prime 2020.1.1.

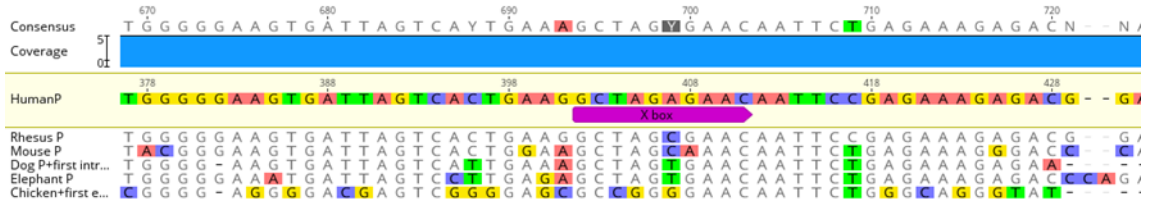


Figure 48. RFX DNA binding motif (X-box promoter motif) conservation in vertebrates. A conserved RFX DNA binding motif in human, mouse, elephant, chicken, dog, and rhesus *GAP43* promoters are depicted. The picture was made in Geneious Prime 2020.1.1.

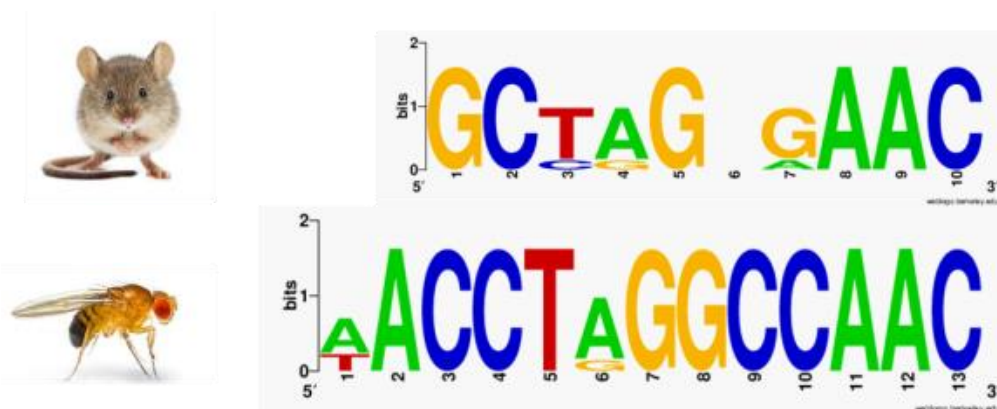
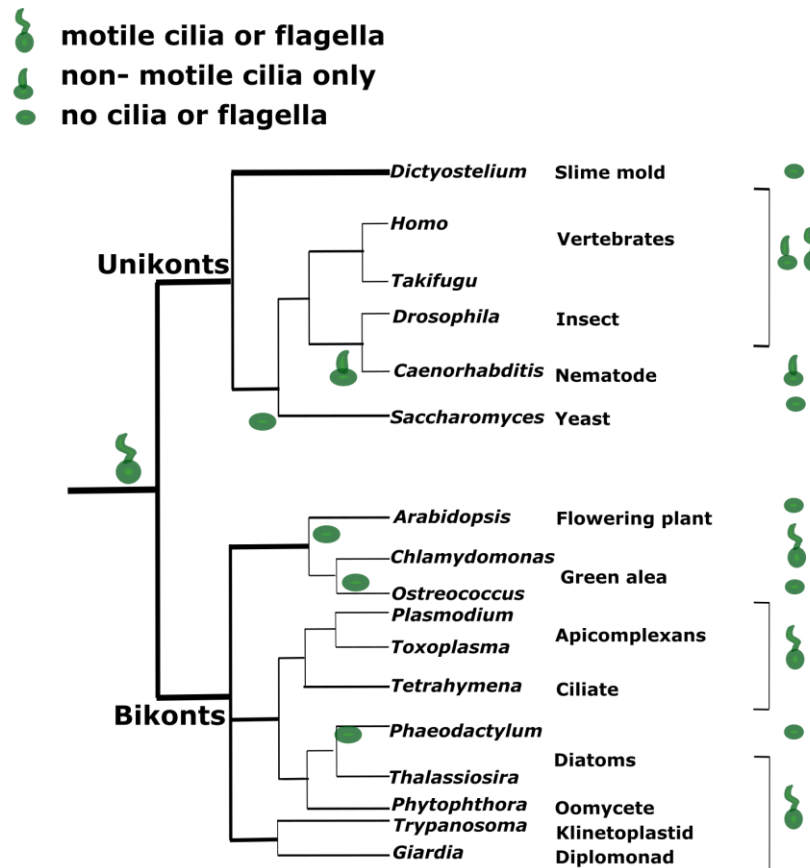


Figure 49. Comparison of X-box motifs in mammalian *GAP43* and *Drosophila igl*. Made by (<http://weblogo.berkeley.edu/logo.cgi>)

2.2.3.2. IGL conservation in ciliated eukaryotes

Additional evidence for *igl* as a cilium compartment gene comes from the IGL BLAST I performed in ciliated and non-ciliated eukaryotes. The BLAST results demonstrated that IGL co-occurs with intraflagellar transport (IFT) and is present in a large group of ciliated eukaryotes (Figure 50).



	IGL Blast P	IFT		Inner arm		outer arm
		IFT88	IFT140	IC140	IC138	IC70, 78
Dictyostelium	x	x	x	x	x	x
Homo	✓0.005	✓	✓	✓	✓	✓
Takifugu	✓4e-07	✓	✓	✓	✓	✓
Drosophila	✓	✓	✓	x	✓	✓
Caenorhabditis	✓0.007	✓	✓	x	x	x
Saccharomyces	x	x	x	x	x	x
Arabidopsis	✓0.59	x	x	x	x	x
Chlamydomonas	✓2e-06	✓	✓	✓	✓	✓
Ostreococcus	x	x	x	x	✓	x
Plasmodium	x	x	x	x	x	✓
Toxoplasma	x	✓	✓	✓	✓	✓
Tetrahymena	x	✓	✓	✓	✓	✓
Phaeodactylum	x	x	x	x	x	x
Thalassiosira	x	✓	x	x	x	✓
Phytophthora	✓0.011	✓	✓	✓	✓	✓
Trypanosoma	✓0.23	✓	✓	✓	✓	✓
Giardia	x	✓	✓	x	✓	✓

Figure 50. *igl* is conserved in ciliated eukaryotes.

Unikonts and bikonts are the two main branches of the eukaryotic evolutionary tree. IGL co-occurs with intraflagellar transport (IFT) more than axonemal dynein intermediate chains (IC) both from the outer and inner dynein arms. Each data is determined by the top score from the BLASTP searches. *igl* orthologs and *E*-values are shown in the table. Modified from (Kavlie et al., 2010).

2.2.3.3. *igl* expression pattern in *Rfx* mutant flies

I demonstrated a conserved RFX DNA binding motif in the *Drosophila igl* promoter (Figure 47). Furthermore, for supporting the hypothesis of *igl* as a cilium compartment gene, I analyzed the *igl* expression level in pupae and antennae of the *Rfx* mutant (*Rfx*^{c02503}) flies. The expression level of *igl* was reduced in the antennae but elevated in the pupae (Figure 51) and the whole *Rfx*^{c02503} mutant flies (data not shown). However, the expression level of *iav* as a known ciliary gene (Kim et al., 2003; Gong et al., 2004) was elevated, both in the *Rfx*^{c02503} mutant antennae and pupae (Figure 51). It seems that the *iav* expression level is positively affected by the *Rfx*^{c02503} mutation. The *iav* gene has a restricted expression pattern, and for that reason, it was expected to see the same pattern in the antenna and pupa of the *Rfx*^{c02503} mutant flies. Although the *igl* expression level changes do not have the same pattern as the *iav* expression, its deviation from control flies demonstrates that *igl* expression is dependent on the RFX transcription factor.

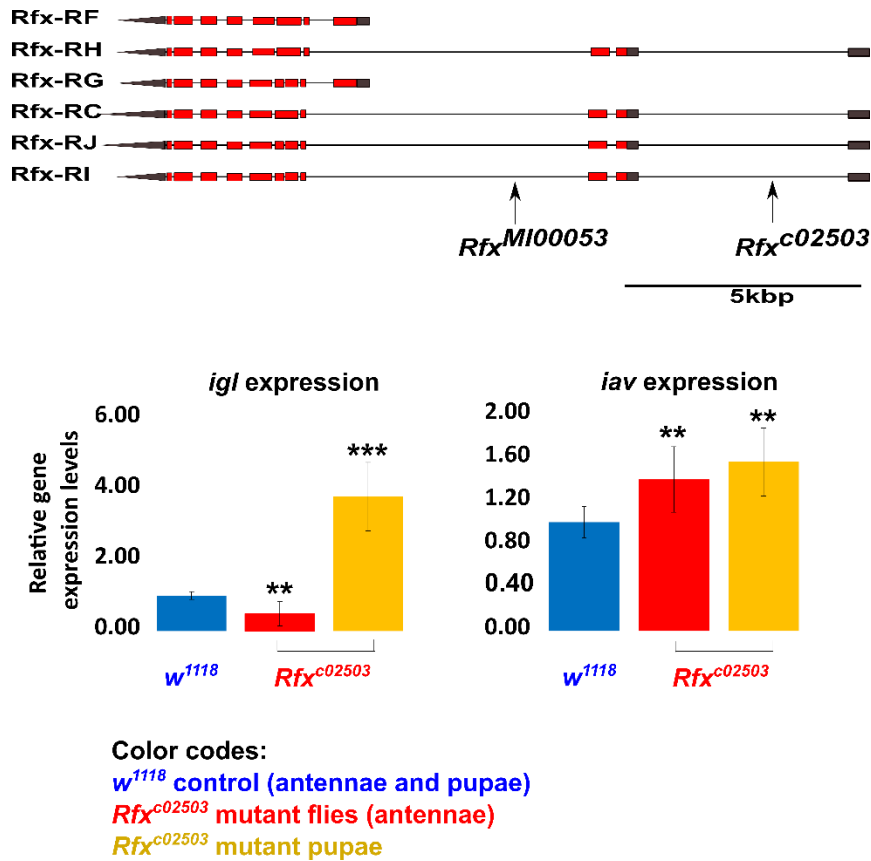


Figure 51. *igl* and *iav* expression dependency on the RFX transcription factor.

The six transcripts of the *Rfx* gene, plus the positions of the two *Rfx* mutations (*Rfx*^{MI00053} and *Rfx*^{c02503}), are depicted. The MiMIC mutant flies for the *Rfx* gene are homozygous lethal, for that reason, I used the homozygous *Rfx*^{c02503} mutant flies for analyzing the effect of *Rfx* mutation on the *iav* and *igl* expression levels. In the pupa, the expression levels of *igl* and *iav* (known cilia gene) were increased compared to control flies. The samples from the antennae, however, demonstrated reduced *igl* but elevated *iav* expression levels. Mann-Whitney-U tests with the Bonferroni correction were used for statistical analysis. Significances are indicated with ** ($P \leq 0.01$), *** ($P \leq 0.001$). $n = 3$ biological replicates with five pupae and hundred antennae for each biological replicate were used. The error bars represent standard deviations.

2.2.3.4. IGL localization in *Rfx* mutant flies

I showed that the *igl* expression level is dependent on the integrity of the RFX transcription factor (Figure 52). If IGL is a cilium compartment protein, its localization must be disrupted in the *Rfx* mutant flies (due to the effect of the RFX transcription factor on the *igl* gene expression). Labeling the IGL in the *Rfx* mutant larvae (*Rfx*^{MI00053} or *Rfx*^{c02503}) demonstrated missing IGL protein in the lateral chordotonal organ (Ich5). In addition, the HRP band signals were disrupted in the respective *Rfx* mutant larvae (Figure 52). This observation is strong evidence that IGL is regulated by the RFX transcription factor and is in the cilia of the auditory neurons.

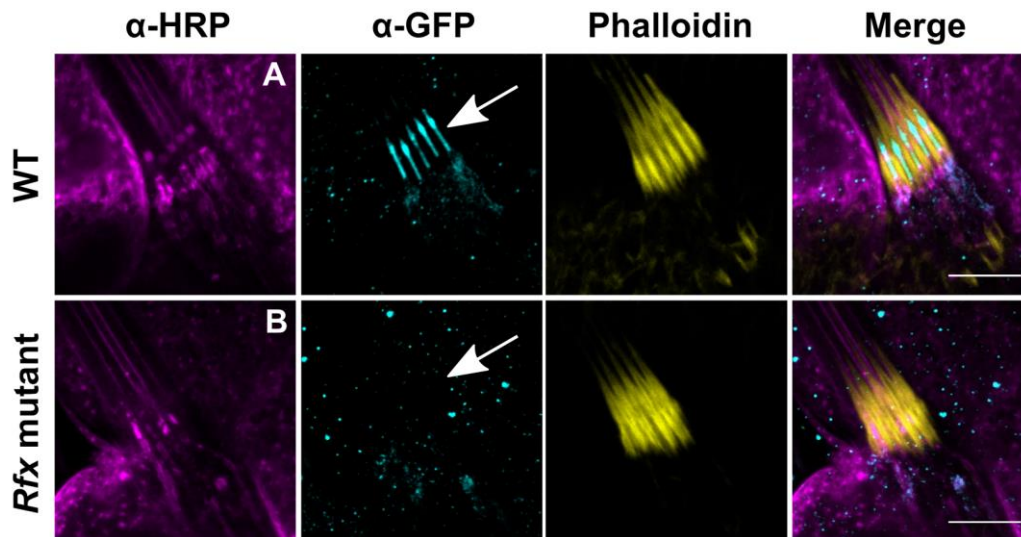


Figure 52. IGL localization in the *Rfx* mutant larva.

I used the GFP-tagged IGL-L in both WT and *Rfx* mutant backgrounds. In the first panel (A), the IGL (cyan) in the WT larva is localized in the cilia of the lch5; however, in the second panel (B), the IGL signal in the *Rfx* mutant larva is absent in the cilia of the lch5 (white arrow). The results for the two *Rfx* mutants, *Rfx*^{M100053} and *Rfx*^{c02503}, were the same. In addition, the HRP band signals demonstrate enormous abnormality (magenta). Phalloidin labels the actin in scolopale rods (yellow). Scale bars: 10 μ m.

2.2.4. Hearing impairment in *igl* mutant flies

I showed the *igl* expression in the JO neurons (Figure 44) and the IGL protein localization in the cilium (Figure 46). Based on the idea that *igl* is a ciliary gene and the presumable function of IGL in the establishment or maintenance of neurons (Neel and Young, 1994), its mutation might cause a hearing defect in the mutated flies. Due to a lack of proper *igl* mutant flies, I replaced the MiMIC cassette in *igl*^{M102290} with a not-in-frame GFP cassette. In this scenario, only the IGL-L, which showed the localization in the cilia, must be affected. The not-in-frame GFP sequence in the N-terminal of the protein will lead to a premature stop codon and a truncated protein. The analysis of the respective mutant flies revealed that IGL-L is required for the mechanical amplification by the JO neurons and sensitive hearing (Figure 53). Driving *UAS-igl* with the chordotonal receptor driver, *Dnai2-Gal4*, (*Dnai2-Gal4>igl*) in the *igl* mutant flies recovered the hearing perception, including the antenna best frequencies, mechanical amplification, and sound-evoked electrical potentials (Figure 54).

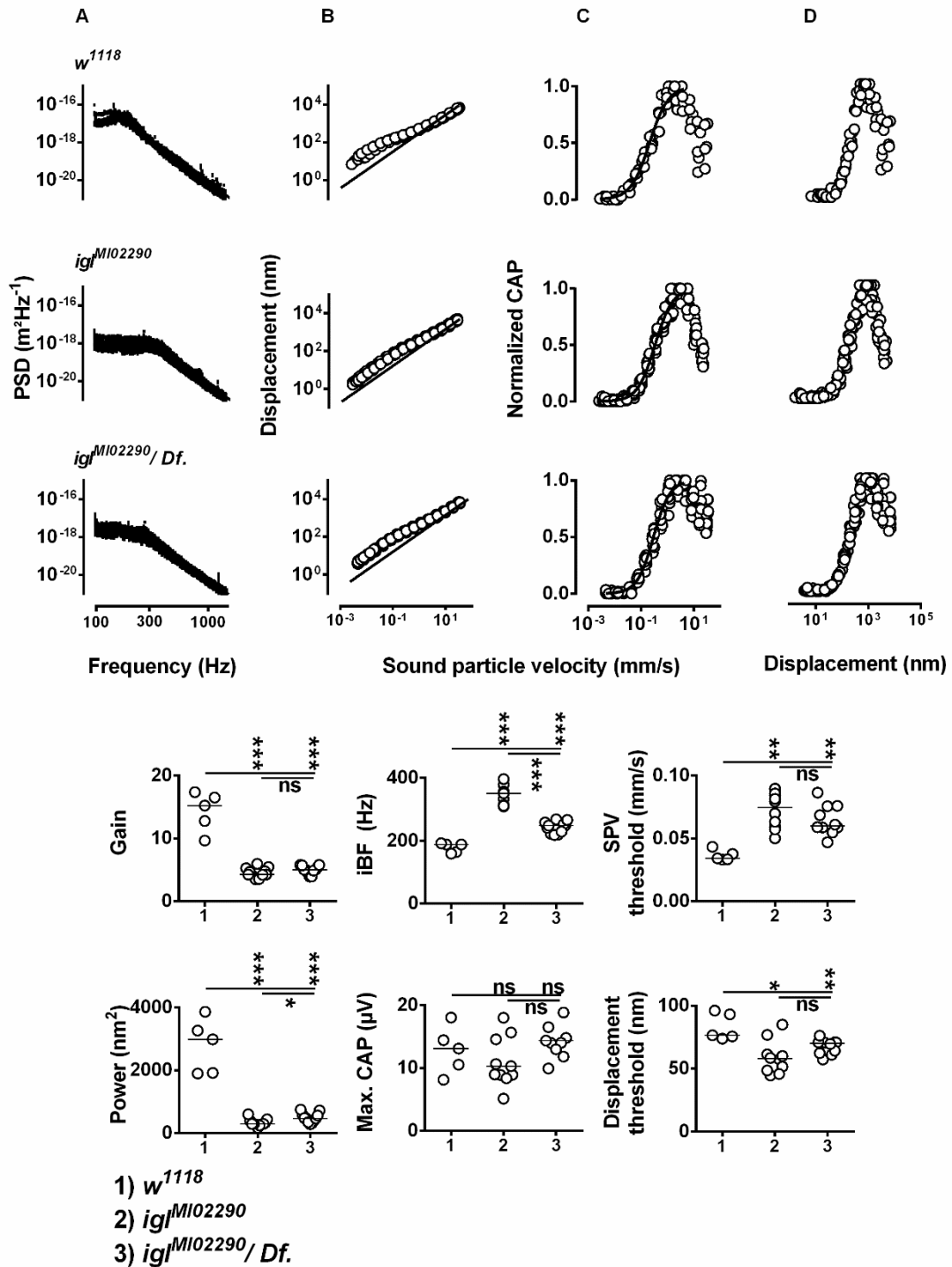
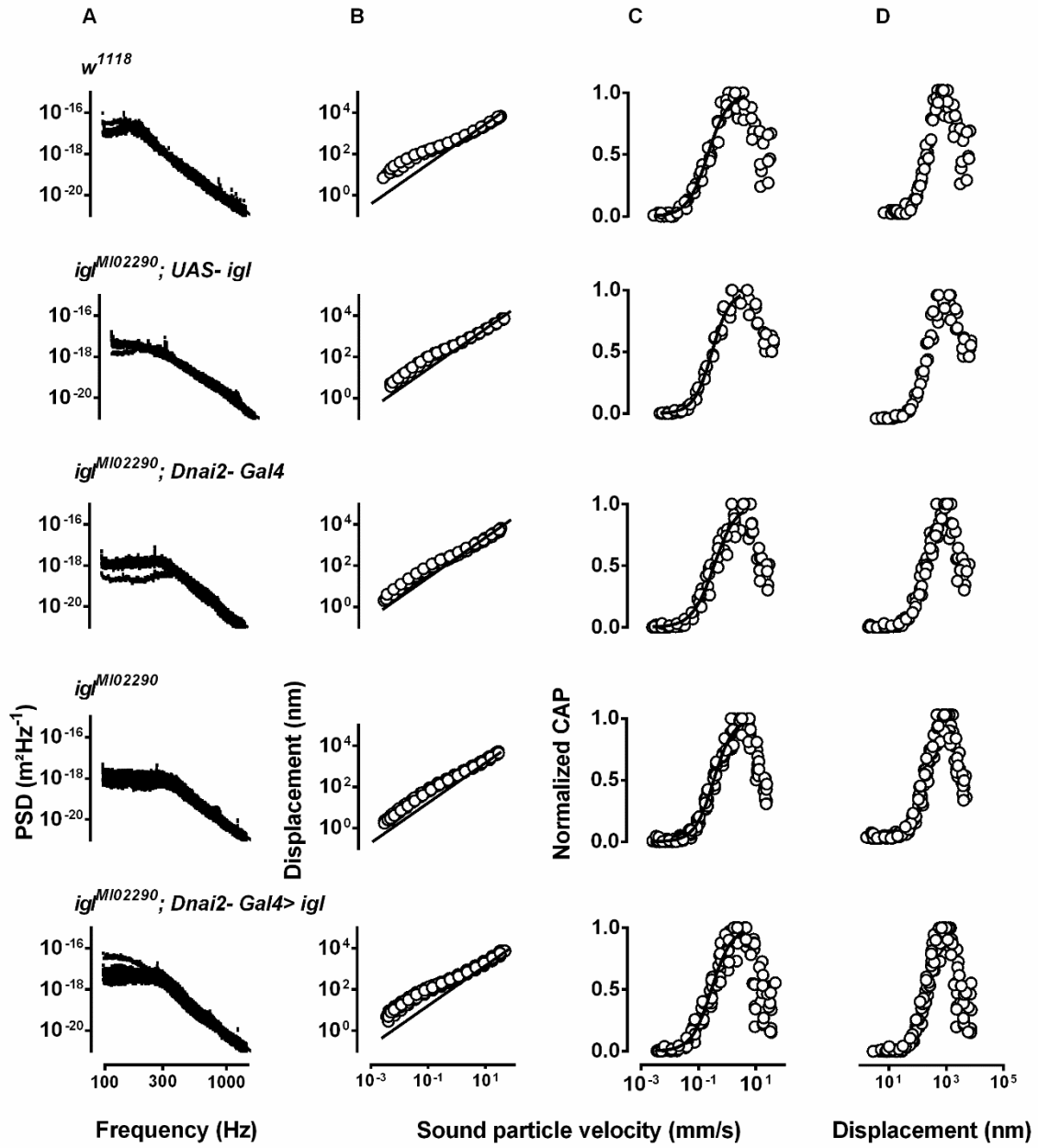


Figure 53. Hearing in *igl* mutant flies compared to w^{1118} control flies.

Top: power spectra of the mechanical fluctuations of the antennal sound receiver (A) as well as antennal displacement (B), normalized compound action potential (CAP) amplitudes (C) as a function of the sound particle velocity, and CAP amplitude as a function of antennal displacement (D) in wild type flies, $igl^{MI02290}$ mutant flies, and flies in which the $igl^{MI02290}$ allele was uncovered by the deficiency $Df(2R)Exel7135$. The $igl^{MI02290}$ represents the line I generated by replacing the MI02290 cassette with a not-in-frame GFP cassette. Bottom: corresponding amplification gain, individual best frequencies, power of the receiver fluctuations, maximum CAP amplitudes, sound particle velocity (SPV) threshold, and displacement threshold. $n \geq 5$ flies/genotype. Two-tailed Mann-Whitney-U tests with the Bonferroni correction were used for statistical analysis. Statistical significances are indicated with ns ($P > 0.05$), * ($P \leq 0.05$), ** ($P \leq 0.01$), *** ($P \leq 0.001$).



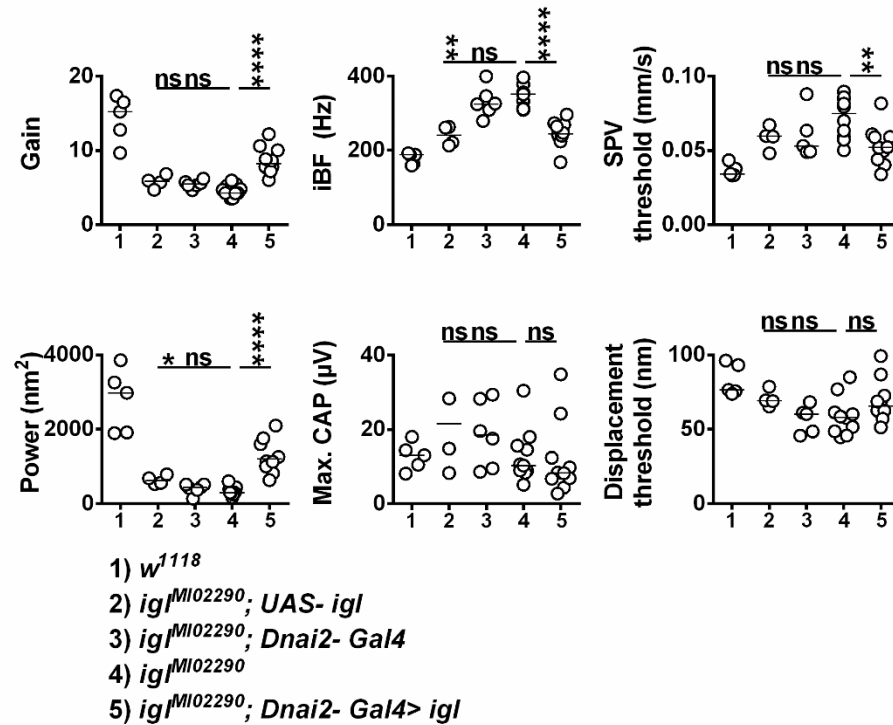


Figure 54. Recovered hearing perception in the *igl* mutant flies.

Top: power spectra of the mechanical fluctuations of the antennal sound receiver (A) as well as antennal displacement (B), normalized compound action potential (CAP) amplitudes (C) as a function of the sound particle velocity, and CAP amplitude as a function of antennal displacement (D) in wild type flies, homozygous $igl^{M102290}; UAS-igl$ control flies, homozygous $igl^{M102290}; Dnai2-Gal4$ control flies, homozygous $igl^{M102290}$ mutant flies, and homozygous igl mutant flies driving $UAS-igl$ with the chordotonal receptor driver, $Dnai2-Gal4$ ($igl^{M102290}; Dnai2-Gal4 > igl$). The $igl^{M102290}$ represents the line I generated by replacing the M102290 cassette with a not-in-frame GFP cassette. Bottom: corresponding amplification gain, individual best frequencies, power of the receiver fluctuations, maximum CAP amplitudes, sound particle velocity (SPV) threshold, and displacement threshold. Driving $UAS-igl$ with $Dnai2-Gal4$ ($Dnai2-Gal4 > igl$) in the mutant flies recovered the mechanical amplification by JO neurons and sensitive hearing. $n \geq 5$ flies/genotype. Two-tailed Mann-Whitney-U tests with the Bonferroni correction were used for statistical analysis. Statistical significances are indicated with ns ($P > 0.05$), * ($P \leq 0.05$), ** ($P \leq 0.01$), **** ($P \leq 0.0001$).

2.3. Discussion

Cilia are microtubular axoneme-based structures within dynamically assembled proteins. The importance of cilia and flagella, especially in sensory function and cell motility, is undeniable (Pan et al., 2005; Marshall and Nonaka, 2006). Ciliopathies refer to the disease in which cilia assembly or function is disrupted (Badano et al., 2006). Studies for unrevealing players in cilia assembly and function in any model organism can lead to a better understanding of ciliopathies.

The *GAP43* gene is expressing in the growth cones of developing and regenerating neurons. A growth cone in dendrite or axon tips is an actin-based scaffold-looking structure for synaptic targets in growing and regenerating neuritis. A GAP43 cilium connection was first noticed in newborn rat olfactory receptor neurons, the cilia of which are strongly stained by antibodies against GAP43 (Verhaagen et al., 1989). IGL in *Drosophila* is a functional homolog to GAP43 (Neel and Young, 1994). In this thesis, I demonstrated differences in the expression pattern of *igl* transcripts and localization of the respective IGL proteins. Furthermore, I provided evidence for supporting the hypothesis that the *igl* is a cilium compartment gene, and its mutation causes hearing impairment in *Drosophila*.

2.3.1. *igl* expression pattern and its protein localization

In vertebrates, there is a small family of genes related to *GAP43* that share a conserved region containing one PKC phosphorylation site and a calmodulin-binding domain. In *Drosophila*, only one gene, *igl*, with two proteins (IGL-L and IGL-S), each with multiple calmodulin-binding domains (three in IGL-L and two in IGL-S), represents the family of vertebrate *GAP43*-related genes that might cover the functions of all these genes. Besides the different number of the calmodulin-binding sites, the two proteins of the *igl* gene have different sizes, and unlike IGL-S, IGL-L is a membrane-associated protein (Neel and Young, 1994). Studying the features of the two proteins can help us understand the probable different functions of the two IGL proteins.

I showed that *igl* is expressed in the auditory receptor neurons. By applying the Double Header tool and the two *igl* MiMIC lines, I generated two GFP-tagged *igl* lines that designate different IGL proteins. I showed that the IGL-L is confined in the JO neuron

cilium tips, whereas the IGL-S has a widespread localization in the JO neurons. IGL-S is the more abundant IGL protein in the whole fly (especially undifferentiated cells in the eye) and the antenna, whereas the membrane-anchored, less plentiful IGL-L might be absent from the whole fly except the antennae (shown by RT-qPCR on the *igl-RA* transcript). This result is inconsistent with previous data from Neel and Young, in which the long transcript was not detectable in the adult flies (Neel and Young, 1994). These observations indicate the possibility of various IGL functions in *Drosophila*.

2.3.2. RFX regulation of IGL

Besides the cilium localization of the IGL protein, the presence of an RFX DNA binding motif in the *igl* promoter reinforces the idea of IGL-cilium connection. Parts of ciliogenesis genes are regulated by regulatory factor X (RFX) transcription factor (Laurençon et al., 2007). RFX are conserved transcription factors in a broad spectrum of species, including *D. melanogaster*, mammals, and *C. elegans*. They share a winged-helix DNA binding domain that binds to an imperfect inverted DNA sequence called the X-box motif (Gajiwala et al., 2000). There are one, two, and five RFXs in *C. elegans*, *D. melanogaster*, and mammals, respectively (Emery et al., 1996). Functional conservation of RFX in ciliogenesis in all species can be used to recognize ciliogenesis genes by seeking the X-box motifs (RFX DNA binding motifs) in promoters.

Several X-box motifs were found in the *igl* promoter, which can also be found in the promoter of negative control genes. For that reason, I examined the conservation of the assumed X-box motifs in *D. pseudoobscura* as a divergent *Drosophila* species. This species has a most recent common ancestor with *D. melanogaster* from 40 - 60 million years ago (Laurençon et al., 2007). *D. pseudoobscura* has 45 - 50 % and 63 % average identity with *D. melanogaster* in untranslated regions and DNA protein binding sites, respectively (Richards et al., 2005). DNA protein binding sites are in relatively conserved block sequences called cis-regulatory elements. Besides *D. pseudoobscura*, the conservation of the presumed X-box motifs in the *igl* promoter was also observed for other *Drosophila* species extended to the most distant ones (data not shown).

In vertebrates, by looking into the *GAP43* promoter, I found a conserved X-box motif in chicken, human, mouse, elephant, dog, and rhesus. According to T-Gene (Prediction of Target Gene), the regulatory element for the human *GAP43* gene should start 185 nucleotides upstream of the translation start site, and interestingly my

suspected X-box motif is in this region (Bailey et al., 2015). Using Tompton (Motif Comparison Tool), the presumed X-box motif matches RFX2-DBD with a P-value of 1.39e-03 (Gupta et al., 2007).

Assessing the expression level of *igl* in the *Rfx* mutant (*Rfx*^{c02503}) background demonstrated a negative RFX effect on *igl* expression level in the antenna but a positive effect in 40-hour-old complete pupa (freshly differentiated dendrites and cilia). This observation demonstrated a local RFX regulatory effect or the effect on different *igl* transcripts. On the other hand, the *iav* expression as a control cilia gene (Kim et al., 2003; Gong et al., 2004) in the antenna and the complete pupa were positively regulated. This data is inconsistent with previous work by Newton et al. (Newton et al., 2012). One explanation for that can be the application of different *Rfx* mutant lines. I used sterile homozygous *Rfx*^{c02503} flies. This line, from PBac{PB} insertion (Thibault et al., 2004) in the regulatory sequence of *Rfx* might affect *Rfx* function. I showed the absence of the IGL protein in the lateral chordotonal organ (lch5) of the *Rfx*^{c02503} larvae. On the other hand, Newton et al. used the *Rfx*⁴⁹ line, which has lch5 defects and dies before the end of the larval stage (Dubruille et al., 2002). Imprecise excision of the progenitor element caused a deletion encompassing the first three exons of the *Rfx* gene in the *Rfx*⁴⁹ mutants. Moreover, one can analyze the *igl* expression level in the *Rfx*⁴⁹ mutant larvae.

2.3.3. IGL role in hearing

For the ciliary localization of the IGL protein, and the presumable function of IGL in the establishment or maintenance of neurons (Neel and Young, 1994), I was expecting a hearing defect in the flies with *igl* mutation. I used two RNAi (BDSC# 29598, VDRC# v100159) lines for down-regulating *igl* expression and assessing the *Drosophila* hearing function. Although the RT-qPCR results showed a reduction in the level of *igl* transcripts, both RNAi did not show significant hearing defects compared to control flies. One explanation for that can be a dosage effect that, i.e., 1% transcript is enough for IGL function, or long protein stability, and low protein turnover. It might also be false-positive results from the RT-qPCR quantification of the RNAi mediated *igl* knockdown (Onchuru and Kaltenpoth, 2019).

Using *igl*^{Mi02290}, I replaced the MiMIC cassette with a not-in-frame GFP sequence, which must only affect the IGL-L. The not-in-frame GFP will lead to a premature stop codon and truncated proteins.

Using the not-in-frame GFP *igl* mutated line, I showed that *igl* is required for hearing. Compared to control flies, the mutation in the long *igl* transcript decreased the mechanical amplification and the power of the antenna's mechanical free fluctuations. However, the application of the two *igl* MiMIC lines for hearing assessment did not show any hearing defect (data not shown). This observation can be due to alternative splicing and the presence of the WT splice variant of the gene beside the truncated one. The *igl*^{Mi12785}-*Gal4* flies that affect all three *igl* transcripts are homozygous lethal, which indicates that *igl* is a vital gene for fly survival, and the other *igl* mutants that are not homozygous lethal are hypomorphs but not knockout mutants.

Mutations in the flies' single *calmodulin* gene, *nan*, and *iav* cause excess mechanical amplification in hearing (Göpfert et al., 2006; Senthilan et al., 2012). Because of the IQ motifs in IGL proteins, which bind calmodulin (Neel & Young, 1994), one can assume a profound IGL, TRPVs, and calmodulin cooperation for modulating amplification gain in the fly's auditory system.

References

- Abcam. (2013). General Western Blot Protocol: Guidance for running an efficient and accurate experiment. Abcam.
- Ahmad, F. J.; Pienkowski, T. P.; Baas, P. W. (1993). Regional differences in microtubule dynamics in the axon. *Journal of Neuroscience* *13*, 856–866.
- Akella, J. S.; Wloga, D.; Kim, J.; Starostina, N. G.; Lyons-Abbott, S.; Morrissette, N. S.; Dougan, S. T.; Kipreos, E. T.; Gaertig, J. (2010). MEC-17 is an α -tubulin acetyltransferase. *Nature* *467*, 218–222.
- Akitake, B.; Ren, Q.; Boiko, N.; Ni, J.; Sokabe, T.; Stockand, J. D.; Eaton, B. A.; Montell, C. (2015). Coordination and fine motor control depend on *Drosophila* TRP γ . *Nature Communications* *6*, 1–13.
- Albert, J. T.; Nadrowski, B.; Kamikouchi, A.; Gopfert, M. C. (2006). Mechanical tracing of protein function in the *Drosophila* ear. *Nature Protoc* *10*.
- Albert, J. T.; Nadrowski, B.; Göpfert, M. C. (2007). Mechanical Signatures of Transducer Gating in the *Drosophila* Ear. *Current Biology* *17*, 1000–1006.
- Albert, J. T.; Göpfert, M. C. (2015). Hearing in *Drosophila*. *Current Opinion in Neurobiology* *34*, 79–85.
- Alexander, K. A.; Cimler, B. M.; Meier, K. E.; Storm, D. R. (1987). Regulation of calmodulin binding to P-57. A neurospecific calmodulin binding protein. *Journal of Biological Chemistry* *262*, 6108–6113.
- Alexander, K. A.; Wakim, B. T.; Doyle, G. S.; Walsh, K. A.; Storm, D. R. (1988). Identification and characterization of the calmodulin-binding domain of neuromodulin, a neurospecific calmodulin-binding protein. *Journal of biological chemistry* *263*, 7544–7549.
- Apel, E. D.; Byford, M. F.; Au, D.; Walsh, K. A.; Storm, D. R. (1990). Identification of the Protein Kinase C Phosphorylation Site in Neuromodulin. *Biochemistry* *29*, 2330–2335.
- Ashmore, J.; Avan, P.; Brownell, W. E.; Dallos, P.; Dierkes, K.; Fettiplace, R.; Grosh, K.; Hackney, C. M.; Hudspeth, A. J.; Jülicher, F.; Lindner, B.; Martin, P.; Meaud, J.; Petit, C.; Santos Sacchi, J. R.; Canlon, B. (2010). The remarkable cochlear amplifier. *Hearing Research* *266*, 1–17.
- Ashmore, J. F. (1987). A fast motile response in guinea-pig outer hair cells: the cellular basis of the cochlear amplifier. *The Journal of Physiology* *388*, 323–347.
- Audrito, V.; Vaisitti, T.; Rossi, D.; Gottardi, D.; D’Arena, G.; Laurenti, L.; Gaidano, G.;

- Malavasi, F.; Deaglio, S. (2011). Nicotinamide blocks proliferation and induces apoptosis of chronic lymphocytic leukemia cells through activation of the p53/miR-34a/SIRT1 tumor suppressor network. *Cancer Research* *71*, 4473–4483.
- Audrito, V.; Messana, V. G.; Deaglio, S. (2020). NAMPT and NAPRT: Two Metabolic Enzymes With Key Roles in Inflammation. *Frontiers in Oncology* *10*, 358.
- Azusa Kamukouchi, Tkashi Shimada, K. I. (2006). Comprehensive Classification of the Auditory Sensory Projections in the Brain of the Fruit Fly *Drosophila melanogaster*. *Journal of Comparative Neurology* *499*, 317–356.
- Badano, J. L.; Mitsuma, N.; Beales, P. L.; Katsanis, N. (2006). The ciliopathies: An emerging class of human genetic disorders. *Annu. Rev. Genomics Hum. Genet.* *7*, 125–148.
- Bailey, T. L.; Johnson, J.; Grant, C. E.; Noble, W. S. (2015). The MEME Suite. *Nucleic Acids Research* *43*, W39–W49.
- Balan, V.; Miller, G. S.; Kaplun, L.; Balan, K.; Chong, Z. Z.; Li, F.; Kaplun, A.; VanBerkum, M. F. A.; Arking, R.; Freeman, D. C.; Maiese, K.; Tzivion, G. (2008). Life span extension and neuronal cell protection by *Drosophila* nicotinamidase. *Journal of Biological Chemistry* *283*, 27810–27819.
- Bellen, H. J.; Levis, R. W.; Liao, G.; He, Y.; Carlson, J. W.; Tsang, G.; Evans-Holm, M.; Hiesinger, P. R.; Schulze, K. L.; Rubin, G. M.; Hoskins, R. A.; Spradling, A. C. (2004). The BDGP gene disruption project: Single transposon insertions associated with 40% of *Drosophila* genes. *Genetics* *167*, 761–781.
- Bennet-Clark, H. C. (1971). Acoustics of insect song. *Nature* *234*, 255–259.
- Benowitz, L. I.; Routtenberg, A. (1987). A membrane phosphoprotein associated with neural development, axonal regeneration, phospholipid metabolism, and synaptic plasticity. *Trends in Neurosciences* *10*, 527–532.
- Bermingham, N. A.; Hassan, B. A.; Price, S. D.; Vollrath, M. A.; Ben-Arie, N.; Eatock, R. A.; Bellen, H. J.; Lysakowski, A.; Zoghbi, H. Y. (1999). Math 1: An essential gene for the generation of inner ear hair cells. *Science* *284*, 1837–1841.
- Bieganski, P.; Brenner, C. (2004). Discoveries of nicotinamide riboside as a nutrient and conserved NRK genes establish a preiss-handler independent route to NAD⁺ in fungi and humans. *Cell* *117*, 495–502.
- Bitterman, K. J.; Anderson, R. M.; Cohen, H. Y.; Latorre-Esteves, M.; Sinclair, D. A. (2002). Inhibition of silencing and accelerated aging by nicotinamide, a putative negative regulator of yeast Sir2 and human SIRT1. *Journal of Biological Chemistry* *277*, 45099–45107.
- Blum, M.; Chang, H. Y.; Chuguransky, S.; Grego, T.; Kandasamy, S.; Mitchell, A.; Nuka, G.; Paysan-Lafosse, T.; Qureshi, M.; Raj, S.; Richardson, L.; Salazar, G. A.; Williams, L.; Bork, P.; Bridge, A.; Gough, J.; Haft, D. H.; Letunic, I.; Marchler-Bauer,

References

A. et al. (2021). The InterPro protein families and domains database: 20 years on. *Nucleic Acids Research* *49*, D344–D354.

Bockwoldt, M.; Houry, D.; Niere, M.; Gossmann, T. I.; Reinartz, I.; Schug, A.; Ziegler, M.; Heiland, I. (2019). Identification of evolutionary and kinetic drivers of NAD-dependent signaling. *Proceedings of the National Academy of Sciences of the United States of America* *116*, 15957–15966.

Brewster, R.; Bodmer, R. (1995). Origin and specification of type II sensory neurons in *Drosophila*. *Development* *121*, 2923–2936.

Browne, A.; O'Donnell, M. J. (2013). Ammonium secretion by Malpighian tubules of *Drosophila melanogaster*: Application of a novel ammonium-selective microelectrode. *Journal of Experimental Biology* *216*, 3818–3827.

Cachero, S.; Simpson, T. I.; zur Lage, P. I.; Ma, L.; Newton, F. G.; Holohan, E. E.; Armstrong, J. D.; Jarman, A. P. (2011). The gene regulatory cascade linking proneural specification with differentiation in *Drosophila* sensory neurons. *PLoS Biology* *9*, e1000568.

Caldwell, J. C.; Eberl, D. F. (2002). Towards a molecular understanding of *Drosophila* hearing. *Journal of Neurobiology* *53*, 172–189.

Caldwell, J. C.; Miller, M. M.; Wing, S.; Soll, D. R.; Eberl, D. F. (2003). Dynamic analysis of larval locomotion in *Drosophila* chordotonal organ mutants. *Proceedings of the National Academy of Sciences* *100*, 16053–16058.

Campesan, S.; Green, E. W.; Breda, C.; Sathyaikumar, K. V.; Muchowski, P. J.; Schwarcz, R.; Kyriacou, C. P.; Giorgini, F. (2011). The kynurenine pathway modulates neurodegeneration in a *drosophila* model of Huntington's disease. *Current Biology* *21*, 961–966.

Campos-Ortega, J. A.; Hartenstein, V. (2013). *The Embryonic Development of Drosophila melanogaster*. Springer Science & Business Media.

Carlson, J. R. (1996). Olfaction in *Drosophila*: From odor to behavior. *Trends in Genetics* *12*, 175–180.

Chalfie, M.; Au, M. (1989). Genetic control of differentiation of the *caenorhabditis elegans* touch receptor neurons. *Science* *243*, 1027–1033.

Chang, P. (2018). Correction to: ADP-ribosylation and NAD⁺ Utilizing Enzymes. *ADP-ribosylation and NAD⁺ Utilizing Enzymes* 415.

Chapman, E. R.; Au, D.; Alexander, K. A.; Nicolson, T. A.; Storm, D. R. (1991). Characterization of the calmodulin binding domain of neuromodulin. Functional significance of serine 41 and phenylalanine 42. *Journal of Biological Chemistry* *266*, 207–213.

Cheney, R. E.; Mooseker, M. S. (1992). Unconventional myosins. *Current Opinion in*

Cell Biology 4, 27–35.

Cheng, L. E.; Song, W.; Looger, L. L.; Jan, L. Y.; Jan, Y. N. (2010). The Role of the TRP Channel NompC in *Drosophila* Larval and Adult Locomotion. *Neuron* 67, 373–380.

Chintapalli, V. R.; Wang, J.; Dow, J. A. T. (2007). Using FlyAtlas to identify better *Drosophila melanogaster* models of human disease. *Nature Genetics* 39, 715–720.

Covarrubias, A. J.; Perrone, R.; Grozio, A.; Verdin, E. (2021). NAD⁺ metabolism and its roles in cellular processes during ageing. *Nature Reviews Molecular Cell Biology* 22, 119–141.

Crook, M.; McCreynolds, M. R.; Wang, W.; Hanna-Rose, W. (2014). An NAD⁺ biosynthetic pathway enzyme functions cell non-autonomously in *C. elegans* development. *Developmental Dynamics* 243, 965–976.

Crook, M.; Upadhyay, A.; Ido, L. J.; Hanna-Rose, W. (2016). Epidermal growth factor receptor cell survival signaling requires phosphatidylcholine biosynthesis. *G3: Genes, Genomes, Genetics* 6, 3533–3540.

Dallos, P. (1992). The active cochlea. *Journal of Neuroscience* 12, 4575–4585.

Diao, F. F.; Ironfield, H.; Luan, H.; Diao, F. F.; Shropshire, W. C.; Ewer, J.; Marr, E.; Potter, C. J.; Landgraf, M.; White, B. H. (2015). Plug-and-play genetic access to *drosophila* cell types using exchangeable exon cassettes. *Cell Reports* 10, 1410–1421.

Dickson, B. J. (2008). Wired for sex: The neurobiology of *Drosophila* mating decisions. *Science* 322, 904–909.

Dubruille, R.; Laurençon, A.; Vandaele, C.; Shishido, E.; Coulon-Bublex, M.; Swoboda, P.; Couble, P.; Kernan, M.; Durand, B. (2002). *Drosophila* regulatory factor X is necessary for ciliated sensory neuron differentiation. *Development* 129, 5487–5498.

Eberl, D. F. (1999). Feeling the vibes: Chordotonal mechanisms in insect hearing. *Current Opinion in Neurobiology* 9, 389–393.

Effertz, T.; Wiek, R.; Göpfert, M. C. (2011). NompC TRP channel is essential for *Drosophila* sound receptor function. *Current Biology* 21, 592–597.

Effertz, T.; Nadrowski, B.; Piepenbrock, D.; Albert, J. T.; Göpfert, M. C. (2012). Direct gating and mechanical integrity of *Drosophila* auditory transducers require TRPN1. *Nature Neuroscience* 15, 1198–1200.

Elkon, R.; Milon, B.; Morrison, L.; Shah, M.; Vijayakumar, S.; Racherla, M.; Leitch, C. C.; Silipino, L.; Hadi, S.; Weiss-Gayet, M.; Barras, E.; Schmid, C. D.; Ait-Lounis, A.; Barnes, A.; Song, Y.; Eisenman, D. J.; Eliyahu, E.; Frolenkov, G. I.; Strome, S. E. et al. (2015). RFX transcription factors are essential for hearing in mice. *Nature Communications* 6, 1–14.

Emery, P.; Durand, B.; Mach, B.; Reith, W. (1996). RFX proteins, a novel family of DNA

References

binding proteins conserved in the eukaryotic kingdom. *Nucleic Acids Research* 24, 803–807.

Ewing, A. W. (1978). The antenna of *Drosophila* as a ‘love song’ receptor. *Physiological Entomology* 3, 33–36.

Fettiplace, R. (2006). Active hair bundle movements in auditory hair cells. *Journal of Physiology* 576, 29–36.

Fischer, J. A.; Giniger, E.; Maniatis, T.; Ptashne, M. (1988). GAL4 activates transcription in *Drosophila*. *Nature* 332, 853–856.

Fowler, M. A.; Montell, C. (2013). *Drosophila* TRP channels and animal behavior. *Life Sciences* 92, 394–403.

Gajiwala, K. S.; Chen, H.; Cornille, F.; Roques, B. P.; Reith, W.; Mach, B.; Burley, S. K. (2000). Structure of the winged-helix protein hRFX1 reveals a new mode of DNA binding. *Nature* 403, 916–921.

Galli, U.; Colombo, G.; Travelli, C.; Tron, G. C.; Genazzani, A. A.; Grolla, A. A. (2020). Recent Advances in NAMPT Inhibitors: A Novel Immunotherapeutic Strategy. *Frontiers in Pharmacology* 11, 656.

Gaudet, P.; Livstone, M.; Thomas, P. (2010). Gene Ontology annotation inferences using phylogenetic trees. *GO Reference Genome Project*.

Gaudet, P.; Livstone, M. S.; Lewis, S. E.; Thomas, P. D. (2011). Phylogenetic-based propagation of functional annotations within the Gene Ontology consortium. *Briefings in Bioinformatics* 12, 449–462.

Georgiev, P.; Okkenhaug, H.; Drews, A.; Wright, D.; Lambert, S.; Flick, M.; Carta, V.; Martel, C.; Oberwinkler, J.; Raghu, P. (2010). TRPM channels mediate zinc homeostasis and cellular growth during *drosophila* larval development. *Cell Metabolism* 12, 386–397.

Geurten, B.; Spalthoff, C.; Göpfert, M. C. (2013). Insect hearing: Active amplification in tympanal ears. *Current Biology* 23, R950–R952.

Gong, Z.; Son, W.; Chung, Y. D.; Kim, J.; Shin, D. W.; McClung, C. A.; Lee, Y.; Lee, H. W.; Chang, D. J.; Kaang, B. K.; Cho, H.; Oh, U.; Hirsh, J.; Kernan, M. J.; Kim, C. (2004). Two interdependent TRPV channel subunits, inactive and nanchung, mediate hearing in *Drosophila*. *Journal of Neuroscience* 24, 9059–9066.

Göpfert, M. C.; Robert, D. (2002). The mechanical basis of *Drosophila* audition. *Journal of Experimental Biology* 205, 1199–1208.

Göpfert, M. C.; Robert, D. (2003)a. Motion generation by *Drosophila* mechanosensory neurons. *Proceedings of the National Academy of Sciences* 100, 5514–5519.

Göpfert, M. C.; Robert, D. (2003)b. MICROMECHANICS OF DROSOPHILA AUDITION. *Biophysics of the Cochlea: From Molecules to Models* 300–307.

- Göpfert, M. C.; Humphris, A. D. L.; Albert, J. T.; Robert, D.; Hendrich, O. (2005). Power gain exhibited by motile mechanosensory neurons in *Drosophila* ears. *Proceedings of the National Academy of Sciences* *102*, 325–330.
- Göpfert, M. C.; Albert, J. T.; Nadrowski, B.; Kamikouchi, A. (2006). Specification of auditory sensitivity by *Drosophila* TRP channels. *Nature Neuroscience* *9*, 999–1000.
- Göpfert, M. C.; Hennig, R. M. (2016). Hearing in Insects. *Annual Review of Entomology* *61*, 257–276.
- Gossmann, T. I.; Ziegler, M.; Puntervoll, P.; De Figueiredo, L. F.; Schuster, S.; Heiland, I. (2012). NAD⁺ biosynthesis and salvage - A phylogenetic perspective. *The FEBS Journal* *279*, 3355–3363.
- Goswami, C.; Hucho, T. (2008). Submembraneous microtubule cytoskeleton: Biochemical and functional interplay of TRP channels with the cytoskeleton. *The FEBS journal* *275*, 4684–4699.
- Greenspan, R. J.; Ferveur, J. (2000). Courtship in *Drosophila*. *Annual review of genetics* *34*, 205–232.
- Gupta, S.; Stamatoyannopoulos, J. A.; Bailey, T. L.; Noble, W. S. (2007). Quantifying similarity between motifs. *Genome Biology* *8*, R24.
- Halachmi, N.; Nachman, A.; Salzberg, A. (2016). A newly identified type of attachment cell is critical for normal patterning of chordotonal neurons. *Developmental Biology* *411*, 61–71.
- Hammond, J. W.; Cai, D.; Verhey, K. J. (2008). Tubulin modifications and their cellular functions. *Current Opinion in Cell Biology* *20*, 71–76.
- Han, P.; McDonald, H. A.; Bianchi, B. R.; Kouhen, R. El; Vos, M. H.; Jarvis, M. F.; Faltynek, C. R.; Moreland, R. B. (2007). Capsaicin causes protein synthesis inhibition and microtubule disassembly through TRPV1 activities both on the plasma membrane and intracellular membranes. *Biochemical Pharmacology* *73*, 1635–1645.
- Hernandez, I. F.; Marsh, E. B.; Bonaguidi, M. A. (2021). Mechanosensory neuron regeneration in adult *Drosophila*. *Development (Cambridge)* *148*, dev187534.
- Hofmann, T.; Chubanov, V.; Chen, X.; Dietz, A. S.; Gudermann, T.; Montell, C. (2010). *Drosophila* TRPM channel is essential for the control of extracellular magnesium levels. *PLoS ONE* *5*, e10519.
- Holahan, M. R. (2017). A shift from a pivotal to supporting role for the growth-associated protein (GAP-43) in the coordination of axonal structural and functional plasticity. *Frontiers in Cellular Neuroscience* *11*, 266.
- Howard, J.; Bechstet, S. (2004). Hypothesis: A helix of ankyrin repeats of the NOMPC-TRP ion channel is the gating spring of mechanoreceptors [1]. *Current Biology* *14*, R224–

References

R226.

Hu, Y.; Flockhart, I.; Vinayagam, A.; Bergwitz, C.; Berger, B.; Perrimon, N.; Mohr, S. E. (2011). An integrative approach to ortholog prediction for disease-focused and other functional studies. *BMC Bioinformatics* 12, 1–16.

Hudspeth, A. J. (2008). Making an Effort to Listen: Mechanical Amplification in the Ear. *Neuron* 59, 530–545.

Imai, S. ichiro; Guarente, L. (2014). NAD⁺ and sirtuins in aging and disease. *Trends in Cell Biology* 24, 464–471.

Janke, C.; Montagnac, G. (2017). Causes and Consequences of Microtubule Acetylation. *Current Biology* 27, R1287–R1292.

Jarman, A. P.; Grau, Y.; Jan, L. Y.; Jan, Y. N. (1993). atonal is a proneural gene that directs chordotonal organ formation in the *Drosophila* peripheral nervous system. *Cell* 73, 1307–1321.

Jumper, J.; Evans, R.; Pritzel, A.; Green, T.; Figurnov, M.; Ronneberger, O.; Tunyasuvunakool, K.; Bates, R.; Žídek, A.; Potapenko, A.; Bridgland, A.; Meyer, C.; Kohl, S. A. A.; Ballard, A. J.; Cowie, A.; Romera-Paredes, B.; Nikolov, S.; Jain, R.; Adler, J. et al. (2021). Highly accurate protein structure prediction with AlphaFold. *Nature* 1.

K. Venkatachalam, C. M. (2007). TRP channels. *Annu Rev Biochem* 76, 387–417.

Kadowaki, T. (2015). Evolutionary dynamics of metazoan TRP channels. *Pflugers Archiv European Journal of Physiology* 467, 2043–2053.

Kamikouchi, A.; Inagaki, H. K.; Effertz, T.; Hendrich, O.; Fiala, A.; Göpfert, M. C.; Ito, K. (2009). The neural basis of *Drosophila* gravity-sensing and hearing. *Nature* 458, 165–171.

Karak, S.; Jacobs, J. S.; Kittelmann, M.; Spalthoff, C.; Katana, R.; Sivan-Loukianova, E.; Schon, M. A.; Kernan, M. J.; Eberl, D. F.; Göpfert, M. C. (2015). Diverse Roles of Axonemal Dyneins in *Drosophila* Auditory Neuron Function and Mechanical Amplification in Hearing. *Scientific Reports* 5, 17085.

Katana, R.; Guan, C.; Zanini, D.; Larsen, M. E.; Giraldo, D.; Geurten, B. R. H.; Schmidt, C. F.; Britt, S. G.; Göpfert, M. C. (2019). Chromophore-Independent Roles of Opsin Apoproteins in *Drosophila* Mechanoreceptors. *Current Biology* 29, 2961–2969.

Kavlie, R. G.; Kernan, M. J.; Eberl, D. F. (2010). Hearing in *drosophila* requires TilB, a conserved protein associated with ciliary motility. *Genetics* 185, 177–188.

Kawasaki, H.; Nakayama, S.; Kretsinger, R. H. (1998). Classification and evolution of EF-hand proteins. *BioMetals* 11, 277–295.

Kernan, M. J. (2007). Mechanotransduction and auditory transduction in *Drosophila*.

- Pflugers Archiv European Journal of Physiology 454, 703–720.
- Kim, J.; Chung, Y. D.; Park, D. Y.; Choi, S. K.; Shin, D. W.; Soh, H.; Lee, H. W.; Son, W.; Yim, J.; Park, C. S.; Kernan, M. J.; Kim, C. (2003). A TRPV family ion channel required for hearing in *Drosophila*. *Nature* 424, 81–84.
- Klimova, N.; Long, A.; Kristian, T. (2019). Nicotinamide mononucleotide alters mitochondrial dynamics by SIRT3-dependent mechanism in male mice. *Journal of Neuroscience Research* 97, 975–990.
- Kretsinger, R. H.; Schaffer, J. E. (2021). Calcium | Calcium-Modulated Proteins (EF-Hand). *Encyclopedia of Biological Chemistry III*, pp. 630–636.
- Krishnan, A.; Sane, S. P. (2015). Antennal Mechanosensors and Their Evolutionary Antecedents. *Advances in Insect Physiology* 49, 59–99.
- Kung, C. (2005). A possible unifying principle for mechanosensation. *Nature* 436, 647–654.
- Kwon, Y.; Shen, W. L.; Shim, H. S.; Montell, C. (2010). Fine thermotactic discrimination between the optimal and slightly cooler temperatures via a TRPV channel in chordotonal neurons. *Journal of Neuroscience* 30, 10465–10471.
- Lan, S. J.; Henderson, L. M. (1968). Uptake of nicotinic acid and nicotinamide by rat erythrocytes. *Journal of Biological Chemistry* 243, 3388–3394.
- Lane, M. A.; Bailey, S. J. (2005). Role of retinoid signalling in the adult brain. *Progress in Neurobiology* 75, 275–293.
- Larkin, A.; Marygold, S. J.; Antonazzo, G.; Attrill, H.; dos Santos, G.; Garapati, P. V.; Goodman, J. L.; Sian Gramates, L.; Millburn, G.; Strelets, V. B.; Tabone, C. J.; Thurmond, J. (2021). FlyBase: Updates to the *Drosophila melanogaster* knowledge base. *Nucleic Acids Research* 49, D899–D907.
- Laurençon, A.; Dubruille, R.; Efimenko, E.; Grenier, G.; Bissett, R.; Cortier, E.; Rolland, V.; Swoboda, P.; Durand, B. (2007). Identification of novel regulatory factor X (RFX) target genes by comparative genomics in *Drosophila* species. *Genome Biology* 8, R195.
- Lee, J.; Moon, S.; Cha, Y.; Chung, Y. D. (2010). *Drosophila* TRPN(=NOMPC) channel localizes to the distal end of mechanosensory cilia. *PLoS ONE* 5, e11012.
- Lee, P. T.; Zirin, J.; Kanca, O.; Lin, W. W.; Schulze, K. L.; Li-Kroeger, D.; Tao, R.; Devereaux, C.; Hu, Y.; Chung, V.; Fang, Y.; He, Y.; Pan, H.; Ge, M.; Zuo, Z.; Housden, B. E.; Mohr, S. E.; Yamamoto, S.; Levis, R. W. et al. (2018). A gene-specific T2A-GAL4 library for *drosophila*. *eLife* 7, e35574.
- Lehnert, B. P.; Baker, A. E.; Gaudry, Q.; Chiang, A. S.; Wilson, R. I. (2013). Distinct Roles of TRP Channels in Auditory Transduction and Amplification in *Drosophila*. *Neuron* 77, 115–128.

References

- Li-Kroeger, D.; Kanca, O.; Lee, P. T.; Cowan, S.; Lee, M. T.; Jaiswal, M.; Salazar, J. L.; He, Y.; Zuo, Z.; Bellen, H. J. (2018). An expanded toolkit for gene tagging based on MiMIC and scarless CRISPR tagging in *Drosophila*. *eLife* 7, e38709.
- Liberman, M. C.; Gao, J.; He, D. Z. Z.; Wu, X.; Jia, S.; Zuo, J. (2002). Prestin is required for electromotility of the outer hair cell and for the cochlear amplifier. *Nature* 419, 300–304.
- Lin, H. (2007). Nicotinamide adenine dinucleotide: Beyond a redox coenzyme. *Organic and Biomolecular Chemistry* 5, 2541–2554.
- Linzen, B. (1974). The Tryptophan → Ommochrome Pathway in Insects. *Advances in Insect Physiology* 10, 117–246.
- Liu, D.; Pitta, M.; Mattson, M. P. (2008). Preventing NAD⁺ depletion protects neurons against excitotoxicity: Bioenergetic effects of mild mitochondrial uncoupling and caloric restriction. *Annals of the New York Academy of Sciences* 1147, 275.
- Liu, J.; Du, J.; Wang, Y. (2019). CDK5 inhibits the clathrin-dependent internalization of TRPV1 by phosphorylating the clathrin adaptor protein AP2 μ 2. *Science Signaling* 12, eaaw2040.
- Livak, K. J.; Schmittgen, T. D. (2001). Analysis of relative gene expression data using real-time quantitative PCR and the 2- $\Delta\Delta$ CT method. *Methods* 25, 402–408.
- Lu, Q.; Senthilan, P. R.; Effertz, T.; Nadrowski, B.; Göpfert, M. C. (2009). Using *Drosophila* for studying fundamental processes in hearing. *Integrative and Comparative Biology* 49, 674–680.
- Madeira, F.; Park, Y. M.; Lee, J.; Buso, N.; Gur, T.; Madhusoodanan, N.; Basutkar, P.; Tivey, A. R. N.; Potter, S. C.; Finn, R. D.; Lopez, R. (2019). The EMBL-EBI search and sequence analysis tools APIs in 2019. *Nucleic Acids Research* 47, W636–W641.
- Makki, R.; Cinnamon, E.; Gould, A. P. (2014). The development and functions of oenocytes. *Annual Review of Entomology* 59, 405–425.
- Manley, G. A. (2001). Evidence for an active process and a cochlear amplifier in nonmammals. *Journal of Neurophysiology* 86, 541–549.
- Marletta, A. S.; Massarotti, A.; Orsomando, G.; Magni, G.; Rizzi, M.; Garavaglia, S. (2015). Crystal structure of human nicotinic acid phosphoribosyltransferase. *FEBS Open Bio* 5, 419–428.
- Marshall, W. F.; Nonaka, S. (2006). Cilia: Tuning in to the Cell's Antenna. *Current Biology* 16, PR604-R614.
- Matsuo, E.; Yamada, D.; Ishikawa, Y.; Asai, T.; Ishimoto, H.; Kamikouchi, A. (2014). Identification of novel vibration- and deflection-sensitive neuronal subgroups in Johnston's organ of the fruit fly. *Frontiers in Physiology* 5, 179.

- McGrath, J.; Roy, P.; Perrin, B. J. (2017). Stereocilia morphogenesis and maintenance through regulation of actin stability. *Seminars in Cell and Developmental Biology* 65, 88–95.
- McReynolds, M. R.; Wang, W.; Holleran, L. M.; Hanna-Rose, W. (2017). Uridine monophosphate synthetase enables eukaryotic de novo NAD⁺ biosynthesis from quinolinic acid. *Journal of Biological Chemistry* 292, 11147–11153.
- Meiri, K. F.; Gordon-Weeks, P. R. (1990). GAP-43 in growth cones is associated with areas of membrane that are tightly bound to substrate and is a component of a membrane skeleton subcellular fraction. *Journal of Neuroscience* 10, 256–266.
- Meng, Y.; Ren, Z.; Xu, F.; Zhou, X.; Song, C.; Wang, V. Y. F.; Liu, W.; Lu, L.; Thomson, J. A.; Chen, G. (2018). Nicotinamide Promotes Cell Survival and Differentiation as Kinase Inhibitor in Human Pluripotent Stem Cells. *Stem Cell Reports* 11, 1347–1356.
- Michishita, E.; Park, J. Y.; Burneskis, J. M.; Barrett, J. C.; Horikawa, I. (2005). Evolutionarily conserved and nonconserved cellular localizations and functions of human SIRT proteins. *Molecular Biology of the Cell* 16, 4623–4635.
- Montell, C. (2005). The TRP superfamily of cation channels. *Science Signaling* 2005, re3–re3.
- Mori, V.; Amici, A.; Mazzola, F.; Di Stefano, M.; Conforti, L.; Magni, G.; Ruggieri, S.; Raffaelli, N.; Orsomando, G. (2014). Metabolic profiling of alternative NAD biosynthetic routes in mouse tissues. *PLoS ONE* 9, e113939.
- Nadrowski, B.; Albert, J. T.; Göpfert, M. C. (2008). Transducer-Based Force Generation Explains Active Process in *Drosophila* Hearing. *Current Biology* 18, 1365–1372.
- Nadrowski, B.; Effertz, T.; Senthilan, P. R.; Göpfert, M. C. (2011). Antennal hearing in insects - New findings, new questions. *Hearing Research* 273, 7-13.
- Nagarkar-Jaiswal, S.; Lee, P. T.; Campbell, M. E.; Chen, K.; Anguiano-Zarate, S.; Gutierrez, M. C.; Busby, T.; Lin, W. W.; He, Y.; Schulze, K. L.; Booth, B. W.; Evans-Holm, M.; Venken, K. J. T.; Levis, R. W.; Spradling, A. C.; Hoskins, R. A.; Bellen, H. J. (2015). A library of MiMICs allows tagging of genes and reversible, spatial and temporal knockdown of proteins in *Drosophila*. *eLife* 2015, e05338.
- Neel, V. A.; Young, M. W. (1994). igloo, a GAP-43-related gene expressed in the developing nervous system of *Drosophila*. *Development* 120, 2235–2243.
- Nesterov, A.; Spalthoff, C.; Kandasamy, R.; Katana, R.; Rankl, N. B.; Andrés, M.; Jähde, P.; Dorsch, J. A.; Stam, L. F.; Braun, F. J.; Warren, B.; Salgado, V. L.; Göpfert, M. C. (2015). TRP Channels in Insect Stretch Receptors as Insecticide Targets. *Neuron* 86, 665–671.
- Newton, F. G.; zur Lage, P. I.; Karak, S.; Moore, D. J.; Göpfert, M. C.; Jarman, A. P. (2012). Forkhead Transcription Factor Fd3F Cooperates with Rfx to Regulate a Gene Expression Program for Mechanosensory Cilia Specialization. *Developmental Cell* 22,

References

1221–1233.

Nikiforov, A.; Dölle, C.; Niere, M.; Ziegler, M. (2011). Pathways and subcellular compartmentation of NAD biosynthesis in human cells: From entry of extracellular precursors to mitochondrial NAD generation. *Journal of Biological Chemistry* 286, 21767–21778.

Olson, E. S.; Duifhuis, H.; Steele, C. R. (2012). Von Békésy and cochlear mechanics. *Hearing Research* 293, 31–43.

Onchuru, T. O.; Kaltenpoth, M. (2019). Quantitative PCR primer design affects quantification of dsRNA-mediated gene knockdown. *Ecology and Evolution* 9, 8187–8192.

Pan, J.; Wang, Q.; Snell, W. J. (2005). Cilium-generated signaling and cilia-related disorders. *Laboratory Investigation* 85, 452–463.

Patapoutian, A.; Peier, A. M.; Story, G. M.; Viswanath, V. (2003). Thermotrpt channels and beyond: Mechanisms of temperature sensation. *Nature Reviews Neuroscience* 4, 529–539.

Pedersen, S. F.; Owsianik, G.; Nilius, B. (2005). TRP channels: An overview. *Cell Calcium* 38, 233–252.

Porter, J. A.; Yu, M.; Doberstein, S. K.; Pollard, T. D.; Montell, C. (1993). Dependence of calmodulin localization in the retina on the NINAC unconventional myosin. *Science* 262, 1038–1042.

Reese, M. G. (2001). Application of a time-delay neural network to promoter annotation in the *Drosophila melanogaster* genome. *Computers and Chemistry* 26, 51–56.

Reilly, C. A.; Taylor, J. L.; Lanza, D. L.; Carr, B. A.; Crouch, D. J.; Yost, G. S. (2003). Capsaicinoids cause inflammation and epithelial cell death through activation of vanilloid receptors. *Toxicological Sciences* 73, 170–181.

Revollo, J. R.; Körner, A.; Mills, K. F.; Satoh, A.; Wang, T.; Garten, A.; Dasgupta, B.; Sasaki, Y.; Wolberger, C.; Townsend, R. R.; Milbrandt, J.; Kiess, W.; Imai, S. ichiro. (2007). Namp1/PBEF/Visfatin Regulates Insulin Secretion in β Cells as a Systemic NAD Biosynthetic Enzyme. *Cell Metabolism* 6, 363–375.

Richards, S.; Liu, Y.; Bettencourt, B. R.; Hradecky, P.; Letovsky, S.; Nielsen, R.; Thornton, K.; Hubisz, M. J.; Chen, R.; Meisel, R. P.; Couronne, O.; Hua, S.; Smith, M. A.; Zhang, P.; Liu, J.; Bussemaker, H. J.; van Batenburg, M. F.; Howells, S. L.; Scherer, S. E. et al. (2005). Comparative genome sequencing of *Drosophila pseudoobscura*: Chromosomal, gene, and cis-element evolution. *Genome Research* 15, 1–18.

Rongvaux, A.; Andris, F.; Van Gool, F.; Leo, O. (2003). Reconstructing eukaryotic NAD metabolism. *Bioessays* 25, 683–690.

Rosenzweig, M.; Kang, K. J.; Garrity, P. A. (2008). Distinct TRP channels are required

- for warm and cool avoidance in *Drosophila melanogaster*. *Proceedings of the National Academy of Sciences of the United States of America* *105*, 14668–14673.
- Roy, M.; Sivan-Loukianova, E.; Eberl, D. F. (2013). Cell-type-specific roles of Na⁺/K⁺ ATPase subunits in *Drosophila* auditory mechanosensation. *Proceedings of the National Academy of Sciences of the United States of America* *110*, 181–186.
- Ruan, K.; Zhu, Y.; Li, C.; Brazill, J. M.; Zhai, R. G. (2015). Alternative splicing of *Drosophila* Nmnat functions as a switch to enhance neuroprotection under stress. *Nature Communications* *6*, 1–14.
- Ruggero, M. A.; Rich, N. C. (1991). Application of a commercially-manufactured Doppler-shift laser velocimeter to the measurement of basilar-membrane vibration. *Hearing Research* *51*, 215–230.
- Ryskamp, D. A.; Witkovsky, P.; Barabas, P.; Huang, W.; Koehler, C.; Akimov, N. P.; Lee, S. H.; Chauhan, S.; Xing, W.; Rentería, R. C.; Liedtke, W.; Križaj, D. (2011). The polymodal ion channel transient receptor potential vanilloid 4 modulates calcium flux, spiking rate, and apoptosis of mouse retinal ganglion cells. *Journal of Neuroscience* *31*, 7089–7101.
- Sanxaridis, P. D.; Tsunoda, S. (2010). A forward genetic screen in *Drosophila melanogaster* to identify mutations affecting INAD localization in photoreceptor cells. *Fly* *4*, 95–103.
- Sattar, S.; Martinez, M. T.; Ruiz, A. F.; Hanna-Rose, W.; Thompson, G. A. (2019). Nicotinamide Inhibits Aphid Fecundity and Impacts Survival. *Scientific Reports* *9*, 1–11.
- Schöndorf, D. C.; Ivanyuk, D.; Baden, P.; Sanchez-Martinez, A.; De Cicco, S.; Yu, C.; Giunta, I.; Schwarz, L. K.; Di Napoli, G.; Panagiotakopoulou, V.; Nestel, S.; Keatinge, M.; Pruszek, J.; Bandmann, O.; Heimrich, B.; Gasser, T.; Whitworth, A. J.; Deleidi, M. (2018). The NAD⁺ Precursor Nicotinamide Riboside Rescues Mitochondrial Defects and Neuronal Loss in iPSC and Fly Models of Parkinson's Disease. *Cell Reports* *23*, 2976–2988.
- Seiner, D. R.; Hegde, S. S.; Blanchard, J. S. (2010). Kinetics and inhibition of nicotinamidase from mycobacterium tuberculosis. *Biochemistry* *49*, 9613–9619.
- Senthilan, P. R.; Piepenbrock, D.; Ovezmyradov, G.; Nadrowski, B.; Bechstedt, S.; Pauls, S.; Winkler, M.; Möbius, W.; Howard, J.; Göpfert, M. C. (2012). *Drosophila* auditory organ genes and genetic hearing defects. *Cell* *150*, 1042–1054.
- Sun, B.; Salvaterra, P. M. (1995). Characterization of Nervana, a *Drosophila melanogaster* Neuron-Specific Glycoprotein Antigen Recognized by Anti-Horseradish Peroxidase Antibodies. *Journal of Neurochemistry* *65*, 434–443.
- Sun, Y.; Liu, L.; Ben-Shahar, Y.; Jacobs, J. S.; Eberl, D. F.; Welsh, M. J. (2009). TRPA channels distinguish gravity sensing from hearing in Johnston's organ. *Proceedings of the National Academy of Sciences of the United States of America* *106*, 13606–13611.

References

- Talavage, T. M.; Sereno, M. I.; Melcher, J. R.; Ledden, P. J.; Rosen, B. R.; Dale, A. M. (2004). Tonotopic Organization in Human Auditory Cortex Revealed by Progressions of Frequency Sensitivity. *Journal of Neurophysiology* 91, 1282–1296.
- Tearle, R. (1991). Tissue specific effects of ommochrome pathway mutations in *Drosophila melanogaster*. *Genetical Research* 57, 257–266.
- Thibault, S. T.; Singer, M. A.; Miyazaki, W. Y.; Milash, B.; Dompe, N. A.; Singh, C. M.; Buchholz, R.; Demsky, M.; Fawcett, R.; Francis-Lang, H. L.; Ryner, L.; Cheung, L. M.; Chong, A.; Erickson, C.; Fisher, W. W.; Greer, K.; Hartouni, S. R.; Howie, E.; Jakkula, L. et al. (2004). A complementary transposon tool kit for *Drosophila melanogaster* using P and piggyBac. *Nature Genetics* 36, 283–287.
- Tilokani, L.; Nagashima, S.; Paupe, V.; Prudent, J. (2018). Mitochondrial dynamics: Overview of molecular mechanisms. *Essays in Biochemistry* 62, 341–360.
- Todi, S. V.; Sharma, Y.; Eberl, D. F. (2004). Anatomical and molecular design of the *Drosophila* antenna as a flagellar auditory organ. *Microscopy Research and Technique* 63, 388–399.
- Todorovic, V. (2016). Making sense of NAD⁺ subcellular localization. *Nature Methods* 13, 611–611.
- Tracey, W. D.; Wilson, R. I.; Laurent, G.; Benzer, S. (2003). *painless*, a *Drosophila* gene essential for nociception. *Cell* 113, 261–273.
- Tsunoda, S.; Sierralta, J.; Sun, Y.; Bodner, R.; Suzuki, E.; Becker, A.; Socolich, M.; Zuker, C. S. (1997). A multivalent PDZ-domain protein assembles signalling complexes in a G- protein-coupled cascade. *Nature* 388, 243–249.
- Tsunoda, S.; Sun, Y.; Suzuki, E.; Zuker, C. (2001). Independent anchoring and assembly mechanisms of INAD signaling complexes in *Drosophila* photoreceptors. *Journal of Neuroscience* 21, 150–158.
- Turner, H. N.; Armengol, K.; Patel, A. A.; Himmel, N. J.; Sullivan, L.; Iyer, S. C.; Bhattacharya, S.; Iyer, E. P. R.; Landry, C.; Galko, M. J.; Cox, D. N. (2016). The TRP Channels Pkd2, NompC, and Trpm Act in Cold-Sensing Neurons to Mediate Unique Aversive Behaviors to Noxious Cold in *Drosophila*. *Current Biology* 26, 3116–3128.
- Upadhyay, A.; Pisupati, A.; Jegla, T.; Crook, M.; Mickolajczyk, K. J.; Shorey, M.; Rohan, L. E.; Billings, K. A.; Rolls, M. M.; Hancock, W. O.; Hanna-Rose, W. (2016). Nicotinamide is an endogenous agonist for a *C. elegans* TRPV OSM-9 and OCR-4 channel. *Nature Communications* 7, 1–11.
- Venken, K. J. T.; Bellen, H. J. (2005). Emerging technologies for gene manipulation in *Drosophila melanogaster*. *Nature Reviews Genetics* 6, 167–178.
- Venken, K. J. T.; Schulze, K. L.; Haelterman, N. A.; Pan, H.; He, Y.; Evans-Holm, M.; Carlson, J. W.; Levis, R. W.; Spradling, A. C.; Hoskins, R. A.; Bellen, H. J. (2011). MiMIC: A highly versatile transposon insertion resource for engineering *Drosophila*

melanogaster genes. *Nature Methods* 8, 737–747.

Verhaagen, J.; Oestreicher, A. B.; Gispén, W. H.; Margolis, F. L. (1989). The expression of the growth associated protein B50/GAP43 in the olfactory system of neonatal and adult rats. *Journal of Neuroscience* 9, 683–691.

Voolstra, O.; Spät, P.; Oberegelsbacher, C.; Claussen, B.; Pfannstiel, J.; Huber, A. (2015). Light-dependent phosphorylation of the drosophila inactivation no afterpotential D (INAD) scaffolding protein at Thr170 and Ser174 by eye-specific protein kinase C. *PLoS ONE* 10, e0122039.

Vrablik, T. L.; Huang, L.; Lange, S. E.; Hanna-Rose, W. (2009). Nicotinamidase modulation of NAD⁺ biosynthesis and nicotinamide levels separately affect reproductive development and cell survival in *C. elegans*. *Development* 136, 3637–3646.

Vrablik, T. L.; Wang, W.; Upadhyay, A.; Hanna-Rose, W. (2011). Muscle type-specific responses to NAD⁺ salvage biosynthesis promote muscle function in *Caenorhabditis elegans*. *Developmental Biology* 349, 387–394.

Wang, W.; McReynolds, M. R.; Goncalves, J. F.; Shu, M.; Dhondt, I.; Braeckman, B. P.; Lange, S. E.; Kho, K.; Detwiler, A. C.; Pacella, M. J.; Hanna-Rose, W. (2015). Comparative metabolomic profiling reveals that dysregulated glycolysis stemming from lack of salvage NAD⁺ biosynthesis impairs reproductive development in *Caenorhabditis elegans*. *Journal of Biological Chemistry* 290, 26163–26179.

Xie, X.; Harrison, D. H.; Schlichting, I.; Sweet, R. M.; Kalabokis, V. N.; Szent-Györgyi, A. G.; Cohen, C. (1994). Structure of the regulatory domain of scallop myosin at 2.8 Å resolution. *Nature* 368, 306–312.

Yamanaka, M. K.; Saugstad, J. A.; Hanson-Painton, O.; McCarthy, B. J.; Tobin, S. L. (1987). Structure and expression of the *Drosophila* calmodulin gene. *Nucleic acids research* 15, 3335–3348.

Yan, C.; Wang, F.; Peng, Y.; Williams, C. R.; Jenkins, B.; Wildonger, J.; Kim, H. J.; Perr, J. B.; Vaughan, J. C.; Kern, M. E.; Falvo, M. R.; O'Brien, E. T.; Superfine, R.; Tuthill, J. C.; Xiang, Y.; Rogers, S. L.; Parrish, J. Z. (2018). Microtubule Acetylation Is Required for Mechanosensation in *Drosophila*. *Cell Reports* 25, 1051–1065.

Yan, Z.; Zhang, W.; He, Y.; Gorczyca, D.; Xiang, Y.; Cheng, L. E.; Meltzer, S.; Jan, L. Y.; Jan, Y. N. (2013). *Drosophila* NOMPC is a mechanotransduction channel subunit for gentle-touch sensation. *Nature* 493, 221–225.

Yorozu, S.; Wong, A.; Fischer, B. J.; Dankert, H.; Kernan, M. J.; Kamikouchi, A.; Ito, K.; Anderson, D. J. (2009). Distinct sensory representations of wind and near-field sound in the *Drosophila* brain. *Nature* 458, 201–205.

Zanini, D.; Giraldo, D.; Warren, B.; Katana, R.; Andrés, M.; Reddy, S.; Pauls, S.; Schwedhelm-Domeyer, N.; Geurten, B. R. H.; Göpfert, M. C. (2018). Proprioceptive Opsin Functions in *Drosophila* Larval Locomotion. *Neuron* 98, 67–74.

References

Zhai, R. G.; Cao, Y.; Hiesinger, P. R.; Zhou, Y.; Mehta, S. Q.; Schulze, K. L.; Verstreken, P.; Bellen, H. J. (2006). *Drosophila* NMNAT maintains neural integrity independent of its NAD synthesis activity. *PLoS Biology* 4, e416.

Zhang, W.; Yan, Z.; Jan, L. Y.; Jan, Y. N. (2013). Sound response mediated by the TRP channels NOMPC, NANCHUNG, and INACTIVE in chordotonal organs of *Drosophila* larvae. *Proceedings of the National Academy of Sciences of the United States of America* 110, 13612–13617.

Zhang, W.; Cheng, L. E.; Kittelmann, M.; Li, J.; Petkovic, M.; Cheng, T.; Jin, P.; Guo, Z.; Göpfert, M. C.; Jan, L. Y.; Jan, Y. N. (2015). Ankyrin Repeats Convey Force to Gate the NOMPC Mechanotransduction Channel. *Cell* 162, 1391–1403.

Zuber, M. X.; Strittmatter, S. M.; Fishman, M. C. (1989). A membrane-targeting signal in the amino terminus of the neuronal protein GAP-43. *Nature* 341, 345–348.

Appendix

Unveiling the role of the visual scaffolding protein INAD in hearing

Our ability to sense odors, light, or sound relies on dedicated sensory cells transducing these stimuli into electrical signals. Molecularly, this stimulus transduction is mediated by ion channels that are gated directly by the stimuli or indirectly via signaling cascades. The indirect gating characterizes, for example, phototransduction, where photons are first absorbed by rhodopsin molecules whose activation triggers a second messenger cascade that ultimately alters the open probability of chemically gated ion channels. By contrast, mechanical stimulus forces as imposed by sound or touch can directly gate transduction channels without intermittent signaling cascades. Here, the stimulus force promotes gating movements of the transduction channels. Such direct transduction allows the receptor cells to electrically respond to the stimuli with the utmost speed, yet it does not allow for the biochemical signal amplification that can be provided by second messenger cascades. The latter disadvantage has been circumvented by some auditory receptors that, before transduction, mechanically amplify sound-induced vibrations on a cycle-by-cycle basis.

The fastest known second-messenger cascade is the phototransduction cascade of *Drosophila*, which operates about ten times faster than mammalian rods. One reason for this exquisite speed seems related to the structural organization of all the cascade components, which are compacted into one macromolecular signalplex, the transducisome. Central to this transducisome is INAD, a 674 amino acid scaffolding protein with five PDZ domains (Tsunoda et al., 1997). In general, PDZ domains help to hold together signaling complexes at cell membranes, and, in fly photoreceptors, INAD keeps together the transducisome through its PDZ domains. INAD PDZ domains reportedly interact with (i) NINAE, the fly's major visual opsin protein, the (ii) G-protein coupled phospholipase C, NORPA that triggers the gating of the phototransduction channels by hydrolyzing phosphatidyl-inositol (4,5) bisphosphate (PIP2) to generate diacylglycerol (DAG), inositol (1,4,5) trisphosphate (InsP3), and a proton, (iii) TRP phototransduction channels, the (iv) eye-specific protein kinase C (eye-PKC) INAC, which negatively regulates phototransduction, the (v) calmodulin-binding protein NINAC that, together with the protein Retinophilin, terminates the signaling cascade.

Intriguingly, many of the above components seem also to occur in the *Drosophila* hearing organ. Transcriptome analyses have identified various genes that are expressed

in JO, including diverse ion channels and axonemal dyneins. Unexpectedly, also virtually all the components of the phototransduction signalplex were detected in JO, including the opsin NINAE, the PLC NORPA, TRP phototransduction channels, and the INAD scaffolding protein. Functional studies further revealed that mechanosensory JO function requires INAD and visual opsins.

Opsins are expressed in JO mechanoreceptors where they seem to modulate sound transduction (Katana et al., 2019). The expression pattern of INAD in JO, however, has not yet been examined, and the same applies to its subcellular localization, its molecular integration, and its functional role. Might INAD be forming a signalplex, or even a transducisome, in JO as it does in photoreceptors? And if so, what are its binding partners, and how does it contribute to cellular mechanosensitivity? Answering these questions promises surprising fundamental insights in mechanosensory cell function and the evolution of sensory signalplexes and sensory signaling cascades. As it happens, JO mechanoreceptors and fly photoreceptors are evolutionarily related. Both cell types seem to have diversified from common ancestor cells, or ‘protosensory’ cells. Analyzing INAD in JO, as proposed here, thus promises not only insights into mechanosensory cell function, but also might contribute to our understanding of the evolution of sensory signalplexes and signaling cascades.

Transgenic flies

To investigate the role of INAD in JO, I needed flies with a null mutation in the *inaD* gene. One mutant line, *inaD*¹, was kindly provided by Susan Tsunoda (Tsunoda et al., 1997). In this mutant, a stop mutation in exon 4 leads to a truncated and nonfunctional protein. Since this is a chemical-induced mutation, other genes may also be influenced, besides the fact that the first four intact exons in this gene may also have sufficient function in JO but not in the eyes – the mutants are blind. For these reasons, two other *inaD* mutant flies were generated as follows:

inaD^{2, TGEM}-Gal4

Since there was no reported MiMIC insertion in *inaD*, an *inaD*^{2, TGEM}-Gal4 line was generated. In summary, the Trojan-Gal4 expression module (T-GEM) construct (Diao et al., 2015) was inserted in the Intron between exon 1 and 2 of *inaD* by the CRISPR-CAS 9 method (Figure 55). (The injection was performed by the Genetivision Company).

inaD^{3, CRIMIC}-Gal4

While the MiMIC technique was incapable of tagging many genes in *Drosophila*, Bellen et al. developed CRISPR-Mediated Integrated Cassette (CRIMIC) (Lee et al., 2018), which is based on the CRISPR-CAS9 method. *inaD*^{3, CRIMIC}-Gal4 was a kind gift from Hugo Bellen.

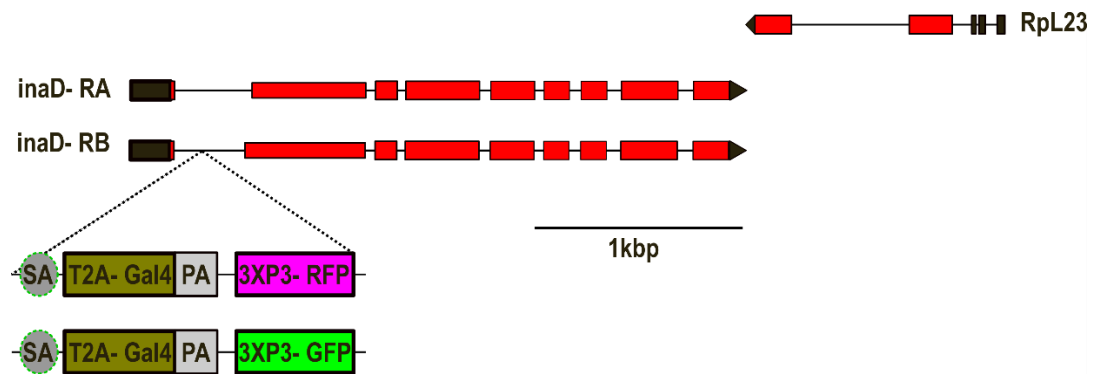


Figure 55. *inaD*^{2, TGEM}-Gal4, and *inaD*^{3, CRIMIC}-Gal4 constructs.

CRISPR-Mediated Integrated Cassette (CRIMIC), or Trojan-Gal4 expression module (T-GEM) were inserted in the first intron between exon1 and 2. RA and RB are two transcripts of *inaD* differing at the beginning of the second exon. Both cassettes have a splicing acceptor (SA), which disrupts the normal splicing of *inaD*, polyadenylation (PA), which terminates transcription, and T2A, which leads to the landing of the ribosome from the beginning of the Gal4 transcription factor. RFP in CRIMIC and GFP in TGEM are the genome cassette integration markers.

In these transgenic flies, *inaD* splicing should be disrupted because of the splicing acceptor sequence in the cassette, which is followed by GAL4 and Polyadenylation signal. Besides the Gal4 transcription factor, alternative splicing can lead to the expression of the WT splice variant of the gene. PCR with specific primers for the two *inaD* WT transcripts on cDNA from *inaD*^{2, TGEM}-Gal4, *inaD*^{3, CRIMIC}-Gal4, and *cn*¹ *bw*¹ flies, confirmed the occurrence of alternative splicing (Figure 56). For quantitative measurement, RT-qPCR was performed, which showed a lower amount of WT transcripts in *inaD*^{3, CRIMIC}-Gal4 than in the *inaD*^{2, TGEM}-Gal4 line (Figure 57).

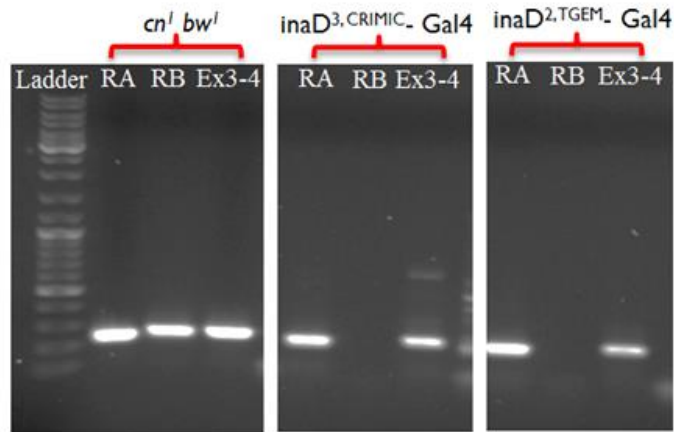


Figure 56. PCR on cDNA of *cn¹ bw¹*, *inaD³, CRIMIC-Gal4*, and *inaD², TGEM-Gal4*. *RA*, the more dominant transcript of *inaD* is present in both the cDNA from *inaD², TGEM-Gal4*, and *inaD³, CRIMIC-Gal4* flies, while the less abundant transcript, *RB*, is absent in these two samples. The PCR with primers spanning exon 3 and 4 was performed to test whether other transcripts exist.

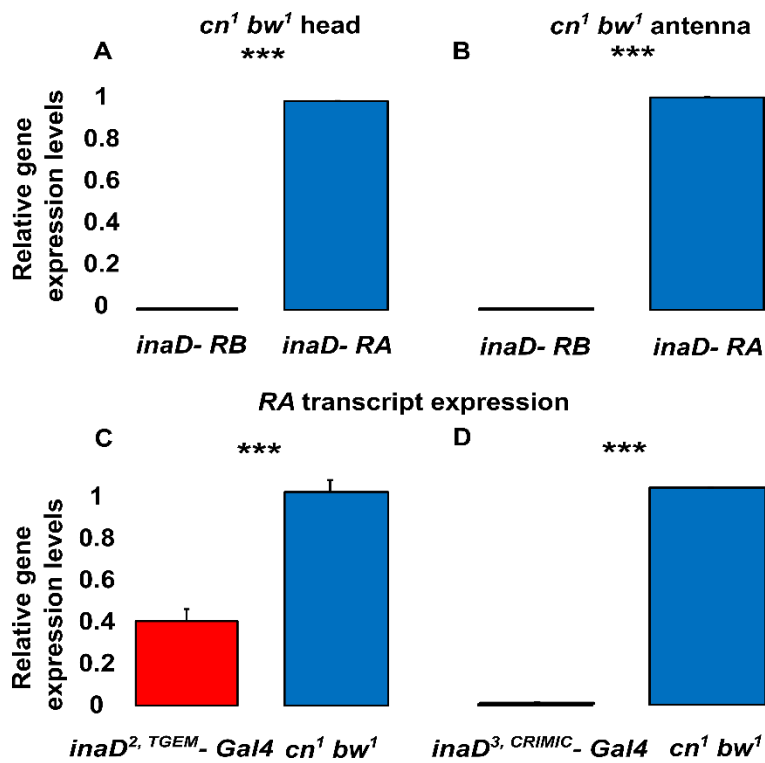


Figure 57. Quantification of *inaD* transcripts in *cn¹ bw¹*, *inaD², TGEM-Gal4*, and *inaD³, CRIMIC-Gal4*. *RA* transcript is more abundant than *RB* in both heads (including antennae) and antennae of *cn¹ bw¹* (A, B). *RA* transcript in *inaD³, CRIMIC-Gal4* is less than *inaD², TGEM-Gal4* and both are less than *RA* transcript in *cn¹ bw¹* (C, D). Mann-Whitney-U tests were used for statistical analysis. Statistical significances are indicated with *** ($p < 0.001$).

For having a proper null mutant, a vector with two gRNAs (one on 5'UTR very close to the first exon and the other one on the sixth exon) was constructed. The gRNAs were chosen based on their efficacy and low off-target effects. This construct was sent for injection to BestGene. If both gRNA lead the CAS9 to cut the desired place in the genome, a deletion spanning the first six exons will be generated. In case only one gRNA works, a smaller deleted area with some modifications due to non-homologous end-joining repair would be the outcome. The modification should be assessed by PCR and subsequent sequencing (This has been stopped because of the final results).

The contribution of INAD to JO function, including auditory transduction and mechanical amplification

Mechanoelectrical transduction and nonlinear mechanical amplification in JO can be used as an indication of auditory integrity. Compound action potentials and displacement of the antennal sound receiver evoked by pure tone stimuli are shown in Figure 58.

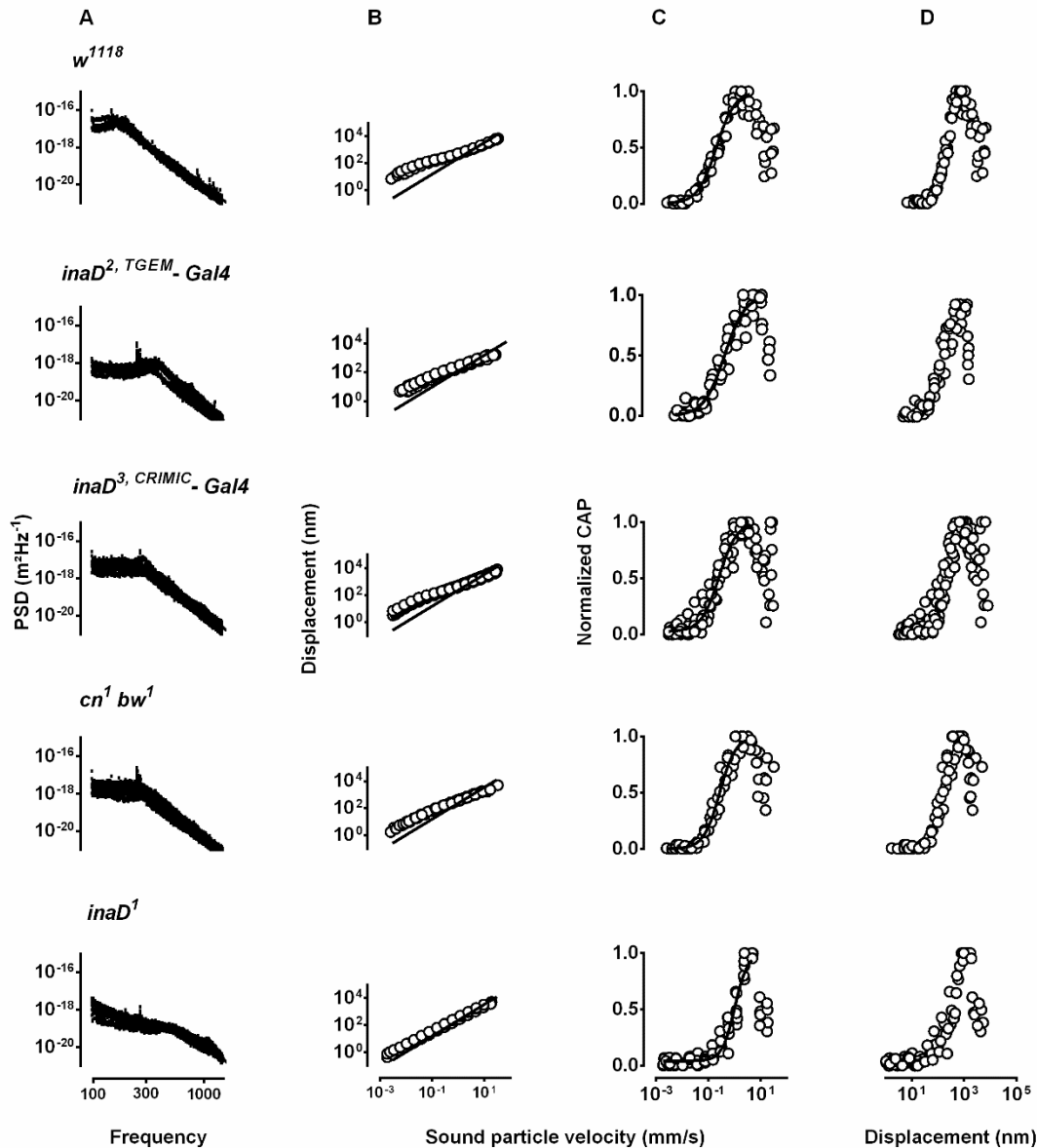


Figure 58. The auditory phenotype in *inaD* mutants compared to the respective control flies (Part I). Power spectra of the mechanical fluctuations of the antennal sound receiver (A) as well as antennal displacement (B), normalized compound action potential (CAP) amplitudes (C) as a function of the sound particle velocity, and CAP amplitude as a function of antennal displacement (D) in *w¹¹¹⁸*, *inaD², TGEM-Gal4*, *inaD³, CRIMIC-Gal4*, *cn¹ bw¹*, and *inaD¹* flies. *inaD², TGEM-Gal4*, and *inaD³, CRIMIC-Gal4* flies, compared to their genetic background (*w¹¹¹⁸*), have normal sensitivity but lower amplification (linearized displacement). (Because of alternative splicing, there is variability in the observed phenotypes). *inaD¹*, compared to its genetic background (*cn¹ bw¹*), shows lower sensitivity (right-shifted CAP response) and lower mechanical amplification. At least 5 flies were measured for each genotype.

Compared to genetic background controls (*w¹¹¹⁸*, *cn¹ bw¹*) strains, mechanical amplifications were reduced in *inaD¹* mutants, however in *inaD², TGEM-Gal4* and *inaD³, CRIMIC-Gal4* mutants, this varied considerably, possibly due to the alternative splicing and thus, varying amounts of the WT protein. While some of the flies show WT-auditory amplification, others showed lowered mechanical amplification (Figure 59).

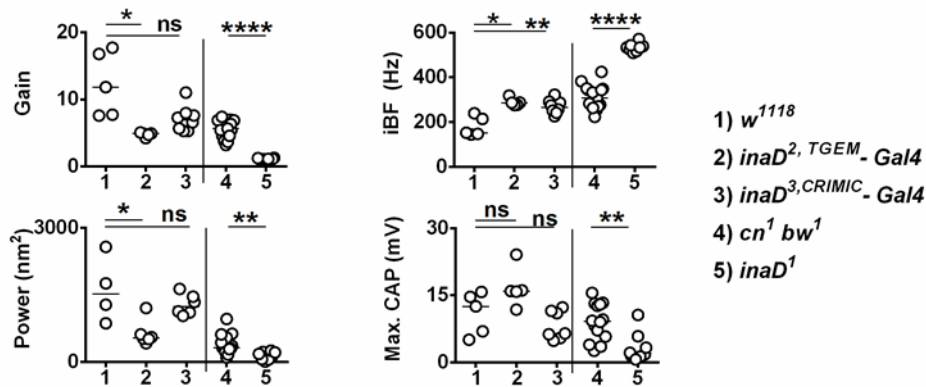


Figure 59. The auditory phenotype in *inaD* mutants compared to the respective control flies (Part II). *inaD¹*, compared to its genetic background (*cn¹ bw¹*), and *inaD^{3, CRIMIC}-Gal4*, *inaD^{2, TGEM}-Gal4*, compared to *w¹¹¹⁸*, show a lower gain, higher iBF, and lower power (not in *inaD^{3, CRIMIC}-Gal4*). Maximum CAP data, due to the different positions of the inserted electrode, is not informative. Mann-Whitney-U tests with the Bonferroni correction were used for statistical analysis. Statistical significances are indicated with ns ($P > 0.05$), * ($P \leq 0.05$), ** ($P \leq 0.01$), **** ($P \leq 0.0001$).

Cellular expression of the *inaD* gene

Gal4 driver in *inaD^{2, TGEM}-Gal4* and *inaD^{3, CRIMIC}-Gal4* flies was used for visualizing *inaD* expression by driving *UAS-GFP* or *RFP* reporters. For that, *inaD^{2, TGEM}-Gal4*, and *inaD^{3, CRIMIC}-Gal4* flies were crossed to *UAS-GFP*, and *UAS-RFP* flies, respectively. Since RFP in *inaD^{2, TGEM}-Gal4*, and GFP in *inaD^{3, CRIMIC}-Gal4* work as genome integration markers, the vice versa staining would not be informative (Figure 60).

The expression of the Gal4 transcription factor under the control of the *inaD* promoter did not drive the expression of GFP or RFP in JO neurons (Supplement Figure 84). For increasing the probable existing faint signal, different reporters, antibodies (Chicken anti GFP, GFP-nanobody, and FluoTag®-X4 anti-GFP), and protocols were tested. In all conditions, no stronger signal than background was observed.

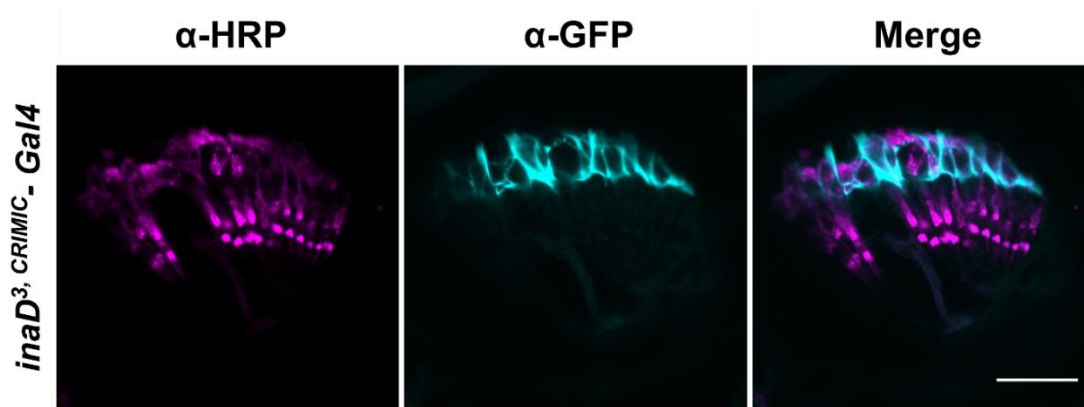


Figure 60. *inaD³, CRIMIC-Gal4* integration marker.

Anti-HRP labels the neurons (magenta), and anti-GFP shows the GFP integration marker of the CRIMIC cassette (cyan) (not the expression pattern of *inaD*). Scale bar: 20 μ m.

In homozygous flies for both the *inaD* Gal4 transcription factor and UAS-GFP, also no signal was observed in the JO.

Western blotting with anti-INAD antibody from Voolstra et al. (Voolstra et al., 2015), which works in western blot but not immunostaining, was performed on protein extracts from *inaD* mutants and respective control flies. As it is shown in Figure 61, INAD protein is absent in extracts from *inaD¹* mutant but not in *inaD², TGEM-Gal4* flies, and it is low in *inaD³, CRIMIC-Gal4* flies. Here, *cn¹ bw¹* was used as a genetic background control and *Canton-S* (CS) as a WT control.

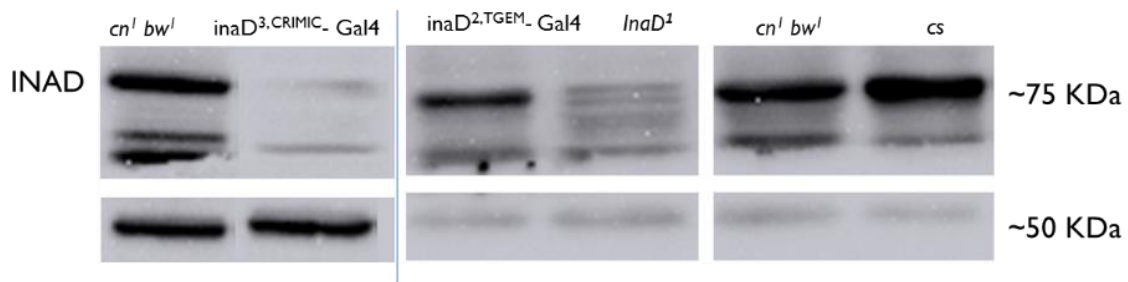


Figure 61. INAD level in *inaD* mutants compared to the respective control flies.

INAD antibody recognizes some unspecific bands, while it also marks a region around 75 KDa, which is pertinent to INAD. β -Tubulin was used as an indication of protein extraction efficacy. While in *cn¹ bw¹* and *Canton-S* (CS), INAD is highly expressed, the amount of INAD is dropped from *inaD², TGEM-Gal4* line to *inaD³, CRIMIC-Gal4*, and *inaD¹*. Western blot on *cn¹ bw¹* and *inaD³, CRIMIC-Gal4* have been done separately (left image).

INAD protein localization

Anti-INAD from Susan Tsunoda (Tsunoda et al., 1997) marks JO in both *inaD*¹ and WT flies (data not shown). I did not expect to see any signal in *inaD*¹ mutants since the antibody recognizes the last 300 amino acids, which is absent in the mutants because of the nonsense mutation. The signal was specific because when the first antibody was used without the secondary antibody, and vice versa, no signal was observed. According to the databases, there is no other protein with high homology to INAD; however, there might be a possibility that another protein in its three-dimensional state binds to the INAD antibody. For purifying the antibody, all proteins from *inaD*¹ mutant flies were extracted and premixed with INAD antibody before usage, though no signal was observed as before.

Uncovering *inaD* mutations with a deficiency line

In the deficiency line, *Df* (*BSC864*), there is an enormous deletion in the second chromosome, including the *inaD* gene. If the hearing defect in the *inaD*¹ mutant flies is due to the *inaD* gene disruption, one should observe the same phenotype when the mutation is uncovered with the deficiency. This deficiency line cannot be balanced with a customary balancer, harboring a visible marker since the deletion also includes a gene called *RpL23*. The *RpL23* gene needs to be present in two copies for fly survival, for that reason, the deficiency chromosome (*Df*) has been kept over a duplicated and inverted chromosome (*Dp*). The duplicated chromosome contains two copies of the *RpL23* and some other genes (the exact position of deletion and duplication is not known). The hearing phenotype in flies with *inaD*¹ and *Df* (*BSC864*) was not recapitulating homozygous *inaD*¹ hearing defect (each progeny of the cross was confirmed by PCR) (data not shown).

Different comparisons on variable crosses of the deficiency line are shown in Figure 62. The mechanical amplification for *inaD*¹ over *Dp* resembles that of *Canton-S* over *Dp*, however, in *inaD*¹ over *Df* it has a lower value than *Canton-S* over *Df*. There could be two explanations for the observed phenotype: first, the mutation in *inaD*¹ causes the difference, or second, the extra copies of some genes in the duplicated chromosome (presumably *RpL23*) causes the phenotype.

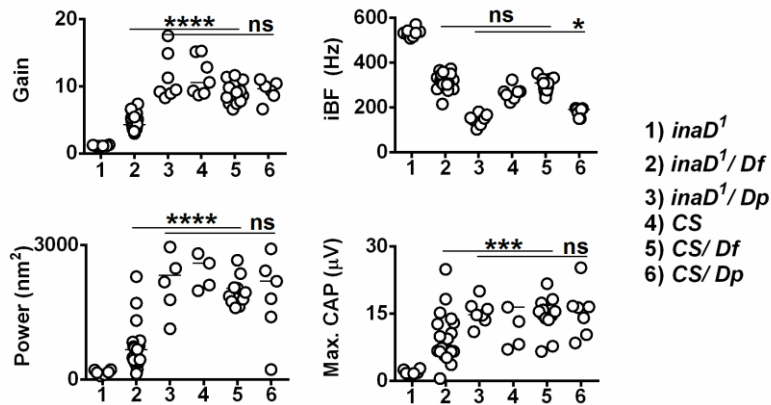


Figure 62. Uncovering *inaD* mutation with a deficiency line.

Gain, power, and Max. CAP (but not iBF) show *CS/Dp* is like *inaD*¹/*Dp*, while *inaD*¹/*Df* is significantly different from *CS/Df* which could be due to the duplicated genes for the first observation or *inaD*¹ mutation in the second one. $n \geq 5$ flies/genotype. Two-tailed Mann-Whitney-U tests with the Bonferroni correction were used for statistical analysis. Statistical significances are indicated with ns ($P > 0.05$), * ($P \leq 0.05$), *** ($P \leq 0.001$), **** ($P \leq 0.0001$).

Since I did not have a decent deficiency line for the *inaD* gene, I crossed *inaD*¹ to *inaD*^{3, CRIMIC}-*Gal4* flies to produce a progeny with a low amount of INAD protein. In case the function of INAD is dose-dependent, I should see a hearing defect more severe than *inaD*^{3, CRIMIC}-*Gal4* homozygous flies. *inaD*^{3, CRIMIC}-*Gal4/inaD*¹ mutants recapitulate the *inaD*^{3, CRIMIC}-*Gal4* phenotype. The analysis on the amplification gain, iBF, power, and maximum CAP in *inaD*^{3, CRIMIC}-*Gal4/inaD*¹ compared to *inaD*^{3, CRIMIC}-*Gal4* showed no significant difference (Figure 63). It could be that a low amount of INAD in *inaD*^{3, CRIMIC}-*Gal4* due to the alternative splicing is sufficient for the hearing organ function.

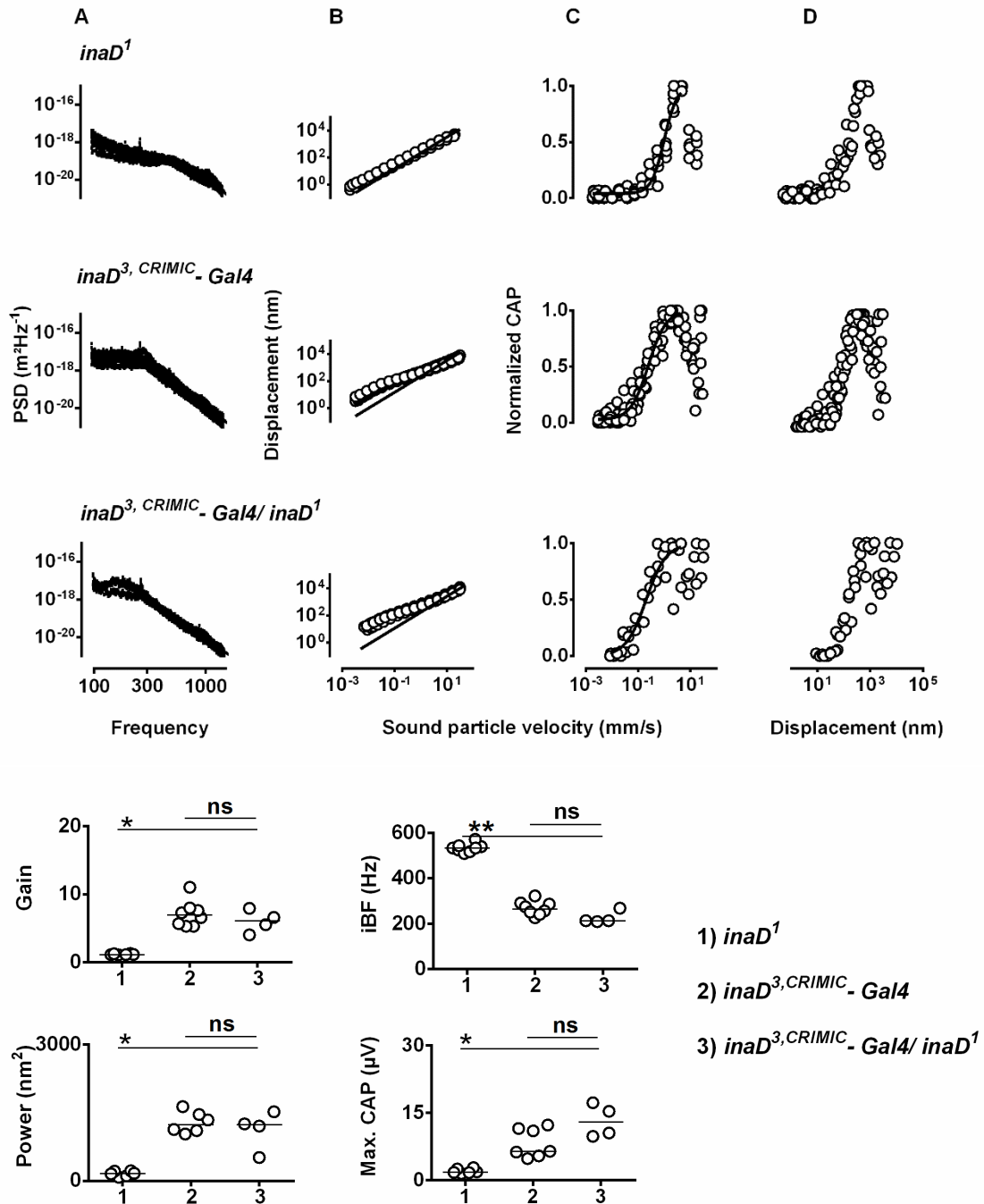


Figure 63. The auditory phenotype in *inaD^{3, CRIMIC-Gal4/inaD¹}* compared to *inaD^{3, CRIMIC-Gal4}*.

Top: power spectra of the mechanical fluctuations of the antennal sound receiver (A) as well as antennal displacement (B), normalized compound action potential (CAP) amplitudes (C) as a function of the sound particle velocity, and CAP amplitude as a function of antennal displacement (D) in *inaD¹*, *inaD^{3, CRIMIC-Gal4}*, and *inaD^{3, CRIMIC-Gal4/inaD¹}* flies. Bottom: corresponding amplification gain, individual best frequencies, power of the receiver fluctuations, and maximum CAP amplitudes. *inaD^{3, CRIMIC-Gal4/inaD¹}* hearing phenotype is similar to *inaD^{3, CRIMIC-Gal4}* without any deterioration. $n \geq 5$ flies/genotype. Two-tailed Mann-Whitney-U tests with the Bonferroni correction were used for statistical analysis. Statistical significances are indicated with ns ($P > 0.05$), * ($P \leq 0.05$), ** ($P \leq 0.01$).

Rescuing the mutant phenotype

Rescuing the *inaD* mutant phenotype can support the correlation of the observed hearing defect with the *inaD* mutations (Figure 58). One possibility for rescuing the mutant phenotype was using *hs-inaD* flies, provided by Susan Tsunoda (Tsunoda et al., 2001). The *hs-inaD* flies only express *inaD* after heat shock, though this line turned out not to rescue hearing (data not shown).

The flies, *P(GMR-inaD-GFP); inaD¹*, provided by Susan Tsunoda (Sanxaridis and Tsunoda, 2010), could also be used for rescuing the *inaD¹* mutation. These flies carry *inaD* tagged with *GFP* on the first chromosome under the *GMR* promoter control and the *inaD¹* mutation on the second chromosome. The *GMR* promoter is used for deriving expression in photoreceptors. I expected to have an improved auditory perception due to the *inaD* mutation rescue. Besides, the rescue phenotype has already been reported in vision (Sanxaridis and Tsunoda, 2010).

The audition in these flies was similar to the mutant (data not shown), and staining with anti-GFP showed no signal in the JO (data not shown). One possibility for the observed phenotype could be the absence of *GMR* expression in the JO. To test that, I stained the progeny of *GMR-Gal4* crossed to the *20XUAS-6XGFP*. A very weak signal appeared in the JO, while the driver is strong (Figure 64). This needs to be taken into consideration when interpreting hearing perception recovery or GFP signals in the *P(GMR-inaD-GFP); inaD¹* flies.

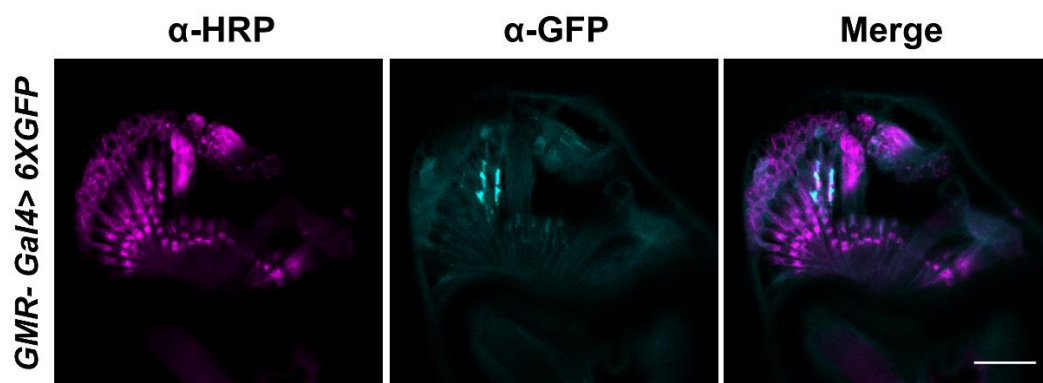


Figure 64. GMR expression pattern.

Driving *20XUAS-6XGFP* with *GMR-Gal4* (*GMR-Gal4>6XGFP*) (cyan) partially labels the JO. Anti-HRP labels the neurons (magenta). Scale bar: 20 μ m.

As another approach for rescue, an area (19914 *CH322-163010* on *2R:22853474...22873387*) was chosen to be integrated into the third chromosome by *attB*-P[acman]. Since the *RpL23* gene is very close to the *inaD* (Figure 55), the selected area also contains the *RpL23*.

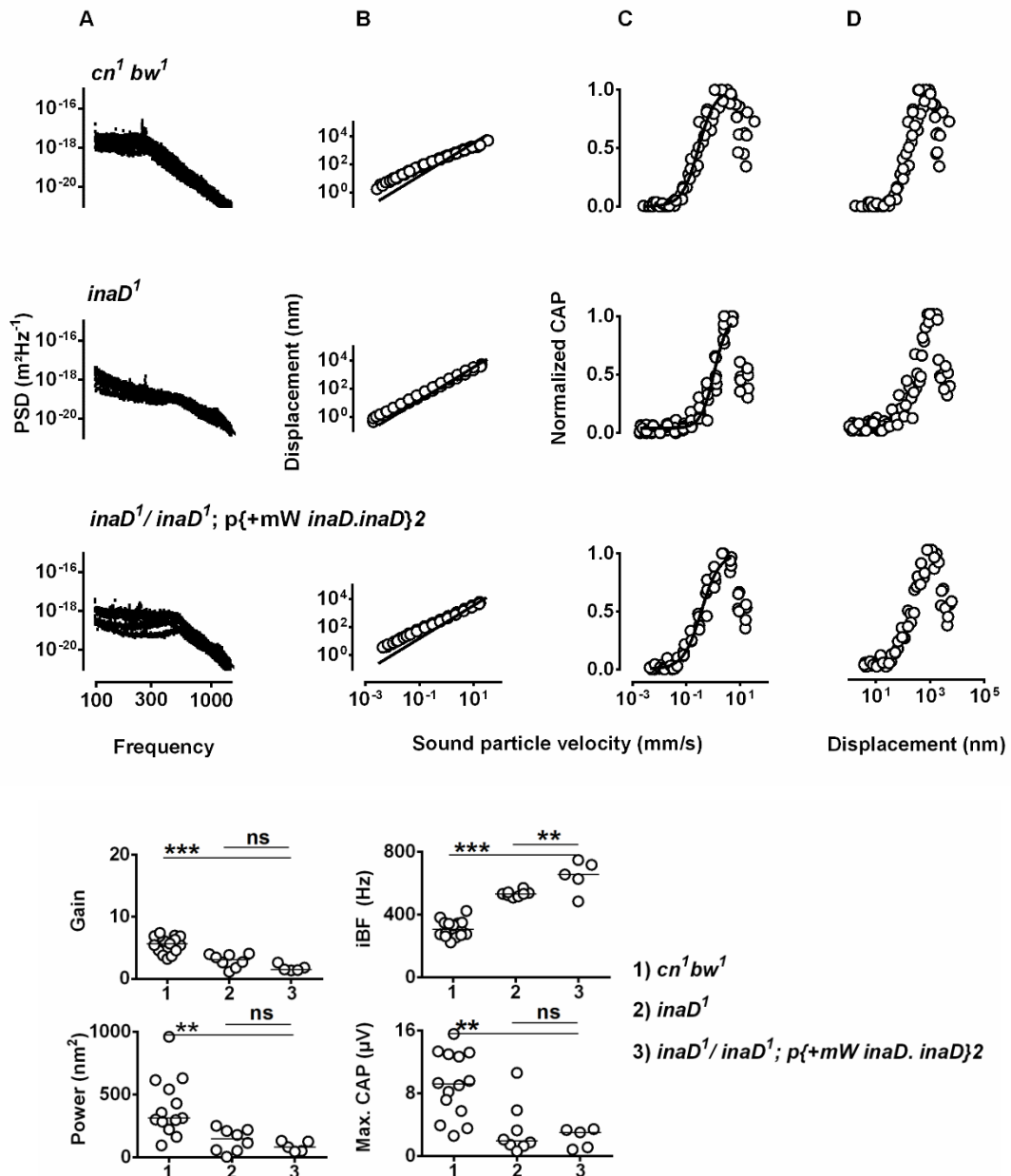


Figure 65. The auditory phenotype of *inaD¹* compared to genomic rescued flies.

Top: power spectra of the mechanical fluctuations of the antennal sound receiver (A) as well as antennal displacement (B), normalized compound action potential (CAP) amplitudes (C) as a function of the sound particle velocity, and CAP amplitude as a function of antennal displacement (D) in *cn¹bw¹*, *inaD¹*, and *inaD¹/inaD¹; p{+mW inaD.inaD}²* flies. Bottom: corresponding amplification gain, individual best frequencies, power of the receiver fluctuations, and maximum CAP amplitudes. The *inaD¹/inaD¹; p{+mW inaD.inaD}²* flies did not show an improved auditory perception. $n \geq 5$ flies/genotype. Two-tailed Mann-Whitney-U tests with the Bonferroni correction were used for statistical analysis. Statistical significances are indicated with ns ($P > 0.05$), ** ($P \leq 0.01$), *** ($P \leq 0.001$).

It is shown in Figure 65 that *inaD¹/inaD¹; p {+mW inaD. inaD}2* flies did not show an improved auditory perception.

By Western blotting, the presence of INAD was confirmed in the respective flies (data not shown). The flies also showed rescued vision phenotype (Figure 66). One explanation for the observed phenotype can be the interferences of the *RpL23* or another redundant gene next to the *inaD* gene with hearing but not vision.

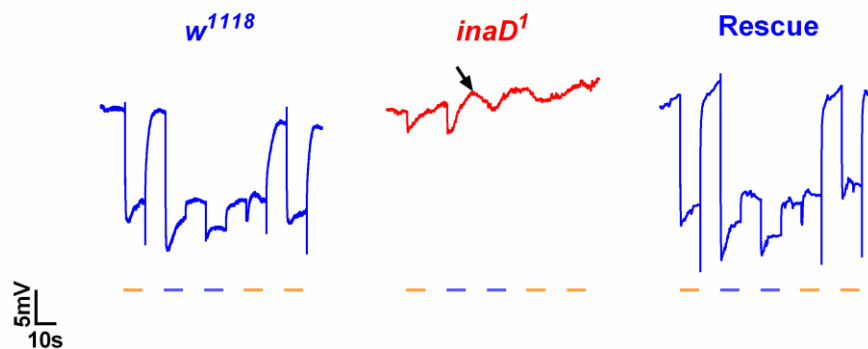


Figure 66. PDA phenotype in *w¹¹¹⁸* as a control, *inaD¹*, and rescue flies.

Prolonged depolarizing afterpotential (PDA) is a simple and efficient way for phototransduction functional assessment. In the WT genotype, PDA appears after the end of the first blue stimulus, when most of the rhodopsin molecules activate and are in a metarhodopsin state. The stimulus protocol is shown at the bottom as lines. Each represents a 10 s stimulus separating with 10 s intervals (one orange stimulus followed by two blue stimuli and two subsequent orange stimuli). In *inaD¹*, there is an inactivation after the first blue stimulus but no PDA (black arrow), while in *w¹¹¹⁸* and rescue, both inactivation and PDA exist.

Since the previously generated fly did not lead to any conclusive result about *inaD* function in hearing, I made *UAS-inaD* and *UAS-inaD::GFP* flies that only carry the *inaD* but not extra adjacent genes.

Driving *UAS-inaD::GFP* with *Dnai2-Gal4* (*Dnai2-Gal4>inaD::GFP*), I probed the derived INAD expression in the respective flies (Figure 67). Co-staining of these flies with anti-INAD antibody from Susan Tsunoda (Tsunoda et al., 1997) did not show any overlapping signals; this led to the conclusion that the antibody from Susan Tsunoda (Tsunoda et al., 1997) binds unspecifically.

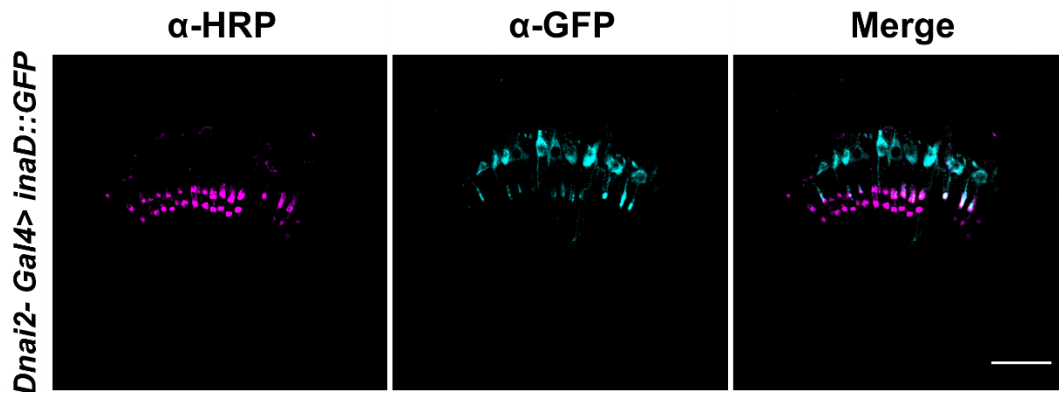


Figure 67. Derived expression pattern of *inaD*.

Driving *UAS-inaD::GFP* with *Dnai2-Gal4* (*Dnai2-Gal4>inaD::GFP*) (cyan) labels the JO neurons. Anti-HRP labels the neurons (magenta). Scale bar: 20 μ m.

Unfortunately, driving *UAS-inaD* or *UAS-inaD::GFP* with *Dnai2-Gal4* (*Dnai2-Gal4>inaD* or *inaD::GFP*) also did not recover the hearing perception in the *inaD*¹ mutant flies (data not shown); however, driving *UAS-inaD::GFP* with *Tub85-Gal4* (*Tub85-Gal4>inaD::GFP*) (provided by Radoslaw Katana) leads to a significant change in iBF but not mechanical amplification, power of the receiver fluctuations, and maximum CAP amplitudes compared to the *inaD*¹ mutant flies (Figure 68).

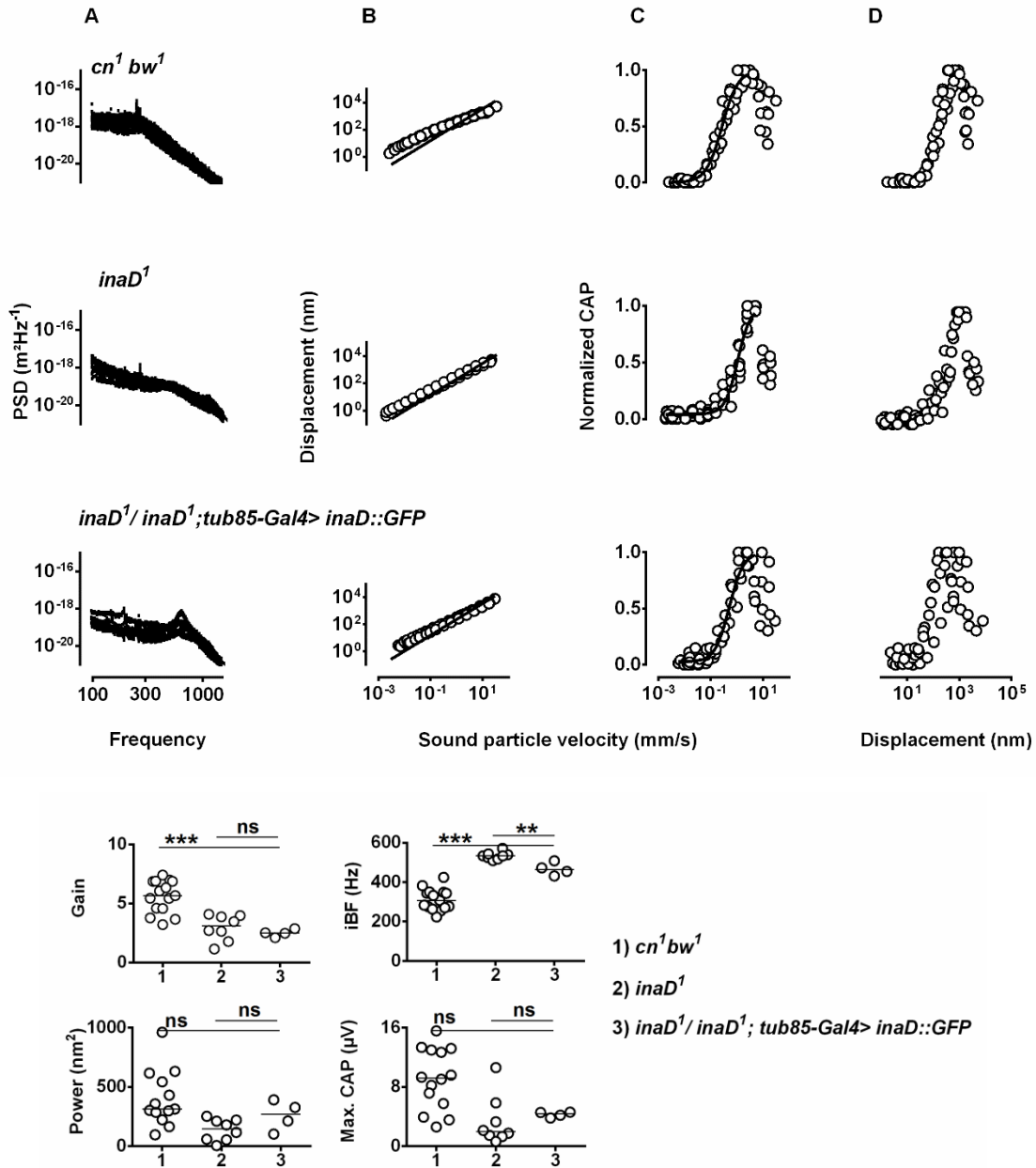


Figure 68. The auditory phenotype in *inaD¹* compared to UAS rescued flies.

Top: power spectra of the mechanical fluctuations of the antennal sound receiver (A) as well as antennal displacement (B), normalized compound action potential (CAP) amplitudes (C) as a function of the sound particle velocity, and CAP amplitude as a function of antennal displacement (D) in *cn¹bw¹*, homozygous *inaD¹*, and *inaD¹/inaD¹; tub85-Gal4 > inaD::GFP* flies. Bottom: corresponding amplification gain, individual best frequencies, power of the receiver fluctuations, and maximum CAP amplitudes. The *inaD¹* hearing phenotype is similar to the rescued flies, without any improvement. $n \geq 5$ flies/genotype. Two-tailed Mann-Whitney-U tests with the Bonferroni correction were used for statistical analysis. Statistical significances are indicated with ns ($P > 0.05$), ** ($P \leq 0.01$), *** ($P \leq 0.001$).

One reason for the unsuccessful rescued hearing could be an insufficient amount or an incorrect location for the expressed INAD in the JO of the respective flies.

In conclusion, JO function is impaired in the *inaD*¹, *inaD*^{2, TGEM-Gal4}, and *inaD*^{3, CRIMIC-Gal4} mutant flies since there is a reduction in the average of the mechanical amplification. The sensitivity is also reduced in the *inaD*¹ mutants, as CAPs are only evoked by loud sounds. A deficiency line did not uncover the mutation, and rescuing the phenotype in the *inaD*¹ mutant flies was unsuccessful. Besides, immunohistochemistry reinforced the absence of INAD localization in the JO.

Based on the obtained data, there can be a possibility for INAD involvement in hearing (Table 11). For making clear conclusions about the role of INAD in hearing, one can continue characterizing the *inaD*^{DEL} flies.

Table 11. Brief summary of INAD project.

	<i>inaD</i> ¹	<i>inaD</i> ^{2, TGEM-Gal4}	<i>inaD</i> ^{3, CRIMIC-Gal4}	<i>inaD</i> ^{1/ inaD} ¹ ; p{+mW <i>inaD. inaD</i> }2	WT (control)	<i>inaD</i> ^{DEL}
Vision	-	+	-	+	+	?
Hearing	-	+	+	-	+	?
RA	+	+ (~40%)	-(very low)	+ (not tested)	+	?
RB	+	-	-	+ (not tested)	+	?
Protein (western blot)	-	+	-	+	+	?
Protein (Immunohist ochemistry)		-	-			?

Supplement pictures

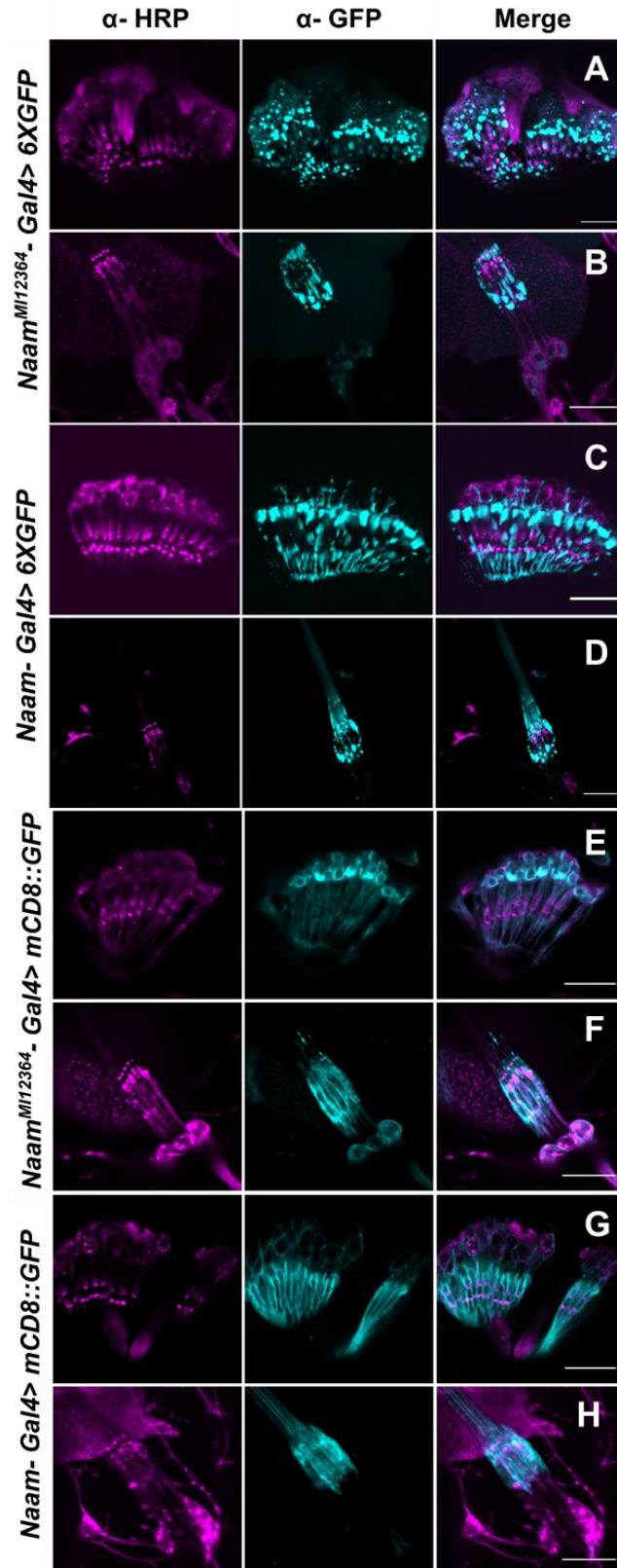


Figure 69. *Naam* expression in scolopale and cap cells (different reporters).

Driving *20XUAS-6XGFP* or *UAS-mCD8::GFP* with *Naam^{MI12364}-Gal4* (cyan) (*Naam^{MI12364}-Gal4>6XGFP* or *mCD8::GFP*) labels neurons, scolopale, and cap cells of the adult *Drosophila* JO (A, E) and the larval chordotonal organ Ich5 (B, F), however, driving the same reporters with *Naam-Gal4* (cyan) (*Naam-Gal4>6XGFP* or *mCD8::GFP*) does not label the neurons of the adult *Drosophila* JO (C, G) and the larval chordotonal organ Ich5 (D, H). Anti-HRP labels the neurons (magenta). Scale bars: 20 μ m.

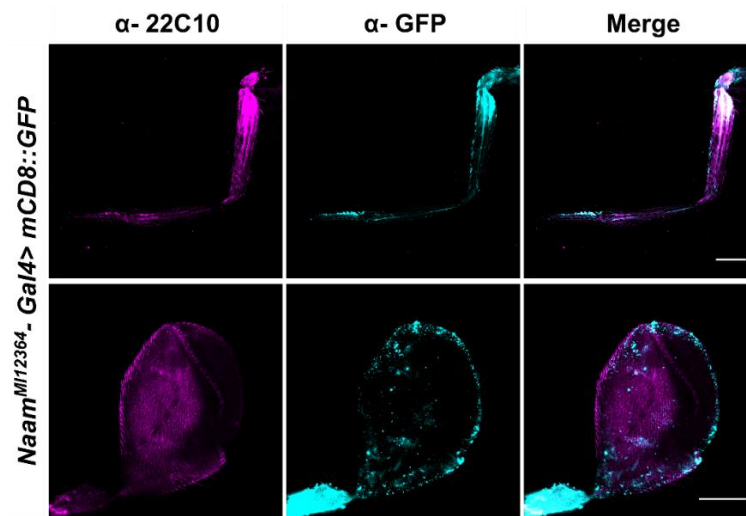


Figure 70. *Naam* expression in the leg chordotonal and haltere pedicelum.

Driving *UAS-mCD8::GFP* with *Naam^{MI12364}-Gal4* (cyan) (*Naam^{MI12364}-Gal4>mCD8::GFP*) labels the femoral chordotonal organ in the leg of adult flies (A) and their haltere pedicel (B). Anti-22C10 labels the neurons (magenta). Scale bars: 2 mm in panel A, 50 μ m in panel B.

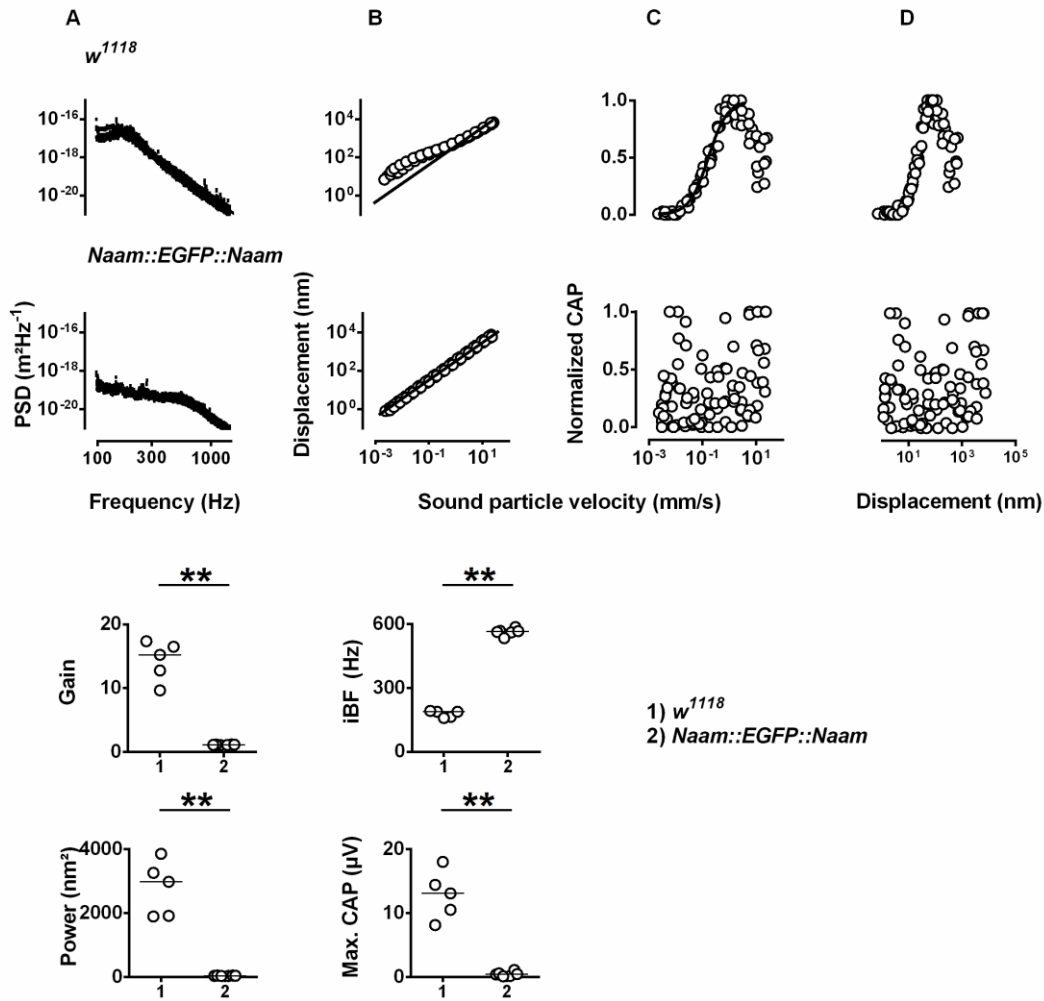


Figure 71. Hearing defect in the internally GFP-tagged NAAM flies.

Top: power spectra of the mechanical fluctuations of the antennal sound receiver (A) as well as antennal displacement (B), normalized compound action potential (CAP) amplitudes (C) as a function of the sound particle velocity, and CAP amplitude as a function of antennal displacement (D) in *w¹¹¹⁸*, and *Naam::EGFP::Naam* flies. Bottom: corresponding amplification gain, individual best frequencies, power of the receiver fluctuations, and maximum CAP amplitudes. The integration of the GFP cassette in the middle of the *Naam* gene caused hearing loss in the respective flies. $n \geq 5$ flies/genotype. Two-tailed Mann-Whitney-U tests were used for statistical analysis. Statistical significance is indicated with ** ($P \leq 0.01$).

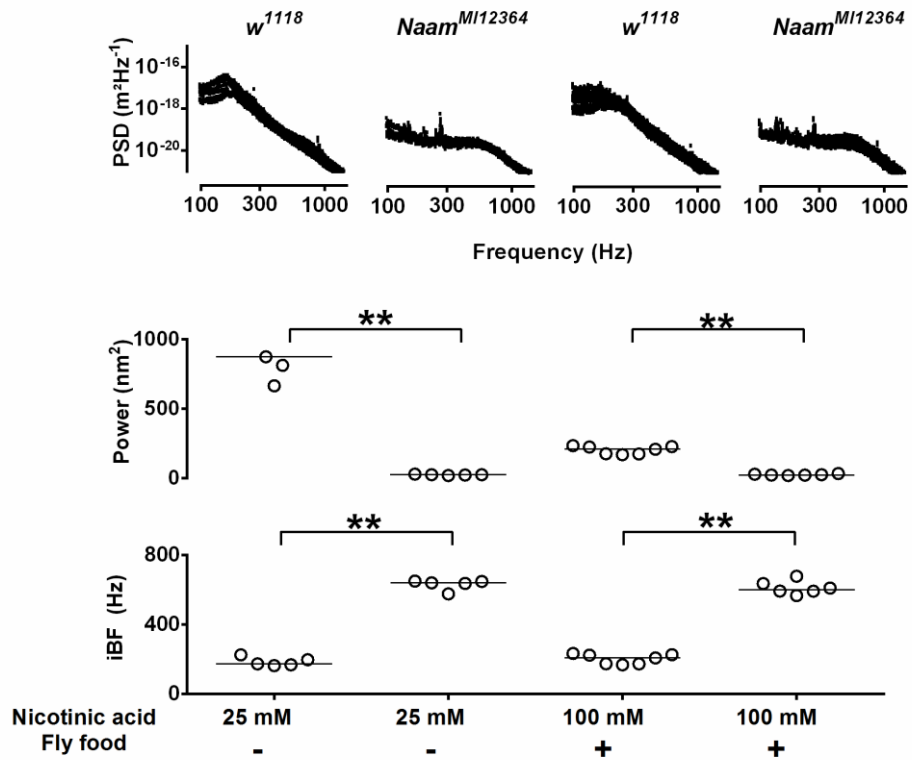


Figure 72. Absence of nicotinic acid rescue effect on hearing of the *Naam* mutant flies.

Naam^{M12364} mutant flies were treated with 25 mM nicotinic acid for 3 hours after overnight starvation or 100 mM nicotinic acid plus fly food (from the larval stage). In neither case, an improved auditory perception was obtained. $n \geq 5$ flies/genotype. Mann-Whitney-U tests were used for statistical analysis. Statistical significance is indicated with ** ($P \leq 0.01$).

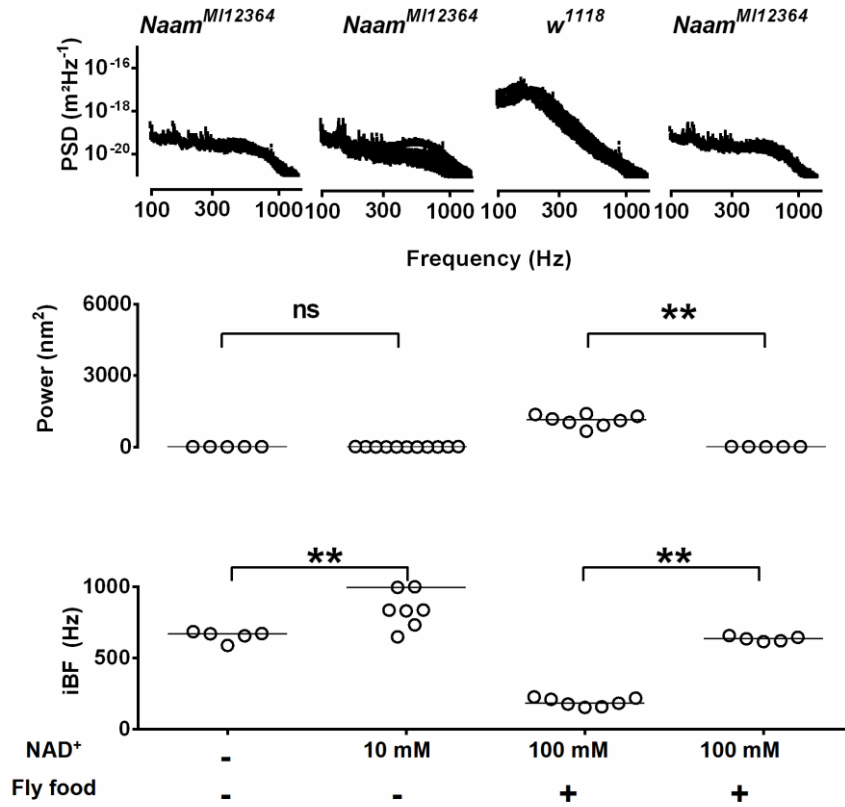


Figure 73. Absence of NAD⁺ rescue effect on hearing of the *Naam* mutant flies.

Naam^{MI12364} mutant flies were treated with 10 mM NAD⁺ for 3 hours after overnight starvation or 100 mM NAD⁺ plus fly food (from the larval stage). In neither case, an improved auditory perception was obtained. $n \geq 5$ flies/genotype. Mann-Whitney-U tests were used for statistical analysis. Statistical significances are indicated with ns ($P > 0.05$), ** ($P \leq 0.01$).

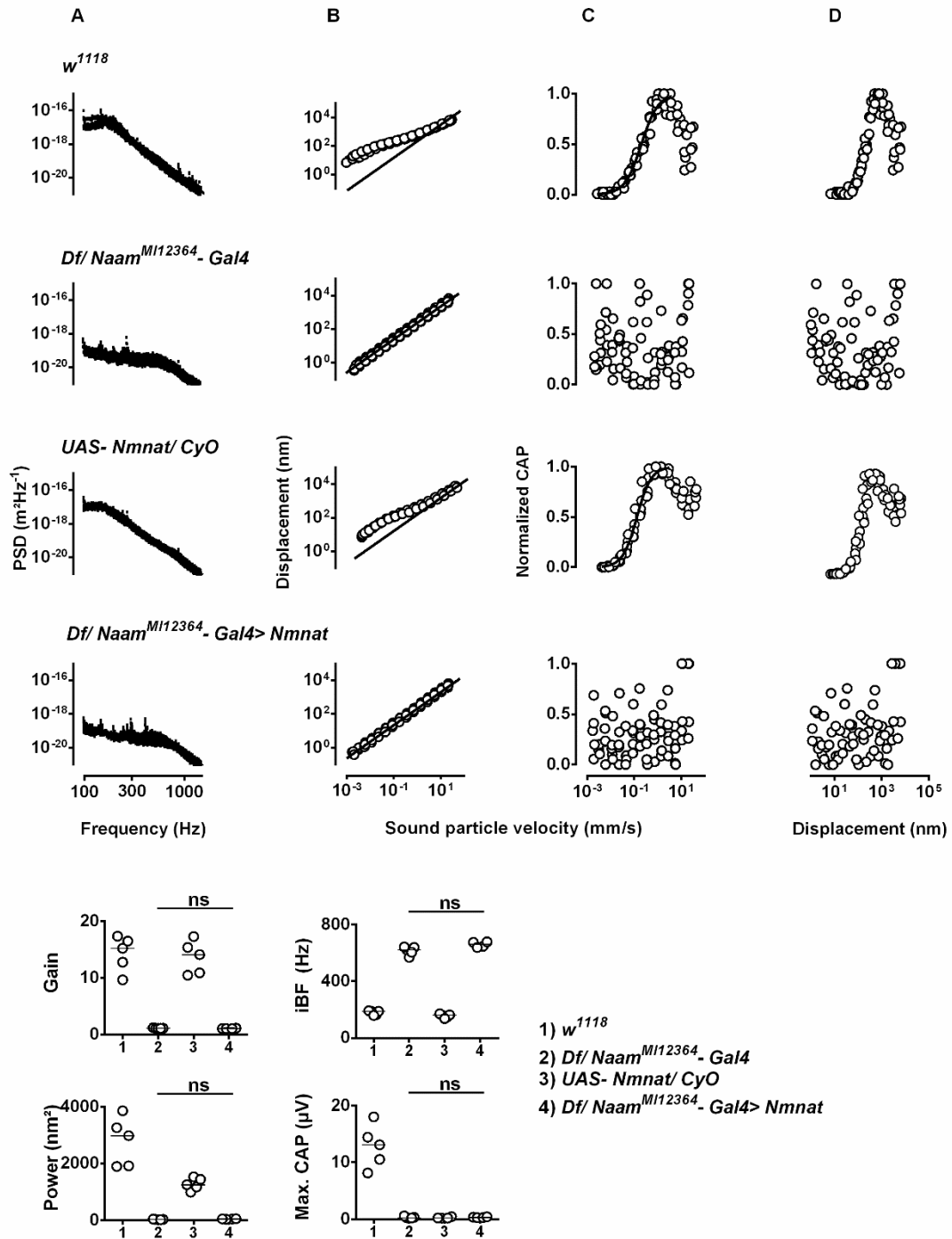


Figure 74. Absence of overexpressed *Nmnat* rescue effect on hearing of the *Naam* mutant flies.

Top: power spectra of the mechanical fluctuations of the antennal sound receiver (A) as well as antennal displacement (B), normalized compound action potential (CAP) amplitudes (C) as a function of the sound particle velocity, and CAP amplitude as a function of antennal displacement (D) in *w¹¹¹⁸*, *Df(3R)BSC809/Naam^{MI12364}-Gal4*, *UAS-Nmnat/CyO*, and *Df(3R)BSC809/Naam^{MI12364}-Gal4>Nmnat* flies. The *Nmnat* overexpression did not recover the hearing perception in the *Naam* mutant flies. Bottom: corresponding amplification gain, individual best frequencies, power of the receiver fluctuations, and maximum CAP amplitudes. $n \geq 5$ flies/genotype. Two-tailed Mann-Whitney-U tests were used for statistical analysis. Statistical significance is indicated with ns ($P > 0.05$).

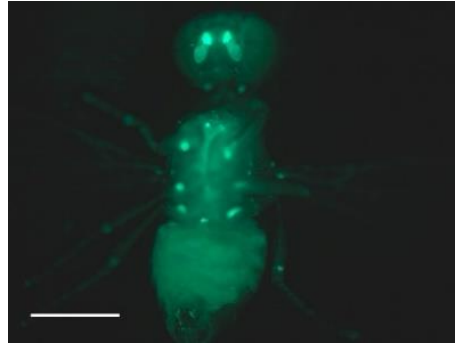


Figure 75. Fluorescent picture of *Naam*^{MI12364}-Gal4>*Naam*::GFP flies.
 Driving *UAS-Naam*::GFP construct with *Naam*^{MI12364}-Gal4 driver (*Naam*^{MI12364}-Gal4>*Naam*::GFP) in green labels antenna and the femoral chordotonal organ in the leg of adult *Drosophila*. Scale bar: 1 mm.

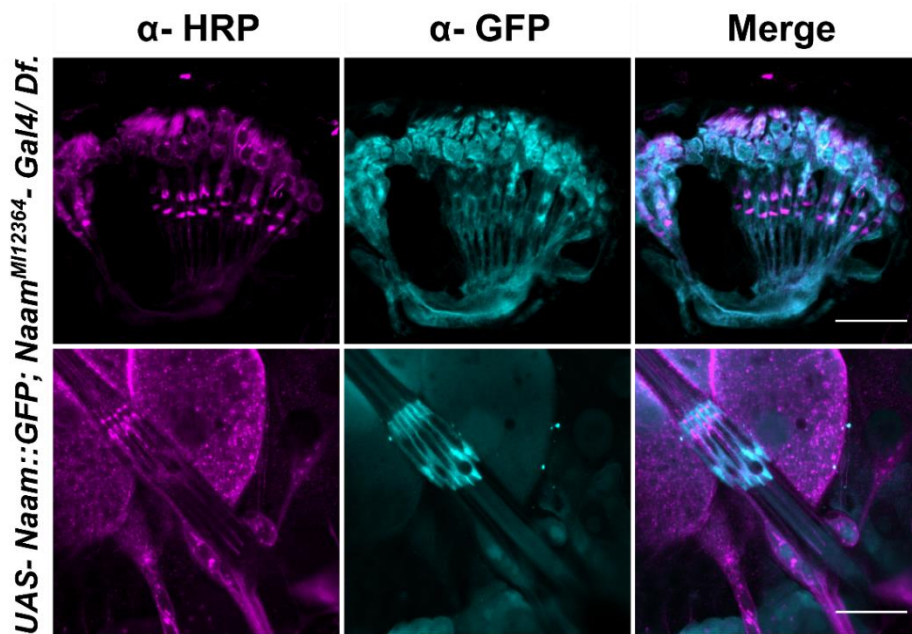
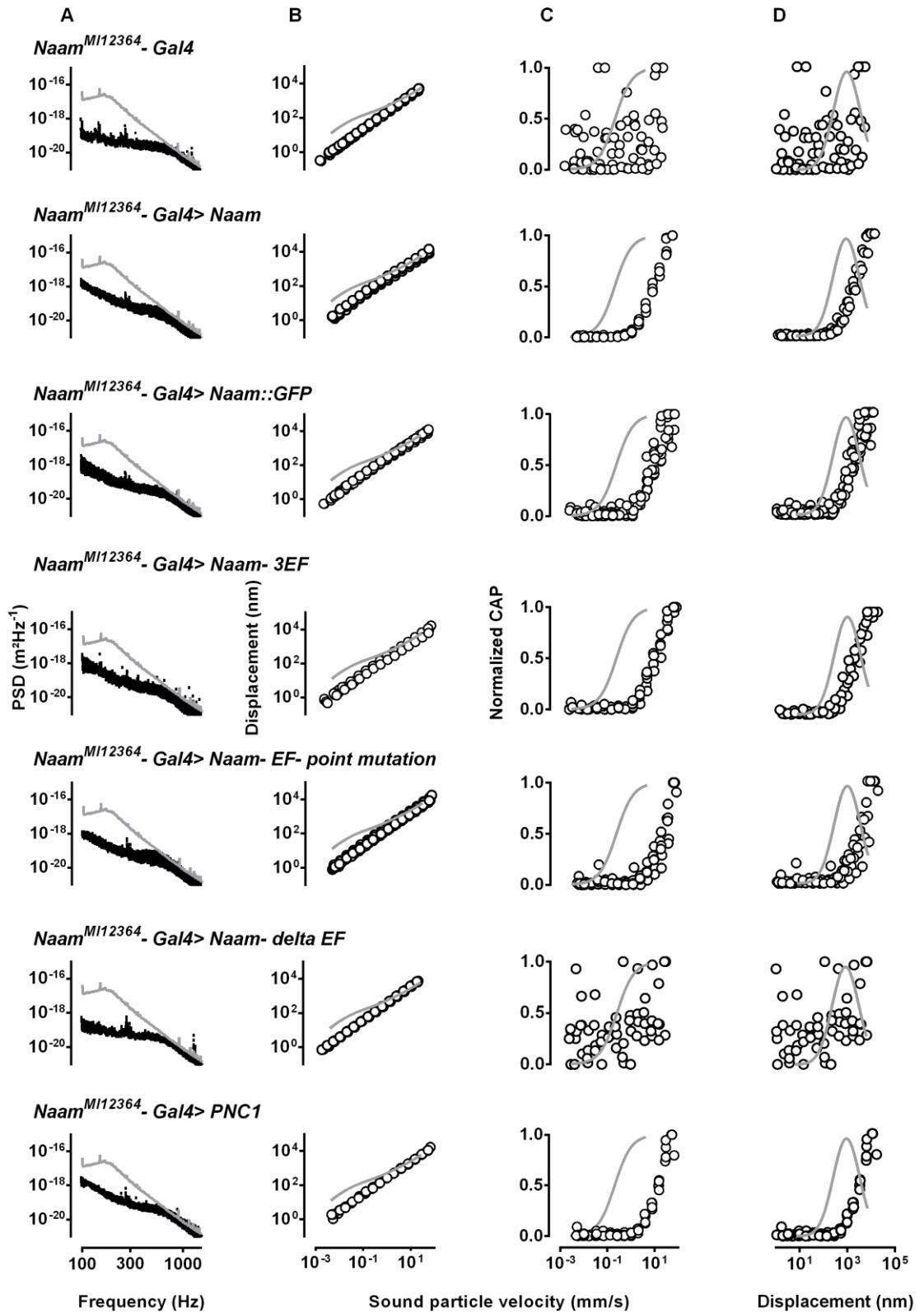
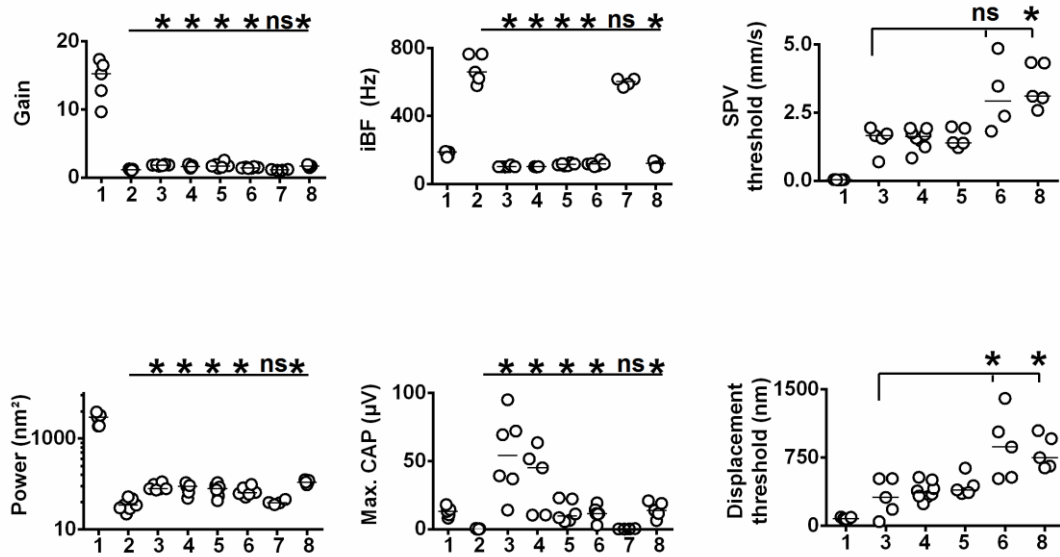


Figure 76. NAAM localization in the *Naam* mutant flies with recovered hearing perception.
 Driving *UAS-Naam*::GFP construct with *Naam*^{MI12364}-Gal4 driver (*Naam*^{MI12364}-Gal4>*Naam*::GFP) in the mutant *Naam*^{MI12364}-Gal4/Df(3R)BSC809 flies labels neurons, scolopale and cap cells (cyan) in both adult JO (upper panel), and larvae lch5 (lower panel). Anti-HRP labels the neurons (magenta). Scale bars: 20 μ m.



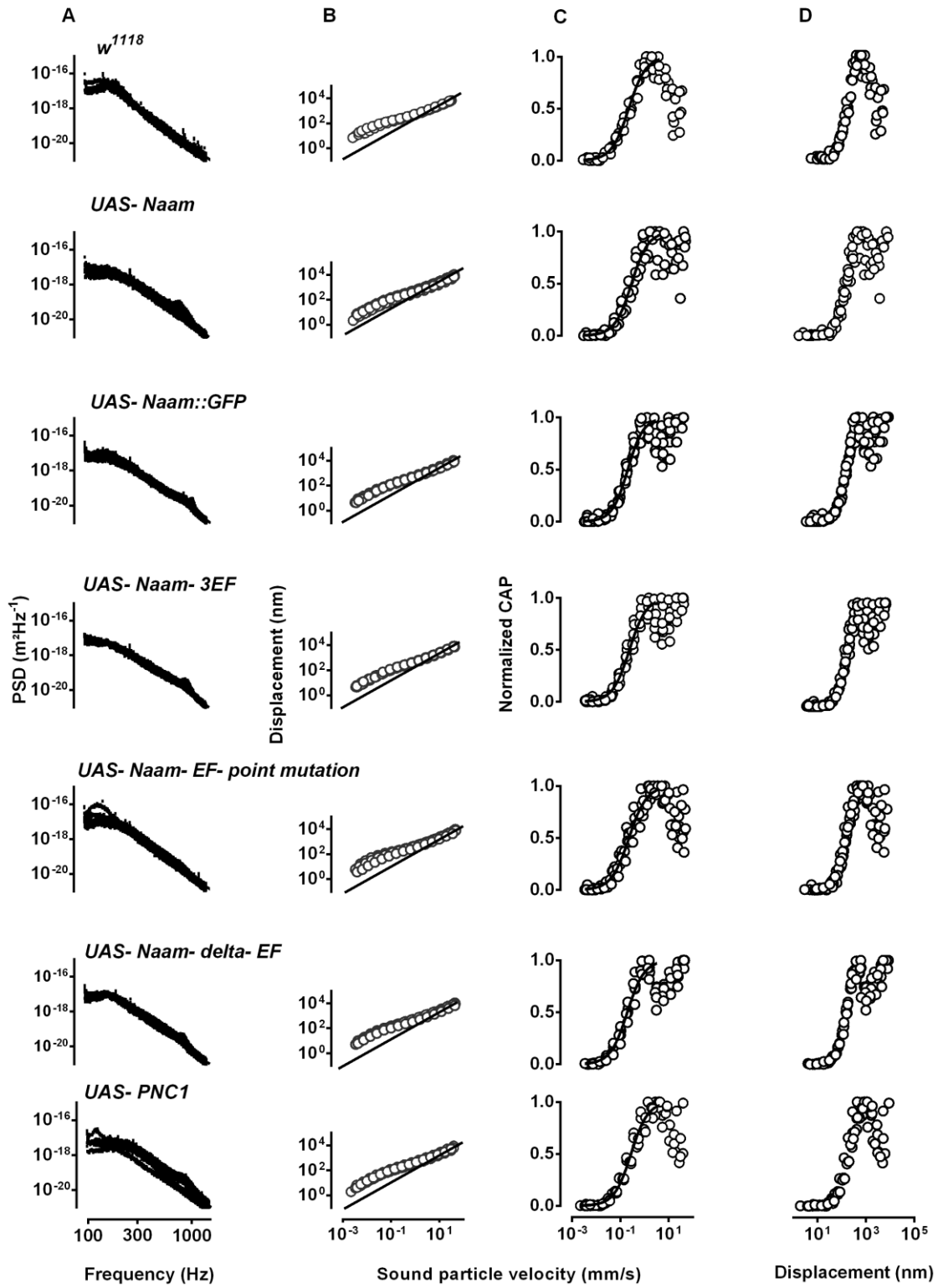


	1	2	3	4	5	6	7	8
Gain	14.30 3.117	1.150 0.1051	1.820 0.1000	1.642 0.2170	1.798 0.4160	1.460 0.1023	1.143 0.06625	1.653 0.1773
iBF	178.2 15.43	677.4 83.86	103.7 4.590	102.2 0.8367	115.5 7.503	118.8 14.19	598.0 23.41	117.2 15.79
Power	2782 861.8	35.59 10.71	86.62 15.05	80.61 23.26	76.21 24.02	69.74 17.16	39.71 4.449	111.6 11.35
Max. CAP	12.84 3.772	0.2320 0.2451	54.43 29.51	36.21 24.45	12.80 7.817	11.76 5.352	0.2361 0.1239	14.28 5.814
SPV threshold (mm/s)	0.03639 0.00429	-	1.514 0.4784	1.551 0.3692	1.581 0.3481	3.131 1.342	-	3.479 0.8041
Displacement threshold (nm)	83.08 10.70	-	315.1 208.2	383.6 97.50	437.8 114.5	871.2 369.4	-	809.5 183.9

- 1) w^{1118}
- 2) $Naam^{MI12364} - Gal4$
- 3) $Naam^{MI12364} - Gal4 > Naam$
- 4) $Naam^{MI12364} - Gal4 > Naam::GFP$
- 5) $Naam^{MI12364} - Gal4 > Naam - 3EF$
- 6) $Naam^{MI12364} - Gal4 > Naam - EF - point\ mutation$
- 7) $Naam^{MI12364} - Gal4 > Naam - delta\ EF$
- 8) $Naam^{MI12364} - Gal4 > PNC1$

Figure 77. Unsuccessful hearing perception recovery in homozygous $Naam^{MI12364}-Gal4$ flies.

Top: power spectra of the mechanical fluctuations of the antennal sound receiver (A) as well as antennal displacement (B), normalized compound action potential (CAP) amplitudes (C) as a function of the sound particle velocity, and CAP amplitude as a function of antennal displacement (D) in w^{1118} flies, homozygous $Naam^{MI12364}-Gal4$ mutant flies, and flies expressing various $UAS-Naam$ constructs with homozygous $Naam^{MI12364}-Gal4$ driver. Bottom: corresponding amplification gain, individual best frequencies, power of the receiver fluctuations, maximum CAP amplitudes, sound particle velocity (SPV) threshold, and displacement threshold. Driving $UAS-Naam$ constructs in $Naam^{MI12364}-Gal4$ homozygous flies resulted in nerve response recovery but not the mechanical amplification. The ghost graphs represent w^{1118} as a control. The power graph is on a logarithmic scale. The first number in the table represents the mean, and the second one stands for standard deviation. $n \geq 5$ flies/genotype. Two-tailed Mann-Whitney-U tests with the Bonferroni correction were used for statistical analysis. Statistical significances are indicated with ns ($P > 0.05$), and * ($P \leq 0.05$).



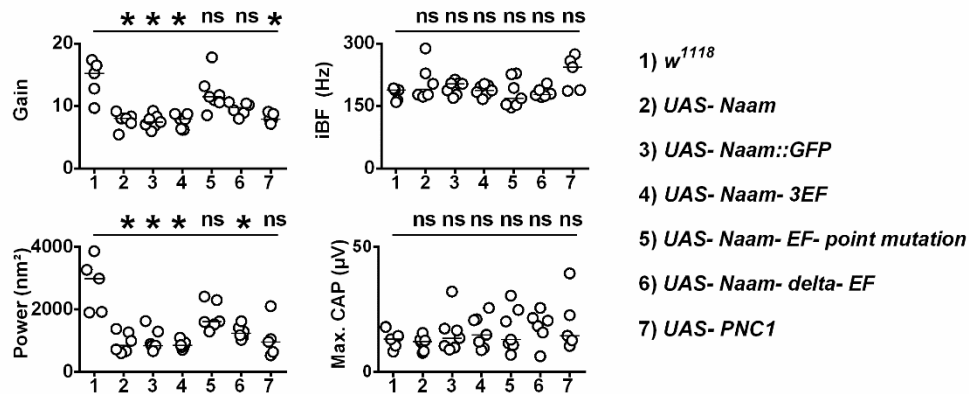


Figure 78. Absence of hearing defect in *UAS-Naam* constructs.

Top: power spectra of the mechanical fluctuations of the antennal sound receiver (A) as well as antennal displacement (B), normalized compound action potential (CAP) amplitudes (C) as a function of the sound particle velocity, and CAP amplitude as a function of antennal displacement (D) in w^{1118} , *UAS-Naam*, *UAS-Naam::GFP*, *UAS-Naam-3EF*, *UAS-Naam-EF-point mutation*, *UAS-Naam-delta-EF*, and *UAS-PNC1*. Bottom: corresponding amplification gain, individual best frequencies, power of the receiver fluctuations, and maximum CAP amplitudes. $n \geq 5$ flies/genotype. Two-tailed Mann-Whitney-U tests with the Bonferroni correction were used for statistical analysis. Statistical significances are indicated with ns ($P > 0.05$), and * ($P \leq 0.05$).

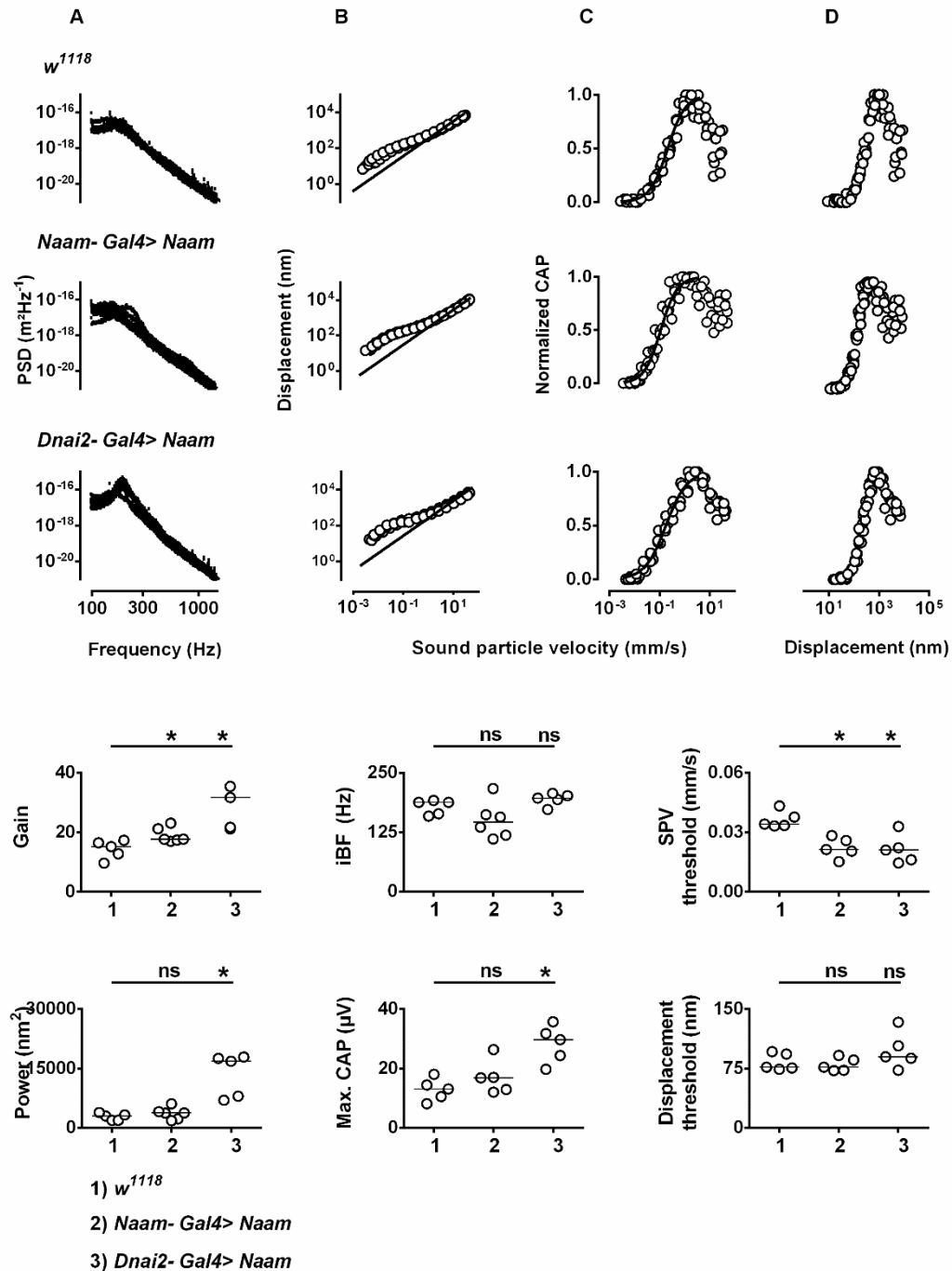


Figure 79. Overexpressed *Naam* with cell-type-specific drivers.

Top: power spectra of the mechanical fluctuations of the antennal sound receiver (A) as well as antennal displacement (B), normalized compound action potential (CAP) amplitudes (C) as a function of the sound particle velocity, and CAP amplitude as a function of antennal displacement (D) in wild type flies, and flies overexpressing *Naam* with the chordotonal receptor driver, *Dnai2-Gal4* (*Dnai2-Gal4>Naam*) or scolopale driver, *Naam-Gal4* (*Naam-Gal4>Naam*). Bottom: corresponding amplification gain, individual best frequencies, power of the receiver fluctuations, maximum CAP amplitudes, sound particle velocity (SPV) threshold, and displacement threshold. The power of the antenna's mechanical free fluctuations of flies overexpressing *Naam* with a neuronal driver is significantly higher compared to the scolopale driver. $n \geq 5$ flies/genotype. Two-tailed Mann-Whitney-U tests with the Bonferroni correction were used for statistical analysis. Statistical significances are indicated with ns ($P > 0.05$), * ($P \leq 0.05$).

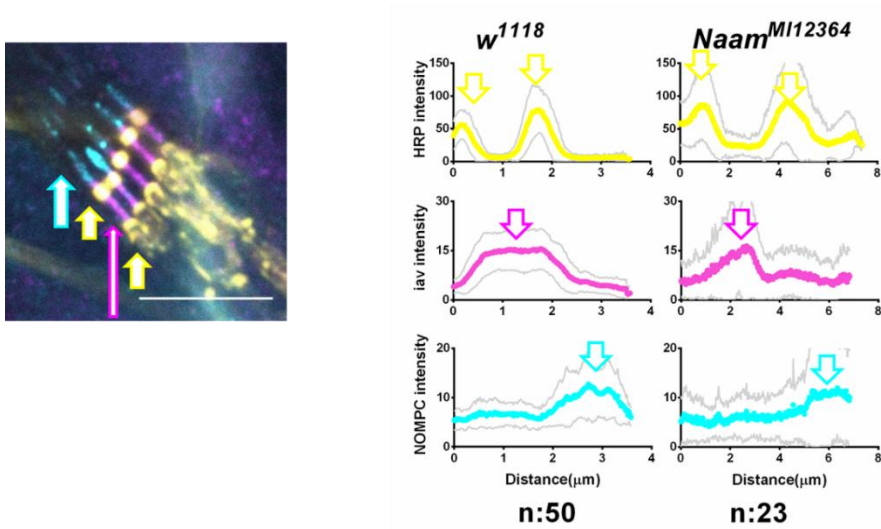


Figure 80. lav and NOMPC signal amplitudes in *Naam* mutant larvae. Plotting (the existing) signal amplitudes of NOMPC(cyan), lav(magenta), and HRP (yellow) along the longitudinal neuronal axis showed the same pattern as in *w¹¹¹⁸*, control flies, however, with a higher deviation from the mean. Scale bar: 20 μ m.

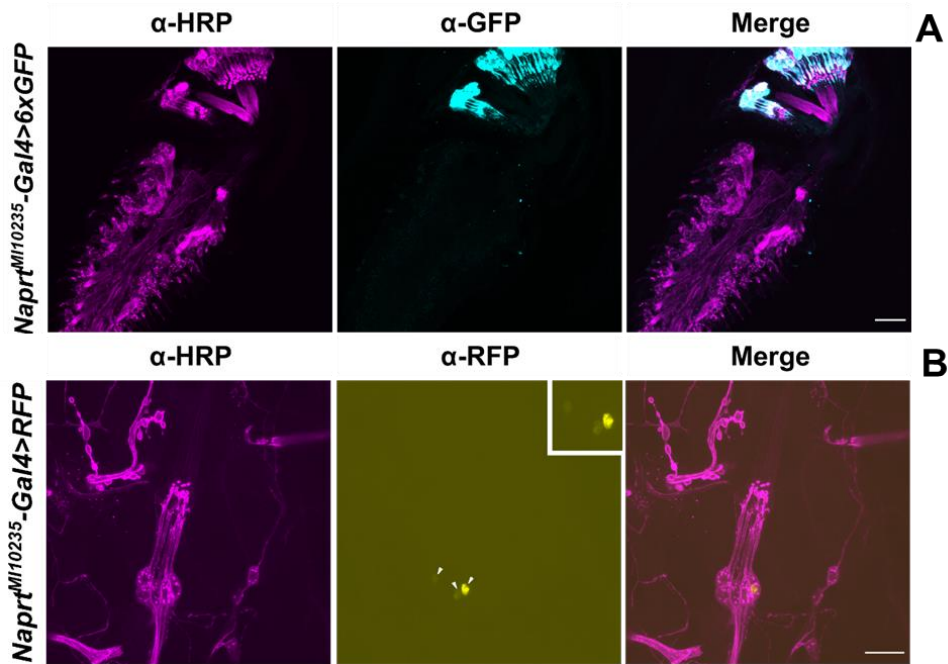


Figure 81. *Naprt* expression pattern. Driving 20XUAS-6XGFP with *Naprt^{M110235}-Gal4* driver (*Naprt^{M110235}-Gal4*>6XGFP) (cyan) labels the JO in the antenna of adult *Drosophila* (A) and driving nuclear RFP (*UAS-red-stinger*) with *Naprt^{M110235}-Gal4* (*Naprt^{M110235}-Gal4*>RFP) (yellow) labels lch5 in larvae (B). Anti-HRP labels the neurons (magenta). The expression of *Naprt* is not present in all five lateral chordotonal organs. Scale bars: 10 μ m.

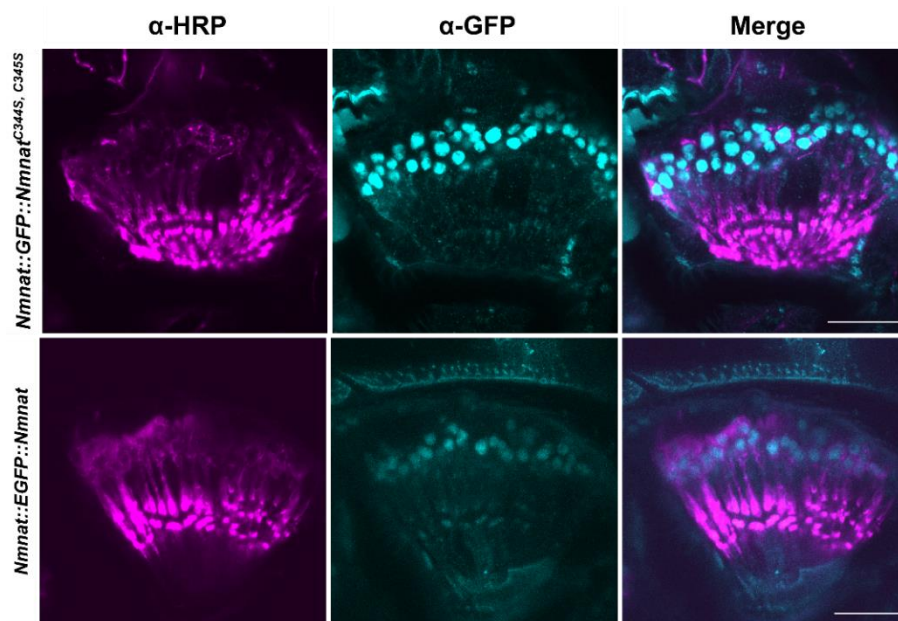
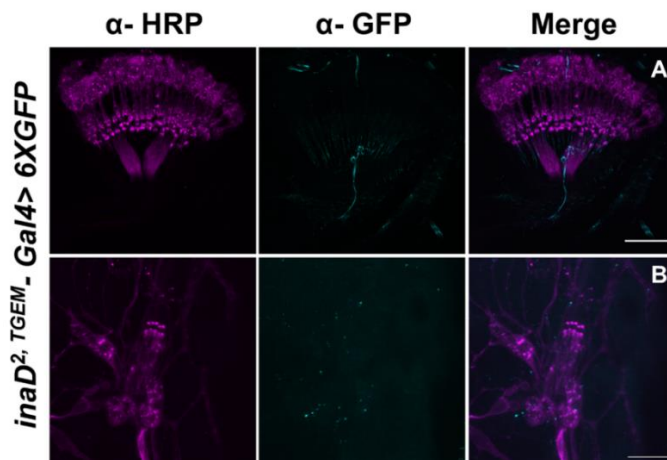
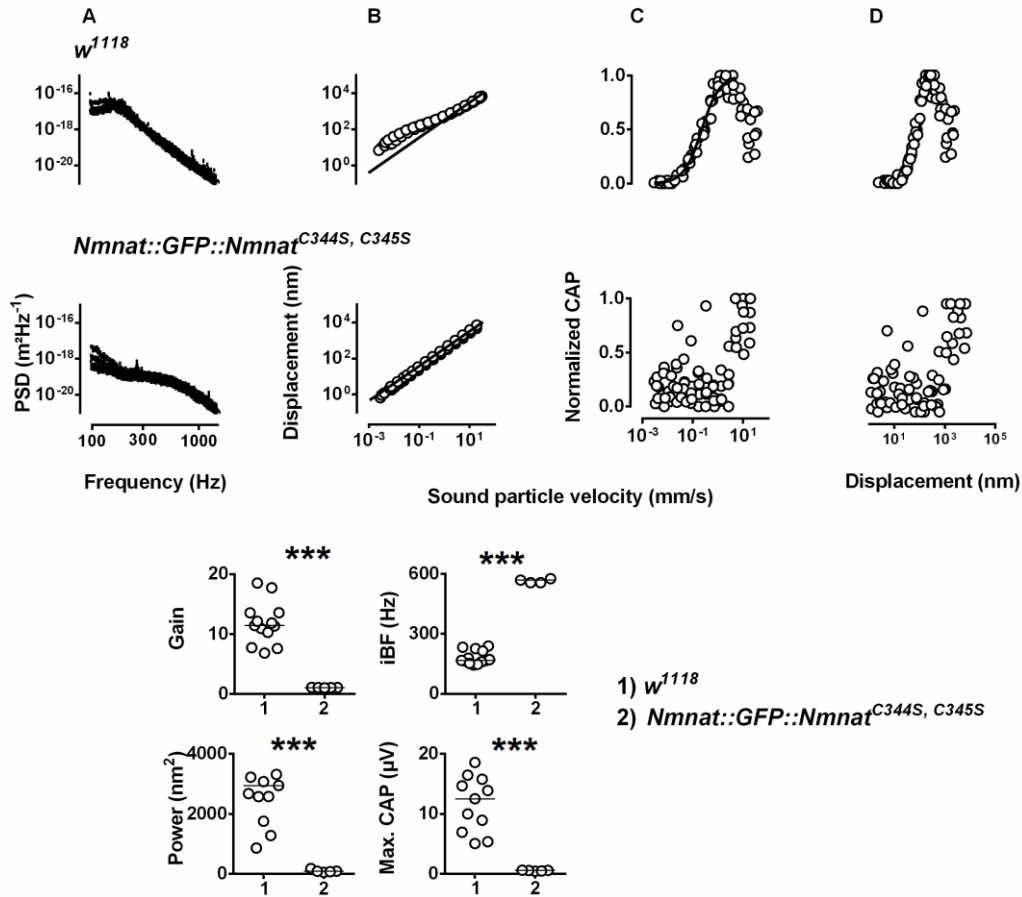


Figure 82. NMNAT protein localization.

GFP tagged NMNAT demonstrates localization in the nuclei of JO mechanoreceptors (cyan). Anti-HRP labels the neurons (magenta). Scale bars: 20 μ m.



List of figures

Figure 1. <i>Drosophila</i> hearing organ.	11
Figure 2. Experimental plan.....	21
Figure 3. Schematic of Gal4/UAS system.....	22
Figure 4: Generated plasmid map.	26
Figure 5. Double Header tool.	29
Figure 6: Laser Doppler vibrometry (LDV) set up.	33
Figure 7. Schematic of NAAM assay.	36
Figure 8. Salvage pathway of NAD ⁺ synthesis.....	42
Figure 9. The evolutionary conservation of the EF-hand domains in the NAAM enzyme.	45
Figure 10. <i>Naam</i> transcripts.	47
Figure 11. <i>Naam</i> expression in JO and Ich5 chordotonal organs.....	48
Figure 12. <i>Naam</i> expression pattern in the <i>Drosophila</i> brain.	49
Figure 13. NAAM localization in scolopale cells and JO neurons.....	50
Figure 14. Localization of NAAM relative to the scolopale rods.	51
Figure 15. <i>Naam</i> expression analysis.....	52
Figure 16. Auditory defects in <i>Naam</i> mutant flies.	53
Figure 17. Effects of a NAAM inactivator on hearing.	54
Figure 18. Nicotinamide and nicotinic acid feeding effects on hearing.	56
Figure 19. Absence of nicotinic acid or NAD ⁺ rescue effect on hearing of the <i>Naam</i> mutant flies.....	57
Figure 20. <i>Nmnat</i> overexpression effects on the hearing of the <i>Naam</i> mutant flies.....	59
Figure 21. Crossing scheme of the cell type-specific rescue of hearing in the <i>Naam</i> mutant flies.....	61
Figure 22. Cell type-specific rescue of the <i>Naam</i> mutant flies.	62
Figure 23. Schematic picture of the generated NAAM constructs.	63
Figure 24. The differences between the two NAAM GFP-tagged proteins.	64
Figure 25. Rescue potential of <i>UAS-Naam</i> with and without EF-hand domains mutation.	67
Figure 26. <i>In vitro</i> NAAM enzymatic activity with or without EF-hand domains ablation.	69
Figure 27. <i>Naam</i> overexpression effects on hearing.....	72
Figure 28. Nicotinamide effects on flies with overexpressed <i>Naam</i>	73
Figure 29. The auditory phenotype in double <i>Naam</i> and <i>iav</i> mutant flies.....	75
Figure 30. <i>nompC</i> and <i>iav</i> expression levels in the <i>Naam</i> mutant flies compared to <i>w¹¹¹⁸</i>	76
Figure 31. Disrupted channel localization in <i>Naam</i> mutant larvae.....	77
Figure 32. Absence of apoptosis in <i>Naam</i> mutant flies.	78
Figure 33. Absence of apoptosis in nicotinamide or nicotinic acid-treated <i>w¹¹¹⁸</i>	79
Figure 34. Altered mitochondrial features in <i>Naam</i> mutant flies.	80
Figure 35. Disrupted tubulin acetylation pattern in <i>Naam</i> mutant flies.....	81
Figure 36. Disrupted tubulin acetylation pattern upon nicotinamide treatment.	81
Figure 37. Predicted 3D structure of NAAM.....	86
Figure 38. Schematic picture of the proposed NAAM function in the JO.....	87
Figure 39. GAP43 mode of action.	93
Figure 40. <i>igl</i> transcripts and the position of two MiMIC insertions.....	94
Figure 41. Two IGL translated proteins.....	95

Figure 42. IGL and its human orthologs.....	96
Figure 43. <i>igl</i> transcripts levels.	98
Figure 44. <i>igl</i> expression pattern.	100
Figure 45. <i>igl</i> expression pattern in <i>Drosophila</i> brain.....	101
Figure 46. Cellular localization of IGL in JO and lch5.....	102
Figure 47. RFX DNA binding motif (X-box promoter motif) conservation in <i>Drosophila</i> specious.....	103
Figure 48. RFX DNA binding motif (X-box promoter motif) conservation in vertebrates.	103
Figure 49. Comparison of X-box motifs in mammalian GAP43 and <i>Drosophila igl</i>	103
Figure 50. <i>igl</i> is conserved in ciliated eukaryotes.....	105
Figure 51. <i>igl</i> and <i>iav</i> expression dependency on the RFX transcription factor.	107
Figure 52. IGL localization in the <i>Rfx</i> mutant larva.....	108
Figure 53. Hearing in <i>igl</i> mutant flies compared to <i>w¹¹¹⁸</i> control flies.....	109
Figure 54. Recovered hearing perception in the <i>igl</i> mutant flies.....	111
Figure 55. <i>inaD^{2, TGEM}-Gal4</i> , and <i>inaD^{3, CRIMIC}-Gal4</i> constructs.....	133
Figure 56. PCR on cDNA of <i>cn¹ bw¹</i> , <i>inaD^{3, CRIMIC}-Gal4</i> , and <i>inaD^{2, TGEM}-Gal4</i>	134
Figure 57. Quantification of <i>inaD</i> transcripts in <i>cn¹ bw¹</i> , <i>inaD^{2, TGEM}-Gal4</i> , and <i>inaD^{3, CRIMIC}-Gal4</i>	134
Figure 58. The auditory phenotype in <i>inaD</i> mutants compared to the respective control flies (Part I).....	136
Figure 59. The auditory phenotype in <i>inaD</i> mutants compared to the respective control flies (Part II).....	137
Figure 60. <i>inaD^{3, CRIMIC}-Gal4</i> integration marker.	138
Figure 61. INAD level in <i>inaD</i> mutants compared to the respective control flies.	138
Figure 62. Uncovering <i>inaD</i> mutation with a deficiency line.	140
Figure 63. The auditory phenotype in <i>inaD^{3, CRIMIC}-Gal4/inaD¹</i> compared to <i>inaD^{3, CRIMIC}-Gal4</i>	141
Figure 64. GMR expression pattern.....	142
Figure 65. The auditory phenotype of <i>inaD¹</i> compared to genomic rescued flies.....	143
Figure 66. PDA phenotype in <i>w¹¹¹⁸</i> as a control, <i>inaD¹</i> , and rescue flies.....	144
Figure 67. Derived expression pattern of <i>inaD</i>	145
Figure 68. The auditory phenotype in <i>inaD¹</i> compared to UAS rescued flies.	146
Figure 69. <i>Naam</i> expression in scolopale and cap cells (different reporters).	148
Figure 70. <i>Naam</i> expression in the leg chordotonal and haltere pedicelum.	149
Figure 71. Hearing defect in the internally GFP-tagged NAAM flies.....	150
Figure 72. Absence of nicotinic acid rescue effect on hearing of the <i>Naam</i> mutant flies.	151
Figure 73. Absence of NAD ⁺ rescue effect on hearing of the <i>Naam</i> mutant flies.....	152
Figure 74. Absence of overexpressed <i>Nmnat</i> rescue effect on hearing of the <i>Naam</i> mutant flies.....	153
Figure 75. Fluorescent picture of <i>Naam^{MI12364}-Gal4>Naam::GFP</i> flies.	154
Figure 76. NAAM localization in the <i>Naam</i> mutant flies with recovered hearing perception.	154
Figure 77. Unsuccessful hearing perception recovery in homozygous <i>Naam^{MI12364}-Gal4</i> flies.....	156
Figure 78. Absence of hearing defect in <i>UAS-Naam</i> constructs.	158
Figure 79. Overexpressed <i>Naam</i> with cell-type-specific drivers.....	159
Figure 80. <i>iav</i> and NOMPC signal amplitudes in <i>Naam</i> mutant larvae.....	160
Figure 81. <i>Naprt</i> expression pattern.	160
Figure 82. NMNAT protein localization.	161

Figure 83. Hearing defect in *Nmnat* mutant flies.....162
Figure 84. *inaD* expression pattern.....162

List of tables

Table 1. Fly lines	17
Table 2. List of clonings.....	23
Table 3. Used Primers.....	24
Table 4. Quantitative RT-PCR protocol	27
Table 5. Used antibodies.....	31
Table 6. Auditory phenotypes based on amplification gain values (Senthilan et al., 2012).....	34
Table 7. Screening result for <i>Naam</i> gene	43
Table 8. NAD salvage pathway enzymes.	89
Table 9. Screening result for <i>igl</i> gene	97
Table 10. Possible <i>igl</i> <i>GAL4</i> and <i>GFP</i> lines	99
Table 11. Brief summary of INAD project.	147

List of abbreviations

aa	amino acid
AMMC	antennal mechanosensory and motor center
<i>ato</i>	<i>atonal</i>
BDSC	Bloomington Drosophila Stock Center
<i>C. elegans</i>	<i>Caenorhabditis elegans</i>
CaM	Calmodulin
CamKII	Ca ²⁺ /calmodulin-dependent protein kinase II
CAP	compound action potential
cDNA	complementary DNA
CRIMIC	CRISPR-Mediated Integrated Cassette
DH	Double Header
<i>D. melanogaster</i>	<i>Drosophila melanogaster</i>
Dnai2 dynein	axonemal, intermediate chain 2
GAP	Growth-associated protein
GFP	green fluorescent protein
iav	inactive
iBF	individual best frequency
IFT	intraflagellar transport
<i>igl</i>	<i>invertebrate GAP43 like</i>
INAD	inactivation no afterpotential D
JO	Johnston's organ
lch	lateral chordotonal organ
LDV	Laser Doppler Vibrometer
LIMk	LIM kinase
MiMIC	Minos-Mediated Integration Cassette
NA	Not Applicable
NA	nicotinate
NAAM	nicotinamidase
NAD ⁺	nicotinamide adenine dinucleotide
NADA	nicotinamide deamidase
NADS	NAD synthetase
NAM	nicotinamide
NAMPT	nicotinamide phosphoribosyltransferase

List of abbreviations

nan	nanchung
NAPRTase	nicotinate phosphoribosyltransferase
NMN	nicotinamide mononucleotide
NMNAT	nicotinamide mononucleotide adenylyltransferase
nompC	no mechanoreceptor potential C
NR	nicotinamide riboside
ns	not significant
PARP	poly ADP-ribose polymerase
PBS	phosphate buffer saline
PBST	phosphate buffer saline with triton-X100
pcof	phosphorylation of cofilin
PCR	polymerase chain reaction
PDA	prolonged depolarizing afterpotential
PFA	paraformaldehyde
PIP2	phosphatidylinositol 4,5-bisphosphate
PKC	protein kinase C
PNC1	pyrazinamidase/nicotinamidase 1
PSD	power spectral density
RT-qPCR	Quantitative reverse transcription PCR
rab	rabatin
RFP	red fluorescent protein
RT	room temperature
sirtuins	silent information regulators
SNAP-25	synaptosomal-associated protein 25
SPV	sound particle velocity
synp	synaptophysin
T-GEM	Trojan-Gal4 expression module
TRP	transient receptor potential
TRPN	transient receptor potential nompC
TRPV	transient receptor potential vanilloid
TUNEL	TdT-mediated dUTP-X nick end labeling
UAS	upstream activating sequence
VDRC	Vienna Drosophila Resource Center
WT	wild type

Acknowledgments

First of all, I would like to thank my Doctoral Advisor, Martin Göpfert, for allowing me to work on different projects in his laboratory, as well as for his dedicated support.

Many thanks to Tobias Moser and Jörg Großhans for their scientific input into my project and acceptance to be in my 'Thesis Committee'.

Many thanks to Ralf Heinrich, Jan Clemens, and Gerd Vorbrueggen for their acceptance to be on the examination board.

I also want to thank everyone from whom I have received a lot of help:

Natascha Zhang, Thomas Effertz, Radoslaw Katana, Debbra Yasemin Knorr, Nicola Schwedhelm-Domeyer, Stephanie Pauls, Silvia Gubert, and Hanna Pies

as well as my students: Lucas Sebastian and Sabrina Weber

I would like to specially express my thanks to Dr. Philipp Hehlert for his constructive discussions and corrections.

I would also like to thank all other people in my working group who accompanied me during my doctorate.

Gudrun Matthes, Prof. Andreas Stumpner, Prof. Ralf Heinrich, and Dr. Bart Geurten

Last but not least, I want to thank the loves of my life, my parents, and specially my husband, Lenard Lux.

I also appreciate the financial support from DAAD: German Academic Exchange Service.

Narges Bodaghabadi (Lux)

Declaration

I herewith declare that the PhD thesis entitled “Regulation of mechanical feedback amplification in the *Drosophila* ear” was written independently, with no other sources and aids than quoted.

Narges Bodaghabadi (Lux)

Göttingen, 17.11.2021

Curriculum vitae

Name: Narges Bodaghabadi (Lux)

Date of birth: December 20th, 1989

Place of birth: Tehran, Iran

Nationality: Iranian

Education

- 09.2017 – Present Ph.D. student, Georg-August-Universität Göttingen - Department of Cellular Neurobiology
Ph.D. thesis: Regulation of mechanical feedback amplification in the *Drosophila* ear
- 2012 – 2015 M.Sc. in Cellular & Molecular Biology-Genetics, (GPA: 18.82/20)
University of Tarbiat Modares - Department of Genetics, Faculty of Biology
Master thesis: Preparation and Evaluation of Rifampicin and Co-trimoxazole-loaded Nanocarrier Efficacy against *Brucella Melitensis* Infection
Supervisor: Prof. M. Sadeghizadeh. Thesis defense Grade: 19.80/20
- 2008 - 2012 B.Sc. in Cellular & Molecular Biology-Genetics, (GPA: 18.44/20)
Shahed University - Department of Biology, Faculty of Basic Sciences.
- 2007 - 2008 Pre-University in Experimental Science (GPA: 19.54/20) Fazilat High school, Tehran, Iran.
- 2004 - 2007 High school in Experimental Science, (GPA: 19.83/20) Fazilat High school, Tehran, Iran.

Honors

- First rank student in B.Sc & second rank student in M.Sc.
- 7th rank in nationwide M.S. entrance examination on Genetics, 2012 (Held by Ministry of Science and Technology between more than 10,000 examinees).

- Top 1 % rank in B.S. entrance exam, 2008 (Held by Ministry of Science and Technology between more than 400,000 examinees).
- I was awarded a scholarship from the German Academic Exchange (DAAD) for Doctoral student for more than 4 years

Conference attendance and presentations

- Ph.D.
- 12th Göttingen Meeting of the German Neuroscience Society (NWG) (22.03.2017)
 - Women's Careers and Networks 2017 (13.10.2017)
 - 11th Molecular Biology of Hearing and Deafness meeting in Göttingen (24.05.2018) (poster presentation)
 - Neurobiological practice course hearing (19. - 23.03.2018) (poster presentation)
 - Force Gated Ion Channels Conference (17. - 20.10.2018)
 - Flying Senses Symposium 2018 (26. - 27.10.2018)
 - 13th Göttingen Meeting of the German Neuroscience Society (NWG) (20. - 23.03.2019) (poster presentation)
 - NEURO DoWo 2019 (28. - 31.08.2019) (poster presentation)
- Master
- 10th Royan International Congress on "Stem Cell Biology & Technology" Royan Institute, Tehran, Iran, September (3. - 5. 2014) (poster presentation)
 - First International and 13th Iranian Genetic Congress, Shahid Beheshti University Conference Center, Tehran, Iran, May (24. - 26. 2014) (poster presentation)
 - 5th International Congress on Nanoscience and Nanotechnology, Tarbiat Modares University, Tehran, Iran, October (22. - 24. 2014) (poster presentation)
 - 15th International Iranian Congress of Microbiology, Tehran University, Tehran, Iran, August (26. - 28. 2014) (poster presentation)

Publications

- Preparation and Evaluation of Rifampicin and Co-trimoxazole-loaded Nanocarrier against *Brucella melitensis* Infection. DOI: 10.29252/ibj.22.4.275 (first author)

- Radiation-induced surge of macrophage foam cell formation, oxidative damage, and cytokine release is attenuated by a nanoformulation of curcumin. DOI: 10.1080/09553002.2016.1242817
- One-pot exfoliation, functionalization, and size manipulation of graphene sheets: efficient system for biomedical applications. DOI: 10.1007/s10103-017-2422-4
- Nanoformulation of curcumin protects HUVEC endothelial cells against ionizing radiation and suppresses their adhesion to monocytes: potential in prevention of radiation-induced atherosclerosis. DOI: 10.1007/s10529-016-2189-x
- Nano Packaged Tamoxifen and Curcumin; Effective Formulation against Sensitive and Resistant MCF-7 Cells. 2018 winter; 17(1): 1–10.
- Techniques for Evaluation of LAMP Amplicons and their Applications in Molecular Biology. DOI: 10.7314/APJCP.2015.16.17.7409

Skills

Molecular biology (RNA extraction, cDNA synthesis, qPCR, cloning, protein extraction, enzymatic reaction, western blot), Immunohistochemistry, Mammalian cell culture, Microbiology, Cell biology

Languages

Persian, Turkish (Azari):	Native Language
English:	Fluent (TOEFL score: 101/120 Reading: 28 listening: 24 Speaking: 22 Writing: 27)
German:	B2.2

Attendant courses

Laboratory animal science (17.03.2017)

Neurobiological Practical Course - HEARING, 2018 (23.03.2018)

Workshop "Good Scientific Practice for Biologists" (24.08.2018)

Adobe Illustrator Beginners' Course (21.08.2018)

Basic methods of transmission electron microscopy - from tissue preparation to 3D reconstruction (6.2018)

Networking for academics (4.11.2018)

Curriculum vitae

Preparation and patch-clamp recording of adrenal chromaffin cells (11.01.2019)

A Brief Introduction to Statistics for PhDs Part I (21.08.2018)

Neuronal circuit dissection in *Drosophila* - Brief information (01.10.2018)

Introduction to image processing in biology with ImageJ and FIJI

Deutsch - Grundkurs (A1.1), (A1.2), (A2.1), (A2.2), (B1.1), (B1.2), (B2.1), and (B2.2).

Teaching experiences

Bachelor (Lucas Sebastian) 01. - 03.2019

Erasmus internship (Laura Martín Herrero) 03. - 04.2019

Lab rotation (Sabrina Weber) 04. - 06.2021